Transition and Flow-Induced Scattering of Acoustic Modes in Ducts

Alexander Francis Smith

DEPARTMENT OF MATHEMATICS
UNIVERSITY COLLEGE, LONDON

A THESIS PRESENTED FOR THE DEGREE OF
DOCTOR OF PHILOSOPHY

SUPERVISORS
DR N. C. OVENDEN & DR R. I. BOWLES

August 2011

I, Alexander Francis Smith, confirm that the work presented in this thesis is my own. Where information has been derived from other sources, I confirm that this has been indicated in the thesis.

SIGNED

Abstract

The propagation of unsteady disturbances in ducts of slowly-varying geometry, such as those typical of an aero-engine, can be successfully modelled using a multiple scales approach. The multiple-scales approach has a number of distinct advantages over full numerical methods. Previous authors have validated the accuracy and usefulness of the multiple scales approach by comparing with results obtained using the finite element method, using realistic aero-engine configurations.

Cut-on cut-off transition of acoustic modes in hard-walled ducts with irrotational mean flow is well understood. However, previous finite-element simulations of this phenomenon appear to indicate the possibility of energy scattering into neighbouring modes at large Helmholtz numbers. In this thesis, an attempt is made to explain such scattering phenomena in slowly varying aero-engine ducts using multiple-scales techniques.

In order to model modal scattering a good understanding of cut-on cut-off transition is necessary. Here, the well known single turning point is revisited, and our understanding of cut-on cut-off transition is extended to include an analysis of a double turning point. Then using a similar apparatus, modal scattering in the case where a mode undergoes cut-on cut-off transition is investigated. It is found that, for sufficiently high frequencies, a mechanism exists whereby a propagating incident mode can be scattered into neighbouring modes provided that a mean flow exists within the duct. An asymptotic analysis of this mechanism is presented and, by solving numerically a composite solution, results in a duct of rectangular cross section are obtained.

The energy distribution of the incident and neighbouring scattered modes reveals an interaction and exchange of energy with the mean flow. This work now allows greater insight as well as more accurate and fast computations of high frequency mode propagation in slowly-varying hard walled ducts using multiple-scales approaches.

Contents

Acknowledgements

First and foremost I would like express my deepest gratitude to my doctoral supervisors Dr Nicholas Ovenden and Dr Robert Bowles. I am truly grateful for their encouragement, guidance and support right throughout this process, without which I doubt this thesis would have been finished. One could not ask for better supervisors, and I very much hope that we may be able to work together again in some capacity soon.

I would like to thank Professor Frank Smith for giving me the opportunity to complete a PhD, and to EPSRC for their financial support. I would also like to thank everyone at the department of mathematics at UCL; professors, fellow PhD students and office staff, for the countless acts of friendship and support shown to me over the last five years.

I am grateful to everyone who has encouraged me throughout my career as a mathematician. I would like to give particular special thanks to my pre-undergraduate teachers Mr V. Knight and Mr T. Larson who were nothing short of truly inspirational. The world needs more maths teachers like them! I also received a fantastic education from the University of Manchester, and I would like to thank all of those who helped to make this such an enjoyable and worthwhile experience.

I would like to give thanks to all my friends and family for their encouragement and belief throughout my life. A special mention goes out to my two very good friends Simon Little and Joe Carroll from whom I learnt a lot about programming, web development and linux.

Finally, I would like to thank my beautiful and amazing wife Kremena for her love, friendship and support, and to congratulate her on making such a fine choice of husband.

List of Figures

List of Tables

Part I

Propagation & Transmission of Acoustic Modes

Chapter 1

Introduction

1.1 The Problem of Aeroacoustic Noise

Aeroacoustic noise, such as the noise emitted by a low flying aircraft, has been of great importance to engineers and scientists ever since such machines came into widespread commercial deployment. The health effects associated with elevated sound levels produced by commercial aircraft can include stress, annoyance, sleep deprivation and hypertension among other things [30]. These effects on humans are well known, and in an effort to protect citizens from exposure to adverse levels of noise governments all over the world have introduced various forms of regulation to combat the problem. For example, a recent (2003) UK government white paper outlined several measures to protect citizens that live within the close vicinity of airports, such as imposing noise limits for departing aircraft, and plans to phase out older types of aircraft and replace them with newer and quieter aircraft [41]. These measures have put pressure on commercial aircraft engineers to combat the problem of

aeroacoustic noise, and as a result modern aircraft have become significantly quieter over the last 30 years. ISO standards currently use a method that is used to measure the Effective Perceived Noise Level (EPNL) of passenger planes and certification of aircraft noise levels are awarded using this scale. Reductions in EPNL levels over the years can be seen in Figure 1.1.

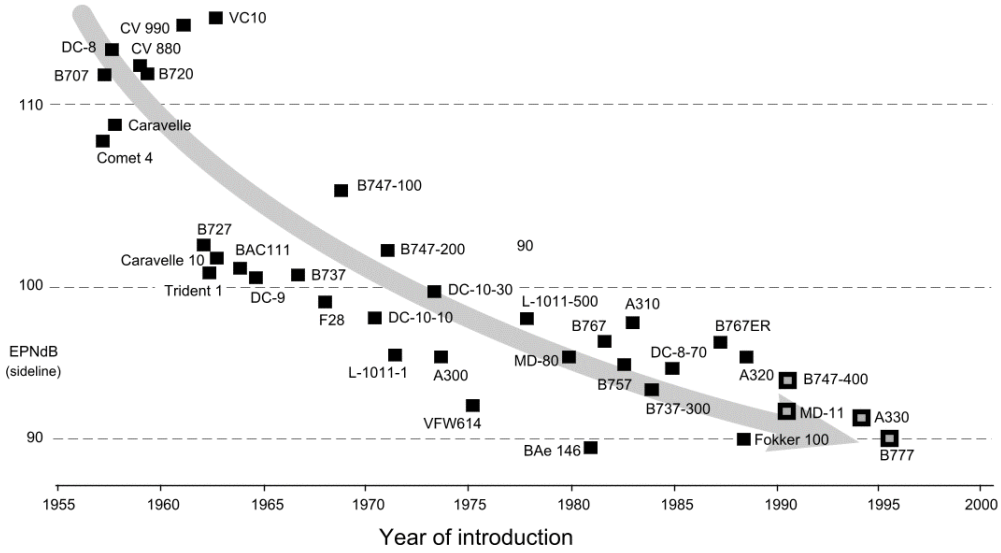

Figure 1.1: Improvements in the Effective Perceived Noise Level (EPNL) of passenger aircraft between 1955 and 1995

However despite the achievements over the last 40 or so years, there are still problems as modern aircraft can still by no means be considered to be quiet, plus the sheer increase in the number of aircraft over the last decade has partially offset the reduction in noise per aircraft. Thus more needs to be done to control the level of noise produced by this very necessary form of transportation.

The problem with aircraft noise in particular is that there are several mechanisms for sound production, the three principle mechanisms being aerodynamic noise, mechanical noise, and noise produced by the aircraft's systems which include cockpit and cabin pressurisation/conditioning systems and auxiliary power unit. If one's aim is to significantly reduce aircraft noise then all of these mechanisms need to be addressed and understood.

Aerodynamic noise arises due to the flow of air around the airframe (i.e. the aircraft's fuselage and it's control surfaces). However to any listeners not on board the aircraft this aerodynamically generated noise is only significant during the take-off and landing phases of the aircraft operation [59].

Noise producing systems that fall into the mechanical noise category include aircraft propulsion systems. These include the jet, turbofan engine and the turbine driven propellers and undoubtedly form a major source of mechanical noise generated by an aircraft. The noise produced by the jet follows Lighthill's famous eighth power law, which states that the total acoustic power scales with the eighth power of the jet velocity [31].

As mentioned above, one key contributor to the degree of aeroacoustic noise is the noise produced by the aircraft's turbofan engines. A turbofan engine is a type of aircraft jet engine whose purpose is to provide the thrust necessary to keep the aeroplane in steady motion whilst airborne. Although several types of turbofan exist, the main principle behind all turbofan engines is that thrust is generated by drawing in and then discharging a fast moving jet of fluid,

and a natural by-product of this action is aeroacoustic noise. Figure 1.2 shows some typical features of a modern turbofan engine.

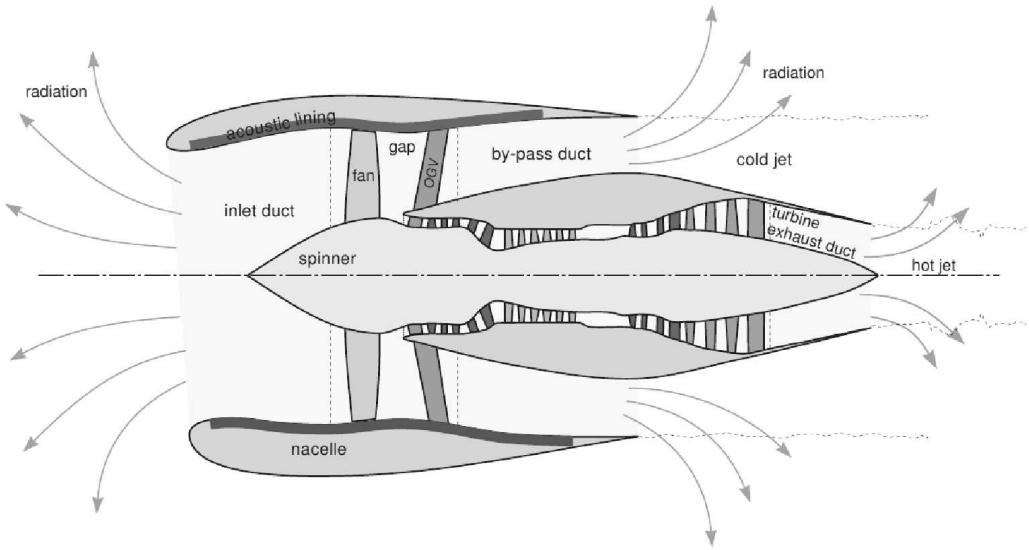

Figure 1.2: Sketch of a typical turbofan engine

The airstream passes into the engine via the inlet duct, a process that is assisted by the fan. Then part of this airstream passes though the core of the engine, providing oxygen to burn fuel and create power, whilst the rest of the air flow passes through the by-pass duct, mixing with the faster stream from the core at the exhaust. This method of splitting the flow field up using the by-pass duct has two advantages; Firstly it allows some of the thrust to be generated by allowing air to pass through the by-pass duct and thus reducing fuel consumption resulting in greater energy efficiency, and secondly this method of mixing the hot and cool air at the exhaust actually leads to a reduction of sound being produced at the exhaust.

The engine by-pass ratio is defined as the ratio between the mass flow rate

of air that is drawn in by the fan that by-passes the engine core to the mass flow rate passing through the engine core. A higher by-pass ratio gives a lower exhaust speed, less noise and higher efficiency in terms of fuel level consumption when compared to a low-by-pass duct. Prior to the early 1960s, low-by-pass ducts were mainly used in civil aviation, but were slowly phased out of use in favour of high-by-pass engines. Today high by-pass engines are deployed throughout the entire civil aircraft industry and low-by-pass ducts are no longer used. One distinct feature of figure 1.1 is the large gap in EPNL that occurred around the early 1960s, and this gap is a direct consequence of many aircraft switching from low to high ratio by-pass engines. This period in history is sometimes referred to as the 'high by-pass revolution'.

The presence of the rotating fan within a turbofan engine is known to be a significant source of broadband noise, broadband noise being noise that spans a large range of the audible frequency spectrum. One of the largest contributions to this broadband noise is believed to come from the interaction between the turbulent flow in the rotor wake and the stator vanes, known as *rotor wake-stator interaction noise* (see, for example studies by Tyler-Sofrin [26], Kester-Pickett [29], Sijtsma and Schulten [56] and Britchford *et al* [27]). Another very important mechanism of broadband noise is believed to be the interaction between the turbulence generated in the boundary layer on the rotor blades and it's trailing edge, a mechanism that is often referred to as rotor *self-noise* [5].

Although engineers have some degree of control of noise production at the

exhaust and broadband noise produced by the fans, noise produced at the inlet duct is also a big issue, and this is an area that engineers have less control over. It is known that the degree of sound production within this area of the duct is effected by the geometry of the duct and the acoustic impedance of the duct walls. As shown in figure 1.2 some turbofan engines are lined with an acoustic lining, and the acoustic impedance of this acoustic lining may vary with the duct geometry. It is the understanding the mechanisms that occur within the inlet duct area of the turbofan engine that is the main focal point of this thesis.

1.2 Literature Review

Propagation of sound in straight ducts with a constant cross section, a constant impedance type boundary condition contained within a homogeneous medium is a classical and well understood problem [33, 34]. In this case the solution for the sound field is found in the case of frequency ω by solving the reduced wave (Helmholtz) equation $(\nabla^2 + k^2)\phi = 0$, where ϕ is the acoustic potential and $k = \omega/c$, where c is the speed of sound. The solution for ϕ is constructed by means of a modal expansion, and each modal solution is related to the two-dimensional Laplacian operator acting on the cross section. These modes are interesting because they form, in general, a complete basis from which any solution can be represented. Also from a physical point of view, each mode is actually a solution in it's own right, and is not just a small part of a larger mathematical framework. From understanding these modes and the way in which they are constructed, the (usually) complicated structure of

the total acoustic field becomes easier to understand and analyse.

The next major development in the asymptotic analysis of duct acoustics was made by Nayfeh and Telionis [40], who in 1973 utilised the method of multiple scales to describe the spatial and temporal variation of amplitudes and phases of an acoustic wave propagating through a duct of slowly varying square or circular cross-section in both lined and hard walled ducts. They were able to show that by slowly reducing the cross section it is possible to eliminate some of the acoustic modes, and it appears that the behaviour of each mode can be separated into two distinct regions within the duct, known as the 'propagating region' and the 'attenuating region'. Within the propagating region the mode is said to be 'cut-on', which means that the geometry and boundary conditions are suitable to allow a particular mode to propagate in the axial direction, and therefore acoustic energy may be transmitted in the direction of axial propagation throughout this region by the mode. Throughout the propagating region the amplitude of the mode varies algebraically according to the variation of duct cross section. Within the attenuating region the mode is said to be 'cut-off', meaning that the geometry and boundary conditions are such that the isolated mode is unable to transmit acoustic energy within this region. A cut-off mode decays exponentially along the duct, and no further propagation of acoustic energy by this mode occurs within this region.

The point at which the mode undergoes this cut-on cut-off transition is known as a 'turning point', and the propagating/attenuating solutions that were obtained by Nayfeh and Telionis are not valid within the neighbourhood of this

(usually small) region, because the assumption of the acoustic potential ϕ being slowly-varying with respect to the axial direction is not true here, and therefore a different treatment of the governing equations is required. From a physical point of view, a mode undergoing cut-on cut-off transition means that the wavelength of the axially propagating mode is too large to allow further propagation into the constricting channel, and so the mode reflects at the transition point, exchanging all of its acoustic energy with its opposite running counterpart, causing a standing (or trapped) wave within the duct.

The research was further extended by Nayfeh, Telionis and Kaiser [37] and then by Nayfeh, Telionis and Lekoudis [38] to include the effects of mean flow. The introduction of the mean flow made the scenario a lot more complicated, as the spatially varying mean flow velocities consequently give non-constant coefficients in the governing acoustic equations, which usually means that a modal expansion is not possible. The simplest non-trivial case with mean flow is that with almost uniform mean flow in the case of vanishing viscosity. In this case, a modal solution may be found that is quite similar to the case without flow. However although the authors did manage to produce an exact expression for the modal amplitude in the case of no mean flow, the differential equation governing the modal amplitude in the case of mean flow appeared to be unsolvable analytically.

In attempting to derive an analytical solution for the mean flow case, one process that requires thorough attention is the way that the sound field is transmitted through the vanishing boundary layer. The reduction of the boundary

layer to an infinitesimally small size essentially modifies the impedance boundary condition at the duct wall to an equivalent condition in the limit to the duct wall. In other words a boundary condition should not be applied at the wall, but instead should be applied at a point very close to the wall, just inside where the effects of the mean flow can be felt. For straight ducts with non-varying cross section, a modified boundary condition was proposed first by Ingard [24], and then later proved by Eversman and Beckemeyer [18] and Tester [60]. However this boundary condition only works for uniform mean flow, and for non uniform mean flow this condition must be significantly modified. A corrected form of the boundary condition was derived in 1980 by Myers [35], but of course this modification was unknown when Nayfeh *et al* produced their 1975 work, which is the reason why they could not solve the acoustic field exactly in the mean flow case.

In 1999 Nayfeh *et al*'s solution was corrected by Rienstra [47], who used Myers' boundary condition plus a consistent description of the mean flow to derive an exact modal solution for slowly varying circular and annular ducts lined with slowly varying impedance walls. One of the unique features of Rienstra's solution was that it provided a systematic approximation to the hollow-to-annular cylinder transition problem which has direct applications to turbofan engines. Rienstra's solution also showed that for hard-walled ducts, the so-called turning points observed by Nayfeh *et al* do exist within the duct, and that this phenomenon is true irrespective of the presence of a mean flow. Cooper and Peake extended this study to include elliptic cross sections [14], and then in 2003 Rienstra [49] described a modal solution of acoustic propagation in a

slowly varying duct of arbitrary cross section. Cooper and Peake [13, 15] then extended their study to model situations with mean swirling flow and trapped modes, and a more recent development by Brambley and Peake [8] has seen the model extended to include modal propagation in strongly curved ducts.

Several developments were then made in the study of turning points in hard-walled ducts [48, 49]. In these studies the equation within the vicinity of the turning point was derived, solved and then matched to the known outer solution, a process that allowed explicit forms of the reflection and transmission coefficients of the mode in question to be obtained. This study of turning points was extended by Ovenden [42] who demonstrated that a similar phenomenon occurs for lined walls of finite impedance. Ovenden showed that in the case of lined walls a partial modal reflection is possible, and that the magnitude of this partial reflection is dependent upon the mean flow and the magnitude and phase of the wall impedance. It was also shown that the results were consistent with the results obtained for hard walls by finding the limit as the impedance was increased to infinity. In this thesis the subject of turning points is dealt with in chapter 3, which also includes a new set of results for the so-called double turning point case.

One of the problems with only knowing an inner and outer solution is that it is difficult to use these when attempting to numerically simulate the acoustic field within the duct. However in 2005 Ovenden developed a uniformly valid composite solution for cut-on cut-off transition for hard walled ducts [44]. This solution encompasses both the outer modal solution and the inner turning

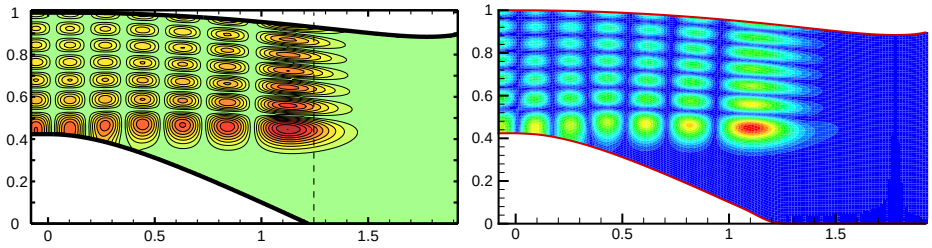

(a) Multiple Scales Solution (b) Finite Element Solution

Figure 1.3: Comparing multiple scales and finite element solutions: Pressure contour plots for high frequency and no mean flow with parameters $\omega = 50.2, m = 20, n = 7$. Transition point $X_t \approx 1.25$.

.

point solution and remains valid throughout the entire duct, completely removing any singularities that were present in previous modal solutions. Ovenden's contribution meant that numerical computations using the multiple scales theory could now be performed with ease.

With the availability of this composite solution Ovenden, Eversman and Rienstra compared this multiple scales solution to the solutions obtained from the finite-element method [43]. For the vast majority of cases the results obtained from both approaches were in excellent agreement. Figure 1.3 shows a direct comparison of the results obtained from multiple scales and finite-element methods for case of zero mean flow, and figure 1.4 shows a comparison of the results obtained from the two methods with mean flow included. In both of these cases the mode in question undergoes cut-on cut-off transition, and the transition point has been indicated.

There was at least one case however where the results differed significantly

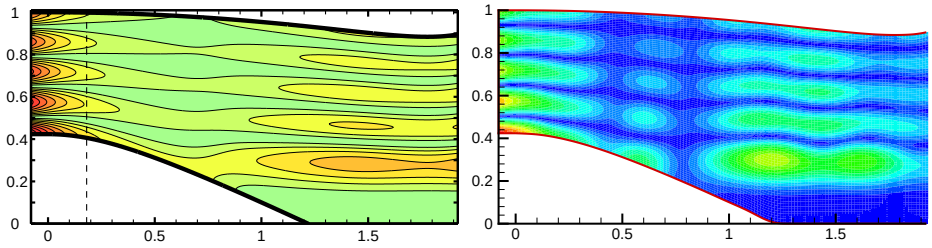

(a) Multiple Scales Solution (b) Finite Element Solution

Figure 1.4: Comparing multiple scales and finite element solutions: Pressure contour plots for a cut-off cut-on acoustic mode with mean flow. Parameters are $\omega = 19.8, n = m = 5, M = 0.5$. Transition point $X_t \approx 0.18$.

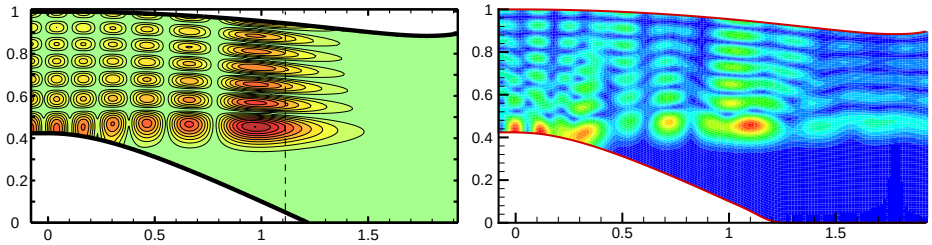

(a) Multiple Scales Solution (b) Finite Element Solution

Figure 1.5: Comparing multiple scales and finite element solutions for high frequency and mean flow. Parameters are $M = 0.5, m = 20, n = 7, \omega = 44.4$. For the critical point $X_t \approx 1.11$.

between the two methods, and differences seemed to occur when attempting to model cut-on cut-off transition for very high frequency and mean flow. In such a scenario the finite-element method showed a significant degree of modal scattering into neighbouring modes, whereas the multiple scales solution showed no indication of any scattering. Figure 1.5 shows a comparison of the results obtained in this case. It may be seen from figure 1.5(a) that according to the multiple scales solution the mode undergoes cut-on cut-off transition via precisely the same mechanism as with the previous cases, and

so no acoustic energy may propagate beyond the turning point X_t. However looking at the finite element solution 1.5(b) it is clear that acoustic energy is in fact present beyond X_t, although this energy cannot be attributed to the incident mode because that incident mode cannot propagate beyond the turning point. Hence the only conclusion that may be drawn is that a non-incident neighbouring that is cut-on for $X > X_t$ has been excited and has absorbed sufficient energy from the incident cut-on cut-off mode that it may propagate axially and out of the duct.

The main aim of this thesis is to use asymptotic analysis to understand and model the modal scattering of an acoustic mode undergoing cut-on cut-off transition in the case of high frequency and mean flow for a hard-walled duct of slowly varying cross section. In chapter 5 the acoustic wave equation within a duct is studied using an asymptotic framework, the terms responsible for the modal scattering are identified and a differential equation that describes the scattering mechanism within the inner region is obtained. The inner equation is then used to form a composite solution, valid throughout the entire duct. This composite solution is then used in chapter 6 to demonstrate that modal scattering can be modelled using the multiple scales technique.

Modal scattering of acoustic modes has recently been successfully modelled under some circumstances, usually involving a sudden change in the properties of the boundaries of the acoustic duct. For example, in 2007 Rienstra successfully developed an explicit Wiener-Hopf solution to model the scattering of an acoustic mode in a straight duct that contains a hard-soft impedance

transition at arbitrary frequency [51]. In the same paper Rienstra then went on to perform an asymptotic analysis for very low frequency (where very little modal energy is transmitted) and to study the properties of the reflection coefficient. Rienstra's results for the reflection coefficient appeared to be significantly different depending upon whether a Kutta-like condition was applied, which corresponds to the inclusion or exclusion of an instability wave over the impedance wall (assuming an impedance independent of frequency). The suggestion then was that for certain choices of parameter the differences in this reflection coefficient are so large that it could be used as an experimental test to check for the presence of stability waves over the surface of impedance linings. However in 2009 Brambley rederived Rienstra's low frequency analysis by considering a frequency dependant locally reacting impedance wall [6]. Brambley's results proved to be very different from Rienstra's, and were not dependant on whether a Kutta-like condition is chosen or not, and appeared to cast doubt on the usefulness of the reflection coefficient to experimentally test for instability waves over an impedance wall for small frequency. Another recent and interesting development in the modelling of modal scattering was performed by Brambley and Peake, who used the Wiener-Hopf technique to model the scattering of acoustic modes within a cylindrical duct where the boundaries of the duct change from being completely rigid to that of a thin shell [9].

Other notable developments in the field are that of Cooper and Peake [15], who described the propagation of acoustic waves in a flow duct with mean swirling flow. This model adds an extra layer of complexity to the problem as

the flow is assumed to have a swirling component, meaning that the associated eigenvalue problem is not self-adjoint as it is for irrotational mean flow.

1.3 Mathematical Framework

This section discusses how to construct a modal solution for sound propagation through a slowly varying duct of arbitrary cross section. A detailed discussion can be found in Rienstra's 2003 paper on the subject [49].

Consider a compressible inviscid perfect isentropic irrotational gas flow contained within a duct of slowly varying cross section. It is convenient to make parameters dimensionless: spatial dimensions can be made dimensionless using a typical duct radius R_∞, densities using a reference density at the inlet ρ_∞, velocities on a typical sound speed c_∞, time on R_∞/c_∞, pressure on $\rho_\infty c_\infty^2$ and velocity potential on $R_\infty c_\infty$. Note that the corresponding reference pressure p_∞ satisfies $\rho_\infty c_\infty^2 = \gamma p_\infty$, where γ is the (constant) ratio of specific heats at constant pressure and volume. Within the acoustic region the non-dimensional quantities of pressure $\tilde{p}$, velocity $\tilde{\mathbf{v}}$, density $\tilde{\rho}$, entropy $\tilde{s}$ and sound speed $\tilde{c}$ must obey the Euler equations (see for example Acheson [25] and Batchelor [28]), which consists of the equation for continuity and the momentum equation (subject to boundary conditions described in section 1.3)

$$\frac{\partial \tilde{\rho}}{\partial t} + \nabla.(\tilde{\rho}\tilde{\mathbf{v}}) = 0, \quad \tilde{\rho}\left(\frac{\partial \tilde{\mathbf{v}}}{\partial t} + \tilde{\mathbf{v}}.\nabla\tilde{\mathbf{v}}\right) + \nabla\tilde{p} = 0, \tag{1.1}$$

and the perfect gas equations

$$\gamma\tilde{p} = \tilde{\rho}^{\gamma}, \quad \tilde{c}^2 = \frac{\mathrm{d}\tilde{p}}{\mathrm{d}\tilde{\rho}} = \tilde{\rho}^{\gamma-1}, \quad \frac{\mathrm{d}\tilde{s}}{\mathrm{d}t} = 0,$$
$$\tilde{s} = C_V \log\tilde{p} - C_P \log\tilde{\rho}, \quad \gamma = \frac{C_P}{C_V}, \tag{1.2}$$

where C_V, C_P and γ are constants. C_V is the heat capacity at constant volume, C_P is the heat capacity at constant pressure and γ is the ratio of specific heats.

The entire fluid flow is assumed to be irrotational in the region of interest ($\nabla \times \tilde{\mathbf{v}} = \mathbf{0}$) and therefore one can write $\tilde{\mathbf{v}} = \nabla\tilde{\phi}$ for some scalar potential $\tilde{\phi}$. Then making use of the Lamb formula

$$(\tilde{\mathbf{v}}.\nabla)\tilde{\mathbf{v}} = \frac{1}{2}\nabla|\tilde{\mathbf{v}}|^2 + (\nabla \times \tilde{\mathbf{v}}) \times \tilde{\mathbf{v}},$$

and the equations relating $\tilde{p}$ and $\tilde{\rho}$, the momentum equation (1.1) may be integrated immediately to give a variant of Bernoulli's equation

$$\frac{\partial\tilde{\phi}}{\partial t} + \frac{1}{2}|\nabla\tilde{\phi}|^2 + \frac{\tilde{c}^2}{\gamma - 1} = C(t). \tag{1.3}$$

It is then assumed that the entire flow field may be split up into a steady mean flow component, which is assumed near-uniform with no swirling component, plus infinitesimally-small time-harmonic perturbations of a non-dimensional frequency (Helmholtz number) ω,

$$(\tilde{\mathbf{v}}, \tilde{\rho}, \tilde{p}, \tilde{c}) = (\mathbf{V}, D, P, C) + (\nabla\phi, \rho, p, c)\, e^{\mathrm{i}\omega t}. \tag{1.4}$$

Substituting (1.4) into (1.1), (1.2) and (1.3) plus some subsequent linearisation yields the following expressions: For the mean flow field

$$\begin{aligned} \nabla.(D\mathbf{V}) &= 0, & (1.5)\\ \frac{1}{2}|\mathbf{V}|^2 + \frac{C^2}{\gamma-1} &= E, & (1.6)\\ C^2 = \frac{\gamma P}{D} &= D^{\gamma-1}, & (1.7) \end{aligned}$$

where E is some constant. For the acoustic field

$$\begin{aligned} \nabla.(D\nabla\phi + \rho\mathbf{V}) &= -\mathrm{i}\omega\rho, & (1.8)\\ \mathrm{i}\omega\phi + \mathbf{V}.\nabla\phi &= -\frac{p}{D}, & (1.9)\\ pD^{-(\gamma+1)/2} &= \frac{2c}{\gamma-1}, & (1.10)\\ p &= C^2\rho. & (1.11) \end{aligned}$$

The constant of integration in the momentum equation can be absorbed into the definition of ϕ. For the acoustic field it is desirable to form one single differential equation for the acoustic potential ϕ. Manipulation of equations (1.8) - (1.11) via elimination of p and ρ gives rise to what is known as the general convected reduced wave equation

$$D^{-1}\nabla.(D\nabla\phi) - (\mathrm{i}\omega + \mathbf{V}.\nabla)[C^{-2}(\mathrm{i}\omega + \mathbf{V}.\nabla)\phi] = 0, \qquad (1.12)$$

which is subject to the Myers' boundary condition, described in more detail later in this section. Once ϕ is known the density ρ (and hence p) may be recovered from

$$(\mathrm{i}\omega + \mathbf{V}.\nabla)\rho + \rho\mathbf{V}.\nabla + \nabla.(D\nabla\phi) = 0.$$

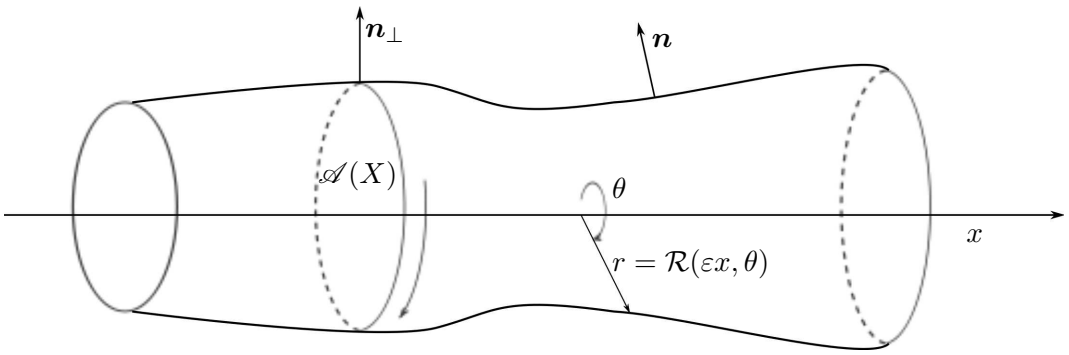

Figure 1.6: Sketch of a typical duct geometry

The Geometry

One establishes a three-dimensional cylindrical polar co-ordinate system (x, r, θ) with unit vectors $\mathbf{e}_x$, $\mathbf{e}_r$ and $\mathbf{e}_\theta$. The problem domain (shown in figure 1.6) consists of a duct $\mathcal{D}$ that is slowly varying in the axial direction with boundary $\partial\mathcal{D}$. The entire duct region may be precisely defined in terms of a function Σ as

$$\Sigma(X, r, \theta) = r - \mathcal{R}(X, \theta) \leq 0,$$

where $\mathcal{R}$ is the duct radius at a given point (X, θ). Then define the so-called slow (axial) variable X as $X = \varepsilon x$, where ε is a small parameter. The small parameter ε may be thought of as a typical duct gradient and will form the basis of our asymptotic expansions as it's presence is required to legitimise and support the use of a systematic perturbation method. To avoid coupling between the acoustic field and ε it is assumed that each acoustic amplitude is significantly smaller than any relevant power of ε. In this notation a cross section of the duct $\mathscr{A}(X)$ has area $\mathcal{A}(X)$. In order to keep the notation simple, $\Sigma = 0$ corresponds to the surface of a hollow duct, although the analysis presented here is easily extended to topologically more complex shapes, and

the final results presented in this section will be valid for both hollow and annular ducts.

At the duct surface $\Sigma = 0$ the surface gradient $\nabla\Sigma$ is

$$\nabla\Sigma = -\varepsilon \mathbf{e}_x \frac{\partial R}{\partial X} + \mathbf{e}_r - \mathbf{e}_\theta \frac{1}{R}\frac{\partial R}{\partial \theta}, \tag{1.13}$$

which is derived from the gradient operator in cylindrical polar coordinates given by

$$\nabla = \mathbf{e}_x \frac{\partial}{\partial x} + \mathbf{e}_r \frac{\partial}{\partial r} + \mathbf{e}_\theta \frac{1}{r}\frac{\partial}{\partial \theta}.$$

The quantity $\nabla\Sigma$ is a vector quantity that is normal to the duct surface, and so the unit normal to the duct surface is given as

$$\mathbf{n} = \frac{\nabla\Sigma}{|\nabla\Sigma|}.$$

The transverse gradient $\nabla_\perp\Sigma$ lies in the same plane as the cross-section $\mathcal{A}(X)$, is perpendicular to the x axis and is given by

$$\nabla_\perp\Sigma = \mathbf{e}_r - \mathbf{e}_\theta \frac{1}{R}\frac{\partial R}{\partial \theta}, \quad \text{where} \quad \nabla_\perp = \mathbf{e}_r \frac{\partial}{\partial r} + \mathbf{e}_\theta \frac{1}{r}\frac{\partial}{\partial \theta}. \tag{1.14}$$

Thus if $\mathbf{n}_\perp$ denotes a normal that is the component of the surface normal $\mathbf{n}$ that is projected in the same plane as $\mathcal{A}$ then

$$\mathbf{n} = \mathbf{n}_\perp - \varepsilon \frac{R\frac{\partial R}{\partial X}}{\sqrt{R^2 + \left(\frac{\partial R}{\partial \theta}\right)^2}} + O(\varepsilon^2).$$

The Boundary Conditions

As far as the mean flow is concerned the wall of the duct is solid and impermeable, meaning that fluid cannot pass through the walls of the duct. The

usual condition of normal velocity vanishing at the wall is applied, which is expressed mathematically as

$$\mathbf{V}.\mathbf{n} = 0 \quad \text{on} \quad \Sigma = 0. \tag{1.15}$$

To the acoustic field, the duct is lined with an impedance wall of acoustic impedance $Z \in \mathbb{C}$ which is allowed to vary with position provided that it varies slowly with x, and so $Z = Z(X, \theta)$. The acoustic boundary condition of an impedance wall along a curved wall in the presence of mean flow was given by Myers [35] as

$$\mathrm{i}\omega(\mathbf{v}.\mathbf{n}) = [\mathrm{i}\omega + \mathbf{V}.\nabla - \mathbf{n}.(\mathbf{n}.\nabla\mathbf{V}]\left(\frac{p}{Z}\right) \quad \text{at} \quad \Sigma = 0. \tag{1.16}$$

When formulating his boundary condition, Myers dealt with a fluid whose viscosity was vanishing and whose boundary layer was an infinitesimally small strip that lined the duct wall. This boundary condition could not be applied directly at the wall, but instead was to be applied at a point very close to the wall that lies just inside the mean flow region. The Myers boundary condition above has been well established since 1980, but some very recent papers have actually called this boundary condition into question [53, 7]. It has been known for some time that the Myers condition has lead to some numerical instability issues within the time domain [50], and that some mathematical problems exist concerning the stability analysis of this boundary condition. These instabilities occur in the form of surface waves [52] yet these surface waves have not been shown to exist in reality. Both Brambley and Rienstra [7, 53] have recently shown that viscosity within the vanishing boundary layer must be taken into account in order to avoid such instabilities, and in doing so they have both independently developed a modified Myers condition,

though at time of writing there are still some small disagreements between their solutions. Recent improvements to the Myers boundary condition are for straight ducts only, and at the time of writing a modified Myers condition for a slowly varying duct has not yet been developed. Therefore in this thesis the original boundary condition of Myers will be used, though it should be noted that for hard walled ducts the Myers condition simplifies significantly and the difficulties that have recently been studied are not present.

The Mean Flow

If the mean flow is sub-divided as follows

$$\mathbf{V} = U\mathbf{e}_x + \mathbf{V}_\perp, \tag{1.17}$$

with U representing the axial variation and $\mathbf{V}_\perp$ representing the cross-sectional variation, the mean flow mass flux is given by

$$\iint_{\mathcal{A}} DU \mathrm{d}\sigma = \mathcal{F}, \tag{1.18}$$

where $\mathcal{F}$ is a constant that is independent of x. It is assumed here that only knowledge of the slowly varying geometry is required to determine the mean flow. Further to this, by balancing terms in the mass conservation equation (1.5) it follows that $O(\varepsilon)$ axial variations in mean flow can only be balanced

by $O(\varepsilon)$ radial variations, meaning that $\mathbf{V}_\perp = O(\varepsilon)$ and so

$$U = U_0(X) + O(\varepsilon^2), \tag{1.19}$$

$$\mathbf{V}_\perp = \varepsilon \mathbf{V}_{\perp 0} + O(\varepsilon^3), \tag{1.20}$$

$$C = C_0 + O(\varepsilon^2). \tag{1.21}$$

$$D = D_0 + O(\varepsilon^2). \tag{1.22}$$

$$P = P_0 + O(\varepsilon^2). \tag{1.23}$$

Substitution of the above expressions into equations (1.5), (1.6) and (1.7) and equating to leading order yields the following relationship between P_0, D_0, and C_0:

$$\frac{1}{2}U_0^2 + \frac{C_0^2}{\gamma - 1} = E, \quad C_0^2 = \frac{\gamma P_0}{D_0}, \quad \frac{P_0}{D_0^\gamma} = \frac{1}{\gamma}.$$

and thus it follows that C_0, D_0 and P_0 are functions of X only. Substitution of (1.19) and (1.20) into (1.18) gives an equation that may be integrated immediately and yields an expression for U_0 as

$$U_0(X) = \frac{F}{D_0(X)\mathcal{A}(X)}, \tag{1.24}$$

meaning that $D_0(X)$ (and hence P_0 and C_0) is the root of the algebraic equation

$$\frac{\mathcal{F}^2}{2D_0\mathcal{A}^2} + \frac{D_0^{\gamma-1}}{\gamma - 1} = E.$$

For the cross-wise component of the mean flow $\mathbf{V}_{\perp 0}$ this is defined by the partial differential equation

$$\frac{\partial}{\partial X}(D_0 U_0) + \nabla_\perp . (D_0 \mathbf{V}_{\perp 0}) = 0 \tag{1.25}$$

subject to the zero normal flow condition at the wall

$$\mathbf{V}_{\perp 0} . \mathbf{n}_\perp = \frac{R U_0 \frac{\partial R}{\partial X}}{\sqrt{R^2 + \left(\frac{\partial R}{\partial \theta}\right)^2}} \quad \text{on} \quad r = R. \tag{1.26}$$

The Acoustic Field

Applying the slowly-varying assumptions of the mean flow described in section 1.3 the wave equation (1.12) becomes

$$\begin{aligned} & \left(1-\frac{U_0^2}{C_0^2}\right)\frac{\partial^2\phi}{\partial^2 x}-\frac{2\mathrm{i}\omega U_0}{C_0^2}\frac{\partial\phi}{\partial x}+\nabla_\perp^2\phi-\frac{\omega^2}{C_0^2}\phi \\ + \quad & \varepsilon\Big\{D_0^{-1}D_0'\frac{\partial\phi}{\partial x}-\mathrm{i}\omega U_0(C_0^{-2})'\phi-U_0(U_0C_0^{-2})'\frac{\partial\phi}{\partial x} \\ - \quad & 2\mathrm{i}\omega C_0^{-2}(\mathbf{V}_{\perp 0}.\nabla_\perp\phi)-2U_0C_0^{-2}\left(\mathbf{V}_{\perp 0}\nabla_\perp\frac{\partial\phi}{\partial x}\right)\Big\} \\ + \quad & O(\varepsilon^2)=0, \end{aligned} \tag{1.27}$$

where the dashes denote derivatives with respect to the slow variable X, and the cross-sectional Laplacian operator $\nabla_\perp^2$ for cylindrical polar coordinates is given by

$$\nabla_\perp^2=\frac{\partial^2}{\partial r^2}+\frac{1}{r}\frac{\partial}{\partial r}+\frac{1}{r^2}\frac{\partial^2}{\partial\theta^2}.$$

For a completely straight axisymmetric duct the solution for ϕ would consist of a cross-sectional function in r multiplied by a complex exponential in θ and x. For example the modal solution for a straight circular cylinder is given by $N\,\mathrm{J}_m(\alpha r)\exp(-\mathrm{i}kx-\mathrm{i}m\theta)$, and for an annular cylinder the modal solution is of the form $[N\,\mathrm{J}_m(\alpha r)+M\,\mathrm{Y}_m(\alpha r)]\exp(-\mathrm{i}kx-\mathrm{i}m\theta)$, where J_m and Y_m are Bessel functions of the first and second kind, k, α and m are the axial, radial and circumferential wavenumbers respectively, and N and M are modal amplitudes. In this formulation a slowly varying mode-like solution is sought using the method of multiple scales, and thus the axial wavenumber and amplitude are assumed to vary slowly with X. Therefore under this assumption the solution for ϕ takes on the WKB-Ansatz:

$$\phi(x,r,\theta;\varepsilon)=\Phi(X,r,\theta;\varepsilon)\exp\left(-\frac{\mathrm{i}}{\varepsilon}\int_X\mu(X')\mathrm{d}X'\right), \tag{1.28}$$

where m is the (constant) circumferential wavenumber, μ is the slowly varying axial wavenumber and Φ is the slowly varying amplitude function. From equation (1.28) it is simple to compute the first and second derivatives with respect to x as

$$\begin{aligned} \frac{\partial \phi}{\partial x} &= -\mathrm{i}\mu\Phi + \varepsilon\frac{\partial \Phi}{\partial X}\exp\left(-\frac{\mathrm{i}}{\varepsilon}\int_X \mu(X')\mathrm{d}X'\right), \qquad (1.29) \\ \frac{\partial^2 \phi}{\partial x^2} &= -\mu^2\Phi - \mathrm{i}\varepsilon\frac{\partial \mu}{\partial X}\Phi - 2\mathrm{i}\varepsilon\mu\frac{\partial \Phi}{\partial X} + \varepsilon^2\frac{\partial^2 \Phi}{\partial X^2} \\ &\times \exp\left(-\frac{\mathrm{i}}{\varepsilon}\int_X \mu(X')\mathrm{d}X'\right). \qquad (1.30) \end{aligned}$$

Defining

$$\Omega = \omega - \mu U_0, \qquad (1.31)$$

and substituting (1.28) - (1.31) into (1.27) yields (after some manipulation)

$$\begin{aligned} \nabla_\perp^2\Phi + \left(\frac{\Omega^2}{C_0^2} - \mu^2\right)\Phi &= \frac{\mathrm{i}\varepsilon}{D_0\Phi}\left[\frac{\partial}{\partial X}\left[\left(\frac{\Omega U_0}{C_0^2} + \mu\right)D_0\Phi^2\right]\right. \\ &+ \left.\nabla_\perp.\left(\frac{\Omega D_0}{C_0^2}\Phi^2\mathbf{V}_{\perp 0}\right)\right] + O(\varepsilon^2), \qquad (1.32) \end{aligned}$$

and for the boundary conditions at $r = R$

$$\begin{aligned} \mathrm{i}\omega(\mathbf{n}_\perp.\nabla_\perp\Phi) &- \frac{\Omega^2 D_0}{Z}\Phi = \varepsilon\omega\mu\frac{R\frac{\partial R}{\partial X}}{\sqrt{R^2 + \left(\frac{\partial R}{\partial \theta}\right)^2}}\Phi - \mathrm{i}\varepsilon\left[U_0\frac{\partial}{\partial X}\left(\frac{D_0\Omega\Phi}{Z}\right)\right. \\ &+ \left. U_0\left(\frac{D_0\Omega}{Z}\right)\frac{\partial \Phi}{\partial X} + D_0\Omega\mathbf{V}_{\perp 0}.\nabla_\perp\left(\frac{\Phi}{Z}\right) + \frac{D_0\Omega}{Z}\mathbf{V}_{\perp 0}.\nabla_\perp\Phi\right] \\ &+ \mathrm{i}\varepsilon\mathbf{n}_\perp.(\mathbf{n}_\perp.\nabla_\perp\mathbf{V}_{\perp 0})\frac{D_0\Omega\Phi}{Z}. \qquad (1.33) \end{aligned}$$

The amplitude function Φ and axial wavenumber μ are then expanded by means of a Poincaré expansion about the parameter ε as

$$\begin{aligned} \Phi(X, r, \theta; \varepsilon) &= \Phi_0(X, r, \theta) + \varepsilon\Phi_1(X, r, \theta) + O(\varepsilon^2), \qquad (1.34) \\ \mu(X) &= \mu_0(X) + \varepsilon\mu_1(X) + O(\varepsilon^2). \qquad (1.35) \end{aligned}$$

Substitution of (1.34) and (1.35) into (1.32) yields, to leading order

$$\nabla_{\perp}^2 \Phi_0 + \left(\frac{\Omega_0^2}{C_0^2} - \mu_0^2 \right) \Phi_0 = 0, \tag{1.36}$$

where $\Omega_0 = \omega - \mu_0 U_0$. The above is subject to the boundary condition

$$\mathrm{i}\omega(\mathbf{n}_{\perp}.\nabla_{\perp}\Phi_0) - \frac{\Omega_0^2 D_0}{Z}\Phi_0 = 0 \quad \text{on} \quad r = R. \tag{1.37}$$

The differential equation (1.36) subject to boundary condition (1.37) constitutes an eigenvalue problem that is to be solved in the cross-sectional plane $\mathscr{A}$ for some cross-sectional eigenfunction $\psi(r, \theta; X)$ at each X station, with X acting as a parameter in this sense, i.e.

$$-\nabla_{\perp}^2 \psi = \alpha^2 \psi, \quad \text{with} \quad \mathrm{i}\omega(\mathbf{n}_{\perp}.\nabla_{\perp}\psi) - \frac{\Omega_0^2 D_0}{Z}\psi = 0 \quad \text{on} \quad r = R, \tag{1.38}$$

where the cross sectional wavenumber α satisfies the dispersion relation

$$\frac{\Omega_0^2}{C_0^2} - \frac{(\omega - \Omega_0)^2}{U_0^2} = \alpha^2. \tag{1.39}$$

It is then assumed that for the n th eigenvalue α_n with corresponding eigenfunction ψ_n the function satisfies

$$\iint_{\mathcal{A}} |\psi_n|^2 \mathrm{d}\sigma \neq 0,$$

so that ψ_n can be normalised as

$$\iint_{\mathcal{A}} |\psi_n|^2 \mathrm{d}\sigma = 1,$$

and so for each X one arrives at

$$\Phi_0 = N(X)\psi_n(r, \theta; X). \tag{1.40}$$

The amplitude function $N(X)$ is still unknown and must be determined from the solvability condition for the next order equation for Φ_1 [39]. Subsequently

the amplitude function Φ_1 cannot be determined fully unless the equation for Φ_2 is considered. However it is not necessary to determine the full expression for Φ_1 as all that is required in this analysis is to determine a condition that allows a solution for Φ_1 to exist, and in forming this condition the expression for the modal amplitude $N(X)$ is obtained.

The differential equation for Φ_1 is

$$\begin{aligned}&\nabla_\perp^2\Phi_1+\left(\frac{\Omega_0^2}{C_0^2}-\mu^2\right)\Phi_1\\&=\frac{\mathrm{i}\varepsilon}{D_0\Phi_0}\left[\frac{\partial}{\partial X}\Big[\left(\frac{\Omega_0U_0}{C_0^2}+\mu\right)D_0\Phi_0^2\Big]+\nabla_\perp.\left(\frac{\Omega_0D_0}{C_0^2}\Phi_0^2\mathbf{V}_{\perp0}\right)\right],\end{aligned}\tag{1.41}$$

subject to the boundary condition at $r=R$

$$\begin{aligned}\mathrm{i}\omega(\mathbf{n}_\perp.\nabla_\perp\Phi_1) &- \frac{\Omega_0^2D_0}{Z}\Phi_1=\omega\mu\frac{R\frac{\partial R}{\partial X}}{\sqrt{R^2+\left(\frac{\partial R}{\partial\theta}\right)^2}}\Phi_0-\mathrm{i}\Bigg[U_0\frac{\partial}{\partial X}\left(\frac{D_0\Omega_0\Phi_0}{Z}\right)\\&+ U_0\left(\frac{D_0\Omega_0}{Z}\right)\frac{\partial\Phi_0}{\partial X}+D_0\Omega_0\mathbf{V}_{\perp0}.\nabla_\perp\left(\frac{\Phi_0}{Z}\right)+\frac{D_0\Omega_0}{Z}\mathbf{V}_{\perp0}.\nabla_\perp\Phi_0\Bigg]\\&+ \mathrm{i}\mathbf{n}_\perp.(\mathbf{n}_\perp.\nabla_\perp\mathbf{V}_{\perp0})\frac{D_0\Omega_0\Phi_0}{Z}\end{aligned}\tag{1.42}$$

Multiply equation (1.41) by $D_0\Phi_0$ and also multiply (1.36) by $D_0\Phi_1$ and integrate their difference over the cross section to yield (after some manipulation)

$$\begin{aligned}D_0\iint_{\mathcal{A}}\left(\Phi_0\nabla_\perp^2\Phi_1-\Phi_1\nabla_\perp^2\Phi_0\right)\mathrm{d}\sigma&=\mathrm{i}\frac{\mathrm{d}}{\mathrm{d}X}\left[\Big(\frac{\Omega_0U_0}{C_0^2}+\mu\Big)D_0\iint_{\mathcal{A}}\Phi_0^2\mathrm{d}\sigma\right]\\&-\mathrm{i}\left(\frac{\Omega_0U_0}{C_0^2}+\mu\right)D_0\int_0^{2\pi}\left(\Phi_0^2(X,R,\theta)R\frac{\partial R}{\partial X}\right)\mathrm{d}\theta\end{aligned}\tag{1.43}$$

Then the boundary condition (1.42) can be manipulated and combined with (1.43) to obtain for the adiabatic invariant

$$\frac{\mathrm{d}}{\mathrm{d}X}\left[\mathrm{i}\omega\Big[\left(\frac{\Omega_0U_0}{C_0^2}+\mu\right)D_0N^2\Big]+D_0^2\Omega_0U_0N^2\int_{\partial\mathcal{A}}\frac{1}{Z}\psi_n^2\mathrm{d}l\right]=0.\tag{1.44}$$

It is useful at this stage to introduce a very important quantity, known as the reduced axial wavenumber σ

$$\sigma^2(X) = 1 - (C_0^2(X) - U_0^2(X))\frac{\alpha^2(X)}{\omega^2}. \tag{1.45}$$

The reduced axial wavenumber σ may be thought of as μ scaled by ω without the purely convective effects included, such that

$$\mu = -\frac{\omega U_0}{C_0^2 - U_0^2} + \frac{\omega C_0 \sigma}{C_0^2 - U_0^2},$$

and therefore allowing a clearer distinction between the purely convective and acoustic parts of the axial wavenumber. The first term in the above constitutes a phase variation brought about by the presence of the mean flow, and is zero if no mean flow is present inside the duct. The positive choice for the first term corresponds to a mode propagating in the positive x direction, and the negative choice corresponds to a negatively propagating mode. Note that the reduced axial wavenumber σ also has the following properties:

$$\frac{U_0\Omega_0}{C_0^2} + \mu = \frac{\omega\sigma}{C_0}, \quad \Omega_0 = \omega C_0 \frac{C_0 - U_0\sigma}{C_0^2 - U_0^2}.$$

Therefore of the amplitude $N(X)$

$$\frac{Q^2}{N^2} = \frac{\omega\sigma D_0}{C_0} + \frac{D_0^2\Omega_0}{\mathrm{i}\omega}U_0 \int_{\partial\mathcal{A}} \frac{1}{Z}\psi_n^2 \mathrm{d}l, \tag{1.46}$$

where Q is a constant of integration that is obtained via integration of equation (1.44). The constant Q represents the conserved quantity, and is fixed at a point $X = X_0$.

An important special case of (1.46) is that of hard walled ducts ($Z = \infty$), where the modal amplitude reduces to

$$N(X) = Q\sqrt{\frac{C_0(X)}{\omega\sigma(X)D_0(X)}}, \tag{1.47}$$

and examining the consequences of the above result is a key focal point of this thesis. When $\sigma \sim 1$ equation (1.47) forms a good approximation for the modal amplitude, but as $\sigma \to 0$ a singularity forms within the above expression for the amplitude, and so if the medium varies in such a way that σ vanishes at some point $X = X_t$ the above approximation breaks down and a different method for approximating the modal amplitude is required. In the language of matched asymptotic expansions a boundary layer in the variable X exists within the vicinity of the point X_t, and X_t is known as a *turning point*. The nature by which σ varies as $X \to X_t$ largely determines the outcome of the system. If σ^2 is linear as it approaches X_t then no acoustic energy may propagate beyond X_t and the mode undergoes a total reflection with a phase shift of $\pi/2$, causing a standing wave to be formed within the duct for $X < X_t$ [49]. If the mode behaves quadratically as $X \to X_t$ then the mode undergoes a partial reflection, causing a partial standing wave to be formed for $X < X_t$ and modal propagation continues for $X > X_t$ with reduced modal energy. Precise details of the turning point analysis for these two cases is discussed in chapter 3.

1.4 Alternative Strategies and Methods

As well as the considerable advances that have been achieved within the field of aeroacoustics using multiple scales theory, it is important to note that there have also been advances in the modelling of aeroacoustic problems using methods other than the asymptotic approach. Whilst the field of aeroacoustics dates back to James Lighthill's first groundbreaking paper [31], the use of

computational methods to treat acoustics problems is more recent, dating back to the 1980s, where Hardin and Lamkil [22] modelled the sound field generated by uniform flow over a cylinder at the moderate Reynolds number. In this paper, the authors first modelled the flow field using standard CFD techniques such as a stream function/vorticity formulation. The acoustic field was then obtained by integrating over the flow field using the Coriolis acceleration as the source term and a low frequency Green's function technique. Several properties of the acoustic field were obtained using their method, and these compared favourably against experimental data, indicating the feasibility of their approach. In 1986 the same authors coined the acronym CAA, short for computational aeroacoustics, which has since been widely adopted by the aeroacoustics community [23]. Since then several different techniques within CAA have subsequently been developed, and the main features of some of these are described in this section.

Within all CAA methods, several technical challenges are common. Any CAA algorithm that is designed must not be dispersive or dissipative. Also as all computational domains are finite in size, one must take care to avoid spurious reflections of acoustic waves at the boundary of the computational domain. There are several ways in which one can avoid these reflections, such as the implementation of a buffer zone, perfectly matched layers or by designing a non-reflecting boundary condition. In chapter 6 non reflecting boundary conditions are discussed in some detail.

Direct Numerical Simulation (DNS)

The compressible Navier-Stokes equations contain information regarding both the mean flow field and the aerodynamically generated acoustic field, and thus it is possible to obtain a description of the acoustic field via direct numerical simulation (DNS) of the governing Navier Stokes equations. The use of this method has led to recent successes by Freund, who's utilised direct numerical simulations methods to model the mechanisms of sound generation in a turbulent jet [19], a model which was shown to have excellent agreement when compared to experimental data.

The direct numerical simulation of sound generation and propagation within a given medium is a difficult numerical problem, particularly when the mean flow field is turbulent, and the main reason for this computational difficulty is due to the large differences in magnitude between the mean flow and acoustic variables. When compared to the kinetic energy associated with the mean flow, acoustic waves are phenomena of very low energy which may propagate over large distances, whereas the fluid flow may be affected by significantly small fluid structures containing a large amount of energy, one example being vortices in a turbulent flow. These differences in lengthscale combined with the differences in their physical behaviour mean that to successfully utilise the DNS approach one must overcome significant numerical issues. For these reasons the DNS approach is generally considered to be impractical for industrial use.

Linearised Euler Equations

The influence of viscosity on the sound propagation is generally very small, and this is one reason why noise is so difficult to suppress. Also perturbations of the acoustic field have very little influence on the mean flow field, and for these reasons the acoustic field can be described by the Linearised Euler Equations or LEE's as in [2].

For example, consider the superpositioning of small disturbances on a uniform flow field with mean flow velocity u_0 (that consists of an x component only) with fluid density ρ_0 and pressure p_0. Then the two dimensional linearised Euler equations for the sound field are

$$\frac{\partial \mathbf{U}}{\partial t} + \frac{\partial \mathbf{F}}{\partial x} + \frac{\partial \mathbf{G}}{\partial y} = \mathbf{S},$$

where

$$\mathbf{U} = \begin{pmatrix} \rho \\ u \\ v \\ p \end{pmatrix}, \quad \mathbf{F} = \begin{pmatrix} \rho u_0 + \rho_0 u \\ u_0 u + p/\rho_0 \\ u_0 v \\ u_0 p + \gamma p_0 u \end{pmatrix}, \quad \mathbf{G} = \begin{pmatrix} \rho_0 v \\ 0 \\ p/\rho_0 \\ \gamma p_0 v \end{pmatrix},$$

where p, ρ, u and v are the acoustic variables, and the source term on the right hand side represents distributed unsteady sources. Generally speaking this representation works better for low Mach number flows as higher Mach numbers tend to mean that non-linear disturbances that have been ignored in this formulation become more important and thus need to be considered when modelling the acoustic field. One recent example of LEE usage relevant to the topics covered in this thesis is presented by Chen *et al* [11], who in

2003 modelled sound propagation from a straight duct using a high order computational scheme, and this analysis was shown to have good agreement with analytical techniques used to solve a similar problem.

Finite Element Method

The finite element method (FEM) is a numerical method for finding approximate solutions to partial differential equations, and is particularly useful when attempting to solve systems over complex spatial domains (vehicles, pipes etc) or when the domain changes over time. The domain $\mathscr{D}$ is divided into a finite number of sub-domains known as *elements*, where adjacent elements are then assumed to be be connected by a finite number of nodes. The elements may be all kinds of shapes, but simple shapes such as quadrilaterals and triangles are commonly used. Within the finite element method the computational mesh may be irregular and thus may be adapted to complex boundaries. Another advantage of this method is that, due to the freedom that one has in terms of selecting elements within the domain, this allows an increase in the numerical precision within certain areas within the computational domain where larger accuracy may be required. Finite element models of modal propagation of acoustic modes within a turbofan engine for non-uniform mean flow is presented in detail in papers by Dander Roy and Eversman [54, 55]. For some more specific details relating to finite element applications for duct flows terminated by reflection free boundary conditions, the reader is referred to papers by Eversman [16, 17].

1.5 Outline of Thesis

The structure of this thesis is as follows:

Chapter 2 utilises the results discussed in section 1.3 to discuss modal propagation through circular and annular ducts with near uniform mean flow and a constant impedance lining on one of the duct walls, and within this chapter the propagation of an acoustic mode is considered. The progress of several characteristics of this mode are tracked throughout the duct, such as the modal amplitude, axial and radial wavenumbers and acoustic sound pressure. Thanks to the power of the asymptotic approach these properties may be computed throughout the duct very quickly. The examples presented on this chapter are based on realistic turbofan engine configurations and are therefore of practical importance to a turbofan engine designer. The chapter ends by discussing results for hard-walled ducts and the problems that may occur when attempting to model modal propagation through a hard-walled duct, such as the existence of turning points.

Chapter 3 follows on from chapters 1 and 2 and focuses entirely on the topic of turning points; this chapter discusses in detail the situation in which the modal solution presented in section 1.3 breaks down and how this difficulty is overcome. The technique involves analysing the behaviour of the reduced axial wavenumber σ in the situation where it vanishes, and compares this behaviour to that of the second order derivative of ϕ with respect to X. This analysis gives rise to an axial boundary layer and formulates a new differen-

tial equation for ϕ, valid within the inner region that may be matched to the outer solution, and in doing so reflection and transmission coefficients for the outer modal solution are obtained. Within this chapter two situations are discussed, one where σ^2 varies linearly as in [49], and a new result where σ^2 varies quadratically, which is referred to here as the double turning point case. This chapter also outlines the composite solution devised by Ovenden [44].

Chapter 4 discusses the topic of a modal (outer) solution at large Helmholtz number. Since the main emphasis behind the work presented in this thesis is to understand acoustic scattering, it is necessary to understand the structure of the outer modal solution at high frequency because it is only when the frequency is sufficiently high that modal scattering occurs to leading order [43]. This chapter lays out the framework for constructing an outer modal solution for high frequency.

Chapter 5 builds on the knowledge of the outer solution discussed in chapter 4 to discuss the phenomenon of modal scattering of acoustic modes in some detail. This chapter starts by reviewing the results obtained by Ovenden, Eversman and Rienstra [43], where the finite element showed modal scattering at high frequency and mean flow, but the multiple scales solution did not. A brief discussion by the papers authors suggested that in order to induce modal scattering for order one mean flow the frequency should be sufficiently high in that $\omega \sim \varepsilon^{-2}$. Chapter 5 begins by considering the situation where $\omega \sim \varepsilon^{-2}$, and it is shown here that for flow-induced scattering this original estimate is in fact an overestimate (although it is shown by Smith, Ovenden and Bowles

that this is a suitable estimate for geometry induced scattering [58]). The wave equation is then re-analysed, and a new estimate for the order of magnitude of the modal frequency is obtained, given by $\omega \sim \varepsilon^{-\frac{1}{2}}$. However this estimate for the frequency allows leading order scattering into the incident mode only, and weak scattering for all other modes. The wave equation is re-visited once more in an effort to obtain an estimate for ω that gives leading order scattering for all modes, and an estimate of $\omega \sim \varepsilon^{-1}$ is obtained. The knowledge obtained from the asymptotic analysis of the inner solution leads to the development of a model for the equation governing the composite solution (valid throughout the entire duct as in Ovenden [44]), featured at the end of the chapter.

The composite model developed at the end of Chapter 5 is an ODE for the modal amplitude throughout the entire duct in terms of a stretched axial variable. Chapter 6 starts out by noting that the stretched variable can be difficult to work with so instead for numerical purposes the composite model is revised slightly so that rather than working with the stretched variable it works with the physical axial variable x, making it much easier to apply finite difference methods. Once this revision to the composite equation is made it is solved numerically are the results obtained are compared against the theory shown in chapter 5. This chapter presents results for two and three dimensional acoustic scattering given at least one incident mode and mean flow. The results obtained in this chapter demonstrate that when a mode undergoes cut-on cut-off transition, that mode may exchange energy with neighbouring modes, yielding results that are similar to the finite element results obtained by Ovenden, Eversman and Rienstra [43]. It is also revealed, in contrast to most previous

multiple scales analyses of cut-on cut-off modal interaction so far, that there is evidence that the acoustic fields may exchange energy with the mean flow during the scattering process.

Chapter 2

Modal Propagation Within Circular & Annular Ducts

Chapter one section 1.3 described the main features of a multiple-scales solution concerning the propagation of a mode through a slowly varying duct of arbitrary cross-section. In this chapter, this theory is used to briefly discuss the special case of a cylindrical duct. Hollow and annular cylindrical ducts are of considerable practical importance as they can both used as realistic approximations to the geometry of a turbofan engine. It will be shown in this chapter that for a cylindrical duct of slowly varying circular cross section the acoustic potential ϕ exhibits an analytical solution, which is due to the relative simplicity of the solution in the duct cross section.

The purpose of this chapter is to give the reader an idea of how the theory is applied in practice, and how the theory can be used to model and track the variation of modes and their properties as they propagate through a duct.

The discussions present in this chapter was first shown by Rienstra [47], and the results shown in this chapter replicate these results accurately. For a more in depth discussion on the ideas presented in this chapter, the reader is referred to his 1998 paper.

A cylindrical duct of slowly varying cross section is considered. To the mean flow, the duct is impermeable, but to the acoustic field, the duct is lined with a slowly varying impedance wall. Suppose a cylindrical polar coordinate system (x, r, θ) is established, with unit vectors $\mathbf{e}_x, \mathbf{e}_r, \mathbf{e}_\theta$, with the slowly varying duct radii R_1 and R_2 respectively given by

$$r = R_1(X), \quad r = R_2(X), \quad X = \varepsilon x, \quad -\infty < x < \infty, \quad 0 \leq \theta < 2\pi,$$

where R_1 denotes the inner wall radius and R_2 is the outer wall radius. In this problem the walls R_1 and R_2 are lined with an impedance wall of constant acoustic impedance Z_1 and Z_2 respectively.

The Mean Flow

Following on from the discussion presented in the last chapter, for the mean flow, the mass flux F can be defined such that

$$2\pi \int_{R_1}^{R_2} D(X, r; \varepsilon) U(X, r; \varepsilon) r \mathrm{d}r \mathrm{d}\theta = \pi F$$

which, given the asymptotic expansions given by equations (1.19) - (1.23), may be integrated immediately to yield

$$U_0(X) = \frac{F}{D_0(X)\left(R_2^2(X) - R_1^2(X)\right)},$$

with the quantities D_0, P_0 and C_0 being given by

$$\frac{1}{2}\left(\frac{F}{D_0\left(R_2^2-R_1^2\right)}\right)^2+\frac{1}{\gamma-1}D_0^{\gamma-1}=E,\quad P_0=\frac{1}{\gamma}D_0^{\gamma},\quad C_0=D_0^{(\gamma-1)/2},$$

where D_0 must be evaluated numerically at each X station. For the radial component of the mean flow velocity one arrives at

$$V_1(X,r)=-\frac{F}{2rD_0}\frac{\partial}{\partial X}\left(\frac{r^2-R_1^2}{R_2^2-R_1^2}\right).$$

The Acoustic Field

The acoustic potential ϕ satisfies the general acoustic wave equation (1.27). Recall that modal type approximation for ϕ is of the WKB form

$$\phi=N(X;\varepsilon)\psi(r,\theta;X,\varepsilon)\exp\left(-\frac{\mathrm{i}}{\varepsilon}\int^X\mu(X';\varepsilon)\mathrm{d}X'-\mathrm{i}m\theta\right).$$

Substituting the above into the governing wave equation (1.27) using the cylindrical polar form of the Laplacian operator ∇^2 yields the differential equation for ψ as

$$D_0\mathscr{L}(\psi)=\frac{\mathrm{i}}{\psi}\left\{\frac{\partial}{\partial X}\left[\left(\frac{U_0\Omega}{C_0^2}+\mu\right)D_0\psi^2\right]+\frac{1}{r}\frac{\partial}{\partial r}\left[r\frac{V_1\Omega}{C_0^2}D_0\psi^2\right]\right\},$$

where the linear operator $\mathscr{L}$ is given by

$$\mathscr{L}=\frac{\partial^2}{\partial r^2}+\frac{1}{r}\frac{\partial}{\partial r}+\frac{\Omega^2}{C_0^2}-\mu^2-\frac{m^2}{r^2}.$$

The Myers boundary condition on $R=R_1$ is

$$\mathrm{i}\omega\frac{\partial\psi}{\partial r}+\frac{\Omega^2D_0\psi}{Z_1}=\varepsilon\omega\mu R_1'\psi+\frac{\mathrm{i}\varepsilon}{\psi}\left[U_o\frac{\partial}{\partial X}+V_1\frac{\partial}{\partial r}-\frac{\partial V_1}{\partial r}\right]\left(\frac{\Omega D_0\psi^2}{Z_1}\right),$$

and for $R=R_2$ the boundary condition is given by

$$\mathrm{i}\omega\frac{\partial\psi}{\partial r}-\frac{\Omega^2D_0\psi}{Z_2}=\varepsilon\omega\mu R_2'\psi-\frac{\mathrm{i}\varepsilon}{\psi}\left[U_o\frac{\partial}{\partial X}+V_1\frac{\partial}{\partial r}-\frac{\partial V_1}{\partial r}\right]\left(\frac{\Omega D_0\psi^2}{Z_2}\right),$$

with the special case

$$\left[\mathrm{i}\Omega + \varepsilon\left(U_0\frac{\partial}{\partial X} + V_1\frac{\partial}{\partial r}\right)\right]\psi = 0 \quad \text{at} \quad r = R_i \quad \text{if} \quad Z_i = 0.$$

Suppose then that the cross-sectional wavefunction ψ is expanded via a Poincaré expansion about the small parameter ε as

$$\psi = \psi_0(r,\theta;X) + \varepsilon\psi_1(r,\theta;X) + \ldots,$$

then the differential equations for ψ_0 and ψ_1 are given by

$$\begin{aligned}
\mathscr{L}(\psi_0) &= 0, \\
D_0\mathscr{L}(\psi_1) &= \frac{\mathrm{i}}{A_0}\left\{\frac{\partial}{\partial X}\left[\left(\frac{U_0\Omega}{C_0^2} + \mu\right)D_0\psi_0^2\right] + \frac{1}{r}\frac{\partial}{\partial r}\left[r\frac{V_1\Omega}{C_0^2}D_0\psi_0^2\right]\right\},
\end{aligned}$$

subject to the following boundary conditions on $R = R_1$:

$$\begin{aligned}
\mathrm{i}\omega\frac{\partial\psi_0}{\partial r} + \frac{\Omega^2 D_0\psi_0}{Z_1} &= 0 \\
\mathrm{i}\omega\frac{\partial\psi_1}{\partial r} + \frac{\Omega^2 D_0\psi_1}{Z_1} &= \omega\mu R_1'\psi_0 + \frac{\mathrm{i}}{\psi_0}\left[U_0\frac{\partial}{\partial X} + V_1\frac{\partial}{\partial r} - \frac{\partial V_1}{\partial r}\right] \\
&\times \left(\frac{\Omega D_0\psi_0^2}{Z_1}\right)
\end{aligned}$$

and for the $R = R_2$ the boundary conditions are given by

$$\begin{aligned}
\mathrm{i}\omega\frac{\partial\psi_0}{\partial r} + \frac{\Omega^2 D_0\psi_0}{Z_2} &= 0 \\
\mathrm{i}\omega\frac{\partial\psi_1}{\partial r} - \frac{\Omega^2 D_0\psi_1}{Z_2} &= \omega\mu R_1'\psi_0 - \frac{\mathrm{i}}{\psi_0}\left[U_0\frac{\partial}{\partial X} + V_1\frac{\partial}{\partial r} - \frac{\partial V_1}{\partial r}\right] \\
&\times \left(\frac{\Omega D_0\psi_0^2}{Z_1}\right).
\end{aligned}$$

The differential equation for $\psi_0(r,\theta;X)$ is just Bessel's equation with a radial coordinate stretching, and thus the general normalised solution for the leading order cross sectional eigensolution ψ_0 is

$$\psi_0(r,\theta;X) = \frac{\mathrm{J}_m(\alpha(X)r) - \Upsilon(X)\,\mathrm{Y}_m(\alpha(X)r)}{\sqrt{\frac{2}{\pi}\left(\frac{R_2^2 - m^2/\alpha^2}{[\alpha R_2\,\mathrm{Y}_m'(\alpha(X)R_2)]^2} - \frac{R_1^2 - m^2/\alpha^2}{[\alpha R_1\,\mathrm{Y}_m'(\alpha(X)R_1)]^2}\right)}}e^{\mathrm{i}m\theta},$$

where the (eigenvalue) α and Υ can be determined from the eigenvalue equation

$$\frac{\alpha R_2 J'_m(\alpha R_2) - \zeta_2 J_m(\alpha R_2)}{\alpha R_2 Y'_m(\alpha R_2) - \zeta_2 Y_m(\alpha R_2)} = \frac{\alpha R_1 J'_m(\alpha R_1) + \zeta_1 J_m(\alpha R_1)}{\alpha R_1 Y'_m(\alpha R_1) + \zeta_1 Y_m(\alpha R_1)} = \Upsilon(X), \quad (2.1)$$

where

$$\zeta_1 = \frac{\Omega^2 D_0 R_1}{\mathrm{i}\omega Z_1}, \qquad \zeta_2 = \frac{\Omega^2 D_0 R_2}{\mathrm{i}\omega Z_2},$$

and for the special $Z_i = 0$

$$\frac{J_m(zR_2)}{Y_m(zR_2)} = \frac{J_m(zR_1)}{Y_m(zR_1)} = \Upsilon(X).$$

For a hollow duct ($R_1 = 0$) the expressions reduce to $\Upsilon(X) = 0$, and

$$\psi_0(r, \theta; X) = \frac{J_m(\alpha(X)r)}{J_m(\alpha R_2)} \sqrt{\frac{2}{\pi}} \left(R_2^2 - \frac{m^2}{\alpha^2} \right)^{-\frac{1}{2}} e^{-\mathrm{i}m\theta},$$

and the eigenvalues are determined by the equation

$$\alpha R_2 J'_m(\alpha R_2) - \zeta_2 J_m(\alpha R_2) = 0.$$

Finally, the solvability condition on ψ_1 presented in equation (1.44) gives for the amplitude function $N(X)$

$$\frac{Q^2}{N^2(X)} = \frac{\omega D_0 \sigma}{C_0} + \frac{D_0^2 \Omega U_0}{\mathrm{i}\omega} \left(\frac{2}{Z_1 R_1} \left(1 - \frac{m^2 - \zeta_1^2}{\alpha^2 R_1^2} \right)^{-1} + \frac{2}{Z_2 R_2} \left(1 - \frac{m^2 - \zeta_2^2}{\alpha^2 R_2^2} \right)^{-1} \right)$$

where Q^2 is a constant of integration, obtained via integration of equation (1.44).

Examples of Mode Tracking

This example tracks a single acoustic mode as it propagates through a realistic model of an engine duct.

Code Implementation

In order to write a program modelling the propagation of a mode through a duct, the first requirement is to build an eigensolver to find eigenvalues α satisfying equation (2.1). Thus first define a function $f(z)$ given by

$$f(z) = \frac{zR_2J'_m(zR_2) - \zeta_2 J_m(zR_2)}{zR_2Y'_m(zR_2) - \zeta_2 Y_m(zR_2)} - \frac{zR_1J'_m(zR_1) + \zeta_1 J_m(zR_1)}{zR_1Y'_m(zR_1) + \zeta_1 Y_m(zR_1)},$$

and therefore the values of z satisfying $f(z) = 0$ are the α's that are required. For computational ease, it is useful to replace the derivatives in the above eigenvalue equation using the well known Bessel function identities [61]

$$J'_m(z) = \frac{m}{z}J_m(z) - J_{m+1}(z),$$
$$Y'_m(z) = \frac{m}{z}Y_m(z) - Y_{m+1}(z).$$

Also note that when $\alpha R_1 << 1$ the product $\Upsilon(X)Y_m(\alpha r)$ can be difficult to compute directly as Υ is very small and Y_m very large. To overcome this difficulty, it is useful to make use of the following asymptotic approximations in order to compute this product without any computational difficulties whenever $\alpha r << 1$,

$$Y_m(\alpha r) \sim -\frac{1}{\pi}\Gamma(m)\left(\frac{1}{2}\alpha r\right)^{-m},$$
$$J_m(\alpha r) \sim \frac{1}{\Gamma(m+1)}\left(\frac{1}{2}\alpha r\right)^{m}.$$

In order to find the roots of the above equation, first define a matrix $\boldsymbol{z}$ representing a grid in the complex plane. Start off at the duct inlet, compute a matrix $\boldsymbol{B} = f(\boldsymbol{z})$, and locate positions of any possible roots of f by scanning consecutive elements within B and looking for sign changes (whether real or imaginary). Should a sign change occur anywhere between two points, the two

points are parsed to a root finding algorithm known Riddler's algorithm (described below) in order to find the root. If a root is found, its value is returned and stored in an array $\boldsymbol{\alpha}$. Once all of the roots have been found, Newton's method can be employed to track each α, μ, σ etc as the mode propagates through the duct.

Riddler's Algorithm

There are several useful root finding algorithms available, but one of interest here is known as Riddler's algorithm [46]. The algorithm works as follows: If a root is bracketed between values z_1 and z_2, the midpoint z_3 is computed and a new value z_4 is given by

$$z_4 = z_3 + \frac{(z_3 - z_1)\text{Sign}\left(\text{R}e(f(z_1) - f(z_2))\right) f(z_3)}{\sqrt{f(z_3)^2 - f(z_1)f(z_2)}},$$

where Re denotes the real part. The above equation has some nice properties. First the point z_4 is guaranteed to lie within the interval (z_1, z_2), and the method never jumps out of the brackets. Also Riddler's' algorithm is a very robust algorithm, and has a convergence rate of $\sqrt{2}$ [45].

Finding ζ_1 and ζ_2

The functions ζ_i, (where $i = 1, 2$) are given by

$$\zeta_i = \frac{-iD_0R_i}{\omega Z_i}\left(\omega - U_0\left(\frac{-\omega U_0}{C_0^2 - U_0^2} \pm \frac{C_0}{C_0^2 - U_0^2}\sqrt{\omega^2 - C_0^2z^2 + z^2U_0^2}\right)\right)^2 \quad (2.2)$$

where again we select positive for forward propagating modes, and negative for backward propagating. For a completely soft wall ($Z_i = 0$), $\zeta_i = 0$.

Geometry and Results

In this example, a lined inlet duct of a CFM56-inspired turbofan engine, from inlet plane via a (hard-walled) spinner to the inlet rotor plane is given by (see figure 2.1)

$$R_2(x) = 1.073 - 0.198(1 - x/2)^2 + 0.109\exp(-11x/2)$$
$$R_1(x) = \max\left(0, 0.689 - [1.131(1 - x/2)^2]^{\frac{1}{2}}\right)$$

for $0 \leq x \leq 2$. The acoustic impedances are taken to be $Z_1 = \infty$ and $Z_2 = 2-\mathrm{i}$. An inlet Mach number ~ 0.6 is chosen, such that $F = 0.559$ and $E = 2.514$. The Helmholtz number is taken to be $\omega = 25$, and the azimuthal eigenvalue $m = 26$.

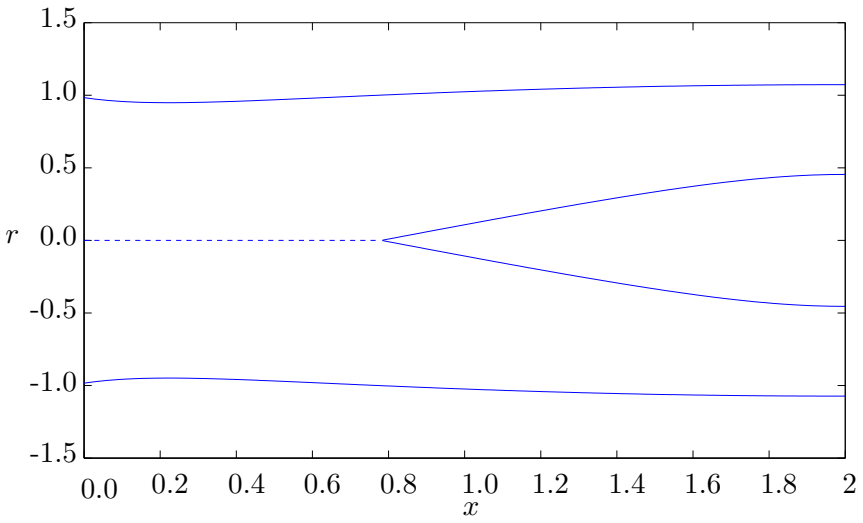

Figure 2.1: A sketch of the cross section of the duct geometry. The dashed line is the duct axis

The mean flow is computered prior to computing the acoustic field, and plots for the Mach number and mean flow density are shown in figure 2.2.

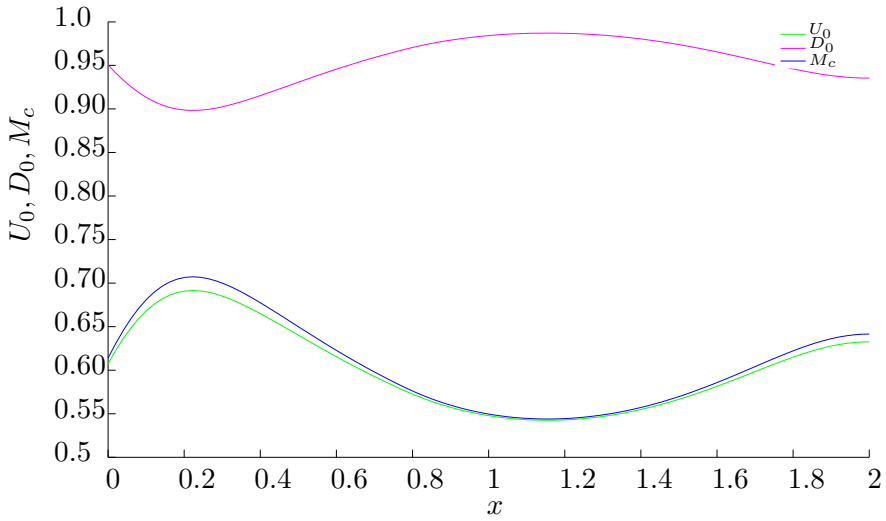

Figure 2.2: Mean flow density, velocity and Mach Number throughout the duct. Here M_c denotes the Mach number

Results for $\omega = 25$

Start with $\omega = 25$. Figures 2.3 - 2.18 show plots of radial wavenumber α, the axial wavenumber μ and reduced axial wavenumber σ in the complex plane, varying parametrically with the duct position x. The open circles indicate the initial position at the inlet plane. To ensure that both the same left and right running mode is being tracked, both are found first at $x = 0$ when $F = 0$, where both of the modes coincide, and then F is increased and the positive and negative modes are tracked as F is increased to $F = 0.559$.

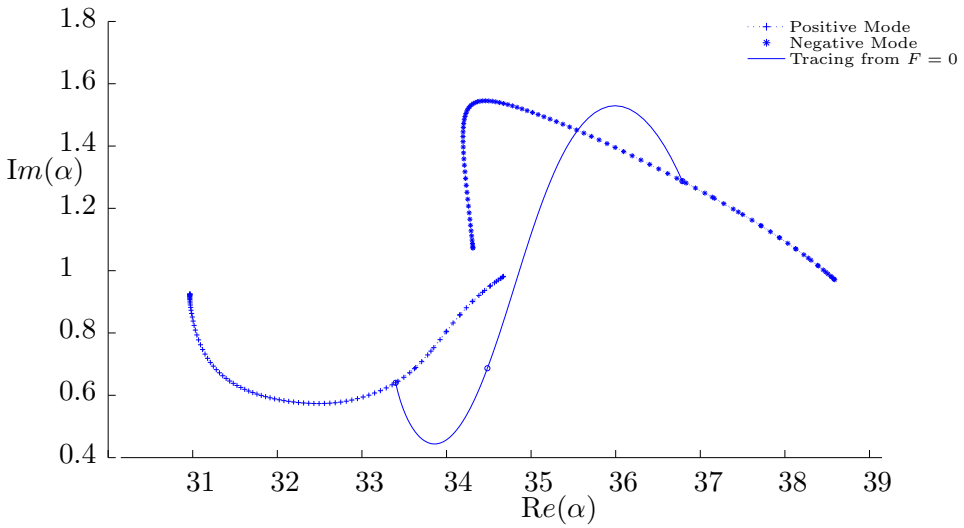

Figure 2.3: Tracking the wavenumber α throughout the duct. The left hand branch is the positive mode, and the right hand branch is it's opposite running counterpart. The solid line denotes the path taken by tracking the two modes forward from $F = 0$

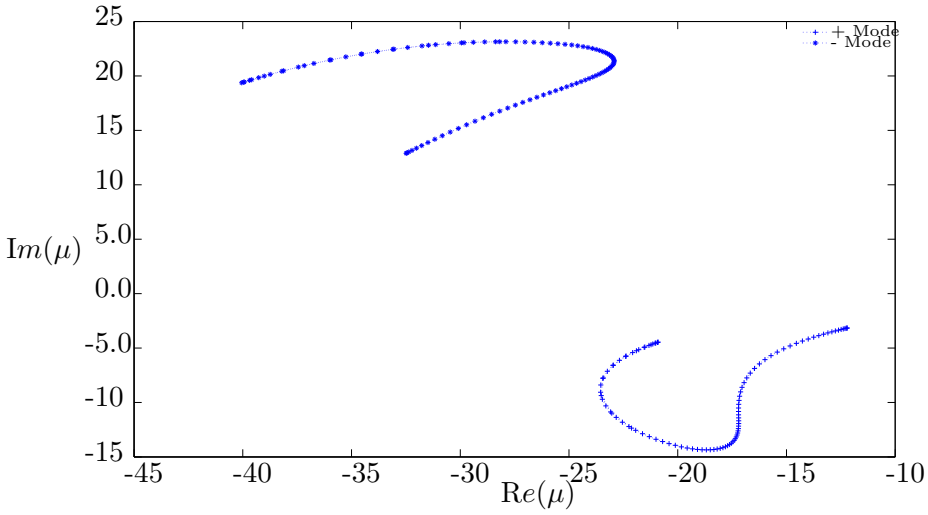

Figure 2.4: Tracking wavenumber μ as it progresses throughout the duct. The top left hand branch is the negative mode, and the other is the positive mode.

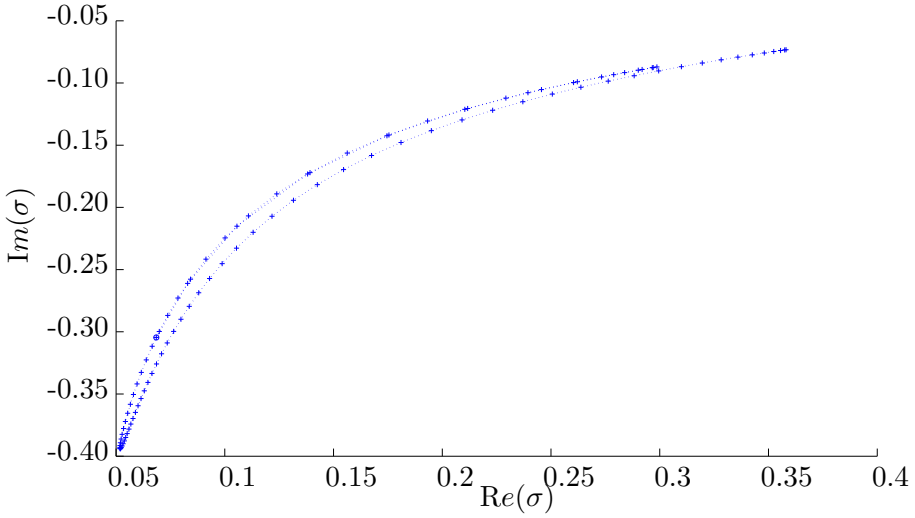

Figure 2.5: Tracking the reduced axial wavenumber σ of the positive mode as it progresses throughout the duct.

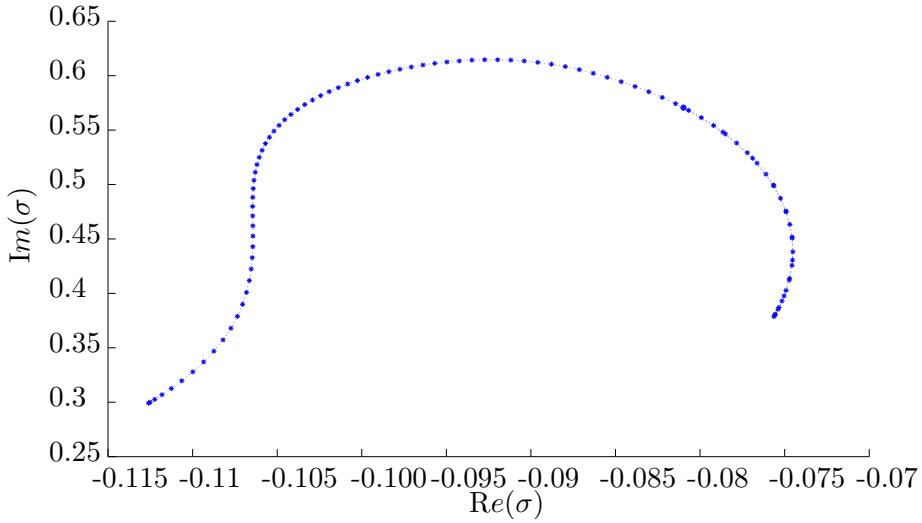

Figure 2.6: Tracking the reduced axial wavenumber σ of the negative mode as it progresses throughout the duct.

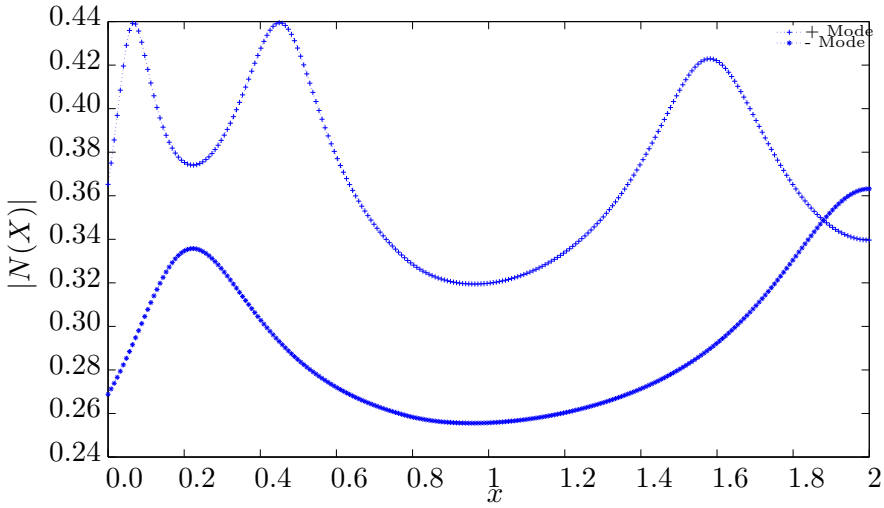

Figure 2.7: Tracking the variation in modal amplitude throughout the duct for both positive and negative modes

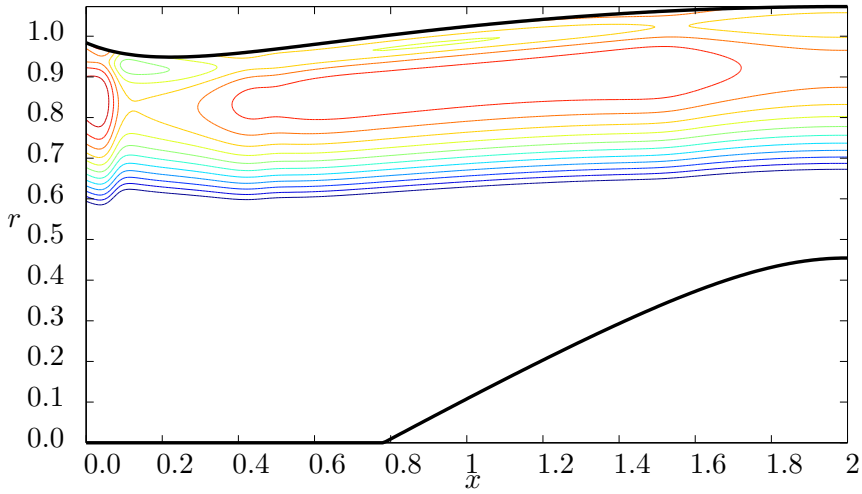

Figure 2.8: Iso-pressure contours for the positively propagating mode for $\omega = 25$, plotted on the decibel scale

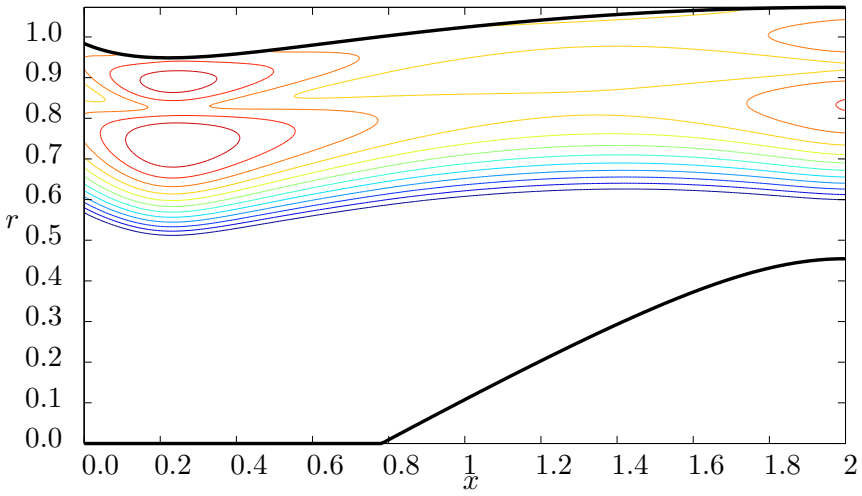

Figure 2.9: Iso-pressure contours for the positively propagating mode for $\omega = 25$, plotted on the decibel scale

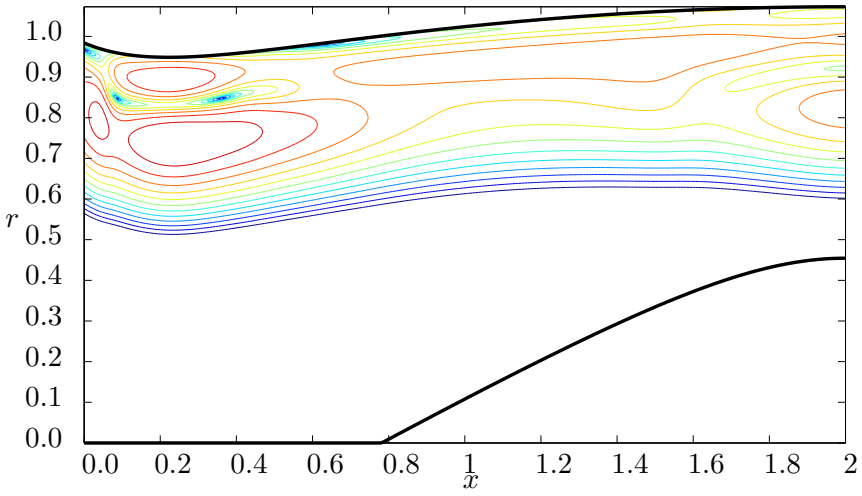

Figure 2.10: Iso-pressure contours for both the positively and negatively propagating modes for $\omega = 25$, plotted on the decibel scale

Results for $\omega = 50$

This section contains the results obtained for the well cut-on second harmonic $\omega = 50$.

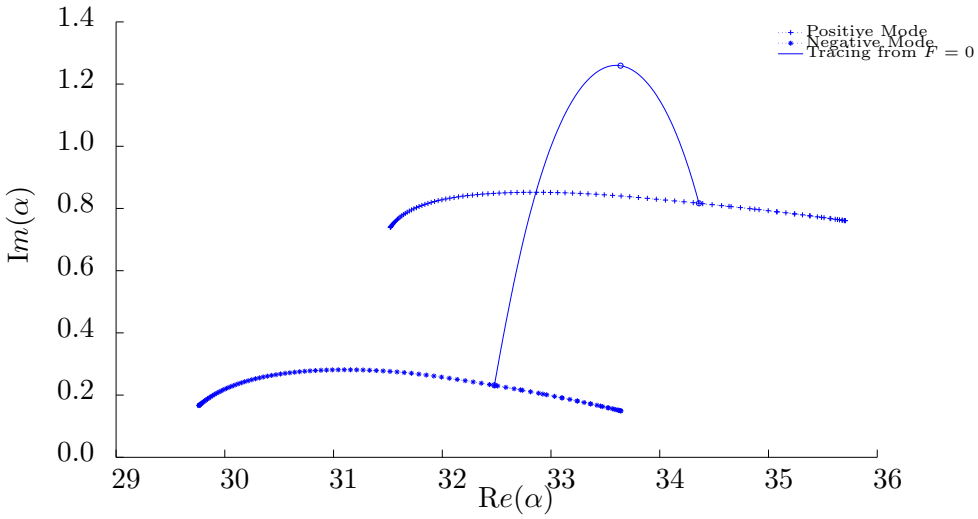

Figure 2.11: Tracking the wavenumber α throughout the duct for $\omega = 50$. The upper branch is the positive mode, and the lower branch is it's opposite running counterpart. The solid line denotes the path taken by tracking the two modes forward from $F = 0$

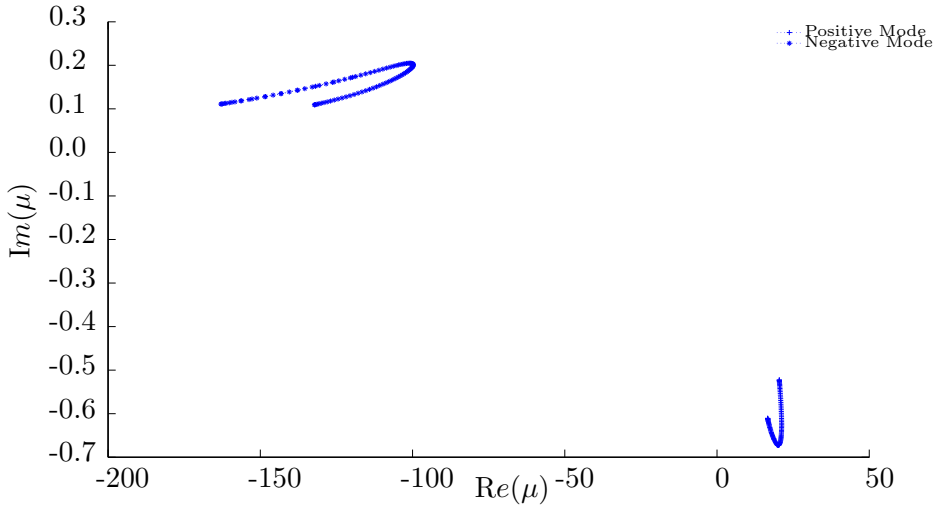

Figure 2.12: Tracking the progress of the wavenumber μ throughout the duct $\omega = 50$.

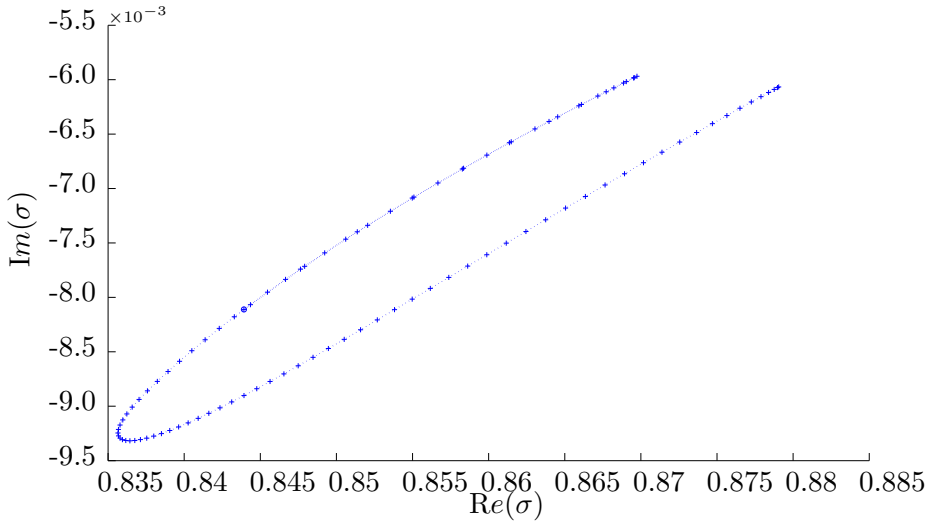

Figure 2.13: Tracking the wavenumber σ throughout the duct of the positively propagating mode for $\omega = 50$.

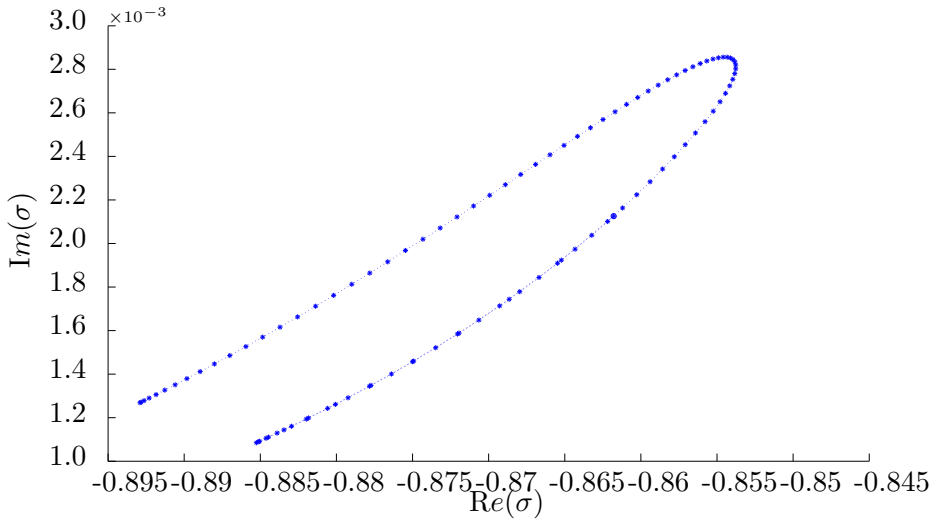

Figure 2.14: Tracking the wavenumber σ throughout the duct of the negatively propagating mode $\omega = 50$.

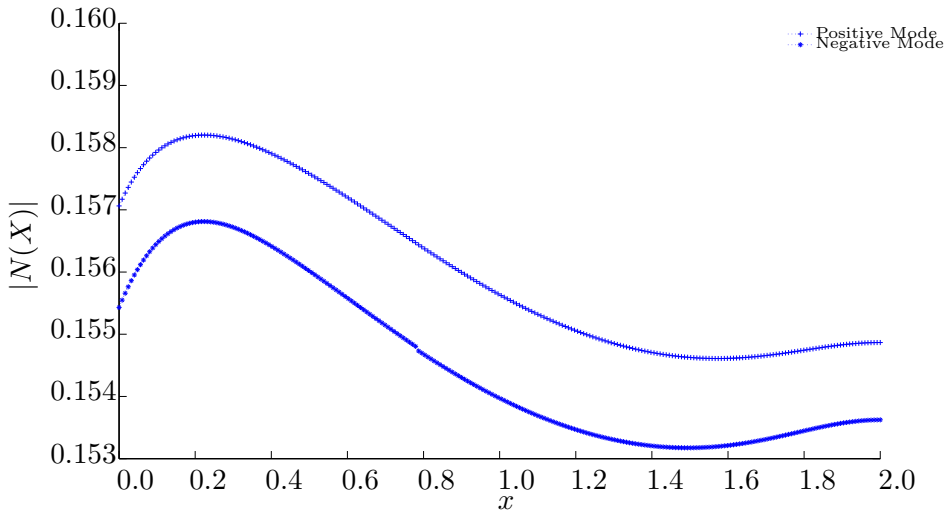

Figure 2.15: Tracking the variation in modal amplitude throughout the duct for both positive and negative modes $\omega = 50$

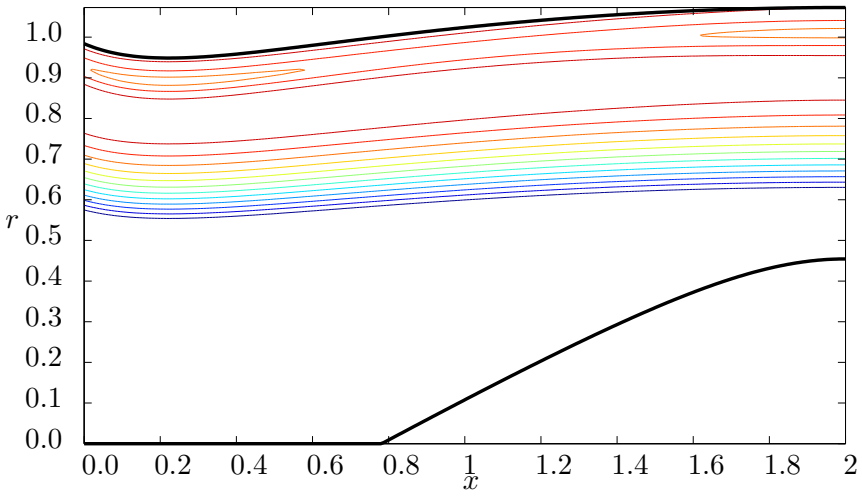

Figure 2.16: Iso-pressure contours for the positively propagating mode for $\omega = 50$, plotted on the decibel scale

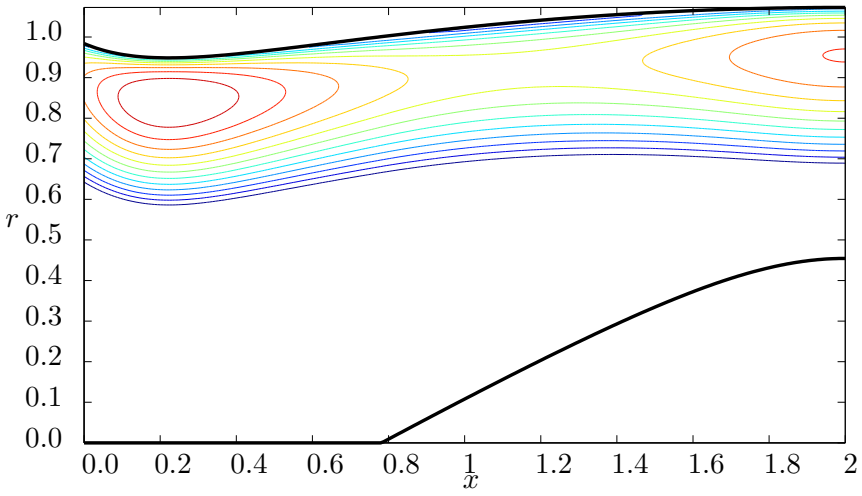

Figure 2.17: Iso-pressure contours for the positively propagating mode for $\omega = 50$, plotted on the decibel scale

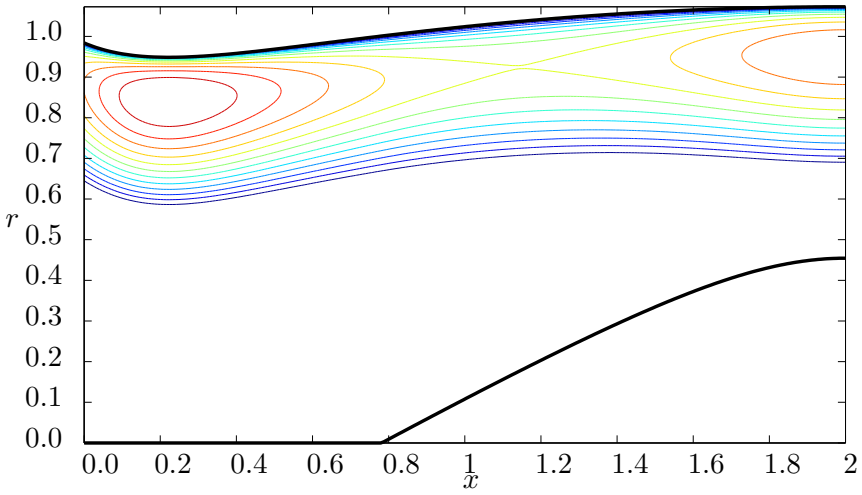

Figure 2.18: Iso-pressure contours for both the positively and negatively propagating modes for $\omega = 50$, plotted on the decibel scale

Example of Hard Walled Ducts

The scenario is now changed slightly as here the case when both walls are hard is considered. Consider now a single mode propagating through a duct with the same geometry as that previously described, the only difference is that the upper impedance wall is replaced with a completely hard wall. It is important to understand the mechanics of modal propagation through an acoustically solid duct as the rest of this thesis deals entirely with hard walled ducts.

Figure 2.21 shows the variation of the radial eigenvalue α as the mode propagates through the duct. Note that in the case of hard walls, the eigenvalue problem for α reduces to

$$\frac{\alpha R_2 J'_m(\alpha R_2)}{\alpha R_2 Y'_m(\alpha R_2)} = \frac{\alpha R_1 J'_m(\alpha R_1)}{\alpha R_1 Y'_m(\alpha R_1)} = \Upsilon(X), \tag{2.3}$$

and so the directional dependence brought about by ζ_1 and ζ_2 is no longer present, and thus α the same for both the positive and negative mode. Another consequence of this is that all α's are now real.

Recall that the reduced axial wavenumber σ is given by

$$\sigma^2 = 1 - (C_0^2 - U_0^2)\frac{\alpha^2}{\omega^2},$$

and if α is real this means that sigma is either real or purely imaginary. The sign of the square root is chosen such that the positive choice corresponds to the right propagating mode, and the negative choice is for the left propagating mode.

Another point to note regarding hard walled ducts is that the expression for the modal amplitude reduces to

$$N^2(X) = \frac{C_0}{Q\omega D_0 \sigma}.$$

Looking at the plot of sigma given in figure 2.19, it becomes quite clear that for a particular mode, the geometry and mean flow may vary in such a way as to make sigma switch from real to imaginary as it propagates along the duct. This is certainly true in this example, and this fact causes problems in terms of calculating the modal amplitude because in order for sigma to change from real to imaginary it must pass through zero. This passing through zero causes a singularity to be introduced into the above expression for the modal amplitude, and the whole modal approximation breaks down. A plot of modal amplitude in the case of hard walls is shown in figure 2.20, and the sharp asymptote type peaks are the points at which the approximation breaks down

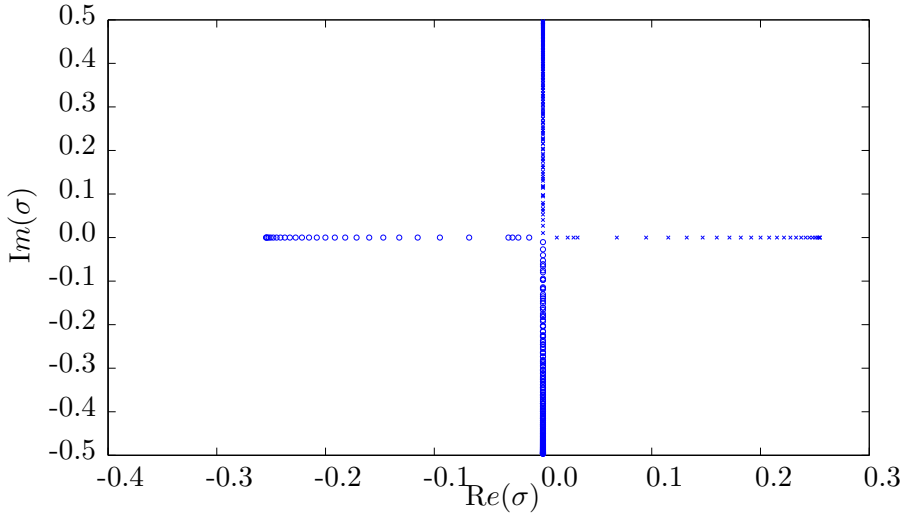

Figure 2.19: Tracking the variation of σ throughout the duct in the case of hard walls. Purely Imaginary σ means that the mode is cut-off

due to a vanishing σ in the denominator of the amplitude.

The problem with the vanishing σ described above is due to the fact that the model developed so far assumes that the mode is slowly varying throughout the duct. Suppose then that a point is defined such that $\sigma(X_t) = 0$. As σ approaches this point the mode does not vary slowly within a small interval around this point, and the whole solution breaks down. This small interval is known as a boundary layer in the variable X. The model with the vicinity of the turning point needs to be considered separately, and details of how this is done will be discussed in the next chapter.

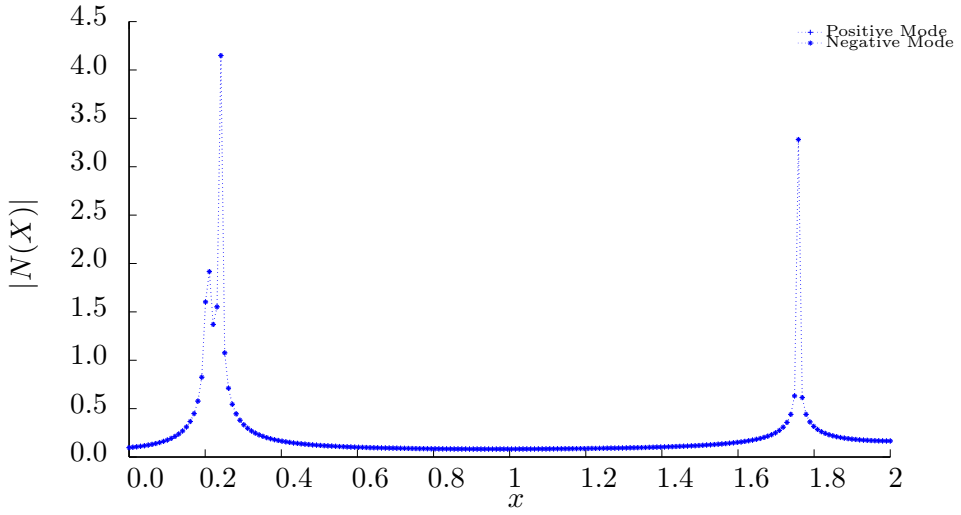

Figure 2.20: Tracking the variation in modal amplitude throughout the duct for both positive and negative modes. The sharp peaks are areas where σ is very small and the slowly varying approximation is not valid.

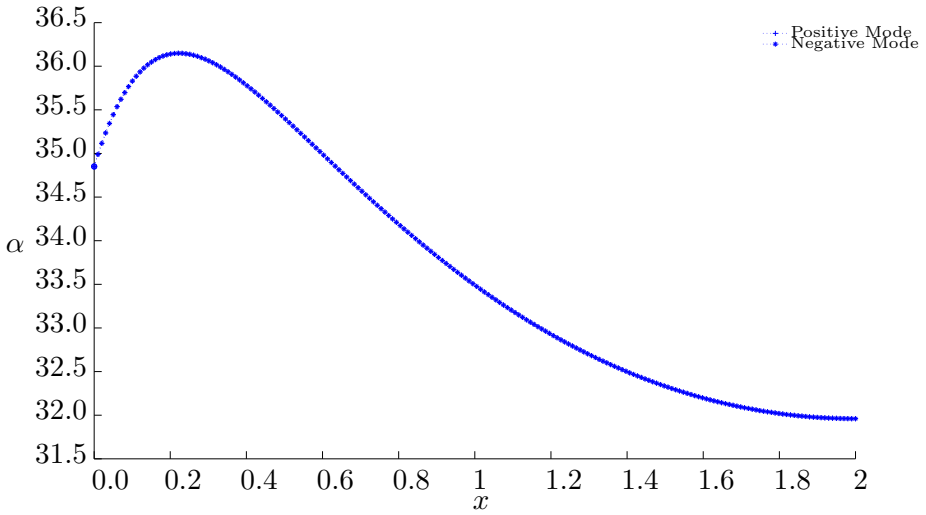

Figure 2.21: Tracking the variation of α throughout the duct in the case of hard walls. In the case of hard walls, α is always real

Summary

This chapter presented an explicit multiple scales solution for sound propagation through a circular and annular duct. This model was used to simulate the propagation of acoustic modes through a geometry that is a realistic geometrical approximation to that of a typical turbofan engine. This modal solution is valid for both hollow and annular ducts, and one of it's unique features is to present a systematic approximation to the hollow-to-annular cylinder transition problem in a turbofan engine. The results shown here are in excellent agreement with Rienstra's 1999 paper on the subject [47].

The model developed in this section made use of the Myers acoustic boundary condition, which models the effect of an impedance wall under a mean flow by assuming that the boundary layer vanishes. All of the results presented in this section make use of this condition. However very recently the Myers condition has been called into question, as there are situations where the Myers gives rise to a certain type of acoustic wave known as a surface wave, but so far these surface waves have not been shown to exist in reality. Further to this, the Myers boundary condition has also recently shown to lead to an ill-posed problem in the time domain [52]. More recently Rienstra and Brambley have independently posed a modified acoustic boundary condition [7, 53], although at present their solutions are similar but not identical. The remainder of this thesis deals with hard walled ducts in which case the problems associated with the instability issues known to be related to the Myers boundary condition do not feature in the analysis.

Chapter 3

Turning Point Analysis

As demonstrated in the last chapter, the outer modal solution presented in Chapter 1 that describes the propagation of an acoustic mode within a duct can break down in the case of a slowly varying hard walled duct, because as the reduced axial wavenumber $\sigma \to 0$ the modal amplitude $N(X)$ (as given in equation (1.47))

$$N(X) = Q\sqrt{\frac{C_0(X)}{\omega\sigma(X)D_0(X)}},$$

becomes singular. Suppose that the medium and duct diameter vary such in a way that within the duct there exists a point $X = X_t$ with $\sigma(X_t) = 0$. The reason for this breakdown in the modal solution is due to the fact that within a small neighbourhood of the point X_t the mode is no longer slowly varying, and so the slowly varying assumption is invalid and therefore a new approximation to the leading order governing equation is required.

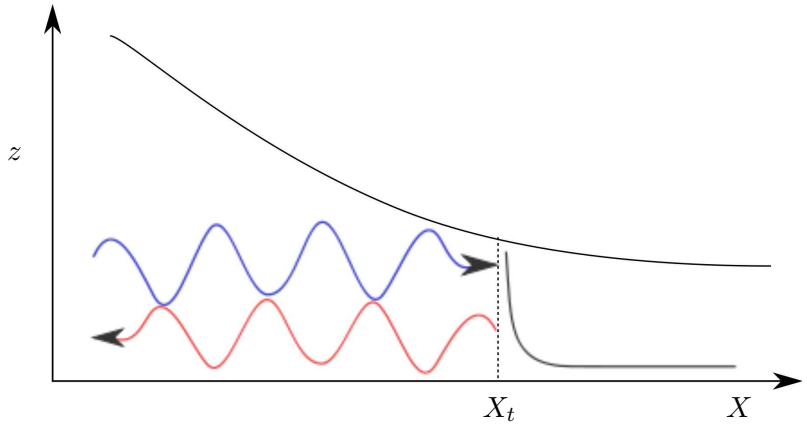

Figure 3.1: Cut-on cut-off Transition for a Single Turning Point: The blue wave represents the incident cut-on mode, the red the reflected cut-on mode, and the black is the exponentially decaying cut-off mode

Recall that the reduced axial wavenumber σ is defined as

$$\sigma^2 = 1 - (C_0^2 - U_0^2)\frac{\alpha^2}{\omega^2}.$$

When σ^2 changes sign from positive to negative, σ changes from real to imaginary. Assuming that there is no interference from other modes around X_t, no energy can transmit beyond X_t and the mode reflects at X_t, leading to the formation of a standing wave within the duct. A sketch illustrating this type of phenomena is shown in figure 3.1. As a result of this reflection, the point X_t is known as a *turning point*.

3.1 Single Turning Point Analysis

In this section the situation in which the reduced axial wavenumber σ^2 decreases linearly within the vicinity of the turning point is discussed. The details in this section summarise the results presented by Rienstra's 2003 paper [49].

Following on from chapter 1 the leading order governing acoustic equation for ϕ is

$$\varepsilon^2\left(1-\frac{U_0^2}{C_0^2}\right)\frac{\partial^2\phi}{\partial X^2}-\frac{2\mathrm{i}\varepsilon\omega U_0}{C_0^2}\frac{\partial\phi}{\partial X}+\left(\frac{\omega^2}{C_0^2}-\alpha^2\right)\phi=O(\varepsilon), \tag{3.1}$$

where the slow variable $X=\varepsilon x$ as before. In the case of a single mode propagating within a hard walled duct where an individual turning point exists within the duct, the modal propagation can be decomposed in accordance with the discussion in Chapter 1 for $X<X_t$ (far from the turning point) as

$$\begin{aligned}\phi=&\frac{A_0}{\sqrt{\sigma}}\psi_0(r,\theta;X)\exp\left(\frac{\mathrm{i}}{\varepsilon}\int_{X_t}^{X}\frac{\omega U_0}{C_0^2-U_0^2}\mathrm{d}X'\right)\\&\times\left[\exp\left(-\frac{\mathrm{i}}{\varepsilon}\int_{X_t}^{X}\frac{\omega C_0\sigma}{C_0^2-U_0^2}\mathrm{d}X'\right)+R\exp\left(\frac{\mathrm{i}}{\varepsilon}\int_{X_t}^{X}\frac{\omega C_0\sigma}{C_0^2-U_0^2}\mathrm{d}X'\right)\right],\end{aligned} \tag{3.2}$$

where R is known as the *reflection coefficient*, a complex number that is to be determined. The argument of the reflection coefficient indicates the phase change that occurs to the reflected left running mode as a result of the wave undergoing cut-on cut-off transition, and the magnitude of R indicates the factor by which the amplitude of the reflected wave is reduced by. The reduced amplitude A_0 is given by

$$A_0(X)=Q\sqrt{\left(\frac{C_0}{\omega D_0}\right)}.$$

For $X>X_t$ at a location that is sufficiently far from the turning point where σ is imaginary negative, the outer solution comprises of an exponentially decaying wave and may be represented as

$$\begin{aligned}\phi\;=&\;\frac{A_0}{\sqrt{\sigma}}\psi_0(r,\theta;X)\left[T\exp\left(-\frac{1}{\varepsilon}\int_{X_t}^{X}\frac{\omega C_0|\sigma|}{C_0^2-U_0^2}\mathrm{d}X'\right)\right]\\&\times\;\exp\left(\frac{\mathrm{i}}{\varepsilon}\int_{X_t}^{X}\frac{\omega U_0}{C_0^2-U_0^2}\mathrm{d}X'\right),\end{aligned} \tag{3.3}$$

where T is known as the *transmission coefficient*, and the branch of the square root is chosen such that $\sqrt{\sigma} = \mathrm{e}^{-\frac{\mathrm{i}\pi}{4}}\sqrt{|\sigma|}$.

Examining the asymptotic behaviour of the outer solution near the transition point X_t and balancing terms in the governing equation leads to the existence of a boundary layer region of thickness $O(\varepsilon^{\frac{2}{3}})$ described by the inner-axial variable ξ as

$$X - X_t = \varepsilon^{\frac{2}{3}}\lambda^{-1}\xi.$$

The coefficient λ was introduced for convenience by Rienstra [49] and is defined in terms of the mean flow variables evaluated at X_t,

$$\lambda^3 = \frac{2\omega^2 C_0^2(X_t)}{(C_0^2(X_t) - U_0^2(X_t))^2}\left[\frac{C_0(X_t)C_0'(X_t) - U_0(X_t)U_0'(X_t)}{C_0^2(X_t) - U_0^2(X_t)} + \frac{\alpha'(X_t)}{\alpha(X_t)}\right]. \tag{3.4}$$

Note that $\sigma \to 0$ as $X \to X_t$, and thus it is possible to form an asymptotic approximation to σ^2 for $\varepsilon \to 0$ in the boundary layer for $\lambda \sim 1$. Using Taylor's theorem in the form

$$f(x_0 + \delta x) = f(x_0) + \delta x f'(x_0) + O((\delta x)^2),$$

where $x \equiv x_0 + \delta x$, the following is true in the boundary layer;

$$\begin{aligned}\sigma^2(X) &= \sigma^2(X_t + \varepsilon^{\frac{2}{3}}\lambda^{-1}\xi) \\ &= -2\varepsilon^{\frac{2}{3}}\lambda^{-1}\xi\left(\frac{C_0(X_t)C_0'(X_t) - U_0(X_t)U_0'(X_t)}{C_0^2(X_t) - U_0^2(X_t)} + \frac{\alpha'(X_t)}{\alpha(X_t)}\right) \\ &+ O(\varepsilon^{\frac{4}{3}}\xi^2)\end{aligned} \tag{3.5}$$

and thus $\sigma^2 \sim \varepsilon^{\frac{2}{3}}$ to leading order.

It is assumed that the boundary layer is very thin and so within the boundary

layer the duct may be assumed to be locally parallel, thus the modal behaviour in the radial direction is unchanged and the inner solution takes the form

$$\phi = \chi(\xi)\psi(r,\theta;X_t)\exp\left[\frac{\mathrm{i}}{\varepsilon}\int_{X_t}^{X}\frac{\omega U_0}{C_0^2-U_0^2}\mathrm{d}X'\right], \tag{3.6}$$

where $\psi(r,\theta;X_t)$ is the solution to the cross sectional eigenvalue problem evaluated at X_t, and $\chi(\xi)$ is the axial amplitude of the mode within the inner region which is to be determined. Substitution of the above model into the reduced governing equation (3.1) yields

$$\psi(r,\theta;X)\left(\varepsilon^{\frac{2}{3}}\lambda^2\frac{\mathrm{d}^2}{\mathrm{d}\xi^2}\chi(\xi)+\frac{\omega^2C_0^2\sigma^2}{\left(C_0^2-U_0^2\right)^2}\chi(\xi)\right)=O(\varepsilon).$$

Inspection of the above equation together with the information gathered from the Taylor expansion of σ^2 shown in equation (3.5) that within the boundary layer the χ'' and σ^2 terms will balance because they are both of order $\varepsilon^{\frac{2}{3}}$. Substitution of the Taylor approximation to σ^2 given in equation (3.5) yields

$$\varepsilon^{\frac{2}{3}}\left(1-\frac{U_0^2(X_t)}{C_0^2(X_t)}\right)\lambda^2\psi(r,\theta;X_t)\left(\frac{\mathrm{d}^2}{\mathrm{d}\xi^2}\chi(\xi)-\xi\chi(\xi)\right)=O(\varepsilon),$$

which to leading order is Airy's equation in the variable ξ

$$\frac{\mathrm{d}^2}{\mathrm{d}\xi^2}\chi(\xi)-\xi\chi(\xi)=0.$$

The general solution for $\chi(\xi)$ is therefore given by

$$\chi(\xi)=\mathscr{A}\,\mathrm{Ai}(\xi)+\mathscr{B}\,\mathrm{Bi}(\xi),$$

where $\mathrm{Ai}(\xi)$ and $\mathrm{Bi}(\xi)$ Airy functions of the first and second kind respectively and $\mathscr{A}$ and $\mathscr{B}$ are arbitrary constants of integration.

The task now is to determine the constants $\mathscr{A}$, $\mathscr{B}$ and the reflection and

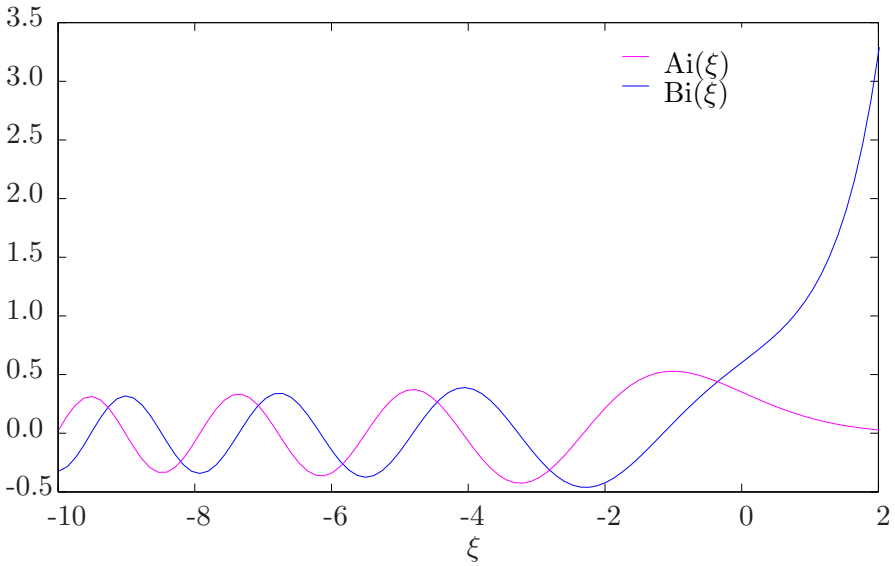

Figure 3.2: Airy Functions of the First and Second Kind

transmission coefficients R and T, and this is achieved by balancing the outer solution in the limit $X \to X_t$ with the inner solution in the limit $\xi \to \pm\infty$. The limiting behaviour of the outer solution is obtained by studying the limit of the integral that corresponds to the modal propagation in the axial direction, i.e.

$$\mathscr{L} = \lim_{X \to X_t} \left(\frac{1}{\varepsilon} \int_{X_t}^{X} \frac{\omega C_0(X')\sigma(X')}{C_0^2(X') - U_0^2(X')} \mathrm{d}X' \right).$$

In analysing $\mathscr{L}$ independently for $X \nearrow X_t$ and $X \searrow X_t$ (using the asymptotic approximation to σ given by equation (3.5)) one arrives at

$$\mathscr{L} = \begin{cases} -\frac{2}{3}(-\xi)^{\frac{3}{2}} = -\zeta & \text{for} \quad \xi < 0 \\ -\mathrm{i}\frac{2}{3}(\xi)^{\frac{3}{2}} = -\mathrm{i}\zeta & \text{for} \quad \xi > 0 \end{cases} \tag{3.7}$$

where $\zeta = \frac{2}{3}|\xi|^{\frac{3}{2}}$ has been introduced for convenience. Thus, for the outer solution in the limit $X \nearrow X_t$ one arrives at

$$\phi \simeq \frac{A_0(X_t)}{\varepsilon^{\frac{1}{6}}(-\xi)^{\frac{1}{4}}} \left(\frac{\omega C_0(X_t)}{\lambda(C_0^2(X_t) - U_0^2(X_t))} \right)^{\frac{1}{2}} \psi(r, \theta; X_t)(e^{\mathrm{i}\zeta} + Re^{-\mathrm{i}\zeta}), \tag{3.8}$$

and for $X \searrow X_t$ one arrives at

$$\phi \simeq \frac{A_0(X_t)}{\varepsilon^{\frac{1}{6}}\xi^{\frac{1}{4}}}\left(\frac{\omega C_0(X_t)}{\lambda(C_0^2(X_t)-U_0^2(X_t))}\right)^{\frac{1}{2}} e^{\frac{\mathrm{i}\pi}{4}}\psi(r,\theta;X_t)Te^{-\zeta}. \tag{3.9}$$

On the other hand, for the limiting behaviour of $\chi(\xi)$ is determined using the following well documented limits [1]

$$\begin{aligned}
\mathrm{Ai}(\xi) \quad &\rightarrow \quad \begin{cases} \frac{\cos\left(\zeta-\frac{\pi}{4}\right)}{\sqrt{\pi}|\xi|^{\frac{1}{4}}} & \text{as} \quad \xi \rightarrow -\infty, \\ \frac{\exp\left(-\zeta\right)}{2\sqrt{\pi}\xi^{\frac{1}{4}}} & \text{as} \quad \xi \rightarrow \infty, \end{cases} \\
\mathrm{Bi}(\xi) \quad &\rightarrow \quad \begin{cases} \frac{\cos\left(\zeta+\frac{\pi}{4}\right)}{\sqrt{\pi}|\xi|^{\frac{1}{4}}} & \text{as} \quad \xi \rightarrow -\infty, \\ \frac{\exp\left(\zeta\right)}{\sqrt{\pi}\xi^{\frac{1}{4}}} & \text{as} \quad \xi \rightarrow \infty. \end{cases}
\end{aligned} \tag{3.10}$$

Thus for $\xi \rightarrow \infty$ the inner solution is

$$\phi \sim \mathscr{A}\frac{\exp\left(-\zeta\right)}{2\sqrt{\pi}\xi^{\frac{1}{4}}} + \mathscr{B}\frac{\exp\left(\zeta\right)}{\sqrt{\pi}\xi^{\frac{1}{4}}}, \tag{3.11}$$

and for $\xi \rightarrow -\infty$ the inner solution is

$$\phi \sim \mathscr{A}\frac{\cos\left(\zeta-\frac{\pi}{4}\right)}{\sqrt{\pi}|\xi|^{\frac{1}{4}}} + \mathscr{B}\frac{\cos\left(\zeta+\frac{\pi}{4}\right)}{\sqrt{\pi}|\xi|^{\frac{1}{4}}}. \tag{3.12}$$

The first step in the asymptotic matching is performed by comparing the outer solution in the limit $X \searrow X_t$ with the inner solution as $\xi \rightarrow \infty$. Upon doing so it is noted that e^{ζ} is an exponentially growing term and is dismissed from the solution giving $\mathscr{B} = 0$ and thus

$$\mathscr{A} = \frac{2A_0(X_t)\sqrt{\pi}}{\varepsilon^{\frac{1}{6}}}\left(\frac{\omega C_0(X_t)}{\lambda(C_0^2(X_t)-U_0^2(X_t))}\right)^{\frac{1}{2}} e^{\frac{\mathrm{i}\pi}{4}}T.$$

The second step in the matching procedure is performed by comparing the outer solution in the limit $X \nearrow X_t$ with the inner solution as $\xi \rightarrow -\infty$ which yields

$$\mathscr{A}\frac{\cos\left(\zeta-\frac{\pi}{4}\right)}{\sqrt{\pi}|\xi|^{\frac{1}{4}}} \sim \frac{A_0(X_t)}{\varepsilon^{\frac{1}{6}}(-\xi)^{\frac{1}{4}}}\left(\frac{\omega C_0(X_t)}{\lambda(C_0^2(X_t)-U_0^2(X_t))}\right)^{\frac{1}{2}}(e^{\mathrm{i}\zeta}+Re^{-\mathrm{i}\zeta}), \tag{3.13}$$

which is equivalent to the identity

$$T\exp(\mathrm{i}\zeta) + T\mathrm{i}\exp(-\mathrm{i}\zeta) \equiv \exp(\mathrm{i}\zeta) + R\exp(-\mathrm{i}\zeta),$$

and this holds if and only if

$$T = 1, \qquad R = \mathrm{i}.$$

Therefore, the argument of the reflection coefficient is $\pi/2$ which indicates that the mode undergoes a phase shift of $\pi/2$ on reflection at the turning point. Note also that the reflected amplitude is equal to the incident amplitude as $|R| = 1$, creating a standing wave. This also conserves energy as the transmitted (cut-off) wave carries no energy.

The Composite Solution

The outer solution breaks down as $X \to X_t$ because the second order derivatives with respect to X that were neglected in forming the approximation are the dominant terms in this region. For the inner region the inner solution is only valid in the region where $|X - X_t| \sim \varepsilon^{\frac{2}{3}}$. Generally speaking it is desirable to form the so-called *composite solution*, which is a solution that is uniformally valid throughtout the entire duct to leading order. The composite solution encompasses both the slowly varying outer solution (both upstream and downstream) and the inner boundary later solution near the transition point X_t. There are several advantages to the composite solution in that there is no need to calculate the size of the boundary layer, and there is no need for asymptotic matching of two solutions. The solution will be valid for both $|X - X_t| \sim 1$ and $|X - X_t| \sim \varepsilon^{\frac{2}{3}}$. The composite solution due to Ovenden [44]

is given by

$$\phi = \hat{Q}\sqrt{\frac{C_0}{\omega D_0}}\psi(y,z;X)\left(-\frac{3}{2\varepsilon\sigma^3}\int_{X_t}^{X}\frac{\omega C_0\sigma}{C_0^2-U_0^2}\mathrm{d}X'\right)^{\frac{1}{6}} \times \mathrm{Ai}\left[\left(\frac{3\mathrm{i}}{2\varepsilon}\int_{X_t}^{X}\frac{\omega C_0\sigma}{C_0^2-U_0^2}\mathrm{d}X'\right)^{\frac{2}{3}}\right],$$

where it should be noted that the term

$$\left(-\frac{3}{2\varepsilon\sigma^3}\int_{X_t}^{X}\frac{\omega C_0\sigma}{C_0^2-U_0^2}\mathrm{d}X'\right)^{\frac{1}{6}},$$

is not singular as $X \to X_t$. The availability of composite solution means that simulations of wave propagation where a mode undergoes cut-on cut-off via a single turning point mechanism may now be easily obtained.

As well as using the composite solution it is also possible to simulate cut-on cut-off transition using a numerical scheme similar to that described in Chapter 6. The methods described in chapter 6 describe a numerical method that is derived from a composite-type equation, the derivation of which is similar to the derivation of the composite solution described above.

Consider a rectangular duct defined by

$$-2.5 < x < 2.5, \quad 0 \le z \le h(x),$$

where the wall function $h(x)$ is defined by

$$h(x) = 1 - 0.1 - 0.1\tanh(3x),$$

and then consider an example of a mode indexed by $n = 6$ propagating from left to right throughout this realm with unit incident amplitude $A_6 = 1$ and

Helmholtz number $\omega = 20$. The traditional theory of modal propagation fails when $\sigma \to 0$, and the solution develops a singularity around the vicinity of the tuning point X_t. However when a composite solution is used the solution is valid throughout the entire duct and a singularity does not develop anywhere.

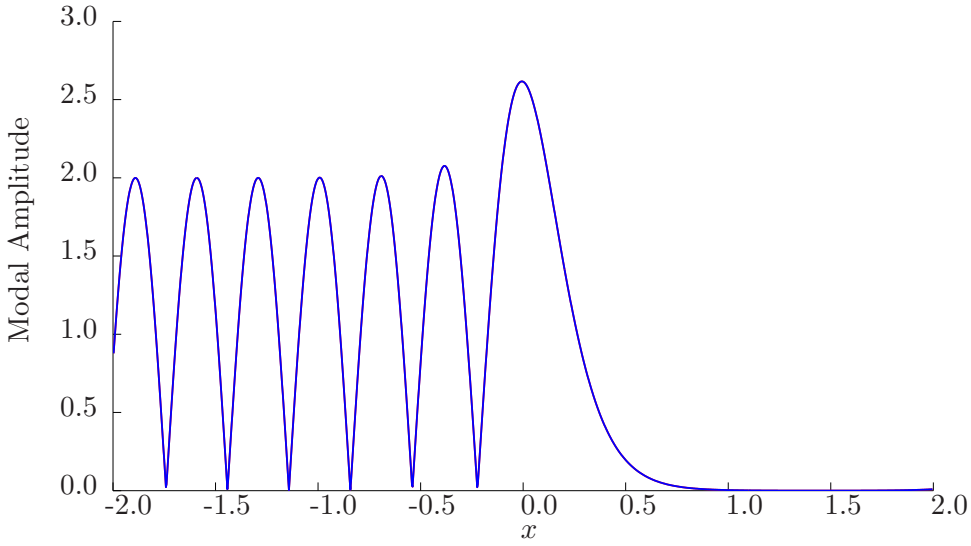

Figure 3.3: Plot of the modal amplitude in the case of a single turning point.

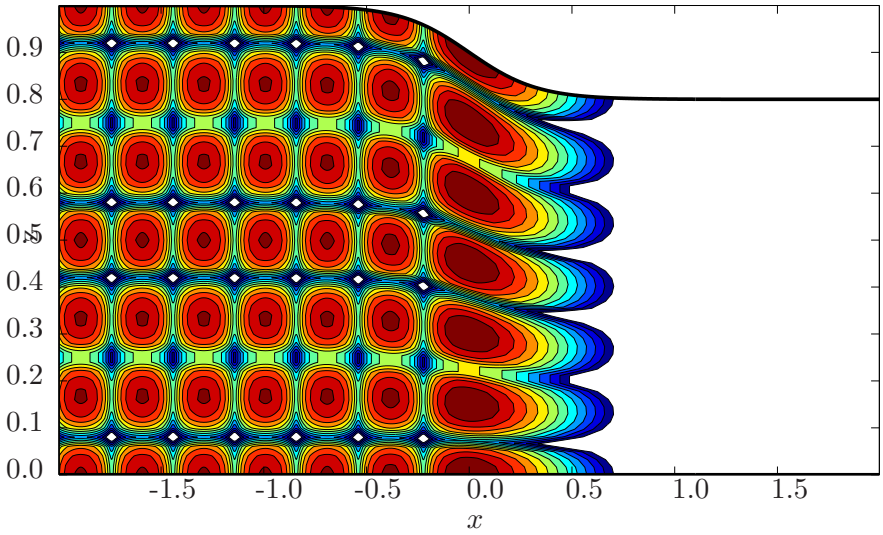

Figure 3.4: Pressure Contours for a single turning point case.

3.2 Double Turning Point Analysis

In the work described in the previous section it was assumed that the leading order behaviour of σ^2 was linear with respect to ξ within the vicinity of the turning point. Here a different scenario is considered, where σ^2 is assumed to be quadratic to leading order within the neighbourhood of X_t, a condition which gives rise to the so-called double turning point. The work described here extends the work of Rienstra [49], and is a completely new formulation.

The Outer Solution

In constructing the inner solution for the single turning point analysis the non-parallel terms on the right hand side of the reduced governing equation (3.1) are negligible throughout the entire analysis. In this formulation it is necessary to consider these non parallel terms of the inner solution because at first glance, they appear to be important.

As before, the governing acoustic equation is given by

$$\varepsilon^2\left(1-\frac{U_0^2}{C_0^2}\right)\frac{\partial^2\phi}{\partial X^2}-\varepsilon\frac{2\mathrm{i}\omega U_0}{C_0^2}\frac{\partial\phi}{\partial X}+\left(\frac{\omega^2}{C_0^2}-\alpha^2\right)\phi=O(\varepsilon). \tag{3.14}$$

When considering the single turning point scenario all of the modal energy is reflected at the turning point and no acoustic energy propagated beyond it. However for a double turning point scenario, far from the turning point for both $X < X_t$ and $X > X_t$ the reduced wavenumber σ^2 is positive in both regions and therefore one would expect that there is only a partial reflection of energy at the turning point, with some of the remaining acoustic energy continuing to propagate beyone the turning point. Thus it is assumed that for

$X < X_t, |X - X_t| \sim 1$ the form of the outer solution remains unchanged and is the same as (3.2), i.e.

$$\phi = \frac{A_0}{\sqrt{\sigma}}\psi(r,\theta;X)\exp\left(\frac{\mathrm{i}}{\varepsilon}\int_{X_t}^{X}\frac{\omega U_0}{C_0^2-U_0^2}\mathrm{d}X'\right) \times\left[\exp\left(-\frac{\mathrm{i}}{\varepsilon}\int_{X_t}^{X}\frac{\omega C_0\sigma}{C_0^2-U_0^2}\mathrm{d}X'\right)+R\exp\left(\frac{\mathrm{i}}{\varepsilon}\int_{X_t}^{X}\frac{\omega C_0\sigma}{C_0^2-U_0^2}\mathrm{d}X'\right)\right]. \quad (3.15)$$

For the region $X > X_t, |X - X_t| \sim 1$ there is a difference from the single turning point case in that a propagating mode is expected rather than a mode that exponentially decays. Thus for $X > X_t, |X - X_t| \sim 1$ it is assumed that

$$\phi = \frac{A_0}{\sqrt{\sigma}}\psi(r,\theta;X)\exp\left(\frac{\mathrm{i}}{\varepsilon}\int_{X_t}^{X}\frac{\omega U_0}{C_0^2-U_0^2}\mathrm{d}X'\right) \times T\exp\left(-\frac{\mathrm{i}}{\varepsilon}\int_{X_t}^{X}\frac{\omega C_0\sigma}{C_0^2-U_0^2}\mathrm{d}X'\right). \quad (3.16)$$

As with the single turning point case, in general there may be a finite number of propagating modes ($A_i \neq 0$) and infinitely many cut-off modes ($A_i = 0$). Within this formulation only a single mode is considered, but it is important to note that other modes may exist within the duct. Indeed, this formulation does not in any way prohibit the existence of multiple modes, but instead exploits the fact that within this model energy transfer between neighbouring modes does not occur and energy per mode is fully conserved, and therefore if other modes were included within this formulation they would not be effected by the phenomenon occurring here. All other modes may be considered to be passive within this process, and therefore it is safe to not consider them in this calculation (but bearing in mind that they may still be there). Chapters 5 and 6 deal with the situation where there is an exchange of energy between neighbouring modes, and it will be shown in these chapters that this passive nature of neighbouring modes that is assumed here is not valid under certain

conditions involving high frequency.

Equations (3.15) and (3.16) constitute a set of approximate solutions to the governing equation (3.14) that are valid far from the turning point, referred to as the *outer solution*. Within the turning point region the outer solution breaks down, because the terms in equation (3.14) that were neglected when forming the outer solution are now dominant, and so within this turning point region another approximate equation is to be used.

The Inner Solution

In order to proceed it is necessary to analyse the behaviour of the reduced axial wavenumber σ in the turning point region. The Taylor expansion of σ^2 about the transition point X_t is given by

$$\sigma^2(X) = \sigma^2(X_t) + (X - X_t)\left(\frac{\mathrm{d}}{\mathrm{d}X}\sigma^2(X)\right)_{X_t} + \frac{(X - X_t)^2}{2!}\left(\frac{\mathrm{d}^2}{\mathrm{d}X^2}\sigma^2(X)\right)_{X_t} + O((X - X_t)^3). \tag{3.17}$$

However in this analysis the turning point X_t takes on a slightly different meaning because here the turning point is defined as the point in which the first derivative of σ^2 with respect to X vanishes, i.e.

$$\left(\frac{\mathrm{d}}{\mathrm{d}X}(\sigma^2)\right)_{X_t} = 0, \tag{3.18}$$

and is not necessarily a point where $\sigma^2(X) = 0$ at X_t, although the case where $\sigma^2(X_t) = 0$ is actually a special case that is dealt with by this analysis. Thus given that condition (3.18) holds, it follows that the second term in the Taylor expansion given by equation (3.17) is zero, which reduces the Taylor expansion

to

$$\sigma^2(X) = \sigma^2(X_t) + \frac{(X - X_t)^2}{2}\left(\frac{\mathrm{d}^2}{\mathrm{d}X^2}\sigma^2(X)\right)_{X_t} + O((X - X_t)^3). \qquad (3.19)$$

The Taylor expansions within the neighbourhood of the turning point of the mean flow quantities $U_0(X)$ and $C_0(X)$ and the radial wavenumber $\alpha(X)$ are

$$U_0(X) = U_0(X_t) + (X - X_t)U_0'(X_t) + \frac{1}{2}(X - X_t)^2 U_0''(X_t) + O((X - X_t)^3),$$
$$C_0(X) = C_0(X_t) + (X - X_t)C_0'(X_t) + \frac{1}{2}(X - X_t)^2 C_0''(X_t) + O((X - X_t)^3),$$
$$\alpha(X) = \alpha(X_t) + (X - X_t)\alpha'(X_t) + \frac{1}{2}(X - X_t)^2\alpha''(X_t) + O((X - X_t)^3).$$

Substitution of the above expansions into the expression for σ^2 given in equation (3.19) yields

$$\begin{aligned}\sigma^2(X) &= 1 - \frac{1}{\omega^2}\left((C_0^2(X_t) - U_0^2(X_t)\alpha^2(X_t))\right) \\ &- \frac{1}{\omega^2}\left(\frac{\mathrm{d}}{\mathrm{d}X}\left[(C_0^2(X) - U_0^2(X))\alpha^2(X)\right]\right)_{X_t}(X - X_t) \\ &+ O((X - X_t)^2).\end{aligned}$$

Comparing the above expression with the Taylor expansion for σ^2 given by (3.19), it should be noted that according to the assumption that the first derivative of σ^2 vanishes at the turning point, then local to the turning point there are no terms proportional to $X - X_t$ and therefore

$$\left(\frac{\mathrm{d}}{\mathrm{d}X}[\alpha^2(X)(C_0^2(X) - U_0^2(X))]\right)\Bigg|_{X_t} = 0,$$

which further implies that

$$\frac{C_0(X_t)C_0'(X_t) - U_0(X_t)U_0'(X_t)}{C_0^2(X_t) - U_0^2(X_t)} + \frac{\alpha'(X_t)}{\alpha(X_t)} = 0. \qquad (3.20)$$

One solution to the above equation that has an interesting physical signif-

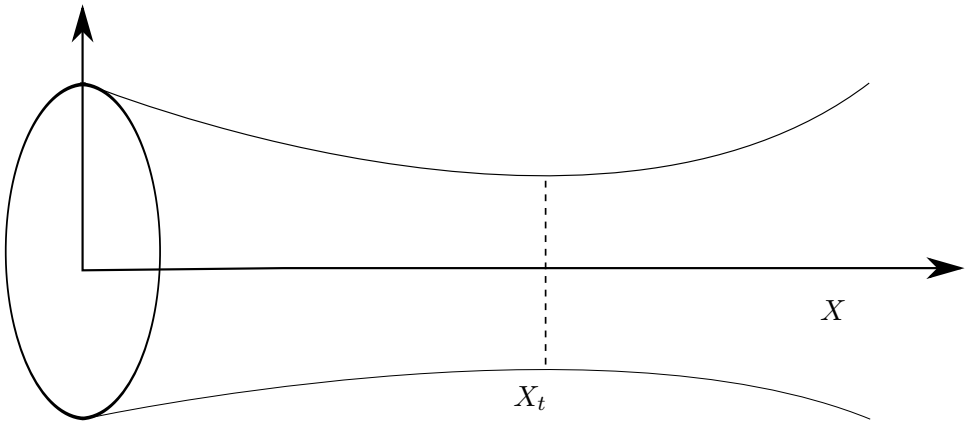

Figure 3.5: An Acoustic Duct that Contains a Choke Point

icance is when the point $X = X_t$ is a choke point, where a choke point is defined as a point within the duct where the derivatives of the mean flow terms with respect to X is zero. Figure 3.5 gives an example of a duct that contains a choke point. Suppose for example that a case of interest is one such that $U_0'(X_t) = 0$. Since the geometry at the point $X = X_t$ has zero gradient the cross flow component $\mathbf{V}_{\perp 0}$ must also be zero at this point. An intuitive way to see this is to note that if the axial mean flow is propagating from left to right then the mean flow must converge for $X < X_t$ near the choke point, so $\mathbf{V}_{\perp 0} < 0$, and as the mean flow passes through the choke point the axial mean flow diverges and so cross flow component must satisfy $\mathbf{V}_{\perp 0} > 0$ for $X > X_t$, and hence at the choke point one finds that $\mathbf{V}_{\perp 0}(X_t, r, \theta) = 0$. Given then that the cross flow component is zero at the choke point the cross-flow continuity equation (1.25) implies that

$$\left(\frac{\mathrm{d}}{\mathrm{d}X}\left(D_0 U_0\right)\right)_{X_t} = 0,$$

and therefore $D_0'(X_t) = 0$. It may also be seen that as the duct is locally stationary at the point X_t then in general $\alpha'(X_t) = 0$, which by (3.20) means that $C_0'(X_t) = 0$. Therefore to summarise, the following conditions hold at the choke point

$$U_0'(X_t) = C_0'(X_t) = \alpha_0'(X_t) = D_0'(X_t) = 0. \tag{3.21}$$

Hence using these mean flow conditions it may be seen that for $X = X_t$ all of the non parallel terms on the right hand side of the governing equation must be zero to leading order, as they all contain terms that are zero as a result of the geometry of the choke point. Using this knowledge regarding the choke point, the governing acoustic equation within the neighbourhood of the turning point can be reduced from what was presented in equation (3.14) to now give

$$\varepsilon^2 \left(1 - \frac{U_0^2}{C_0^2}\right) \frac{\partial^2 \phi}{\partial X^2} - \frac{2\mathrm{i}\varepsilon\omega U_0}{C_0^2} \frac{\partial \phi}{\partial X} + \left(\frac{\omega^2}{C_0^2} - \alpha^2\right) \phi = 0.$$

Analysing the terms in the reduced governing equation above indicates that when the (usually dominant) term becomes comparable to the second derivative term and behaves in a way that is predominantly quadratic in X, then a boundary layer in the variable X exists and can be defined by

$$X - X_t = \varepsilon^{\frac{1}{2}} \lambda_D^{-1} \xi,$$

where ξ is the boundary layer variable. The parameter λ_D is chosen for convenience and its exact value will be defined later.

Based on the knowledge of the form of the outer solution a WKB wave-like

inner solution is assumed in the form

$$\phi(X,r,\theta)=\chi(\xi)\psi(r,\theta;X)\exp\left(\frac{\mathrm{i}}{\varepsilon}\int_{X_t}^{X}\frac{\omega U_0(X')}{C_0^2(X')-U_0^2(X')}\mathrm{d}X'\right), \tag{3.22}$$

and substitution of the above WKB ansatz into the governing equation yields (after suppressing the exponential)

$$\left(\varepsilon\lambda_D^2\frac{\mathrm{d}^2}{\mathrm{d}\xi^2}\chi(\xi)+\frac{\omega^2C_0^2(X)\sigma^2(X)}{\left(C_0^2(X)-U_0^2(X)\right)^2}\chi(\xi)\right)\psi(r,\theta;X)=0 \tag{3.23}$$

In a manner similar to the single turning point case, as $\sigma^2(X)$ is known to be small one can approximate $\sigma^2(X)$ within the boundary layer by rewriting the Taylor expansion (3.19) in terms of the inner variable ξ, i.e.

$$\sigma^2(X)=\varepsilon\bar{\sigma}^2(X_t)+\frac{1}{2}\varepsilon\lambda_D^{-2}\xi^2\left(\frac{\mathrm{d}^2\sigma^2}{\mathrm{d}X^2}\right)_{X_t}+O(\varepsilon^{\frac{3}{2}}\xi^3),$$

where it has been assumed that $\sigma^2(X_t)\sim\varepsilon$ and thus allowing for the rescaling $\sigma^2(X_t)=\varepsilon\bar{\sigma}^2(X_t)$ for $\bar{\sigma}^2(X_t)\sim 1$. Substitution of the above expression for $\sigma^2(X)$ into equation (3.23) and equating leading order terms yields

$$\frac{\mathrm{d}^2}{\mathrm{d}\xi^2}\chi(\xi)+\frac{C_0^2(X_t)\omega^2}{(C_0^2(X_t)-U_0^2(X_t))^2}\left(\frac{1}{2\lambda_D^4}\left(\frac{\mathrm{d}^2}{\mathrm{d}X^2}\sigma^2(X)\right)_{X_t}\varepsilon\xi^2+\frac{\bar{\sigma}^2(X_t)}{\lambda_D^2}\right)=0. \tag{3.24}$$

At this point it is convenient to simplify matters by defining the quantity λ_D as

$$\lambda_D^4=\frac{2C_0^2(X_t)\omega^2}{(C_0^2(X_t)-U_0^2(X_t))^2}\left(\frac{\mathrm{d}^2}{\mathrm{d}X^2}\sigma^2(X)\right)_{X_t}\sim 1, \tag{3.25}$$

and note that since $\sigma^2(X_t)$ is a minimum point one must have

$$\left(\frac{\mathrm{d}^2}{\mathrm{d}X^2}\sigma^2\right)_{X_t}>0,$$

and thus it is clear that λ_D^4 must be a positive quantity. Now that λ_D is defined then define the following paramater a as

$$a=-\frac{\bar{\sigma}^2(X_t)C_0^2(X_t)\omega^2}{\lambda_D^2(C_0^2(X_t)-U_0^2(X_t))^2}=-\frac{\bar{\sigma}^2(X_t)}{2\left(\frac{\mathrm{d}^2\sigma}{\mathrm{d}X^2}\right)_{X_t}}\sim 1, \tag{3.26}$$

and now it may now be seen that the leading order equation is simply the well-known Weber equation [1]

$$\chi''(\xi) + \left(\frac{1}{4}\xi^2 - a\right)\chi(\xi) = 0.$$

Two linearly independent solutions to the Weber equation are the Parabolic Cylinder Functions [1], and are denoted $\mathrm{W}(a, \xi)$ and $\mathrm{W}(a, -\xi)$. Thus the general solution to the inner amplitude $\chi(\xi)$ is

$$\chi(\xi) = \tilde{A}\,\mathrm{W}(a, \xi) + \tilde{B}\,\mathrm{W}(a, -\xi),$$

where $\tilde{A}$ and $\tilde{B}$ are arbitrary constants of integration.

The Matching Procedure

Now that a general form for the outer solution has been found it is necessary to find an explicit form for this solution. This involves determining the values of the amplitudes $\tilde{A}$ and $\tilde{B}$, and the reflection and transmission coefficients R and T. As with the single turning point case this feat is achieved by performing an asymptotic matching of the outer and inner solutions. In order to match the inner and outer solutions it is necessary to find the limit of the outer solution in the limit as $X \to X_t$, and to match this with the inner solution in the limit as $\xi \to \pm\infty$. Careful balancing the two solutions in these limits will give the desired coefficients.

The matching procedure begins by analysing the behaviour of the outer solutions given by expressions (3.15) and (3.16) as $|X - X_t| \sim \varepsilon^{\frac{1}{2}}$. Suppose the

integral $\mathscr{I}$ is defined as

$$\mathscr{I} = \lim_{X \to X_t} \left(\int_{X_t}^{X} \frac{\omega C_0(X')\sigma(X')}{C_0^2(X') - U_0^2(X')} \mathrm{d}X' \right),$$

and then in order to evaluate this integral in the limit as $X \to X_t$ the following substitution involving the inner variable is used

$$X' - X_t = \varepsilon^{\frac{1}{2}} \lambda_D^{-1} \xi', \quad \Rightarrow \quad \mathrm{d}X' = \varepsilon^{\frac{1}{2}} \lambda_D^{-1} \mathrm{d}\xi',$$

and substituting this into the integral $\mathscr{I}$ yields

$$\mathscr{I} = \varepsilon^{\frac{1}{2}} \frac{\lambda^{-1} \omega C_0(X_t)}{C_0^2(X_t) - U_0^2(X_t)} \int_0^{\xi} \sigma(\xi') \mathrm{d}\xi'. \tag{3.27}$$

In order to evaluate the above integral term, Taylors theorem is once again utilised with the assumpton that σ^2 has zero derivative at the turning point, and so

$$\begin{aligned} \sigma^2(X) &= \varepsilon \bar{\sigma}^2(X_t) + \frac{1}{2} \varepsilon \lambda_D^{-2} \xi^2 \left(\frac{\mathrm{d}^2 \sigma^2}{\mathrm{d}X^2} \right)_{X_t} + O(\varepsilon^{\frac{3}{2}} \xi^3), \\ &= \frac{\varepsilon}{2\lambda_D^2} \left(\xi^2 + \eta^2 \right) \left(\frac{\mathrm{d}^2 \sigma^2}{\mathrm{d}X^2} \right)_{X_t} \end{aligned} \tag{3.28}$$

where η^2 has been defined for convenience and is given by

$$\eta^2 = -4a^2.$$

Recalling that it is the quantity σ that is required for the evaluation of the integral $\mathscr{I}$, taking the square root of (3.28) yields

$$\sigma(X) = \pm \frac{\sqrt{2} \varepsilon^{\frac{1}{2}}}{2\lambda_D} (\xi^2 + \eta^2)^{\frac{1}{2}} \sqrt{\left(\frac{\mathrm{d}^2 \sigma^2}{\mathrm{d}X^2} \right)_{X_t}}. \tag{3.29}$$

Substitution of the above into (3.27) causes many terms multiplying the integral to cancel yielding

$$\mathscr{I} = \pm \frac{\varepsilon}{2} \int_0^{\xi} \sqrt{\xi'^2 + \eta^2} \mathrm{d}\xi'.$$

The above integral is a standard integral that may be evaluated to give

$$\mathscr{I} = \pm\frac{\varepsilon}{4}\left(\xi\sqrt{\xi^2+\eta^2} + \eta^2\log\left[\xi+\sqrt{\xi^2+\eta^2}\right] - \eta^2\log\eta\right). \tag{3.30}$$

As far as the outer solution is concerned, for $X < X_t$ the above expression for $\mathscr{I}$ should be negative, and thus the negative solution is chosen. Similarly for the outer solution for $X > X_t$ the above integral should be positive, and thus for this region the positive solution is chosen.

In terms of matching the outer solution for $X < X_t$ as $X \nearrow X_t$, one then evaluates the asymptotic behaviour of the above expression in the limit as $\xi \to -\infty$, giving

$$\lim_{\xi\to-\infty}(\mathscr{I}) = -\varepsilon\zeta,$$

where a new spatial variable ζ is defined as

$$\zeta = \frac{1}{4}\xi^2 - a\log|\xi|.$$

Similarly for the outer solution for $X \searrow X_t$ finding the limit of $\mathscr{I}$ as $\xi \to \infty$ gives

$$\lim_{\xi\to\infty}\mathscr{I} = \varepsilon\zeta. \tag{3.31}$$

Also note that in order to approximate the outer solution as $X \to X_t$ it is required to find an approximation for the singular term $\sigma^{-\frac{1}{2}}$. Note from (3.25) that

$$\left(\frac{\mathrm{d}^2\sigma^2}{\mathrm{d}X^2}\right)_{X_t} = \frac{\lambda_D^4(C_0^2(X_t) - U_0^2(X_t))}{2C_0^2(X_t)\omega^2},$$

and substituting this into (3.28) and taking the appropriate power gives

$$\begin{aligned}\sigma^{-\frac{1}{2}}(X) &= \varepsilon^{-\frac{1}{4}}|\xi|^{-\frac{1}{2}}\left(1+\frac{\eta^2}{\xi^2}\right)^{-\frac{1}{4}}\sqrt{\left(\frac{C_0(X_t)\omega}{\lambda_D(C_0^2(X_t)-U_0^2(X_t))}\right)} \\ &= \varepsilon^{-\frac{1}{4}}|\xi|^{-\frac{1}{2}}\sqrt{\left(\frac{C_0(X_t)\omega}{\lambda_D(C_0^2(X_t)-U_0^2(X_t))}\right)}+O\left(\frac{1}{\xi^2}\right).\end{aligned}$$

Therefore the limiting behaviour of the outer solution for $X < X_t$ is

$$\begin{aligned}\phi \sim \frac{A_0(X_t)}{|\xi|^{\frac{1}{2}}\varepsilon^{\frac{1}{4}}}&\sqrt{\left(\frac{C_0(X_t)\omega}{\lambda_D(C_0^2(X_t)-U_0^2(X_t))}\right)}\psi(r,\theta;X_t) \\ &\times\left(e^{\mathrm{i}\zeta}+Re^{-\mathrm{i}\zeta}\right),\end{aligned}$$

and for the limiting behaviour of the outer solution for $X > X_t$, $X \searrow X_t$ this is given by

$$\phi \sim \frac{A_0(X_t)}{\xi^{\frac{1}{2}}\varepsilon^{\frac{1}{4}}}\sqrt{\left(\frac{C_0(X_t)\omega}{\lambda_D(C_0^2(X_t)-U_0^2(X_t))}\right)}\psi(r,\theta;X_t)\left(Te^{-\mathrm{i}\zeta}\right).$$

Now that the outer solution is understood in the limiting case it is now time to look at the asymptotics of the inner solution as $\xi \to \pm\infty$. If $\xi \to \infty$ then according to Abramowitz and Stegun the asymptotic approximation to $\mathrm{W}(a,\xi)$ to leading order is given by [1]

$$\mathrm{W}(a,\xi) \sim \sqrt{\frac{2k}{\xi}}\cos\left(\frac{1}{4}\xi^2 - a\ln\xi + \frac{1}{4}\pi + \frac{1}{2}\phi_2\right), \tag{3.32}$$

and in a similar way as $\xi \to \infty$

$$\mathrm{W}(a,-\xi) \sim \sqrt{\frac{2}{k\xi}}\sin\left(\frac{1}{4}\xi^2 - a\ln\xi + \frac{1}{4}\pi + \frac{1}{2}\phi_2\right), \tag{3.33}$$

where ϕ_2 is defined as

$$\phi_2 = \arg\left(\Gamma\left(\frac{1}{2}+\mathrm{i}a\right)\right), \tag{3.34}$$

and the constant k is given by

$$k = \sqrt{1+e^{2\pi a}} - e^{\pi a}, \quad \frac{1}{k} = \sqrt{1+e^{2\pi a}} + e^{\pi a},$$

and Γ is the complex Gamma Function [1], i.e

$$\Gamma(z) = \int_0^\infty t^{z-1}\,\mathrm{e}^{-t}\,\mathrm{d}t.$$

Suppose that a real number Θ is defined as

$$\Theta = \frac{1}{4}\pi + \frac{1}{2}\phi_2,$$

and therefore using the composite angle formula for cosine it is possible to say that as $\xi \to -\infty$

$$\begin{aligned}\chi(\xi) &\sim \cos\zeta\left(\tilde{A}\sqrt{\frac{2}{k|\xi|}}\sin\Theta + \tilde{B}\sqrt{\frac{2k}{|\xi|}}\cos\Theta\right)\\ &+ \sin\zeta\left(\tilde{A}\sqrt{\frac{2}{k|\xi|}}\cos\Theta - \tilde{B}\sqrt{\frac{2k}{|\xi|}}\sin\Theta\right),\end{aligned}$$

and in a similar manner one may use the composite angle formula for sine to say that as $\xi \to \infty$

$$\begin{aligned}\chi(\xi) &\sim \cos\zeta\left(\tilde{A}\sqrt{\frac{2k}{\xi}}\cos\Theta + \tilde{B}\sqrt{\frac{2}{k\xi}}\sin\Theta\right)\\ &+ \sin\zeta\left(-\tilde{A}\sqrt{\frac{2k}{\xi}}\sin\Theta + \tilde{B}\sqrt{\frac{2}{k\xi}}\cos\Theta\right).\end{aligned}$$

Thus balancing the outer solution as $X \nearrow X_t$ with the inner solution as $\xi \to -\infty$ gives

$$\begin{aligned}&\frac{A_0(X_t)}{|\xi|^{\frac{1}{2}}\varepsilon^{\frac{1}{4}}}\sqrt{\left(\frac{C_0(X_t)\omega}{\lambda_D(C_0^2(X_t)-U_0^2(X_t))}\right)}\left((1+R)\cos\zeta + \mathrm{i}(1-R)\sin\zeta\right)\\ &\sim \cos\zeta\left(\tilde{A}\sqrt{\frac{2}{k|\xi|}}\sin\Theta + \tilde{B}\sqrt{\frac{2k}{|\xi|}}\cos\Theta\right) + \sin\zeta\left(\tilde{A}\sqrt{\frac{2}{k|\xi|}}\cos\Theta - \tilde{B}\sqrt{\frac{2k}{|\xi|}}\sin\Theta\right).\end{aligned} \tag{3.35}$$

Similarly balancing the outer solution for $X > X_t, X \searrow X_t$ with the inner solution for $\xi \to \infty$ gives

$$\frac{A_0(X_t)}{\xi^{\frac{1}{2}}\varepsilon^{\frac{1}{4}}}\sqrt{\left(\frac{C_0(X_t)\omega}{\lambda_D(C_0^2(X_t)-U_0^2(X_t))}\right)}T\left(\cos\zeta - \mathrm{i}\sin\zeta\right)$$
$$\sim \cos\zeta\left(\tilde{A}\sqrt{\frac{2k}{\xi}}\cos\Theta + \tilde{B}\sqrt{\frac{2}{k\xi}}\sin\Theta\right) + \sin\zeta\left(-\tilde{A}\sqrt{\frac{2k}{\xi}}\sin\Theta + \tilde{B}\sqrt{\frac{2}{k\xi}}\cos\Theta\right). \tag{3.36}$$

Equating terms proportional to $\cos\zeta$ and $\sin\zeta$ in equation (3.35) yields

$$\Delta(1+R) = \tilde{A}(2k^{-1})^{\frac{1}{2}}\sin\Theta + \tilde{B}(2k)^{\frac{1}{2}}\cos\Theta, \tag{3.37}$$

$$\mathrm{i}\Delta(1-R) = \tilde{A}(2k^{-1})^{\frac{1}{2}}\cos\Theta - \tilde{B}(2k)^{\frac{1}{2}}\sin\Theta, \tag{3.38}$$

where Δ is given by

$$\Delta = \frac{A_0(X_t)}{\varepsilon^{\frac{1}{4}}}\sqrt{\left(\frac{C_0(X_t)\omega}{\lambda_D(C_0^2(X_t)-U_0^2(X_t))}\right)}.$$

Solving (3.37) and (3.38) to find $\tilde{A}$ and $\tilde{B}$ in terms of the unknown reflection coefficient R gives

$$\tilde{A} = \Delta(2k^{-1})^{-\frac{1}{2}}\left[(1+R)\sin\Theta + \mathrm{i}(1-R)\cos\Theta\right]$$

$$\tilde{B} = \Delta(2k)^{-\frac{1}{2}}\left[(1+R)\cos\Theta + \mathrm{i}(R-1)\sin\Theta\right].$$

Similarly for the right hand matching, equating terms proportional to $\cos\zeta$ and $\sin\zeta$ in equation (3.36) yields

$$\Delta T = \tilde{A}(2k)^{\frac{1}{2}}\cos\Theta + \tilde{B}(2k^{-1})^{\frac{1}{2}}\sin\Theta,$$

$$-\mathrm{i}\Delta T = -\tilde{A}(2k)^{\frac{1}{2}}\sin\Theta + \tilde{B}(2k^{-1})^{\frac{1}{2}}\cos\Theta,$$

and solving for $\tilde{A}$ and $\tilde{B}$ yields

$$\tilde{A} = \Delta T(2k)^{-\frac{1}{2}}\left[\cos\Theta + \mathrm{i}\sin\Theta\right], \tag{3.39}$$

$$\tilde{B} = \Delta T(2k^{-1})^{-\frac{1}{2}}\left[\sin\Theta - \mathrm{i}\cos\Theta\right]. \tag{3.40}$$

Equating the expressions for $\tilde{A}$ and $\tilde{B}$ and solving for R and T then finally yields for the reflection and transmission coefficients

$$R = \frac{k^2 - 1}{k^2 + 1} \exp(-2\mathrm{i}\Theta), \quad T = \frac{2\mathrm{i}k}{k^2 + 1} \exp(-2\mathrm{i}\Theta). \tag{3.41}$$

For both the reflection and transmission coefficients the magnitude denotes the degree to which the wavetrain is reflected or transmitted, and the argument specifies the phase shift that occurs as a result of the transition. Note also that $|R|^2 + |T|^2 = 1$, indicating that modal energy is entirely conserved throughout the process.

An interesting special case of the above is when $a = 0$, which constitutes to

$$\sigma^2(X_t) = \left(\frac{\mathrm{d}\sigma^2}{\mathrm{d}X}\right)_{X_t} = 0,$$

yielding for the reflection and transmission coefficients

$$R = \frac{\sqrt{2}}{2}\mathrm{i}, \quad T = \frac{\sqrt{2}}{2},$$

which means that precisely half of the modal energy reflects and at the turning point and the other half transmits beyond it. Interestingly enough, in this case the reflected mode undergoes a phase shift of $\pi/2$ and the transmitted mode does not undergo any phase shift, which is precisely the same as that observed for the single turning point case.

Single turning points are very likely to occur in aeroplane turbofan engines due to the shape of the duct, as the slowly constricting geometry means that some cut-on modes will inevitably cut off somewhere within the duct. Double

turning points can also occur within an annular duct due to the combined effect of the inner and outer wall radii. A double turning point is also likely to occur in a duct that contains a 'pinch' (i.e. one that constricts and then widens again shortly downstream), one such geometry being that of a de Laval nozzle, which is a type of nozzle widely found in steam turbines and rockets.

Discussion of Results

In order to demonstrate the nature of a mode that undergoes transition via a double turning point it is useful to look at some examples in which this type of transition occurs.

Consider the reduced axial wavenumber σ_n of a mode that is about to undergo transition via a double turning point as it propagates through an acoustic duct. That mode may undergo transition via a double turning point can be effected in one of two possible ways, either the mode σ becomes very close to zero (but never quite reaches it), or σ_n^2 just dips below zero. Guided by the special case highlighted for $a = 0$ at the end of the last section one would expect that in the first scenario (where $0 << \sigma_n^2(X_t) < 1$) the solution would exhibit a small partial reflection of the mode, and for the second case scenario (where $0 << |\sigma_n^2(X_t)| < 1$ and $\sigma_n^2(X_t) < 0$) one would expect the majority of the modal energy to be reflected with only a small amount being transmitted beyond the turning point.

In order to simulate some cases, define a three dimensional rectangular duct

as

$$x_{min} \leq x \leq x_{max}, \quad 0 \leq y \leq 1, \quad 0 \leq z \leq h(x),$$

where the wall function $h(x)$ is defined as

$$h(x) = h_{\text{step}} - b\,\text{sech}\,(cx)$$

where h_{step}, b and c are positive constants. In order to compare the values obtained from the numerical simulation with the values predicted by the asymptotic analysis it is necessary to establish a numerical value for ε. In all of the cases outlined in this section the value of ε may be estimated as the average gradient of the duct wall $h(x)$ between the points $x = X_t$ (i.e. the point at which the value of $h(x)$ is at a minimum), and some point x_1 which is local to X_t which has $x_1 > X_t$. A sensible value for x_1 should be one that gives a fair representation of the gradient throughout the part of the duct whose geometry is slowly varying and the transition is taking place. Thus x_1 is usually chosen as a value within the duct with $x_1 > 0$ such the the effects of the slowly varying geometry are just beginning to wear off. The average value of the gradient $\bar{h'}$ between $X_t = 0$ and x_1 may be approximated by noting that,

$$h'(x) = bc\,\text{sech}\,(cx)\tanh\,(cx),$$

and therefore $\bar{h'}$ is given by

$$\begin{aligned}\bar{h'} &= \frac{1}{x_1}\int_0^{x_1} h'(x)\mathrm{d}x = -\frac{1}{x_1}\left[b\,\text{sech}\,(cx)\right]_0^{x_1} \\ &= \frac{b}{x_1}\left[1 - \text{sech}\,(cx_1)\right],\end{aligned}$$

and thus ε will be approximated using

$$\varepsilon \simeq \frac{b}{x_1}\left[1 - \text{sech}\,(cx_1)\right], \tag{3.42}$$

for some suitably chosen point x_1.

The equation that is to be solved numerically using a finite difference scheme is

$$\Phi(X)\left(\chi_n''(x) + \frac{\bar{\omega}^2 C_0^2 \sigma_m^2}{(C_0^2 - U_0^2)^2}\chi_n(x)\right) = 0,$$

where $\chi_n(x)$ is the modal amplitude, σ_n behaves quadratically within the vicinity of the turning point, and Φ is the so-called slowly varying coefficient, given by

$$\Phi(X) = \sqrt{\frac{C_0(X)}{(C_0^2(X) - U_0^2(X))D_0(X)h(X)}}.$$

Full details of the finite difference method used to solve this system may be found in chapter 6 section 6.1. Details of how to compute the modal amplitudes, reflection and transmission coefficients and pressure may be found in chapter 6 section 6.1.1.

Case 1

In this case the duct geometry is defined with parameters $h_{\text{step}} = 0.985, b = 0.07$ and $c = 3$, i.e

$$h(x) = 0.975 - 0.07\,\text{sech}\,(3x),$$

where $-2.5 < x < 2.5$, and the flow is modelled as two dimensional flow with Helmholtz number $\omega = 10$. A single incident left running mode indexed by $n = 3$ is initialised with unit amplitude, so $\mathcal{A}_n = 1$ for $n = 3$ and incident amplitude zero for all other modes. A non-zero mean flow with $U(-\infty) = 0.1$ that propagates from left to right is also established. In this example, ε is estimated as the average gradient of the wall between $x = 0$ and $x = 1.2$, and

applying the necessary values to equation (3.42) gives $\varepsilon \simeq 0.07$ to two decimal places. The minimum value of σ^2 within the duct is equal to the value of σ^2 at the point $x = 0$, and this may be shown to be $\sigma^2(x_t) = -0.068$, which is clearly of the same order as ε as required for the asymptotic analysis to be valid.

The simulation code was run and the results obtained for the reflection and transmission coefficients are obtained and are compared against the results predicted by the asymptotic analysis of the double turning point case. Figure 3.6 shows the modal amplitude of the $n = 3$ mode as it propagates throughout the duct. It is interesting to compare this to the single turning point case discussed earlier. In this case there is a similarity to the single turning point case in that within the vicinity of the point X_t the mode exchanges energy with it's opposite running counterpart. However where this case differs from that of a single turning point is that the reflection is only a *partial* reflection of the mode's energy, as opposed to a total reflection, and the mode is able to continue propagating downstream with a finite non-zero amplitude that has reduced significantly as a result of the partial reflection. This is in contrast to the single turning point case where no energy can propagate beyond the turning point. Another interesting feature of this result is the nature of the resulting wave that is formed due to the reflection of the incident wave. Due to the fact that a small amount of the modal energy is transmitted beyond the turning point, the reflected wave has a slightly smaller amplitude than that of the incident mode, meaning that the resulting wave for $x < x_t$ is actually a *partial standing wave*, which consists of a stationary component and

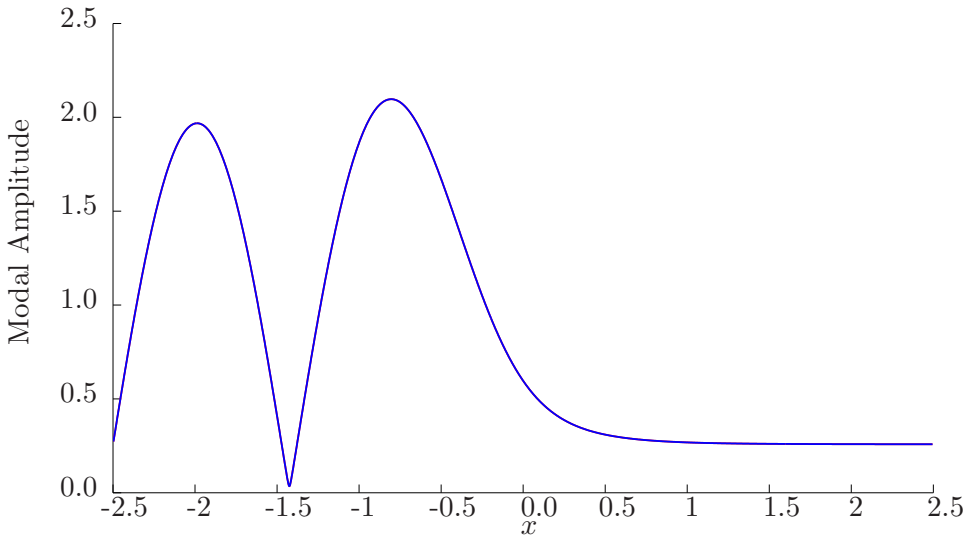

Figure 3.6: Modal amplitude variations throughout the duct for the incident mode in case 1, clearly exhibiting non zero amplitude for $x > x_t$ in contrast to the single turning point case.

a propagating component (see for example [4]). This explains why the modal amplitude of the resulting wave shown in figure 3.6 is never zero, a key component of a partial standing wave compared to a full standing wave.

It is useful to get an idea of exactly how much energy has exchanged with the left running mode, and an indication of this may be obtained by considering the values of the reflection and transmission coefficients obtained by the two models. Calculating the reflection coefficients predicted by the asymptotic analysis is precisely as described in the previous section. For the computational method, details of how these coefficients is achieved is described in chapter 6.

Considering first then the reflection coefficients: the asymptotic analysis de-

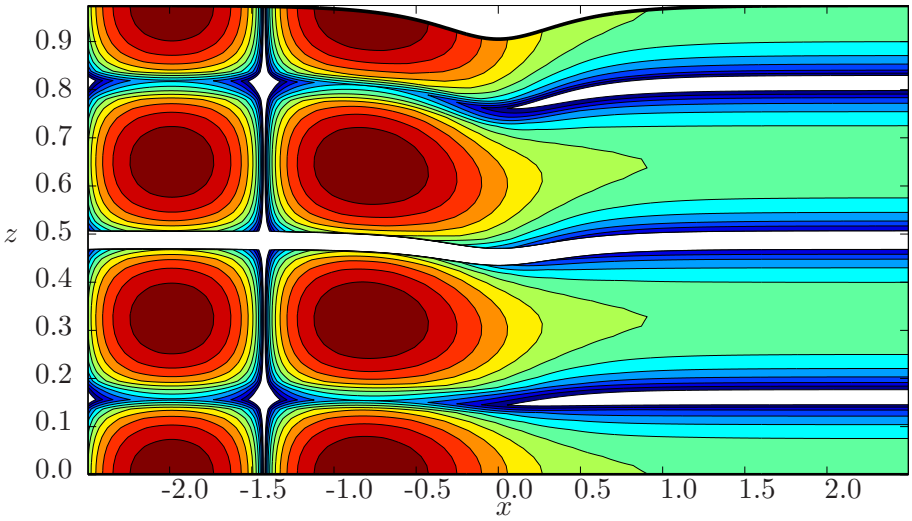

Figure 3.7: Acoustic pressure contours for case one, clearly exhibiting a region of low yet non-zero acoustic pressure for $x > x_t$ in contrast with the single turning point case.

scribed earlier in this chapter predicts that the theoretical value of the reflection coefficient is $|R| = 0.9630$, and this is in very good agreement with the value of the reflection coefficient obtained using the simulation code, which gives $|R| = 0.9580$, and so the absolute error between the two approximations is $O(10^{-3})$. For the transmission coefficient, the theoretical value predicted by the asymptotic analysis is $|T| = 0.2694$, and this is again in very good agreement with the result obtained from the numerical simulation, which was $|T| = 0.2868$. Figure 3.7 shows the acoustic pressure within the duct in this case, and it can be seen that regions of very high acoustic pressure exist for $x < x_t$ as a result of the partial standing wave, with relatively small disturbances when $x > x_t$.

Case 2

According to the multiple scales prediction, if $\sigma(X_t) = 0$ then precisely half the energy will continue to propagate downstream and the other half would be exchanged with the left running counterpart, and therefore for $\sigma^2(X_t) > 0$ the majority of the energy would continue to propagate downstream, with less than half the energy being handed over to the left running mode. In the previous, case due to the fact that the mode slightly cuts off within the transition region the majority of the modal energy is actually reflected with only a small proportion of the energy propagating downstream, which is very much in agreement with the theory predicted by the multiple scales analysis. Suppose then that the system were to be reconfigured such that the mode almost momentarily cuts off, but does not cut off exactly, or in other words $0 < \sigma^2(X_t) << 1$. Such a phenomenon can be modelled using the numerical code simply by altering the computational domain slightly. One such configuration is to define the duct wall $h(x)$ by

$$h(x) = 1.04 - 0.07\,\mathrm{sech}\,(3x),$$

and within this configuration the small parameter ε may approximated using (3.42) and is given by

$$\varepsilon \simeq \frac{0.6}{1.0}\,(1 - \mathrm{sech}\,(3)) = 0.054,$$

and the Helmholtz number and mean flow are given by $\omega = 10$ and $U(\infty) = 0.1$ as in the previous case. In this example, $\sigma_3^2(X_t) = 0.0681$, and therefore the mode does not fully cut off despite getting quite close, and $\sigma_3^2 \sim \varepsilon$ as required for the asymptotic analysis to be valid. Given that the mode does not completely cut off it is then expected that only a small amount of modal energy

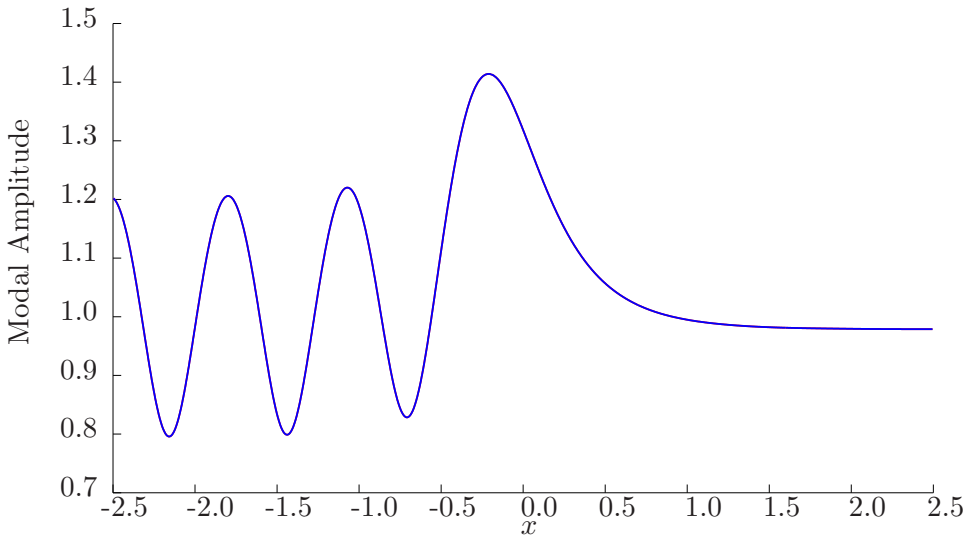

Figure 3.8: Modal amplitude variations throughout the duct for the incident mode in case 2, clearly exhibiting a much larger amplitude for $x > x_t$ than on case 1, but with partial standing wave properties for $x < x_t$.

is partially reflected within the turning point region, and that the majority of the modal energy passes through this region of the duct and propagates downstream. The results are run using the same numerical simulation scheme as in the previous case, and the results obtained for the reflection and transmission coefficients are compared to the results predicted using the asymptotic approach.

Figure 3.8 shows the plot of the amplitude profile for the mode in question. It can be seen from this plot that due to the slowly varying geometry the incident mode undergoes a partial reflection. The key point to note however is that due to the fact that σ_3 does not cut-off fully only a small amount of energy is reflected and the majority of the modal energy actually propagates downstream and transmits out of the duct. Similarly to the previous case a partial

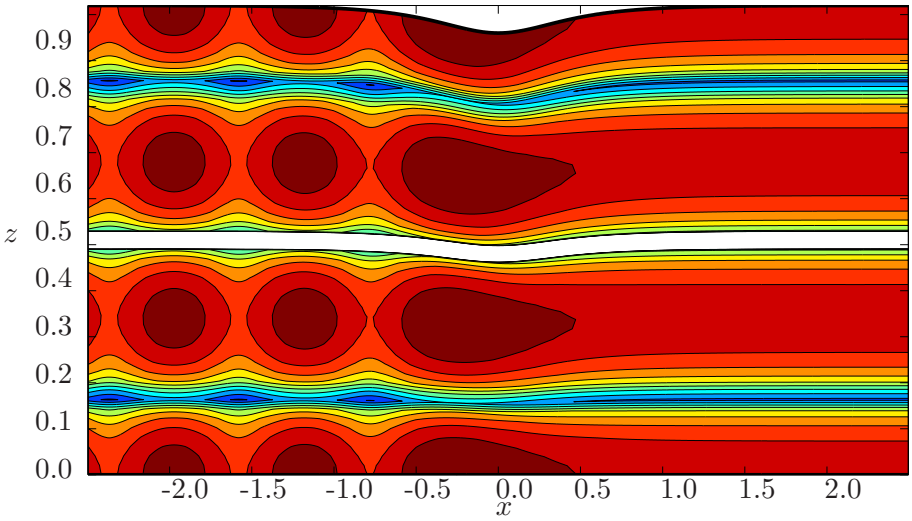

Figure 3.9: Acoustic pressure contours for case two, clearly exhibiting the effects of a small reflected mode for $x < x_t$.

standing wave is formed for $x < x_t$. However in this case the amplitude of the reflected wave is small compared to the amplitude of the incident mode, and the stationary component of the resulting wave is quite small meaning that the propagating component of the wave dominates. The effects of the stationary component can still be seen from the perturbations of the amplitude about it's mean position. The degree to which the mode reflects and transmits is indicated by the reflection and transmission coefficients which may be obtained using both the computational and asymptotic predictions. Once again the values obtained for $|R|$ and $|T|$ are in excellent agreement: For the reflection coefficient the asymptotic theory gives a value of $|R| = 0.2392$, and the computational result is $|R| = 0.2043$. For the transmission coefficient the asymptotic model gives a value of $|T| = 0.9710$, whereas the computational value is 0.9789, so in very good agreement with an absolute error to the order

of 10^{-3}.

Summary

This chapter focused on the subject of turning point analysis for the propagation of an acoustic mode. The subject of turning point analysis is of great importance in the case of hard-walled ducts whenever the geometry and mean flow of the duct vary in such a way that $\sigma^2 \to 0$.

If σ^2 behaves linearly, then this phenomenon may be modelled as a single turning point using the method of multiple scales, and the axial variations in amplitude within the vicinity of the turning point are given by Airy functions. The mode reflects at the turning point causing a standing wave to be formed within the duct. Details of this type of single turning point analysis are well understood as reported by Rienstra [47] and Ovenden [44]. It should also be noted that if the duct is lined with an impedance wall then a similar but partial reflection of the mode occurs, as reported by Ovenden [42].

A new result presented in this chapter deals with the case when σ^2 behaves quadratically within the vicinity of the turning point. The equations governing the axial amplitude within the inner region are Weber functions, leading to a partial transmission and reflection of the mode's energy, and the reflected wave causes a partial standing wave to be formed within the duct. It was also shown in this chapter that this inner solution may be asymptotically matched with the outer solution, leading to the analytic formulation of the

reflection and transmission coefficients. Some simulations were then run to model the double turning point phenomena using the numerical method outlined in chapter 6, and it was shown in both of the cases run that there is very good agreement between the reflection and transmission coefficient obtained by the two methods.

Chapter 4

Propagation of Acoustic Modes at High Frequency

In a recent paper [43], comparisons were made between multiple scales and finite element simulations of a single mode undergoing cut-on cut-off transition in a slowly varying hard walled annular duct. In most cases both sets of results were in remarkable agreement. However it was noted that if the Helmholtz number (frequency) was large and a mean flow was present inside the duct, the finite element results appeared to indicate that a significant degree of modal energy is scattered into neighbouring modes. Multiple scales simulations did not reveal any scattering because the multiple scales solution assumed that energy is conserved for each mode. In the same paper it was estimated that in order for modal scattering to occur, the Helmholtz number must be $O(\varepsilon^{-2})$, assuming that the mean flow is $O(1)$ as described in chapter 1.

Recall that a hard walled duct is a duct that does not allow any acoustic

energy to propagate through it's walls, so in other words a hard walled duct is one with infinite acoustic impedance $Z = \infty$. In the case of hard walls the Myers boundary condition (1.16) reduces to

$$\mathbf{v}.\mathbf{n} = 0 \quad \text{at} \quad \Sigma = 0. \tag{4.1}$$

where Σ describes the duct surface as described in Chapter 1. A consequence of this simplification means that the cross-sectional eigenvalues α are always real.

In simplistic terms, the numerical results obtained by the finite-element method presented in [43] indicate that if the frequency is large enough, the structure of the solution changes. However in this paper it is not entirely clear exactly how or exactly where this solution changes, although observations seem to suggest that scattering occurs within the vicinity of the turning point, and that neighbouring cut-on scattered modes may propagate beyond the turning point and out of the duct. If one is to study the scattering phenomenon using the method of multiple scales then it is necessary to go back to the asymptotics, beginning with the solution in the outer region for high frequency which is valid far from any turning points and to verify that a modal solution still exists. If a modal solution does still exist in the outer region, efforts can then be focused on describing how the solution structure within the inner region changes, solving for the inner region and then matching to the outer solution.

In this chapter, an explicit model of sound transmission through a slowly varying duct of rectangular cross-section with mean flow and high Helmholtz number is derived using the method of multiple scales, the purpose of which

is to enable one to understand the modal solution in the situation where scattering is expected. Then, in analysing that solution it is possible to determine under what conditions the solution breaks down.

Preliminaries

The Geometry

The problem domain here is a slowly-varying rectangular duct, and so a three-dimensional cartesian co-ordinate system (x, y, z) with unit vectors $\mathbf{e}_x$, $\mathbf{e}_y$ and $\mathbf{e}_z$ is established. The duct domain is denoted $\mathscr{D}$, with boundary $\partial\mathscr{D}$ and is given by

$$-\infty < x < \infty, \quad 0 \leq y \leq 1, \quad 0 \leq z \leq h(X), \qquad X = \varepsilon x,$$

where h is by assumption only dependent upon ε through εx. In this model, it is assumed for simplicity that $\mathscr{D}$ has a fixed unit length with respect the the y direction.

Recall from equation (1.15) that for the mean flow the wall of the duct is impermeable, and so in this geometry the boundary condition is

$$\mathbf{V}.\mathbf{n}_i = 0 \qquad \text{on} \quad \mathscr{D}, \quad i = 1, 2, 3, 4 \tag{4.2}$$

where each $\mathbf{n}_i$ denotes an outward pointing unit vector to $\partial\mathscr{D}$. The outward directed normal vector at the duct roof is given by

$$\mathbf{n}_1 = \frac{\mathbf{e}_z - \varepsilon h'(X)\mathbf{e}_x}{\sqrt{1 + \varepsilon^2 R_1'^2}},$$

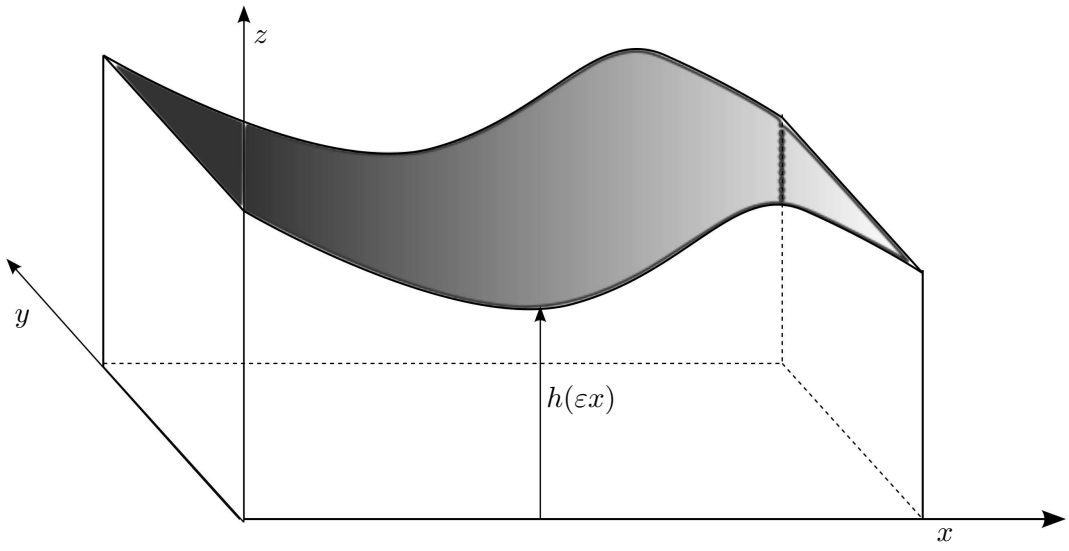

Figure 4.1: Sketch of the duct geometry

and the remaining outward normals are

$$\mathbf{n}_2 = -\mathbf{e}_y, \qquad \mathbf{n}_3 = -\mathbf{e}_z, \quad \mathbf{n}_4 = \mathbf{e}_y.$$

For the acoustic boundary condition this is easily derived from equation (4.1) and is given by

$$\nabla\phi.\mathbf{n}_i = 0 \qquad \text{on} \quad \partial\mathscr{D}, \quad i = 1, 2, 3, 4. \tag{4.3}$$

The Mean Flow and Acoustic Field

The cross sectional area of the duct is given by $\mathcal{A} = h(X)$ due to the unit duct width in the y direction, and so from equation (1.24) the axial component of the mean flow is given by

$$U_0(X) = \frac{F}{D_0(X)h(X)}. \tag{4.4}$$

Recall from (1.17) and (1.20) that the mean flow is axial to leading order with a small cross-wise component

$$\mathbf{V} = U\mathbf{e}_x + \mathbf{V}_\perp \quad \text{and} \quad \mathbf{V}_\perp = \varepsilon \mathbf{V}_{\perp 0} + O(\varepsilon^3). \tag{4.5}$$

By letting $\mathbf{V}_{\perp 0} = W_1(X, z)\mathbf{e}_z$, it is straightforward to show that by substituting (4.4) and (4.5) into the conservation of mass equation (1.5) one may deduce that

$$W_1 = \widetilde{W_1}(X)z + \widetilde{F}(X) \qquad \text{where} \qquad \widetilde{W_1}(X) = -\frac{1}{D_0}(D_0 U_0)_X. \tag{4.6}$$

for some as-yet unknown function $\widetilde{F}(X)$. However the mean flow boundary condition (4.2) dictates that

$$W_1 = 0 \qquad \text{at} \qquad z = 0, \tag{4.7}$$

and

$$W_1 = h'(X)U_0(X) \qquad \text{at} \qquad z = h. \tag{4.8}$$

Clearly substitution of (4.7) into (4.6) yields $\widetilde{F}(X) = 0$. For the boundary condition (4.8) it is simple to show that this boundary condition is automatically satisfied as substituting (4.4) into (4.6) gives

$$W_1(X, z) = \frac{Fh'(X)}{D_0(X)h^2(X)}z, \tag{4.9}$$

which can be further simplified by rearranging (4.4) to make D_0 the subject and substituting to the above to give

$$W_1(X, z) = \frac{h'(X)}{h(X)}U_0(X)z, \tag{4.10}$$

and therefore substituting $z = h$ into the above to obtain the value W_1 at the upperboundary of the duct gives

$$W_1(X, h) = h'(X)U_0(X),$$

which equals (4.8), and hence it has been shown that $W_1(X, z)$ satisfies this boundary condition.

4.1 The Modal Solution for $\omega \sim \varepsilon^{-2}$

For the acoustic field, recall from Chapter 1 equation (1.12) that the general wave equation is given by

$$D^{-1}\nabla.(D\nabla\phi) - (\mathrm{i}\omega + \mathbf{V}.\nabla)[C^{-2}(\mathrm{i}\omega + \mathbf{V}.\nabla)\phi] = 0, \tag{4.11}$$

which is subject to the simplified version of Myers' boundary condition (4.3).

Recall from earlier discussions that it is known that the acoustic frequency ω needs to be sufficiently high in order for modal scattering to be induced [43]. It is the aim of this chapter to obtain and understand how the outer solution behaves at high frequencies. Thus the following rescaling is introduced for the Helmholtz number

$$\omega = \varepsilon^{-2}\bar{\omega}, \tag{4.12}$$

where $\bar{\omega} \sim 1$. Substituting (4.12) into (4.11) then yields the governing wave equation for the acoustic potential ϕ at high Helmholtz number as

$$D^{-1}\nabla.(D\nabla\phi) - (\mathrm{i}\varepsilon^{-2}\bar{\omega} + \mathbf{V}.\nabla)[C^{-2}(\mathrm{i}\varepsilon^{-2}\bar{\omega} + \mathbf{V}.\nabla)\phi] = 0. \tag{4.13}$$

One may already see from this equation that there exists a term that has an order of magnitude $O(\varepsilon^{-4})$. In order to choose a suitable modal-type form, it is vital to determine how a balance with this very large term may be achieved.

The acoustic potential ϕ is assumed at present to consist of a single mode

(indexed by some positive integer j), of high wavenumber that is slowly varying with respect to X and is propagating in the X and z directions, whose amplitude varies slowly in X. This is equivalent to the WKB Ansatz

$$\begin{aligned} \phi &= \Phi_j(X,y,z)\exp\left(-\frac{\mathrm{i}}{\varepsilon^3}\int_{-\infty}^{X}\bar{\mu}_j(X';\varepsilon)\mathrm{d}X'\right) \\ &\times \exp\left(\frac{\mathrm{i}}{\varepsilon^2}\int_0^z \alpha_j(X,z';\varepsilon)\mathrm{d}z'\right), \end{aligned} \tag{4.14}$$

where $\bar{\mu}_j \sim 1$ is the axial-wavenumber, $\alpha_j \sim 1$ is the cross-sectional wavenumber, and $\Phi_j \sim 1$ is the modal amplitude, and that the acoustic potential $\phi \sim 1$ in this model. Note that the first order terms inside both exponentials have large orders of magnitude, $O(\varepsilon^{-3})$ for the axial mode and $O(\varepsilon^{-2})$ for the vertical mode, and hence the corresponding wavelengths are very small. These small wavelengths are required in order to achieve a balance between the terms in equation (4.13) once the derivatives are calculated and substituted. The leading order term inside the exponential corresponding to axial propagation is $O(\varepsilon^{-3})$ to leading order, with the extra factor of ε^{-1} being brought about as a direct consequence of using the slowly-varying model in X, giving $\varepsilon^{-1}\mathrm{d}X = \mathrm{d}x$

The model given by equation (4.14) assumes that a single mode is propagating in the positive X direction. The propagation in the positive X direction is given by $\mu_j > 0$, and consequently negative μ_j would correspond to propagation in the negative axial direction. The aim is to seek a solution in which there there is no interaction between individual modes, and thus it is sufficient to solve the problem for just one single mode. Once the solution is known for one mode, the solution for any given mode becomes clear, and therefore a full solution that consists of potentially infinitely many modes can then be

obtained via a summation of the individual modes, due to the linearity of the leading order problem.

In calculating the necessary derivatives of ϕ from equation (4.14) one obtains (surpressing the exponential terms)

$$\begin{aligned}
\phi_x &= -\frac{\mathrm{i}}{\varepsilon^2}\bar{\mu}_j\Phi_j + \frac{\mathrm{i}}{\varepsilon}\Phi_j\int_0^z \frac{\partial\alpha_j}{\partial X}\mathrm{d}z' + \varepsilon\frac{\partial\Phi_j}{\partial X}, \\
\phi_{xx} &= -\frac{1}{\varepsilon^4}\bar{\mu}^2\Phi_j + \frac{2}{\varepsilon^3}\bar{\mu}_j\Phi_j\int_0^z \frac{\partial\alpha_j}{\partial X}\mathrm{d}z' - \frac{1}{\varepsilon^2}\left(\int_0^z \frac{\partial\alpha_j}{\partial X}\mathrm{d}z'\right)^2\Phi_j \\
&- \frac{\mathrm{i}}{\varepsilon}\left(\frac{\partial\bar{\mu}_j}{\partial X}\Phi_j + 2\bar{\mu}_j\frac{\partial\Phi_j}{\partial X}\right) + O(1), \\
\phi_z &= \frac{\mathrm{i}}{\varepsilon^2}\alpha_j\Phi_j + \frac{\partial\Phi_j}{\partial z}, \\
\phi_{zz} &= -\frac{1}{\varepsilon^4}\alpha_j^2\Phi_j + \frac{1}{\varepsilon^2}\mathrm{i}\left(\Phi_j\frac{\partial\alpha_j}{\partial z} + 2\alpha_j\frac{\partial\Phi_j}{\partial z}\right) + \frac{\partial^2\Phi_j}{\partial z^2}, \\
\phi_{xz} &= \frac{1}{\varepsilon^4}\alpha_j\bar{\mu}_j\Phi_j - \frac{1}{\varepsilon^3}\alpha_j\Phi_j\int_0^z \frac{\partial\alpha_j}{\partial X}\mathrm{d}z' - \frac{\mathrm{i}}{\varepsilon^2}\bar{\mu}_j\frac{\partial\Phi_j}{\partial z} \\
&+ \frac{\mathrm{i}}{\varepsilon}\left(\frac{\partial\Phi_j}{\partial z}\int_0^z \frac{\partial\alpha_j}{\partial X}\mathrm{d}z' + \Phi_j\frac{\partial\alpha_j}{\partial X} + \alpha_j\frac{\partial\Phi_j}{\partial X}\right) + O(\varepsilon). \qquad (4.15)
\end{aligned}$$

It may now be seen from the above expressions that a balance with the large ω^2 term in the governing wave equation equation (4.13) may be achieved through the second derivatives.

The wavenumber and amplitude functions are then expressed via a Poincaré expansion

$$\alpha_j = \alpha_{j0}(X) + \varepsilon\alpha_{j1}(X,z) + \varepsilon^2\alpha_{j2}(X,z) + \varepsilon^3\alpha_{j3}(X,z) + O(\varepsilon^4), \qquad (4.16)$$

$$\bar{\mu}_j = \mu_{j0}(X) + \varepsilon\mu_{j1}(X) + \varepsilon^2\mu_{j2}(X) + \varepsilon^3\mu_{j3}(X) + O(\varepsilon^4), \qquad (4.17)$$

$$\Phi_j = \Phi_{j0}(X) + \varepsilon^3\Phi_{j3}(X,z) + O(\varepsilon^4). \qquad (4.18)$$

In this formulation, the variation of ϕ in X is being described using two separate functions, Φ_j and $\bar{\mu}_j$. In attempting to find a solution, a certain non-

uniqueness occurs between Φ_j and $\bar{\mu}_j$ due to the fact that there are a total of two functions with only one equation to determine them. One is therefore at liberty to choose either one of these functions, or any relation between them, as one so wishes [21]. For matters of convenience in this formulation, Φ_{j0} has been chosen to represent the leading order amplitude of the function, but we note that due to this non-uniqueness property of the WKB method this is not the only option. For example an equivalent problem could be solved by setting $\Phi_{j0} = 1$ and allow the amplitude to be determined by some imaginary part of μ_{j0}.

The function Φ_{j3} has been left within to aid in determining the solvability condition, which is a condition that allows the leading order amplitude Φ_{j0} to be determined.

Formulating the appropriate boundary conditions

It will be shown in this section that for a given μ_{j0}, two valid choices of α_{j0} exist i.e. $\alpha_{j0} = \pm|\alpha_{j0}|$. The positive choice corresponds to a mode propagating in the negative z direction and the negative choice corresponds to a mode propagating in the positive z direction. Whether the positive or negative choice is made, each subsequent α_{ji} (for $i = 1, 2, 3$) will consist of one part that changes sign depending on the choice of α_{j0}, and one part whose sign remains fixed regardless of the choice of α_{j0}. Therefore let the part of each α_{ji} whose sign remains fixed regardless of the choice of α_{j0} be denoted α_{ji}^F, and let the part that changes sign depending upon the choice of α_{j0} be denoted

α_{ji}^V. The cross sectional wavenumber can then be written as

$$\alpha = \pm\alpha_{j0} + \sum_{i=1}^{3} \varepsilon^i \left(\alpha_{ji}^F \pm \alpha_{ji}^V\right) + O(\varepsilon^4). \tag{4.19}$$

with $\alpha_{j0} > 0$. Note that the above expression sums both the positive and negative modes propagating in z, and therefore using the well-known polar identity

$$\cos\theta \equiv \frac{e^{\mathrm{i}\theta} + e^{-\mathrm{i}\theta}}{2},$$

the expression for ϕ can be written in a way that involves a cosine term in z, which gives

$$\begin{aligned} \phi &= 2\Phi_0(X)\cos\left(\frac{1}{\varepsilon^2}\int_0^z \left(\alpha_{j0} + \sum_{i=1}^{3}\varepsilon^i\alpha_{ji}^V\right)\mathrm{d}z'\right) \\ &\times \exp\left(\frac{\mathrm{i}}{\varepsilon^2}\int_0^z \left(\sum_{i=1}^{3}\varepsilon^i\alpha_{ji}^F\right)\mathrm{d}z'\right)\exp\left(-\frac{\mathrm{i}}{\varepsilon^3}\int_{-\infty}^{X}\bar{\mu}(X';\varepsilon)\mathrm{d}X'\right) \\ &+ O(\varepsilon^3), \end{aligned} \tag{4.20}$$

and as the amplitude Φ_{j0} is valid only up to a certain constant coefficient, for the sake of convention it is useful to re-define Φ_{j0} as $\Phi_0 := 2\Phi_{j0}$, in which case ϕ may be expressed as

$$\begin{aligned} \phi &= \Phi_0(X)\cos\left(\frac{1}{\varepsilon^2}\int_0^z \left(\alpha_{j0} + \sum_{i=1}^{3}\varepsilon^i\alpha_{ji}^V\right)\mathrm{d}z'\right) \\ &\times \exp\left(\frac{\mathrm{i}}{\varepsilon^2}\int_0^z \left(\sum_{i=1}^{3}\varepsilon^i\alpha_{ji}^F\right)\mathrm{d}z'\right)\exp\left(-\frac{\mathrm{i}}{\varepsilon^3}\int_{-\infty}^{X}\bar{\mu}(X';\varepsilon)\mathrm{d}X'\right) \\ &+ O(\varepsilon^3). \end{aligned} \tag{4.21}$$

The first partial derivative of ϕ with respect to z can be calculated from (4.21) and is given by

$$\begin{aligned}\frac{\partial\phi}{\partial z} &= \varepsilon^{-2}\Phi_{j0}(X)\left\{\mathrm{i}\left(\sum_{i=1}^{3}\varepsilon^i\alpha_{ji}^F\right)\cos\left(\frac{1}{\varepsilon^2}\int_0^z\left(\alpha_{j0}+\sum_{i=1}^{3}\varepsilon^i\alpha_{ji}^V\right)\mathrm{d}z'\right)\right.\\ &- \left.\left(\alpha_{j0}+\sum_{i=1}^{3}\varepsilon^i\alpha_{ji}^V\right)\sin\left(\frac{1}{\varepsilon^2}\int_0^z\left(\alpha_{j0}+\sum_{i=1}^{3}\varepsilon^i\alpha_{ji}^V\right)\mathrm{d}z'\right)\right\}\\ &\times \exp\left(\frac{\mathrm{i}}{\varepsilon^2}\int_0^z\left(\sum_{i=1}^{3}\varepsilon^i\alpha_{ji}^F\right)\mathrm{d}z'\right)\exp\left(-\frac{\mathrm{i}}{\varepsilon^3}\int_{-\infty}^{X}\bar{\mu}(X';\varepsilon)\mathrm{d}X'\right)\\ &+ \ldots. \end{aligned} \tag{4.22}$$

Recall that the lower boundary condition in z is

$$\frac{\partial\phi}{\partial z}=0 \qquad \text{at} \qquad z=0, \tag{4.23}$$

which is obtained directly from the simplified version of Myers' condition (4.3). The leading order equation (4.21) clearly satisfies this boundary condition because there is only one term within the curley brackets in (4.22) valid at leading order, and this term is always zero when $z=0$ which in turn makes the entire derivative zero. For higher orders there are two terms in the curley bracket have an effect on the derivative, and via inspection of (4.22) one can see that this boundary condition is satisfied only if $\alpha_{ji}^F=0$ when $z=0$. It is in fact true that $\alpha_{ji}^F=0$ when $z=0$, and will be systematically shown later in this section.

The boundary condition at the upper wall is

$$\phi_z=\varepsilon h'\phi_x \qquad \text{on} \qquad z=h, \tag{4.24}$$

and substitution of (4.21) into (4.24) after some simplifications yields

$$\tan\left(\varepsilon^{-2}\theta(X)\right)=\frac{\mathrm{i}\varepsilon}{\alpha_{j0}}\left(\mu_{j0}h'+\alpha_{j1}^F(z=h)\right) \tag{4.25}$$

where

$$\theta(X) = \int_0^{h(X)} \alpha_j(X, z'; \varepsilon) \mathrm{d}z'.$$

Equation (4.25) has the solution

$$\theta = \varepsilon^2 n\pi + \frac{\mathrm{i}\varepsilon^3}{\alpha_{j0}} \left(\mu_{j0} h' + \alpha_{j1}^F(z = h)\right) \quad \text{for} \quad n \in \mathbb{Z}, \tag{4.26}$$

where n must be a large integer so that $\varepsilon^2 n \sim 1$ in order to satisfy the upper boundary condition. Balancing terms in the above equation gives the following conditions on α_{j0} and α_{ji} for $i = 1, 2, 3$:

$$\alpha_{j0} = \frac{N\pi}{h}, \tag{4.27}$$

$$\int_0^h \alpha_{j1}^V \mathrm{d}z' = 0, \tag{4.28}$$

$$\int_0^h \alpha_{j2}^V \mathrm{d}z' = 0, \tag{4.29}$$

$$\int_0^h \alpha_{j3}^V \mathrm{d}z' = \frac{\mathrm{i}}{\alpha_{j0}} \left(\mu_{j0} h' + \alpha_{j1}^F(z = h)\right). \tag{4.30}$$

where $n = \varepsilon^{-2} N$, and N is not necessarily an integer.

At this stage the boundary condition on α_{j3}^V seems peculiar as at first glance it appears to imply that α_{j3}^V may be complex, and if α_{j3}^V were complex that would imply that there exists a small exponential growth or decay in the z direction. A consequence of this would be that there would be an exponentially growing or decaying term that is not expected in this modal solution. However although this may seem the case at this stage, it will be shown on page 124 that in fact $\alpha_{j1}^F(z = h) = -\mu_{j0} h'$ and therefore

$$\int_0^h \alpha_{j3}^V dz' = 0. \tag{4.31}$$

In the following calculation, a dispersion relation relating μ_{ji} and α_{ji}^V is derived at each order, and applying the appropriate boundary condition on α_{ji}^V will

always give an expression for μ_{ji}. The phase variation component α_{ji}^F is usually determined immediately.

The Leading Order $O(\varepsilon^{-4})$ problem

Substitution of (4.21) into (4.13) and balancing all terms proportional to ε^{-4} yields the leading order equation as

$$\left(\frac{\bar{\omega}^2}{C_0^2} - \frac{2\bar{\omega}\mu_{j0}U_0}{C_0^2} + \frac{\mu_{j0}^2U_0^2}{C_0^2} - \mu_{j0}^2 - \alpha_{j0}^2\right)\Phi_{j0} = 0, \tag{4.32}$$

and since it is a non-trivial solution that is being sought, $\Phi_{j0} \neq 0$, which gives rise to the dispersion relation

$$\alpha_{j0}^2 = \frac{\bar{\omega}^2}{C_0^2} - \frac{2\bar{\omega}\mu_{j0}U_0}{C_0^2} + \frac{\mu_{j0}^2U_0^2}{C_0^2} - \mu_{j0}^2 \tag{4.33}$$

and note that there are two choices for α_{j0} for given an initial μ_{j0}, one positive and one negative. In a similar fashion as before, the reduced axial wavenumber σ_{j0} is defined as

$$\sigma_{j0}^2 = 1 - (C_0^2 - U_0^2)\frac{\alpha_{j0}^2}{\bar{\omega}^2}, \tag{4.34}$$

and completing the square in (4.33) making μ_{j0} the subject yields

$$\mu_{j0} = -\frac{\bar{\omega}U_0}{C_0^2 - U_0^2} + \frac{\bar{\omega}C_0\sigma_{j0}}{C_0^2 - U_0^2}. \tag{4.35}$$

The first term on the right hand side of the above is a purely convective term and constitutes a leading order phase alteration that is present due to the presence of the mean flow. If mean flow were not present then this term would equal zero everywhere within the duct and so would not have any influence of the acoustic field. The second term describes how the axial propagation within the duct varies with X. The presence of σ_{j0} demonstrates that a mode can propagate in both positive and negative X directions depending on whether

positive or negative σ is chosen. The second term in the above expression is present whether mean flow exists or not. From (4.35) it is also possible to show the following properties hold for σ_{j0}:

$$\frac{U_0(\bar{\omega}-\mu_{j0}U_0)}{C_0^2}+\mu_{j0}=\frac{\bar{\omega}\sigma_{j0}}{C_0}, \tag{4.36}$$

$$\bar{\omega}-\mu_{j0}U_0=\bar{\omega}C_0\frac{C_0-U_0\sigma_{j0}}{C_0^2-U_0^2}, \tag{4.37}$$

and these properties will be used to simplify some expressions later on this work.

The First Order $O(\varepsilon^{-3})$ problem

Substitution of (4.21) into (4.13) and balancing all terms proportional to ε^{-3} yields the first order equation as

$$\begin{aligned}\alpha_{j1} &= \frac{1}{\alpha_{j0}}\Big(-\frac{\bar{\omega}U_0\mu_{j1}}{C_0^2}-\mu_{j0}\mu_{j1}+\frac{U_0^2}{C_0^2}\mu_{j0}\mu_{j1}+\frac{\bar{\omega}U_0}{C_0^2}\frac{\partial}{\partial X}\alpha_{j0}(X)z\\ &+ \mu_{j0}\frac{\partial}{\partial X}\alpha_{j0}(X)z-\frac{U_0^2\mu_{j0}}{C_0^2}\frac{\partial}{\partial X}\alpha_{j0}(X)z+\frac{\widetilde{W}_1}{C_0^2}\alpha_{j0}(\bar{\omega}-U_0\mu_{j0}).\Big)\end{aligned}$$

As suggested by equation (4.19) the wavenumber α_{j1} is decomposed into two parts as follows

$$\alpha_{j1}=\alpha_{j1}^F+\alpha_{j1}^V.$$

In order to determine which terms in equation (4.38) correspond to α_{j1}^F and which correspond to α_{j1}^V, one must analyse how the behaviour of α_{j1} varies depending upon whether positive or negative choice of α_{j0} is selected. On analysing (4.38) for both positive and negative α_{j0} it can be deduced that

$$\begin{aligned}\alpha_{j1}^V &= \frac{1}{\alpha_{j0}}\left(-\frac{\bar{\omega}U_0\mu_{j1}}{C_0^2}-\mu_{j0}\mu_{j1}+\frac{U_0^2}{C_0^2}\mu_{j0}\mu_{j1}\right)\\ &= -\frac{1}{\alpha_{j0}}\mu_{j1}\frac{\bar{\omega}\sigma_{j0}}{C_0}\end{aligned}$$

where σ_{j0} has been introduced by making use of equation (4.36).

In analysing equation (4.38) the following may be deduced for α_{j1}^F:

$$\begin{aligned}\alpha_1^F &= \frac{z}{\alpha_{j0}}\left(\frac{\bar{\omega}U_0}{C_0^2}\frac{\partial}{\partial X}\alpha_{j0}(X) + \mu_{j0}\frac{\partial}{\partial X}\alpha_{j0}(X) - \frac{U_0^2\mu_{j0}}{C_0^2}\frac{\partial}{\partial X}\alpha_{j0}(X)\right.\\ &+ \left.\frac{\widetilde{W}_1}{C_0^2}\alpha_{j0}(\bar{\omega}-\mu_{j0}U_0)\right)\end{aligned}$$

where it can now bee seen that $\alpha_{j1}^F = 0$ at $z = 0$, so that the boundary condition (4.23) is satisfied to first order. The above expression may be simplified using (4.36) to produce the following

$$\alpha_1^F = \frac{z}{\alpha_{j0}}\left(\frac{\bar{\omega}\sigma_{j0}}{C_0}\frac{\partial}{\partial X}\alpha_{j0}(X) + \frac{\widetilde{W}_1(X)\alpha_{j0}(\bar{\omega}-\mu_{j0}U_0)}{C_0^2}\right), \quad (4.38)$$

and further simplifications may be achieved by noting that

$$\frac{1}{\alpha_{j0}}\frac{\partial}{\partial X}\alpha_{j0}(X) = -\frac{N\pi h(X)h'(X)}{N\pi h^2(X)} = -\frac{h'(X)}{h(X)}.$$

Substituting the above expression, the expression for the cross flow velocity W_1 given by equation (4.10) and using the property of σ_{j0} given by (4.37), means that equation (4.38) reduces to the form

$$\begin{aligned}\alpha_1^F &= -z\frac{h'(X)}{h(X)}\left(\frac{\bar{\omega}C_0\sigma_{j0}}{C_0^2-U_0^2} - \frac{\omega U_0}{C_0^2-U_0^2}\right)\\ &= -z\frac{h'(X)}{h(X)}\mu_{j0}(X). \quad (4.39)\end{aligned}$$

From a physical standpoint the existence of a nonzero α_1^F represents a small (first order) correction to the phase variation in z of the mode as it propagates axially. Part of this small phase variation corresponds purely to the convective part of the flow, and part of it corresponds to the existence and subsequent variation of the mode propagating in the axial direction.

Clearly from (4.39) $\alpha_{j1}^F(z=h) = -\mu_{j0}h'(X)$ which using the boundary condition integral equation (4.30) implies that the boundary condition for α_{j3}^V is in fact exactly as required for a modal solution, i.e.

$$\int_0^{h(X)} \alpha_{j3}^V \mathrm{d}z' = 0. \tag{4.40}$$

Now applying the boundary condition (4.28) yields for α_{j1}^V and μ_{j1}

$$\alpha_{j1}^V = 0 \quad \Longrightarrow \quad \mu_{j1} = 0, \tag{4.41}$$

and thus there are no first order corrections to the axial variation, and there is no first order correction to the magnitude of the radial wavenumber.

The Second Order $O(\varepsilon^{-2})$ problem

In consideration of the third order problem one may deduce that

$$\begin{aligned}
\alpha_{j2} &= \frac{1}{2\alpha_{j0}}\Bigg(-(\alpha_{j1}^F)^2 - \frac{2\omega U_0\mu_{j2}}{C_0^2} - 2\mu_{j0}\mu_{j2} + \frac{2\mu_{j0}\mu_{j2}U_0^2}{C_0^2} \\
&+ \frac{2\omega U_0}{C_0^2}\int_0^z \frac{\partial}{\partial X}\alpha_{j1}^F(X,z')\mathrm{d}z' + 2\mu_{j0}\int_0^z \frac{\partial}{\partial X}\alpha_{j1}^F(X,z')\mathrm{d}z' \\
&- \frac{2U_0^2}{C_0^2}\mu_{j0}\int_0^z \frac{\partial}{\partial X}\alpha_{j1}^F(X,z')\mathrm{d}z' \\
&+ \frac{2W_1\alpha_{j1}^F\Omega}{C_0^2} - \left(\int_0^z \frac{\partial}{\partial X}\alpha_{j0}(X)\mathrm{d}z'\right)^2 + \frac{U_0^2}{C_0^2}\left(\int_0^z \frac{\partial}{\partial X}\alpha_{j0}(X)\mathrm{d}z'\right)^2 \\
&+ \frac{2U_0W_1\alpha_{j0}}{C_0^2}\left(\int_0^z \frac{\partial}{\partial X}\alpha_{j0}(X)\mathrm{d}z'\right) + \frac{W_1^2\alpha_{j0}^2}{C_0^2}\Bigg),
\end{aligned} \tag{4.42}$$

and in analysing the above for both positive and negative α_{j0} we see that in fact all of the above terms change sign. Hence $\alpha_{j2}^V = \alpha_{j2}$ and $\alpha_{j2}^F = 0$, and as this is true this means that the boundary condition (4.29) is satisfied to this order through an appropriate $\mu_{j2}(X)$.

The above expression may be simplified considerably using (4.27) and (4.39) as well as equation (4.36) to give (after some manipulation)

$$\begin{aligned}\alpha_{j2}^{V} &= \frac{\bar{\omega}\sigma_{j0}}{2\alpha_{j0}C_0}\left(-\frac{z^2(h')^2\mu_{j0}}{h^2}-\frac{2\mu_{j2}}{C_0}+2\int_0^{h(X)}\frac{\partial}{\partial X}\alpha_{j1}(X,z')\mathrm{d}z'\right)\\ &- \frac{1}{2\alpha_{0j}}\left(\frac{\mathrm{d}\alpha_{j0}}{\mathrm{d}X}\right)^2 z^2, \end{aligned} \tag{4.43}$$

which further simplifies to

$$\begin{aligned}\alpha_{j2}^{V} &= \frac{\bar{\omega}\sigma_{j0}}{2\alpha_{j0}C_0}\left(-\frac{z^2(h')^2\mu_{j0}}{h^2}-\frac{2\mu_{j2}}{C_0}-\frac{\mathrm{d}}{\mathrm{d}X}\left(\frac{h'(X)}{h(X)}\mu_{j0}\right)z^2\right)\\ &- \frac{1}{2\alpha_{0j}}\left(\frac{\mathrm{d}\alpha_{j0}}{\mathrm{d}X}\right)^2 z^2. \end{aligned} \tag{4.44}$$

Applying the boundary condition (4.29) to the above expression, the expression for $\mu_{j2}(X)$ is obtained as

$$\mu_{j2}(X) = -\frac{C_0}{6}\left((h(X)')^2\mu_{j0}+3h\frac{\mathrm{d}}{\mathrm{d}X}\left(\frac{h'\mu_{j0}}{h}\right)+\frac{C_0h^2}{\omega\sigma_{j0}}\left(\frac{\partial\alpha_{j0}}{\partial X}\right)^2\right). \tag{4.45}$$

The wavenumber $\mu_{j2}(X)$ constitutes a second order correction to the axial propagation, and it can be seen that this is dependent upon the duct geometry and how this geometry varies.

The Third Order $O(\varepsilon^{-1})$ problem

In consideration of the fourth order problem one may deduce that

$$
\begin{aligned}
0 = 2\Phi_0 \Bigg\{ & -\alpha_{j0}\alpha_{j3} - \alpha_{j1}\alpha_{j2} - \frac{\bar{\omega}U_0}{C_0^2}\mu_{j3} - \mu_{j0}\mu_{j3} - \mu_{j1}\mu_{j2} \\
& + \frac{U_0^2}{C_0^2}\left(\mu_{j0}\mu_{j3} + \mu_{j1}\mu_{j2}\right) + \frac{\bar{\omega}U_0}{C_0^2}\int_0^z \frac{\partial}{\partial X}\alpha_{j2}(X,z')\mathrm{d}z' \\
& + \mu_{j0}\int_0^z \frac{\partial}{\partial X}\alpha_{j2}(X,z')\mathrm{d}z' + \mu_{j1}\int_0^z \frac{\partial}{\partial X}\alpha_{j1}(X,z')\mathrm{d}z' \\
& + \mu_{j2}\int_0^z \frac{\partial}{\partial X}\alpha_{j0}(X)\mathrm{d}z' - \left(\frac{U_0^2}{C_0^2}\right)\Big[\mu_{j0}\int_0^z \frac{\partial}{\partial X}\alpha_{j2}(X,z')\mathrm{d}z' \\
& + \mu_{j1}\int_0^z \frac{\partial}{\partial X}\alpha_{j1}(X,z')\mathrm{d}z' + \mu_{j2}\int_0^z \frac{\partial}{\partial X}\alpha_{j0}(X)\mathrm{d}z'\Big] + \frac{W_1\bar{\omega}\alpha_{j2}}{C_0^2} \\
& - \frac{W_1U_0}{C_0^2}\Big(\alpha_{j0}\mu_{j2} + \alpha_{j1}\mu_{j1} + \alpha_{j2}\mu_{j0}\Big) - \int_0^z \frac{\partial}{\partial X}\alpha_{j0}(X)\mathrm{d}z'\int_0^z \frac{\partial}{\partial X}\alpha_{j1}(X,z')\mathrm{d}z' \\
& + \frac{U_0^2}{C_0^2}\int_0^z \frac{\partial}{\partial X}\alpha_{j0}(X)\mathrm{d}z'\int_0^z \frac{\partial}{\partial X}\alpha_{j1}(X,z')\mathrm{d}z' \\
& + \frac{U_0W_1}{C_0^2}\left(\alpha_{j0}\int_0^z \frac{\partial}{\partial X}\alpha_{j1}(X,z')\mathrm{d}z' + \alpha_{j1}\int_0^z \frac{\partial}{\partial X}\alpha_{j0}(X)\mathrm{d}z'\right) + \frac{W_1^2\alpha_{j0}\alpha_{j1}}{C_0^2}\Bigg\} \\
& + \mathrm{i}\Phi_{j0}\Bigg(\alpha_{1,z} + \frac{2\bar{\omega}U_0C_{0,X}}{C_0^3} - \frac{2U_0^2\mu_{j0}C_{0,X}}{C_0^3} - \frac{\mu_{j0}D_{0,X}}{D_0} + \frac{U_0U_{0,X}\mu_{j0}}{C_0^2} \\
& - \mu_{0,X} + \frac{U_0^2\mu_{0,X}}{C_0^2}\Bigg) + 2\mathrm{i}\Phi_{0,X}\left(-\frac{\bar{\omega}U_0}{C_0^2} - \mu_{j0} + \frac{U_0^2\mu_{j0}}{C_0^2}\right) \\
& + \left(\frac{\bar{\omega}^2}{C_0^2} - \frac{2\bar{\omega}\mu_{j0}U_0}{C_0^2} + \frac{\mu_{j0}^2U_0^2}{C_0^2} - \mu_{j0}^2 - \alpha_{j0}^2\right)\Phi_{j3}(X,z)
\end{aligned}
\tag{4.46}
$$

Notice that there are two terms that have been assigned as those responsible for the variation in z at this order, namely $\alpha_{j3}(X,z)$ and $\Phi_{j3}(X,z)$. Recall also that due to the flexibility offered by this redundancy in z at this order, one can choose α_3 to take any form as one wishes with the knowledge that $\Phi_{j3}(X,z)$ will then naturally make up the rest of the the z dependence to give the correct solution[21]. In this case (noting that the term multiplying Φ_3 is identically zero due the the dispersion relation given by equation (4.33)), α_{j3}

is chosen in such a way as to "mop up" all of the z-dependence (or real parts) in the above equation. Choosing α_3 in this way will cause all of the real parts in equation (4.46) to vanish, all that is left with are imaginary parts, which may then be equated to form a first order linear ordinary differential equation in $\Phi_{j0}(X)$. This differential equation in Φ_{j0} is the required solvability condition, and can easily be solved using integration factors, as shown in the next section. Explicit forms for α_{j3} and hence μ_{j3} can be obtained using similar methods to that shown for previous orders, but given the tedious nature of the algebra involved these solutions are omitted here.

In most applications of perturbation theory it is usually not common to see explicit expansions at third order due to the complexity of the algebra that follows, as can be seen in the above expressions. However in this case it was necessary to go to third order because it is at this order that the solvability condition is obtained.

Solvability Condition

Equating imaginary parts in equation (4.46) yields a first order linear ordinary differential equation in X for Φ_{j0}:

$$\Psi_j(X)\frac{\mathrm{d}\Phi_{j0}}{\mathrm{d}X} + \Theta_j(X)\Phi_{j0} = 0 \tag{4.47}$$

where $\Theta_j(X)$ and $\Psi_j(X)$ are given by

$$\begin{aligned}
\Theta_j(X) &= \frac{\partial}{\partial z}\alpha_1(X,z') + \frac{2\omega U_0(X)}{C_0^3(X)}\frac{\mathrm{d}}{\mathrm{d}X}\left(C_0(X)\right) - \frac{2U_0^2(X)\mu_{j0}}{C_0^3(X)}\frac{\mathrm{d}}{\mathrm{d}X}\left(C_0(X)\right) \\
&- \frac{\mu_{j0}(X)}{D_0(X)}\frac{\mathrm{d}}{\mathrm{d}X}\left(D_0(X)\right) + \frac{U_0(X)\mu_{j0}(X)}{C_0^2(X)}\frac{\mathrm{d}}{\mathrm{d}X}\left(U_0(X)\right) - \frac{\mathrm{d}}{\mathrm{d}X}\left(\mu_{j0}(X)\right) \\
&+ \frac{U_0^2(X)}{C_0^2(X)}\frac{\mathrm{d}}{\mathrm{d}X}\left(\mu_{j0}(X)\right), \\
\Psi_j(X) &= 2\left(-\frac{\omega U_0(X)}{C_0^2(X)} - \mu_{j0}(X) + \frac{U_0^2(X)\mu_{j0}(X)}{C_0^2(X)}\right).
\end{aligned}$$

In order to form a solvability condition the differential equation (4.47) is re-arranged as

$$\frac{\mathrm{d}\Phi_{j0}}{\mathrm{d}X} + \frac{\Theta_j(X)}{\Psi_j(X)}\Phi_{j0} = 0 \tag{4.48}$$

and solved using an integrating factor for $\Psi_j(X) \neq 0$ for all X in the domain of interest. Note that $\Psi_j(X) = 0$ corresponds directly to $\sigma_j = 0$ which is known to cause the solution to break down. It is straightforward from equations (4.36) and the expressions for $\alpha_1(X,z)$ and $W_1(X,z)$ to show that

$$\begin{aligned}
\Theta(X) &= \left(\frac{\bar{\omega}\sigma_{j0}(X)}{\alpha_{j0}(X)C_0(X)}\right)\frac{\partial}{\partial X}\alpha_{j0}(X) - \frac{\mathrm{d}}{\mathrm{d}X}\left(\frac{\bar{\omega}\sigma_{j0}(X)}{C_0(X)}\right) - \left(\frac{\bar{\omega}\sigma_{j0}}{C_0}\right)\frac{D_{0,X}}{D_0}, \\
\Psi(X) &= -2\left(\frac{\bar{\omega}\sigma_{j0}}{C_0}\right).
\end{aligned}$$

The integrating factor $\mathscr{I}$ is

$$\begin{aligned}
\mathscr{I} &= \exp\left(\int \frac{\Theta(X)}{\Psi(X)}\mathrm{d}X'\right) \\
&= \exp\left(\frac{1}{2}\int\left(-\frac{1}{\alpha_{j0}}\frac{\mathrm{d}}{\mathrm{d}X}\alpha_{j0}(X) + \frac{1}{\left(\omega\sigma C_0^{-1}\right)}\frac{\mathrm{d}}{\mathrm{d}X}\left(\omega\sigma C_0^{-1}\right) + \frac{1}{D_0}\frac{\mathrm{d}}{\mathrm{d}X}\left(D_0(X)\right)\right)\mathrm{d}X\right) \\
&= \exp\left(\frac{1}{2}\left(-\ln\left(\alpha_{j0}\right) + \ln\left(\frac{\omega\sigma}{C_0}\right) + \ln\left(D_0\right)\right)\right) \\
&= \sqrt{\frac{\bar{\omega}\sigma D_0}{C_0\alpha_{j0}}}
\end{aligned}$$

Hence the right hand side of equation (4.48) can be written as an exact derivative with respect to X, i.e.

$$\frac{\mathrm{d}}{\mathrm{d}X}\left(\Phi_{j0}\sqrt{\frac{\bar{\omega_{j0}}\sigma D_0(X)}{C_0(X)\alpha_{j0}}}\right) = 0 \tag{4.49}$$

and therefore

$$\left(\Phi_{j0}\sqrt{\frac{\bar{\omega}\sigma_{j0}(X)D_0(X)}{C_0(X)\alpha_{j0}(X)}}\right) = Q \tag{4.50}$$

where Q is a constant of integration, which results in the following expression of the amplitude function $\Phi_{j0}(X)$

$$\Phi_{j0}(X) = Q\sqrt{\frac{\alpha_{j0}(X)C_0(X)}{\bar{\omega}\sigma_{j0}(X)D_0(X)}}. \tag{4.51}$$

Note that had we normalised the eigenfunction as described in the first chapter the α_{j0} term would have been omitted from the final expression for Φ_{j0}. .

Summary

It has been demonstrated in this chapter that in fact a modal outer solution does indeed exist for large frequencies. When considering that acoustic scattering may occur within the duct, it is no longer sufficient for the outer solution to consider only one mode. A more general form of the solution must be considered if asymptotic matching between the inner and outer solution is to be attempted. The most general form of the outer solution is given as a summation over all possible modes, i.e.

$$\begin{aligned}
\phi &= \sum_{j=1}^{\infty} \Phi_j(X,z) \exp\left(-\frac{\mathrm{i}}{\varepsilon^3}\int_{-\infty}^{X} \bar{\mu}_j(X';\varepsilon)\mathrm{d}X'\right) \\
&\times \exp\left(\frac{\mathrm{i}}{\varepsilon^2}\int_0^z \alpha_j(X,z';\varepsilon)\mathrm{d}z'\right), \\
&= \sum_{j=1}^{\infty} \Phi_{j0} \exp\left(-\frac{\mathrm{i}}{\varepsilon^3}\int_{-\infty}^{X} \left(\bar{\mu}_{j0}(X') + \varepsilon^2\mu_{j2}(X) + \varepsilon^3\mu_{j3}(X)\right)\mathrm{d}X'\right) \\
&\times \exp\left(\frac{\mathrm{i}}{\varepsilon^2}\int_0^z \left(\varepsilon\alpha^F_{j1}(X,z') + \varepsilon^3\alpha^F_{j2}(X,z')\right)\mathrm{d}z'\right) \\
&\times \cos\left(\int_0^z \left(\alpha_{j0}(X) + \varepsilon^2\alpha^V_{j2}(X,z') + \varepsilon^3\alpha^V_{j3}(X,z')\right)\mathrm{d}z'\right) + \ldots \qquad (4.52)
\end{aligned}$$

where the various wavenumbers up to $O(\varepsilon^2)$ are given by

$$\begin{aligned}
\alpha_{j0}(X) &= \frac{N\pi}{h(X)} \quad \text{where} \quad n = \varepsilon^{-2}N \quad \text{for} \quad n \in \mathbb{Z}, \\
\mu_{j0}(X) &= -\frac{\bar{\omega}U_0}{C_0^2 - U_0^2} + \frac{\bar{\omega}C_0\sigma_{j0}}{C_0^2 - U_0^2}, \\
\Phi_{j0}(X) &= Q\sqrt{\frac{\alpha_{j0}(X)C_0(X)}{\bar{\omega}\sigma_{j0}(X)D_0(X)}}, \\
\alpha_{j1}^F(X,z) &= -z\frac{h'(X)}{h(X)}\mu_{j0}(X), \\
\alpha_{j2}^V(X,z) &= \frac{\bar{\omega}\sigma_{j0}}{2\alpha_{j0}C_0}\left(-\frac{z^2(h')^2\mu_{j0}}{h^2} - \frac{2\mu_{j2}}{C_0} - \frac{\mathrm{d}}{\mathrm{d}X}\left(\frac{h'(X)}{h(X)}\mu_{j0}\right)z^2\right) \\
&- \frac{1}{2\alpha_{0j}}\left(\frac{\mathrm{d}\alpha_{j0}}{\mathrm{d}X}\right)^2 z^2, \\
\mu_{j2}(X) &= \frac{C_0}{6}\left((h(X)')^2\mu_{j0} + 3h\frac{\mathrm{d}}{\mathrm{d}X}\left(\frac{h'\mu_{j0}}{h}\right) + \frac{C_0h^2}{\omega\sigma_{j0}}\left(\frac{\partial\alpha_{j0}}{\partial X}\right)^2\right).
\end{aligned}$$

Now that the outer solution in the case of high frequency is understood, the aim is to understand when this solution is not valid, and to revise the model within any critical regions where the above solution is known to fail. Numerical results have shown that acoustic scattering is expected within a critical region, and a thorough attempt to model the scattering will be tackled in part II.

Part II

Flow Induced Scattering of Acoustic Modes

Chapter 5

Asymptotic Analysis of Modal Scattering

As demonstrated in chapter 3 the phenomenon of cut-on cut-off transition of slowly varying acoustic modes is well understood. For the single turning point case it was demonstrated that at a point $X = X_t$ where the reduced axial wavenumber σ vanished, the mode exchanged energy with it's opposite running counterpart, leading to the formation of a standing wave within the duct. This type of interaction is the only form of modal interaction that has been successfully modelled using the multiple scales approach when cut-on cut-off transition is involved, but it is not the only mechanism by which a particular slowly varying acoustic mode may interact with another mode.

A comparative study between results obtained from analysing cut-on cut-off transition of acoustic modes with flow using both the multiple-scales and finite-element approaches was conducted by Ovenden, Eversman and Rien-

stra [43]. In their paper, the numerical results showed that for a high enough frequency, two different distinct modes (with axial wavenumbers σ_1 and σ_2 say) may interact and exchange energy with one other. One may see from study-

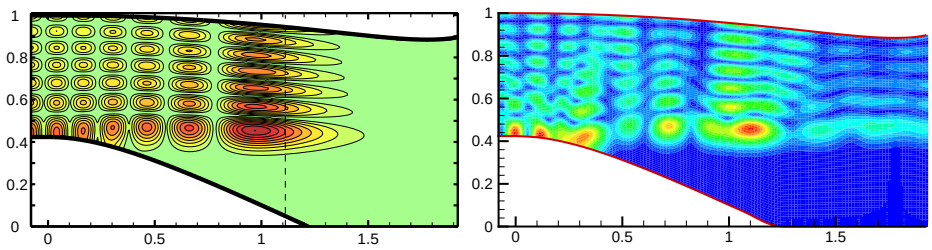

(a) Multiple Scales Solution (b) Finite Element Solution

Figure 5.1: Comparing multiple scales and finite element solutions for high frequency and mean flow

ing the results that there was very good agreement between the two different methods for lower frequencies both with and without mean flow. However significant differences between the result occurred whenever there was high Helmholtz number and mean flow, although there was good agreement whenever the Helmholtz number was high and there was no mean flow present. Case number 6 in the paper considered a slowly varying duct with circumferential eigenvalue $m = 20$, Mach number $M = 0.5$, $\omega = 44.4$ and $\mu = 7$. According to the multiple scales solution (shown in Figure 5.1(a)) there is a turning point at $X_t \sim 1.1$, and as a result of this turning point a standing wave is formed within the duct, meaning that no further propagation of acoustic energy beyond X_t occurs. The results produced by the finite element model (shown in figure 5.1(b)) differ from the results produced by the multiple scales method in that they give a clear indication of scattering of acoustic energy into neighbouring modes. In the finite element results, although there clearly is a reduction in

acoustic pressure beyond X_t modal pressure variations are present beyond X_t. The neighbouring ($n = 6$) mode has been excited and subsequently transmits acoustic energy out of the duct. At this point it appeared that there was no mechanism within the multiple scales solution to model such transition. According to Ovenden, Eversman and Rienstra [43], for scattering to occur sufficiently large ω and n are required, and an estimate for the magnitude of the frequency required was estimated as

$$\omega \simeq \varepsilon^{-2} \frac{2(\Delta\alpha)^3 C_0^2}{(\alpha'/\alpha)^2 (C_0^2 - U_0^2)^{\frac{1}{2}} \xi^3}, \tag{5.1}$$

where $\Delta\alpha$ is the difference between consecutive cross-sectional eigenvalues that tends to a constant for large n. The idea that ω must be sufficiently high in order for scattering to occur was the first indication of how to go about including the scattering phenomenon within the multiple scales solution.

Thus, armed with this idea that ω must be large, it is clear that in order to understand what is happening within the scattering region the frequency ω must be rescaled to a degree that is known to allow scattering to occur. Therefore if Ovenden *et al's* formulation is to be taken the frequency ω is to be rescaled as

$$\omega = \varepsilon^{-2} \bar{\omega},$$

where $\bar{\omega} \sim 1$ is a rescaled Helmholtz number. Recall that the generalised wave equation in this case of large frequency is given by equation (4.13), and writing

this equation in a way that is more convenient to work with one arrives at

$$\varepsilon^2\left(1-\frac{U_0^2(X)}{C_0^2(X)}\right)\frac{\partial^2\phi}{\partial X^2}-\varepsilon^{-1}\frac{2\mathrm{i}\bar{\omega}U_0(X)}{C_0^2}\frac{\partial\phi}{\partial X}+\nabla_\perp^2\phi+\varepsilon^{-4}\frac{\bar{\omega}^2}{C_0^2(X)}\phi$$
$$=-\varepsilon\Bigg[\frac{1}{D_0(X)}\frac{\mathrm{d}}{\mathrm{d}X}\left(D_0(X)\right)\frac{\partial\phi}{\partial x}-\mathrm{i}\varepsilon^{-2}\bar{\omega}U_0(X)\frac{\mathrm{d}}{\mathrm{d}X}\left(\frac{1}{C_0^2(X)}\right)\phi$$
$$-U_0(X)\frac{\mathrm{d}}{\mathrm{d}X}\left(\frac{U_0(X)}{C_0^2(X)}\right)\frac{\partial\phi}{\partial x}-2\mathrm{i}\varepsilon^{-2}\bar{\omega}\frac{1}{C_0^2(X)}(\mathbf{V}_{\perp 0}.\nabla_\perp\phi)$$
$$-2U_0(X)\frac{1}{C_0^2(X)}\left(\mathbf{V}_{\perp 0}.\nabla_\perp\frac{\partial\phi}{\partial x}\right)\Bigg]. \qquad (5.2)$$

For all of the cases of modal interaction dealt with in this thesis so far, the non-parallel terms on the right hand side of the wave equation have not yet come into play to leading order because they have been shown to have been too small to play a significant part in the phenomenon in question. However in this attempt to understand acoustic scattering it will be shown that some of the terms on the right hand side of the equation will in fact come into play here, and that these non-parallel terms that are important to leading order within the boundary layer are actually the source of scattering.

The first step is to find a suitable model for ϕ that is applicable within the scattering region. The situation here is different from those studied in chapter 3, and thus the left hand side and right hand side of equation (5.2) will be dealt with individually, the left hand side being dealt with first. For the non-parallel terms on the right hand side there are several terms that may contribute to the scattering effect, and the idea is to study each one individually, analysing it's order of magnitude within the scattering region in order to determine whether it is large enough to be comparable to the axial acceleration terms that exist on the left hand side.

It will be shown over the course of the next few sections that in order to deduce a model that gives acoustic scattering to leading order for every possible mode, several technical difficulties relating to the asymptotic analysis must be overcome. Several models will be attempted, each one building upon the knowledge gained from the last, until an equation describing acoustic scattering to leading order is achieved. Each stage in the development of the model introduces some new key information regarding the structure of the scattering phenomenon, and these developmental stages are also used in the next chapter to help explain results.

In section 5.1 the model will assume Ovenden et al's deduction that in order for scattering to occur the order of magnitude of the Helmholtz number is given by $\omega \sim \varepsilon^{-2}$. In formulating a model using this assumption the non-parallel terms responsible for the acoustic scattering will be revealed for the first time. It will also be shown that for $\omega \sim \varepsilon^{-2}$ the model requires some further refinement because the introduction of a Helmholtz number of this order of magnitude actually leads to an imbalance of the terms within the inner region. It will be shown in this section that this assumption for ω is actually an overestimate and in fact a smaller ω is required to achieve the desired balance.

Using the knowledge obtained in the previous section, section 5.2 then looks at the terms that are known to be active to leading order within the inner region and asks the question; what should the magnitude of the Helmholtz number be in order to achieve a balance between these leading order terms? Upon ask-

ing this question, a new estimate for the Helmholtz number is achieved and is given by $\omega \sim \varepsilon^{-\frac{1}{2}}$, leading to a refined model for ϕ within the inner region. However it is then shown that by considering the balance between the required terms alone only leads to weak form of modal scattering, where the incident mode experiences leading order modal scattering and the remaining modes only experience a weak form of scattering. The reason for this is because in only considering a balance between all of the required terms in the governing equation means that no consideration is given to whether or not two modes are close enough to each other to give scattering to leading order for every mode. Nonetheless the analysis performed here is useful as weak scattering is a phenomenon that has some physical significance and one could then exploit the fact that the scattering is weak to yield some useful analytical results.

The model is then further refined in section 5.4, where it is posed that not only must all of the important terms balance, but also each mode must lie close enough to every other mode in order to allow scattering to take place. In performing this third refinement leading order scattering for every mode is achieved.

Section 5.5, the final section in this chapter deals with the derivation an equation that describes the composite solution for modal scattering, an equation that has a solution that is valid throughout the entire duct. This composite equation can then be used to produce some results for modal scattering, and the details of these results is described in chapter 6

5.1 Formulation Using Ovenden et al's Assumptions for the Helmholtz Number

This section attempts to build a scattering model based upon the deduction made in Ovenden *et al's* paper [43] that in order for acoustic scattering to occur the order of magnitude of the frequency is given by $\omega \sim \varepsilon^{-2}$. It will be shown here that this is actually an overestimate for the order of magnitude of the frequency, but nonetheless this is enough to be able to identify the terms that are attributed to the scattering source. The problem of how to deal with this overestimate is tackled in section 5.2.

Forming the Appropriate Model for the Inner Region

Using the knowledge gained whilst studying the outer solution in chapter 4 it is then assumed that within the scattering region, the acoustic potential ϕ consists of a whole series of modes with wavenumbers of order $\sim \varepsilon^{-2}$ in the axial and radial directions that vary slowly in x. Let ξ be the axial boundary layer variable which is to be determined. For now it is assumed that the definition of ξ is of a form that is similar to that seen in the turning point analysis, i.e.

$$X - X_t = \varepsilon^{\varsigma}\xi,$$

for some constant ς. The axial amplitude within the turning point region varies on the same scale as ξ, and the rapidly oscillating convective part is unchanged from that of the outer solution. Thus for the inner solution the

following WKB type model for ϕ is assumed:

$$\phi = \sum_{j=1}^{\infty} \chi_j(\xi) \cos\left(\varepsilon^{-2} M \pi y\right) \cos\left(\varepsilon^{-2} \bar{\alpha}_j(X) z\right) \exp\left(\frac{\mathrm{i}}{\varepsilon^3} \int^X \frac{\bar{\omega} U_0}{C_0^2 - U_0^2} \mathrm{d}X'\right), \tag{5.3}$$

where $M \sim 1$ and $\bar{\alpha}_j \sim 1$, as suggested in chapter 4. It is important to note that $\phi \sim 1$ in the boundary layer, and that derivatives of ϕ with respect to x and z will indeed contain some very large terms. This solution assumes an infinite number of modes, although only a finite number of modes are cut-on.

For the turning point analysis studied earlier it was fine to consider only a single propagating mode. This is because although other modes (other than the mode undergoing cut-on cut-off transition) may be present within the acoustic realm, in general these modes are not effected by the energy transfer that takes place during turning point process. With the turning point analysis the mode that underwent cut-on cut-off transition at X_t exchanged energy with it's opposite running counterpart only, and therefore this was the only other mode that required consideration when describing this mechanism; no other modes were active in this process and therefore their consideration within the turning point analysis was not necessary. With the scattering mechanism however, it is necessary to assume that an incident mode that loses energy at the critical point X_t may interact with each and every other mode that exists, and hence every possible mode must be included in the formulation. In fact it will be shown in chapter 6 that when scattering takes place an interaction with the mean flow may also occur, in which case energy is not conserved within the modes.

The Boundary Layer

In this section the magnitude of the boundary layer width is derived by balancing various terms in the governing acoustic equation that are believed to be important within the scattering region. Once the form of the inner region has been obtained it is possible to then fully determine the terms on the left hand side of equation (5.2) that are involved in the scattering process to leading order.

Recall that the boundary layer variable ξ takes the form

$$X - X_t = \varepsilon^{\varsigma}\xi$$

where ς is a real constant that is to be determined. As with the turning point analysis the width of the boundary layer is determined by balancing the second order derivative in X with the term that is vanishing, and thus if this is the case then using equation (5.2) the following must be true in the boundary layer

$$\varepsilon^2\left(1-\frac{U_0^2}{C_0^2}\right)\frac{\partial^2\phi}{\partial X^2} \sim \left(\varepsilon^{-4}\frac{\bar{\omega}^2}{C_0^2} + +\frac{\partial^2}{\partial y^2}+\frac{\partial^2}{\partial z^2}\right)\phi. \tag{5.4}$$

From equation (5.3) it is simple to show that the derivatives in y and z are (supressing the exponential)

$$\frac{\partial^2\phi}{\partial y^2} = -\varepsilon^{-4}M^2\pi^2\sum_{j=1}^{\infty}\chi_j(\xi)\cos(\varepsilon^{-2}M\pi y)\cos(\varepsilon^{-2}\bar{\alpha}_j z), \tag{5.5}$$

$$\frac{\partial\phi}{\partial z} = -\varepsilon^{-2}\sum_{j=1}^{\infty}\bar{\alpha}_j\chi_j(\xi)\cos(\varepsilon^{-2}M\pi y)\sin(\varepsilon^{-2}\bar{\alpha}_j z), \tag{5.6}$$

$$\frac{\partial^2\phi}{\partial z^2} = -\varepsilon^{-4}\sum_{j=1}^{\infty}\bar{\alpha}_j^2\chi_j(\xi)\cos(\varepsilon^{-2}M\pi y)\cos(\varepsilon^{-2}\bar{\alpha}_j z). \tag{5.7}$$

As with the turning point analysis, one would expect that in order for modal scattering to occur a second order derivative of the amplitude in the axial

direction must be present in the leading order analysis, as this term would be the necessary acceleration term driving the scattering. Therefore one would expect there to be a χ'' term in the leading order formulation (where primes here denote a second order derivative with respect to ξ). Thus in computing this second order derivative one arrives at

$$\frac{\partial^2 \phi}{\partial X^2} = \sum_{j=1}^{\infty} \left(\varepsilon^{-2\varsigma} \chi_j'' + \cdots \right), \tag{5.8}$$

and so by substituting the expressions given by equations (5.7) and (5.8) into equation (5.4) yields

$$\varepsilon^{2-2\varsigma} \left(1 - \frac{U_0^2}{C_0^2} \right) \sum_{j=1}^{\infty} \left(\chi_j'' + \cdots \right) \sim \varepsilon^{-4} \sum_{j=1}^{\infty} \left\{ \frac{\bar{\omega}^2}{C_0^2} - M^2 \pi^2 - \bar{\alpha}_j^2(X) \right\} \chi_j(\xi). \tag{5.9}$$

As with the turning point analysis, the term in the curley brackets on the right hand side of (5.9) shrinks to the width of the boundary layer in the limit as $X \to X_t$. Therefore taking this into consideration, balancing the two terms in (5.9) one will yield

$$2 - 2\varsigma = -4 + \varsigma \qquad \Longrightarrow \qquad \varsigma = 2,$$

and hence the boundary layer variable may be expressed as

$$X - X_t = \varepsilon^2 \xi. \tag{5.10}$$

Now that the boundary layer variable has been established the influential terms in the left hand side of equation (5.2) may be fully analysed. First the required derivatives are computed, where it has been noted that because the boundary layer is very thin, the duct is locally parallel within the boundary layer, and so there is virtually no variation of the vertical modal eigenvalues

over such a short lengthscale and therefore the vertical eigenvalues $\bar{\alpha}_j(X)$ can be considered to be constant in the boundary layer. Computing the first derivative of ϕ with respect to X yields

$$\frac{\partial \phi}{\partial X} = \sum_{j=1}^{\infty} \left[\left(\varepsilon^{-1} \chi_j'(\xi) + \mathrm{i}\varepsilon^{-2} \frac{\bar{\omega} U_0}{C_0^2 - U_0^2} \chi_j(\xi) \right) \cos(\varepsilon^{-2} \bar{\alpha}_j z) \right] \times \exp\left(\frac{\mathrm{i}}{\varepsilon^3} \int^X \frac{\bar{\omega} U_0(X')}{C_0^2(X') - U_0^2(X')} \mathrm{d}X' \right), \tag{5.11}$$

and computing the second derivative yields

$$\frac{\partial^2 \phi}{\partial X^2} = \sum_{j=1}^{\infty} \left[\left(\varepsilon^{-2} \chi_j''(\xi) - \frac{\varepsilon^{-4} \bar{\omega}^2 U_0^2}{\left(C_0^2 - U_0^2\right)^2} \chi_j(\xi) + \frac{2\mathrm{i}\varepsilon^{-3} \bar{\omega} U_0}{C_0^2 - U_0^2} \chi_j'(\xi) \right) \cos(\varepsilon^{-2} \bar{\alpha}_j z) \right] \times \exp\left(\frac{\mathrm{i}}{\varepsilon^3} \int^X \frac{\bar{\omega} U_0(X')}{C_0^2(X') - U_0^2(X')} \mathrm{d}X' \right) + O\left(\frac{1}{\varepsilon} \right). \tag{5.12}$$

Substituting (5.11) and (5.12) into the left hand side of equation (5.2) yields to $O(\varepsilon^{-2})$ (after some simplifications),

$$\sum_{j=1}^{\infty} \left[\varepsilon^{-2} \left(1 - \frac{U_0^2}{C_0^2} \right) \chi_j''(\xi) + \frac{\varepsilon^{-4} \bar{\omega}^2 \sigma_{j0}^2}{(C_0^2 - U_0^2)^2} \chi_j(\xi) \right] \cos(\varepsilon^{-2} \bar{\alpha}_j z) = O(\varepsilon^{\tau}), \tag{5.13}$$

where τ will be determined once the terms on the right hand side are examined.

The above expression constitutes the full left hand side that is to be balanced against some terms on the right hand side. The analysis so far seems to indicate that very little has changed than in the single turning point case. However in the following section the right hand side of equation will be examined, and in doing this the terms responsible for the underlying scattering mechanism will be found.

Analysis of the Non-Parallel Terms

In order for scattering to occur there must be a physical effect present in the leading order problem that is not present in the turning point analysis studied in previous chapters. If there is indeed a new physical effect coming onto play, then this effect must be represented by a term that is present within the governing equation. Up until now, the analysis performed so far on the governing equation for high frequency has shown that the left hand side of the equation is precisely the same as what was seen in the turning point analysis. Therefore, this new physical effect must be governed by one of the terms that is available on the right hand side of the governing wave equation. In this section all five terms on the right hand side of equation (5.2) are analysed one-by-one in order to determine which of these contribute to the leading order problem.

The first term on the right hand side of the governing equation is

$$-\varepsilon\frac{1}{D_0(X)}\frac{\mathrm{d}}{\mathrm{d}X}(D_0(X))\frac{\partial\phi}{\partial x} \tag{5.14}$$

and using the form for the derivative of ϕ with respect to x given in equation (5.11) the magnitude of this term is given by

$$-\varepsilon\frac{1}{D_0(X)}\frac{\mathrm{d}}{\mathrm{d}X}(D_0(X))\frac{\partial\phi}{\partial x}\sim\varepsilon\varepsilon^{-2}=\varepsilon^{-1}, \tag{5.15}$$

and therefore this term appears too small to interact with the leading order terms on the left hand side.

The second term on the right hand side of the governing equation is given

by

$$\varepsilon \mathrm{i}\varepsilon^{-2}\bar{\omega}U_0(X)\frac{\mathrm{d}}{\mathrm{d}X}\left(\frac{1}{C_0^2(X)}\right)\phi \sim \varepsilon^{-1} \tag{5.16}$$

and hence it appears that this term is too small to balance with the leading order terms on the left hand side.

The third term on the right hand side of the governing equation is

$$-\varepsilon U_0(X)\frac{\mathrm{d}}{\mathrm{d}X}\left(\frac{U_0(X)}{C_0^2(X)}\right)\frac{\partial\phi}{\partial x} \tag{5.17}$$

and using equation (5.11) for the derivative the magnitude of this term is

$$-\varepsilon U_0(X)\frac{\mathrm{d}}{\mathrm{d}X}\left(\frac{U_0(X)}{C_0^2(X)}\right)\frac{\partial\phi}{\partial x} \sim \varepsilon\varepsilon^{-2} = \varepsilon^{-1}. \tag{5.18}$$

which again is too small to interact with the leading order terms on the left hand side.

The fourth term on the right hand side of the governing equation is

$$\begin{aligned} & \varepsilon\{2\mathrm{i}\varepsilon^{-2}\bar{\omega}C_0^{-2}(X)(\mathbf{V}_{\perp 0}.\nabla_\perp\phi)\} \\ = \;& 2\mathrm{i}\varepsilon^{-1}\bar{\omega}C_0^{-2}(X)W_1(X,z)\frac{\partial\phi}{\partial z} \\ = \;& -2\mathrm{i}\varepsilon^{-3}\bar{\omega}C_0^{-2}(X)W_1(X,z) \\ \times \;& \sum_{j=1}^{\infty}\bar{\alpha}_j\chi(\xi)\cos(\varepsilon^{-2}M\pi y)\sin(\varepsilon^{-2}\bar{\alpha}_j z) \sim \varepsilon^{-3}, \end{aligned} \tag{5.19}$$

and so this term will certainly have some influence due to the fact that it is of a much higher order than the previous terms analysed.

Now considering the fifth non-parallel term in the governing equation

$$\begin{aligned} & 2\varepsilon U_0(X)C_0^{-2}(X)\left(\mathbf{V}_{\perp 0}.\nabla_\perp\frac{\partial\phi}{\partial x}\right) \\ & = 2\varepsilon U_0(X)C_0^{-2}(X)W_1(X,z)\frac{\partial^2\phi}{\partial x\partial z}. \end{aligned} \tag{5.20}$$

In order to determine this quantity in it's entirety it is necessary to compute the cross derivative term, and this is given by

$$\begin{aligned}\frac{\partial^2\phi}{\partial x\partial z} &= \sum_{j=1}^{\infty}\Bigg[-\varepsilon^{-4}\mathrm{i}\bar{\omega}\left(\frac{\bar{\alpha}_j(X)U_0(X)}{C_0^2(X)-U_0^2(X)}\right)\\ &\times \cos(\varepsilon^{-2}M\pi y)\sin(\varepsilon^{-2}\bar{\alpha}_j(X)z)\chi_j(\xi)\\ &- \varepsilon^{-3}\left(\bar{\alpha}_j(X)\cos(\varepsilon^{-2}M\pi y)\sin(\varepsilon^{-2}\bar{\alpha}_j(X)z)\frac{\mathrm{d}}{\mathrm{d}\xi}\left(\chi_j(\xi)\right)\right)\Bigg]\\ &+ O(\varepsilon^{-2}). \end{aligned} \tag{5.21}$$

Substituting equation (5.21) into (5.20) gives for the fifth non-parallel term

$$\begin{aligned}&2\varepsilon U_0C_0^{-2}(\mathbf{V}_{\perp 0}.\nabla_\perp\phi_x)\}\\ =\ &\sum_{j=1}^{\infty}\Bigg[-2\varepsilon^{-3}U_0C_0^{-2}W_1\Bigg[\left(\frac{\mathrm{i}\bar{\alpha}_j\bar{\omega}\sin(\varepsilon^{-2}\bar{\alpha}_jz)U_0\chi_j(\xi_j)}{\left(C_0^2-U_0^2\right)}\right)\\ +\ &\varepsilon^{-2}\left(\bar{\alpha}_j(X)\sin(\varepsilon^{-2}\bar{\alpha}_j(X)z)\frac{\mathrm{d}}{\mathrm{d}\xi}\left(\chi_j(\xi)\right)\right)\Bigg]\Bigg]\cos(\varepsilon^{-2}M\pi y)\\ +\ &O(\varepsilon^{-1}), \end{aligned} \tag{5.22}$$

and thus it can now be seen from the above that to leading order the order of magnitude of the fifth non-parallel term is

$$2\varepsilon U_0C_0^{-2}(\mathbf{V}_{\perp 0}.\nabla_\perp\phi_x)\}\sim\varepsilon^{-3}, \tag{5.23}$$

which appears to be significantly high compared to the first three non-parallel terms analysed, thus this term may play a significant role within the inner region to leading order.

Attempting to balance the terms

From the analysis performed in the previous section it is clear that the fourth and fifth terms on the right hand side of the governing equation (given by expressions (5.19) and (5.22) respectively) are the largest of the terms that exist

on the right hand side. It is these two terms that appear to be responsible for the scattering, because at high frequency they form a dominant physical process within the boundary layer. Notice that both of these terms include the cross-flow component $W_1(X, z)$, which appears to indicate that the existence of the cross flow component of the mean flow is necessary to induce the scattering, provided that the Helmholtz number is large enough. This may also explain why the results shown in Ovenden et al [43] show scattering for high frequency and mean flow, yet there is no scattering for zero mean flow with ω of the same order.

Now although the terms responsible for the scattering appear to have been identified, there appears to be an issue in that the terms do not balance in such a way as to give an asymptotically consistant description of the system to leading order. This can be seen by balancing the important terms on the right hand side (5.19) and (5.22) with the expression (5.13) which yields

$$\begin{aligned} & \sum_{j=1}^{\infty} \left[\varepsilon^{-2} \left(1 - \frac{U_0^2(X)}{C_0^2(X)} \right) \frac{\mathrm{d}^2}{\mathrm{d}\xi^2} \left(\chi(\xi) \right) \cos(\varepsilon^{-2} \bar{\alpha}_j(X) z) \right. \\ + \quad & \varepsilon^{-4} \bar{\omega}^2 \frac{\sigma_j^2(X)}{C_0^2(X) - U_0^2(X)} \chi_j(\xi) \cos(\varepsilon^{-2} \bar{\alpha}_j(X) z) \\ + \quad & \left. 2\varepsilon^{-3} \mathrm{i} \bar{\omega} \frac{\bar{\alpha}_j(X) W_1(X, z)}{C_0^2(X) - U_0^2(X)} \chi_j(\xi) \sin\left(\varepsilon^{-2} \bar{\alpha}_j(X) z \right) \right] = O(\varepsilon^{-1}), \quad (5.24) \end{aligned}$$

and the problem with the balancing can be seen by studying the above expression. The second term on the left hand side includes a $\sigma_j^2(X)$, term, and inside the boundary layer where $X - X_t \sim \varepsilon^2, \sigma_j^2 \sim \varepsilon^2$, meaning that within the boundary layer the second term on left hand side of the above expression shrinks to $O(\varepsilon^{-2})$, and therefore this term balances with the first term in exactly the same way as with the turning point analysis. However the problem

is that this means that there is one term of $O(\varepsilon^{-3})$ remaining that does not seem to balance with any other term. This indicates that this term is likely to be the term responsible for the scattering, but at the moment it is too large to balance the usual terms that dominate the physics within the inner region for $\omega \sim \varepsilon^{-2}$. The fact that there is one term only that is considerably larger than the others implies that the width of the boundary later is incorrect, and that the scattering actually occurs over different lengthscale than the one specified. The $O(\varepsilon^2)$ boundary layer thickness came as a consequence of the assumption that $\omega \sim \varepsilon^{-2}$ in order for scattering to take place, and it now appears that this is not the case and in fact the order of magnitude of the frequency required in order for scattering to occur could be lower than this. The task now therefore is to re-examine this argument and establish the correct order of magnitude for ω that is required in order for scattering to occur.

In consideration of the distance between neighbouring σ_js

It is worth mentioning at this point that although there is currently an imbalance between the terms within the inner modal equation, the neighbouring modes are within the required distance from each other in order to exchange energy. In other words, the distance between neighbouring modes is small enough to allow for modal energy exchange. This can be shown by considering the expression for a general $\sigma_j^2(X)$ and expressing it in terms of the incident mode $\sigma_t^2(X)$, which is the mode that cuts off at X_t. Recall that for a three dimensional duct $\sigma_j^2(X)$ is given by

$$\sigma_j^2 = 1 - \frac{1}{\bar{\omega}^2}(C_0^2 - U_0^2)\left(\bar{\alpha}_j^2 + M^2\pi^2\right),$$

and recall from chapter 4 equation (4.27) that for the cross sectional mode

$$\bar{\alpha}_j = \frac{J\pi}{h(X)} \quad \text{where} \quad j = \varepsilon^{-2}J$$

for some integer $j \sim \varepsilon^{-2}$. The order one index $J \sim 1$ is a real number. Similarly for the mode that cuts off at X_t it's cross-sectional eigenvalue is given by

$$\bar{\alpha_t} = \frac{T\pi}{h(X)} \quad \text{where} \quad t = \varepsilon^{-2}T$$

for some integer $t \sim \varepsilon^{-2}$ and $T \sim 1$ is a real number. The two integers t and j are related by a third integer $p \sim 1$ via $j = t + p$. Thus for the reduced axial wavenumber for a general mode σ_j it is simple to show that

$$\alpha_j(X) = \alpha_t(X) + \frac{\varepsilon^2 p\pi}{h(X)} \quad \Longrightarrow \quad \alpha_j(X) - \alpha_t(X) \sim \varepsilon^2,$$

meaning that the difference between cross sectional eigenvalues is sufficiently small, meaning that it is the same order of magnitude as the width of the boundary layer, which is a necessary condition for modal interaction. Using this expression for α_j^2 above it is then possible to express an arbitrary σ_j^2 in terms of the incident σ_t^2 as

$$\sigma_j^2 = \sigma_t^2 + \delta_{p,t}, \quad \text{where} \quad \delta_{p,t} = -\varepsilon^2\pi p\frac{(C_0^2 - U_0^2)}{h^2\bar{\omega}^2}\left(2\bar{\alpha_t}h + \varepsilon^2 p\pi\right)$$

and thus for the difference between neighbouring modes one has $\sigma_j^2 - \sigma_t^2 \sim \varepsilon^2$, thus satisfying the condition presented in [43] that neighbouring modes must be of a comparable size and be sufficiently close to one another in order for scattering to occur.

5.2 Refining the Model Using Arbitrary Helmholtz Number Scaling

In the previous section the source terms responsible for the scattering were determined, but a balance between the terms in the equation was not achieved for $\omega \sim \varepsilon^{-2}$. Ovenden, Eversman and Rienstra calculated that in order for scattering to take place the required order of magnitude of the frequency is $\sim \varepsilon^{-2}$ (as stated above), and this result was derived by considering an ω such the σ_j's are close enough to induce scattering. In this discussion it is shown that even for the 2D case the magnitude of the frequency required to induce scattering is actually significantly lower than this estimate.

As noted in the previous chapter, $\omega = \varepsilon^{-2}\bar{\omega}$ causes an imbalance in the governing wave equation, and thus an attempt to coordinate a balance between the necessary terms is done by choosing a general scaling for ω, going through the same process as was shown in the previous chapter and then picking the scaling so that all the terms balance.

The first step is to allow ω to have the general form

$$\omega = \varepsilon^{-\vartheta}\bar{\omega}, \tag{5.25}$$

where $0 < \vartheta < 2$ and $\bar{\omega} \sim 1$. This of course now means that the general governing wave equation (1.12) must be rewritten slightly to accommodate

this general ω, and this is given by

$$\left(1-\frac{U_0^2(X)}{C_0^2(X)}\right)\frac{\partial^2\phi}{\partial x^2}-\varepsilon^{-\vartheta}\frac{2\mathrm{i}\bar{\omega}U_0(X)}{C_0^2}\frac{\partial\phi}{\partial x}+\nabla_\perp^2\phi+\varepsilon^{-2\vartheta}\frac{\bar{\omega}^2}{C_0^2(X)}\phi$$
$$=-\varepsilon\Bigg[\frac{1}{D_0(X)}\frac{\mathrm{d}}{\mathrm{d}X}\left(D_0(X)\right)\frac{\partial\phi}{\partial x}-\mathrm{i}\varepsilon^{-\vartheta}\bar{\omega}U_0(X)\frac{\mathrm{d}}{\mathrm{d}X}\left(\frac{1}{C_0^2(X)}\right)\phi$$
$$-U_0(X)\frac{\mathrm{d}}{\mathrm{d}X}\left(\frac{U_0(X)}{C_0^2(X)}\right)\frac{\partial\phi}{\partial x}-2\mathrm{i}\varepsilon^{-\vartheta}\bar{\omega}\frac{1}{C_0^2(X)}(\mathbf{V}_{\perp 0}.\nabla_\perp\phi)$$
$$-2U_0(X)\frac{1}{C_0^2(X)}\left(\mathbf{V}_{\perp 0}.\nabla_\perp\frac{\partial\phi}{\partial x}\right)\Bigg]. \qquad (5.26)$$

Given the scaling introduced in equation (5.25) the acoustic potential ϕ takes the following form in the inner region

$$\begin{aligned}\phi &= \sum_{j=1}^{\infty}\chi_j(\xi)\cos\left(\varepsilon^{-\vartheta}M\pi z\right)\cos\left(\varepsilon^{-\vartheta}\alpha_j(X)z\right)\\ &\times \exp\left(\mathrm{i}\int_{X_t}^{X}\frac{\varepsilon^{-\vartheta-1}\bar{\omega}U_0(X')}{C_0^2(X')-U_0^2(X')}\mathrm{d}X'\right),\end{aligned} \qquad (5.27)$$

where $\bar{\alpha}_j(X)\sim 1$ and $\chi_j(\xi)\sim 1$. In order to determine the thickness of the boundary layer in this case, Rienstra's form for the boundary layer [49] is used, given by

$$X-X_t=\varepsilon^{\frac{2}{3}}\lambda^{-1}\xi,$$

for a parameter λ that was given earlier in equation (3.4). However since $\lambda\sim\omega^{\frac{2}{3}}\sim\varepsilon^{-\frac{2}{3}\vartheta}$ then

$$X-X_t \quad\sim\quad \varepsilon^{\frac{2}{3}}(\omega^{-\frac{2}{3}})\xi \quad\sim\quad \varepsilon^{\frac{2}{3}(1+\vartheta)}\xi, \qquad (5.28)$$

and so for this formulation the boundary layer variable $\xi\sim 1$ is defined by

$$X-X_t=\varepsilon^{\frac{2}{3}(1+\vartheta)}\xi. \qquad (5.29)$$

The derivatives can be calculated using the chain rule as

$$\frac{\partial}{\partial x}=\varepsilon\frac{\partial}{\partial X}=\varepsilon^{\frac{1}{3}(1-2\vartheta)}\frac{\partial}{\partial\xi}, \qquad (5.30)$$

$$\frac{\partial^2}{\partial x^2}=\varepsilon^2\frac{\partial^2}{\partial X^2}=\varepsilon^{\frac{2}{3}(1-2\vartheta)}\frac{\partial^2}{\partial\xi^2}. \qquad (5.31)$$

The first derivative of ϕ with respect to x is

$$\begin{aligned}\frac{\partial\phi}{\partial x} &= \sum_{j=1}^{\infty}\left[\varepsilon^{\frac{1}{3}(1-2\vartheta)}\left\{\chi' + \frac{\mathrm{i}\varepsilon^{-\frac{1}{3}(1+\vartheta)}\bar{\omega}U_0}{C_0^2-U_0^2}\right\}\cos\left(\varepsilon^{-\vartheta}\bar{\alpha}_j z\right)\right] \\ &\times \cos\left(\varepsilon^{-\vartheta}M\pi y\right)\exp\left(\mathrm{i}\int_{X_t}^{X}\frac{\varepsilon^{-\vartheta-1}\bar{\omega}U_0(X')}{C_0^2(X')-U_0^2(X')}\mathrm{d}X'\right), \qquad (5.32)\end{aligned}$$

and the second derivative of ϕ with respect to x is

$$\begin{aligned}\frac{\partial^2\phi}{\partial x^2} = \sum_{j=1}^{\infty}&\left[\varepsilon^{\frac{2}{3}(1-2\vartheta)}\chi'' + \frac{2\mathrm{i}\varepsilon^{-\frac{1}{3}(1-5\vartheta)}\bar{\omega}U_0\chi'}{C_0^2-U_0^2} - \frac{\varepsilon^{-2\vartheta}\bar{\omega}^2U_0^2\chi}{(C_0^2-U_0^2)^2}\right] \\ &\times\cos\left(\varepsilon^{-\vartheta}\bar{\alpha}_j z\right)\cos\left(\varepsilon^{-\vartheta}M\pi y\right)\exp\left(\mathrm{i}\int_{X_t}^{X}\frac{\varepsilon^{-\vartheta-1}\bar{\omega}U_0(X')}{C_0^2(X')-U_0^2(X')}\mathrm{d}X'\right). \qquad (5.33)\end{aligned}$$

The expressions (5.32) and (5.33) may be substituted into the left hand side of the governing wave equation (5.26) to give

$$\begin{aligned}&\sum_{j=1}^{\infty}\left[\left\{\varepsilon^{\frac{2}{3}(1-2\vartheta)}\left(1-\frac{U_0^2}{C_0^2}\right)\chi_j''(\xi) + \frac{\varepsilon^{-2\vartheta}\bar{\omega}^2\sigma_j^2}{C_0^2-U_0^2}\chi_j(\xi)\right\}\cos\left(\varepsilon^{-\vartheta}\bar{\alpha}_j z\right)\right] \\ &\times\cos\left(\varepsilon^{-\vartheta}M\pi y\right)\exp\left(\mathrm{i}\int_{X_t}^{X}\frac{\varepsilon^{-\vartheta-1}\bar{\omega}U_0(X')}{C_0^2(X')-U_0^2(X')}\mathrm{d}X'\right). \qquad (5.34)\end{aligned}$$

In all cases so far, due to the presence of the σ_j^2 term the leading order term reduces to the same order of magnitude as the χ'' term within the boundary layer, achieving a balance between these two terms. It is simple to show that this is in fact true here too, as within the boundary layer a Taylor series expansion of σ_j^2 can be used to show that $\sigma_j^2 \sim \varepsilon^{\frac{2}{3}(1+\vartheta)}$ for $X - X_t \sim \varepsilon^{\frac{2}{3}(1+\vartheta)}$, and therefore for the σ_j^2 term that is reducing to zero one has

$$\varepsilon^{-2\vartheta}\frac{\bar{\omega}^2\chi_i}{C_0^2-U_0^2}\sigma_i^2 \sim \varepsilon^{-2\vartheta}\varepsilon^{\frac{2}{3}}\varepsilon^{\frac{2\vartheta}{3}} = \varepsilon^{\frac{2}{3}(1-2\vartheta)} \qquad (5.35)$$

which is then the same order as the χ'' term in (5.34) within the boundary layer.

It is now a question of studying the terms on the right hand side of equation (5.26), focusing in particular on the terms that are large enough to induce modal scattering. Thus for this purpose the fourth and fifth non-parallel terms previously analysed in section 5.1 will be considered.

Recall that the fourth non-parallel term is given by

$$\varepsilon\left(2\mathrm{i}\varepsilon^{-\vartheta}\bar{\omega}C_0^2W_1(X,z)\frac{\partial\phi}{\partial z}\right), \tag{5.36}$$

and differentiating ϕ with respect to z yields

$$\begin{aligned}\frac{\partial\phi}{\partial z} = &\sum_{j=1}^{\infty}\left[\varepsilon^{-\vartheta}\bar{\alpha}_j(X)\chi_j(\xi)\sin\left(\varepsilon^{-\vartheta}\bar{\alpha}_j(X)z\right)\right]\cos\left(\varepsilon^{-\vartheta}M\pi y\right)\\ &\times\exp\left(\mathrm{i}\int_{X_t}^{X}\frac{\varepsilon^{-\vartheta-1}\bar{\omega}U_0(X')}{C_0^2(X')-U_0^2(X')}\mathrm{d}X'\right),\end{aligned} \tag{5.37}$$

and therefore

$$\begin{aligned}&\varepsilon\left(2\mathrm{i}\varepsilon^{-\vartheta}\bar{\omega}C_0^2W_1(X,z)\frac{\partial\phi}{\partial z}\right)\\ =\;&\varepsilon\left(2\mathrm{i}\varepsilon^{-\vartheta}\bar{\omega}C_0^2W_1(X,z)\right)\sum_{j=1}^{\infty}\left[\varepsilon^{-\vartheta}\bar{\alpha}_j(X)\chi_j(\xi)\sin\left(\varepsilon^{-\vartheta}\bar{\alpha}_j(X)z\right)\right]\\ \times\;&\cos\left(\varepsilon^{-\vartheta}M\pi y\right)\exp\left(\mathrm{i}\int_{X_t}^{X}\frac{\varepsilon^{-\vartheta-1}\bar{\omega}U_0(X')}{C_0^2(X')-U_0^2(X')}\mathrm{d}X'\right)\\ \sim\;&\varepsilon^{1-2\vartheta}.\end{aligned} \tag{5.38}$$

For the fifth non-parallel term is

$$\begin{aligned}&2\varepsilon U_0(X)C_0^{-2}(X)\left(\mathbf{V}_{\perp 0}.\nabla_{\perp}\frac{\partial\phi}{\partial x}\right)\\ &=2\varepsilon U_0(X)C_0^{-2}(X)W_1(X,z)\frac{\partial^2\phi}{\partial x\partial z},\end{aligned} \tag{5.39}$$

which involves a cross derivative term, which is given by

$$\begin{aligned}\frac{\partial^2\phi}{\partial x\partial z} &= \sum_{j=1}^{\infty}\left[-\varepsilon^{-2\vartheta}\mathrm{i}\bar{\omega}\chi_j(\xi)\left(\frac{\bar{\alpha}_j(X)U_0(X)}{C_0^2(X)-U_0^2(X)}\right)\sin(\varepsilon^{-2}\bar{\alpha}_j(X)z)\right]\\ &\times \cos\left(\varepsilon^{-\vartheta}M\pi y\right)\exp\left(\mathrm{i}\int_{X_t}^{X}\frac{\varepsilon^{-\vartheta-1}\bar{\omega}U_0(X')}{C_0^2(X')-U_0^2(X')}\mathrm{d}X'\right)\\ &+ O(\varepsilon^{-2\vartheta+1}),\end{aligned} \tag{5.40}$$

and therefore the fifth non-parallel term is

$$\begin{aligned}&2\varepsilon U_0(X)C_0^{-2}(X)W_1(X,z)\\ \times\ &\sum_{j=1}^{\infty}\left[-\varepsilon^{-2\vartheta}\mathrm{i}\bar{\omega}\left(\frac{\bar{\alpha}_j(X)U_0(X)}{C_0^2(X)-U_0^2(X)}\right)\chi_j(\xi)\sin(\varepsilon^{-2}\bar{\alpha}_j(X)z)\right]\\ \times\ &\cos(\varepsilon^{-2}M\pi y)\exp\left(\mathrm{i}\int_{X_t}^{X}\frac{\varepsilon^{-\vartheta-1}\bar{\omega}U_0(X')}{C_0^2(X')-U_0^2(X')}\mathrm{d}X'\right)\\ +\ &O(\varepsilon^{2-2\vartheta})\end{aligned} \tag{5.41}$$

which is $O(\varepsilon^{1-2\vartheta})$ to leading order, which the same order of magnitude as the forth non parallel term meaning that there is a balance between these two terms.

The aim now is to find a condition on ϑ such that these non parallel terms balance with the left hand side. In order for this balance to occur, the following must be true:

$$\varepsilon^{\frac{2}{3}(1-2\vartheta)} = \varepsilon^{(1-2\vartheta)} \qquad \Longrightarrow \qquad \vartheta = \frac{1}{2},$$

and therefore selecting $\omega \sim \varepsilon^{-\frac{1}{2}}$ will yield a balance between the terms. It then follows that the boundary layer width is given by

$$X - X_t \sim \varepsilon.$$

5.3 Construction of a Model for Weak Modal Scattering

In the previous section it was shown that choosing $\omega \sim \varepsilon^{-\frac{1}{2}}$ appears to yield a balance between all of the required terms in the governing wave equation within the boundary layer. In this section it will be shown that in fact a scaling of this order is sufficient to induce modal scattering, but the degree of modal scattering induced here will only be weak. Section 5.4 takes the ideas discussed in this section further, discusses the reasons why only weak scattering is induced, and refines the method to give a model that yields a differential equation for the inner region for $O(1)$ scattering.

The frequency $\omega \sim \varepsilon^{-\frac{1}{2}}$ has been shown to yield a balancing between the terms in the wave equation that are required in order to induce scattering. Thus a boundary layer variable ξ may be defined as

$$X - X_t = \varepsilon \bar{\lambda}^{-1} \xi$$

where the parameter $\bar{\lambda}$ is defined for convenience as

$$\bar{\lambda}^3 = \frac{2\bar{\omega}^2 C_0^2(X_t)}{(C_0^2(X_t) - U_0^2(X_t))^2} \left(\frac{C_0(X_t)C_0'(X_t) - U_0(X_t)U_0'(X_t)}{C_0^2(X_t) - U_0^2(X_t)} + \frac{\alpha'(X_t)}{\alpha(X_t)} \right)$$

and $\bar{\lambda}$ defined here is simply a rescaled version the λ defined in Rienstra's previous work [49]. The equation governing the scattering mechanism may now be written down as (supressing the both the exponential terms and cosine

term acting the y direction)

$$\sum_{j=1}^{\infty}\left(\left[\bar{\lambda}^2\frac{\mathrm{d}^2}{\mathrm{d}\xi^2}\left(\chi_j(\xi)\right)+\varepsilon^{-1}\frac{\bar{\omega}^2C_0^2(X)\sigma_j^2(X)}{\left(C_0^2(X)-U_0^2(X)\right)^2}\chi_j(\xi)\right]\cos\left(\varepsilon^{-\frac{1}{2}}\alpha_j z\right)\right)$$
$$+\sum_{j=1}^{\infty}\left[\frac{2\mathrm{i}\bar{\omega}C_0^2(X)\alpha_j\widetilde{W}_1(X)z}{\left(C_0^2(X)-U_0^2(X)\right)^2}\chi_j(\xi)\sin\left(\varepsilon^{-\frac{1}{2}}\alpha_j(X)z\right)\right]=O(\varepsilon^{\frac{1}{2}}). \quad (5.42)$$

In a manner similar to the turning point discussions, it is usually convenient to expand the $\sigma_j^2(X)$ term as a Taylor series in ascending powers of ξ about the turning point X_t. However before this is done here it should be noted that, in a similar manner to the method shown in section 5.1, it is usually convenient to represent each $\sigma_j^2(X)$ in terms of the incident mode $\sigma_t^2(X)$, where σ_t is the mode that undergoes transition at the turning point X_t. This representation of each σ_j in terms of σ_t is easily achieved using the definition for the reduced axial wavenumber. Traditionally for $\omega\sim 1$ this mode would undergo cut-on cut-off transition at this point, but in the case of high frequency this mode is expected to cut off at X_t, and a proportion of it's energy may be scattered into neighbouring modes.

Recall once again that for a three dimensional duct $\sigma_j^2(X)$ is given by

$$\sigma_j^2=1-(C_0^2-U_0^2)\left(\frac{\bar{\alpha}_j^2+M^2\pi^2}{\bar{\omega}^2}\right)$$

and in a manner similar to that shown in section 5.1 it is possible to write σ_j^2 as

$$\sigma_j^2=\sigma_t^2+\delta_{p,t} \quad (5.43)$$

where the shift function $\delta_{p,t}$ is now given by

$$\delta_{p,t}=-\varepsilon^{\frac{1}{2}}\pi p\frac{(C_0^2-U_0^2)}{h^2\bar{\omega}^2}\left(2\bar{\alpha}_t h+\varepsilon^{\frac{1}{2}}p\pi\right). \quad (5.44)$$

For the incident mode, multiplying the scattering equation (5.42) by it's cross-sectional eigenfunction $\cos(\varepsilon^{-\frac{1}{2}}\alpha_j z)$ and exploiting the orthogonality of the eigenfunction by integrating over the cross section yields the following equation governing $\chi_t(\xi)$

$$\chi_t''(\xi) - \xi\chi_t(\xi) = \frac{2\mathrm{i}\bar{\omega}C_0^2(X)\widetilde{W}_1(X)}{\left(C_0^2(X) - U_0^2(X)\right)^2}\sum_{k=1}^{\infty}\left[C_{kt}\alpha_k(X)h(X)\chi_k(\xi)\right], \quad (5.45)$$

where a scattering coefficient C_{kt} is identified and defined as

$$C_{kt} = -\frac{2}{h^2(X)}\int_0^h z\cos\left(\frac{\alpha_k z}{\varepsilon^{\frac{1}{2}}}\right)\sin\left(\frac{\alpha_t z}{\varepsilon^{\frac{1}{2}}}\right)\mathrm{d}z, \quad (5.46)$$

and some routine integration gives

$$C_{kt} = \begin{cases} \frac{1}{2t\pi} & \text{for } k = t, \\ \frac{1}{\pi}\left(\frac{(-1)^{t+k}}{t+k} + \frac{(-1)^{t-m}}{t-m}\right) & \text{for } k \neq t. \end{cases} \quad (5.47)$$

For the remaining modes equation (5.42) fails to yield a balance between the terms and hence a rescaling of the boundary layer is necessary. Suppose a change of variables $\xi \to \eta$ is established such that

$$\frac{\mathrm{d}^2}{\mathrm{d}\xi^2} \sim \varepsilon^{-\frac{1}{2}}\frac{\mathrm{d}^2}{\mathrm{d}\eta^2},$$

or $\varepsilon^{\frac{1}{2}}\mathrm{d}\eta^2 \sim \mathrm{d}\xi^2$, noting that the establishment of this type would lead to a balance of all the terms in equation (5.42) for all modes that do not cut-off at X_t. The change of variables described above may be satisfied by setting $\eta = \varepsilon^{-\frac{1}{4}}\xi$. Substitution of this variable into (5.42) yields (up to $O(\varepsilon^{\frac{1}{2}})$)

$$\sum_{j=1}^{\infty}\left(\left[\bar{\lambda}^2\frac{\mathrm{d}^2}{\mathrm{d}\eta^2}(\chi_j(\eta)) + \frac{\bar{\omega}^2C_0^2(X)\delta_{t,p}(X)}{\left(C_0^2(X) - U_0^2(X)\right)^2}\chi_j(\eta)\right]\cos(\varepsilon^{-\frac{1}{2}}\alpha_j z)\right)$$
$$+\varepsilon^{\frac{1}{2}}\sum_{j=1}^{\infty}\left[\frac{2\mathrm{i}\bar{\omega}C_0^2(X)\alpha_j\widetilde{W}_1(X)z}{\left(C_0^2(X) - U_0^2(X)\right)^2}\chi_j(\eta)\sin(\varepsilon^{-\frac{1}{2}}\alpha_j(X)z)\right] = 0. \quad (5.48)$$

Multiplying the above through by $\cos\left(\varepsilon^{-\frac{1}{2}}\alpha_m z\right)$ and integrating over the cross section yields the following for each χ_m,

$$\begin{aligned}&\bar{\lambda}^2\left(\frac{\mathrm{d}^2}{\mathrm{d}\eta^2}\left(\chi_m(\eta)\right)+\frac{\bar{\omega}^2C_0^2(X)\delta_{t,p}(X)}{\bar{\lambda}^2\left(C_0^2(X)-U_0^2(X)\right)^2}\chi_m(\eta)\right)\\ =\;&\varepsilon^{\frac{1}{2}}\sum_{j=1}^{\infty}\left[\frac{2\mathrm{i}\bar{\omega}C_0^2(X)\alpha_j\widetilde{W}_1(X)}{\left(C_0^2(X)-U_0^2(X)\right)^2}C_{jm}\alpha_j(X)h(X)\chi_j(\eta)\right].\end{aligned}\tag{5.49}$$

First note that if $\delta_{t,p}$ is negative this will yield exponentially decaying waves within the immediate vicinity of the turning point. It is possible that a mode with negative $\delta_{t,p}$ may be cut-on somewhere immediately outside the boundary layer, but as it has already been noted that neighbouring σ's are too close to induce scattering to leading order, it seems unlikely that any modes that have negative $\delta_{t,p}$ inside the boundary layer may be scattered in such a way that they are cut-on just outside the boundary layer. Positive $\delta_{t,p}$'s correspond to waves that are able to propagate through the turning point region.

Through studying equations (5.45) and (5.49) it is possible to understand the full problem for weak scattering. Suppose it is assumed that only the mode σ_t is incident within the problem domain, and that all other modes are cut-off. It can then be shown that χ_m for $m \neq t$ is small by expanding χ_m as

$$\chi_m(\eta) = \chi_{m0}(\eta) + \varepsilon^{\frac{1}{2}}\chi_{m1}(\eta) + O(\varepsilon).$$

The above is then substituted into (5.49), and equating leading order terms gives

$$\frac{\mathrm{d}^2}{\mathrm{d}\eta^2}\left(\chi_{m0}(\eta)\right)+\frac{\bar{\omega}^2C_0^2(X)\delta_{t,p}(X)}{\bar{\lambda}^2\left(C_0^2(X)-U_0^2(X)\right)^2}\chi_{m0}(\eta)=0$$

and since there are no incident χ_m modes this gives $\chi_{m0} = 0$ for all m and hence $\chi_m(\eta) \sim \varepsilon^{\frac{1}{2}}$ for all $m \neq t$. The scenario is slightly different if there is

more than one incident mode, and the details of this are discussed at the end of this section.

The knowledge that $\chi_m(\eta) \sim \varepsilon^{\frac{1}{2}}$ for all $m \neq t$ means that for the equation for χ_t given by equation (5.45), most the terms on the right hand side may be considered to be too small to act, and this means that the differential equation for χ_t may be approximated to leading order as

$$\frac{\mathrm{d}^2}{\mathrm{d}\xi^2}\left(\chi_t(\xi)\right) - \left(\frac{2\mathrm{i}\bar{\omega}C_0^2(X)\widetilde{W}_1(X)}{\bar{\lambda}^2\left(C_0^2(X)-U_0^2(X)\right)^2}C_{tt}\alpha_t(X)h(X)+\xi\right)\chi_t(\xi) = 0, \quad (5.50)$$

which is just Airy's equation with an imaginary shift that is approximately constant within the boundary layer. The general solution to the above equation is

$$\begin{aligned}\chi_t(\xi) &= \mathscr{A}\,\mathrm{Ai}\left(\xi + \frac{2\mathrm{i}\bar{\omega}C_0^2(X_t)\widetilde{W}_1(X_t)}{\bar{\lambda}^2\left(C_0^2(X_t)-U_0^2(X_t)\right)^2}C_{tt}\alpha_t(X_t)h(X_t)\right)\\ &+ \mathscr{B}\,\mathrm{Bi}\left(\xi + \frac{2\mathrm{i}\bar{\omega}C_0^2(X_t)\widetilde{W}_1(X_t)}{\bar{\lambda}^2\left(C_0^2(X_t)-U_0^2(X_t)\right)^2}C_{tt}\alpha_t(X_t)h(X_t)\right), \quad (5.51)\end{aligned}$$

where it is concluded that $\mathscr{B} = 0$ must be zero to avoid exponentially growing solutions for $\xi > 0$. For the arbitrary constant $\mathscr{A}$, this may be found via matching with the outer solution, although this analysis is not done here due to the quite complicated manner in which the above solution behaves as $\xi \to -\infty$. A sketch of the nature of this inner solution for the incident mode is shown in figure 5.2. For the modal amplitude χ_m of the other modes, the equation governing the first order amplitude χ_{m1} may be approximated by

$$\bar{\lambda}^2\left(\chi_{m1}''(\eta) + \frac{\bar{\omega}^2C_0^2\delta_{t,p}}{\bar{\lambda}^2\left(C_0^2-U_0^2\right)^2}\chi_{m1}(\eta)\right) = \frac{2\mathrm{i}\bar{\omega}C_0^2\widetilde{W}_1(X)}{\left(C_0^2-U_0^2\right)^2}C_{tt}\alpha_t h\chi_t(\eta). \quad (5.52)$$

One may see from the above equation that the first order evolution of modal amplitude for non-incident modes consists of a propagating wave with the cut-

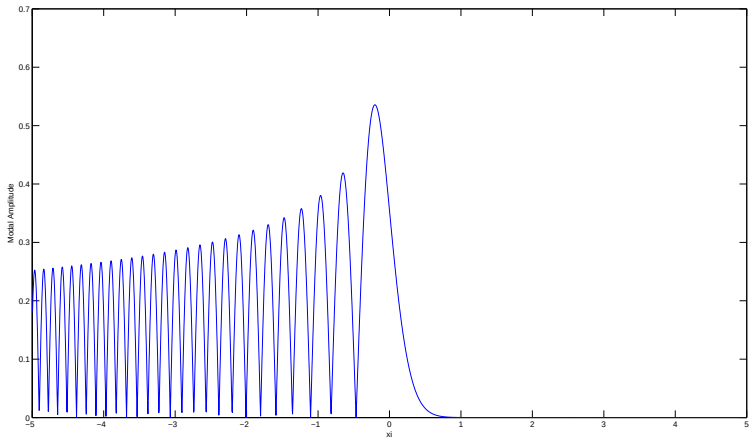

Figure 5.2: Airy Function with a small imaginary shift: $\mathrm{Ai}\,(\xi + a\mathrm{i})$ for real a

on cut-off mode acting as a forcing term and thus provides the source of the scattering for this mode.

It is worth mentioning the case where there are two incident modes, and the second mode is able to propagate beyond the turning point X_t and has amplitude that is of order 1 within the boundary layer. In this scenario then equation (5.50) which governs the cut-on cut-of mode will be inhomogeneous to leading order due to the presence of this extra mode. So to leading order there will be a coupling between these two modes and is more difficult to analyse analytically than the case presented here. The leading order amplitude χ_{m0} for this extra mode will be sinusoidal, as depicted through equation (5.50), and thus for this mode equation (5.52) above constitutes a first order correction to the modal evolution. It will be shown in the next section that scattering to leading order yields a leading order coupling between all modes, whether they are incident or not.

5.4 Construction of a Model for Leading Order Modal Scattering

In the last section an equation governing the modal amplitude within the inner region χ_m in the case of weak scattering was derived. The analysis shown in the previous section is a model for weak scattering only because within the inner region if $\omega \sim \varepsilon^{-\frac{1}{2}}$ then neighbouring modes are not sufficiently close to one another in order for modal scattering to be induced to leading order. In this section a model that describes leading order scattering for each mode is derived, and this is achieved by considering the conditions by which a balancing between all of the required terms is achieved as well as ensuring that the difference between neighbouring modes is of the correct order.

In a manner similar to that shown in section (5.2), a general form for the magnitude of ω is assumed via

$$\omega = \varepsilon^{-\vartheta}\bar{\omega},$$

and consequently the boundary layer ξ is defined as

$$X - X_t = \varepsilon^{\frac{2}{3}(1+\vartheta)}.$$

The acoustic potential function ϕ is assumed to take the form

$$\phi = \sum_{j=1}^{\infty} \chi_j(\xi) \cos(M\pi z) \cos(\alpha_j z) \exp\left(\mathrm{i} \int_{X_t}^{X} \frac{\varepsilon^{-\vartheta-1}\bar{\omega}U_0(X')}{C_0^2(X') - U_0^2(X')} \mathrm{d}X'\right), \quad (5.53)$$

where at this stage, in contrast to the model developed in section 5.2, no assumptions have been made about the various orders of magnitude of the

wavenumbers α_j and M. Taking the above and substituting to the governing wave equation (5.26) yields

$$\sum_{j=1}^{\infty}\left[\varepsilon^{\frac{2}{3}(1-2\vartheta)}\bar{\lambda}^2\chi_j''(\xi)+\varepsilon^{-2\vartheta}\frac{\bar{\omega}^2C_0^2(X)\sigma_j^2(X)}{\left(C_0^2(X)-U_0^2(X)\right)^2}\chi_j(\xi)\right]\cos\left(\varepsilon^{-\frac{1}{2}}\alpha_j z\right)$$
$$+\quad \varepsilon^{1-\vartheta}\sum_{j=1}^{\infty}\left[\frac{2\mathrm{i}\bar{\omega}C_0^2(X)\alpha_j\widetilde{W}_1(X)z}{\left(C_0^2(X)-U_0^2(X)\right)^2}\chi_j(\xi)\sin\left(\varepsilon^{-\frac{1}{2}}\alpha_j(X)z\right)\right]=0. \qquad (5.54)$$

Now use the fact that any given σ_j^2 may be written as

$$\sigma_j^2=1-\left(C_0^2-U_0^2\right)\frac{(\alpha_j^2+\pi^2M^2)}{\omega^2},$$

where now ω is the unscaled Helmholtz number. Note that within all the formulation so far, the above expression for σ_j^2 is entirely equivalent to σ_j^2 when unscaled Helmholtz number and wavenumbers were used because up to this point ω^2, α_j^2 and M^2 were all considered to be of the same order of magnitude, and so if these quantities were to be rescaled as an order one quantity multiplied by ε to some power, the ε terms would always cancel. However in this development the possibility that α_j, M and ω may not be of the same order of magnitude is being taken into account, and thus the expression for σ_j^2 involving unscaled representations of these quantities is considered.

Recall that it is possible to represent and arbitrary σ_j^2 as an incident σ_t^2 plus a shift $\delta_{p,t}$ as.

$$\sigma_j^2=\sigma_t^2+\delta_{p,t}$$

where the shift term $\delta_{p,t}$ is

$$\delta_{p,t}=-\frac{(C_0^2-U_0^2)}{\omega^2h^2}\left(2\alpha_tp\pi h+p^2\pi^2\right),$$

and $j=t+p$ are all integers and $p\sim 1$. It should be noted that for the above expression, the second term in the brackets will be negligible compared

to the first term as $p \sim 1$, and so when this is divided by ω^2 factor this second term will be very small. Substitution of the above expression of $\delta_{p,t}$ into equation (5.54) yields

$$\sum_{j=1}^{\infty}\left[\varepsilon^{\frac{2}{3}(1-2\vartheta)}\bar{\lambda}^2\chi_j''(\xi)+\varepsilon^{-2\vartheta}\frac{\omega^2C_0^2(X)\left(\delta_{p,t}+\sigma_t^2(\xi)\right)}{(C_0^2(X)-U_0^2(X))^2}\chi_j(\xi)\right]\cos\left(\varepsilon^{-\frac{1}{2}}\alpha_j z\right)$$

$$= -\varepsilon^{1-\vartheta}\frac{2\mathrm{i}\bar{\omega}C_0^2\widetilde{W}_1 z}{\left(C_0^2-U_0^2\right)^2}\sum_{j=1}^{\infty}\left[\alpha_j(X)\chi_j(\xi)\sin\left(\varepsilon^{-\frac{1}{2}}\alpha_j(X)z\right)\right]. \tag{5.55}$$

The equation (5.55) contains a summation over all modes, and it may be seen that even for orthogonal eigenfunctions it is not possible to completely decouple the individual modal equations because in general for the cross-sectional part of the forcing term

$$\int_0^{h(X)} z\sin\left(\varepsilon^{-\frac{1}{2}}\alpha_j(X)z\right)\cos\left(\varepsilon^{-\frac{1}{2}}\alpha_m(X)z\right)\mathrm{d}z \neq 0, \tag{5.56}$$

for some integer m. Therefore this new inner solution consists of an entire series of Airy type differential systems, forced via a non-zero right hand side that involves all possible modes and boundary conditions that specify the nature of the incoming waves.

It may be seen that the existence of a non-zero z dependent cross sectional term $W_1(X,z)$ is necessary for this type of scattering phenomenon to take place. The z dependence of $W_1(X,z)$ is a key point that leads to the non zero integral condition illustrated above, plus a system that consists of zero cross sectional component would clearly give a non zero right hand side and thus no scattering would be induced. Equation (5.55) indicates that an incident mode that undergoes cut-on cut-off transition at X_t will influence the behaviour of neighbouring modes via this non zero right hand side.

Due to the orthogonality of the cross sectional cosine eigenfunctions, i.e.

$$\begin{aligned}\int_0^{h(X)} \cos(\alpha_k z)\cos(\alpha_m z)\mathrm{d}z &= 0 \qquad \forall m \neq k,\\ \int_0^{h(X)} \cos^2(\alpha_k z)\mathrm{d}z &= \frac{h}{2},\end{aligned}$$

it is possible to deduce an equation governing each individual χ_m by multiplying equation (5.55) through by the cross sectional eigenfunction $\cos(\alpha_m z)$ and integrate the resulting equation with respect to z over the entire cross section, leading to a differential equation describing the scattering mechanism for each mode as

$$\begin{aligned}&\varepsilon^{\frac{2}{3}(1-2\vartheta)}\bar{\lambda}^2\chi_m''(\xi) + \varepsilon^{-2\vartheta}\frac{\omega^2 C_0^2(X)\left(\delta_{p,t}+\sigma_t^2(\xi)\right)}{(C_0^2(X)-U_0^2(X))^2}\chi_m(\xi)\\ =\ &\varepsilon^{1-\vartheta}\frac{2\mathrm{i}\bar{\omega}C_0^2\widetilde{W}_1}{\left(C_0^2-U_0^2\right)^2}\sum_{j=1}^{\infty}\left[\alpha_j(X)h(X)\mathcal{C}_{jm}\chi_j(\xi)\right].\end{aligned} \tag{5.57}$$

where a scattering coefficient $\mathcal{C}$ is identified and defined as

$$\mathcal{C}_{jm} = -\frac{2}{h^2(X)}\int_0^h z\sin(\alpha_j z)\cos(\alpha_m z)\mathrm{d}z,$$

where some routine integration gives

$$\mathcal{C}_{jm} = \begin{cases} \frac{1}{2m\pi} & \text{for } j = m,\\ \frac{1}{\pi}\left(\frac{(-1)^{j+m}}{j+m} + \frac{(-1)^{j-m}}{j-m}\right) & \text{for } j \neq m.\end{cases} \tag{5.58}$$

Within the inner scaling region the incident σ_t^2 may be approximated using a Taylor series which, on substitution into equation (5.57) leads to the Airy type equation

$$\begin{aligned}&\bar{\lambda}^2\left(\varepsilon^{\frac{2}{3}(1-2\vartheta)}\chi_m''(\xi) + \varepsilon^{-2\vartheta}\left(\hat{\delta}_{p,t}-\xi\right)\chi_p(\xi)\right)\\ =\ &\varepsilon^{1-\vartheta}\frac{2\mathrm{i}\bar{\omega}C_0^2(X)\widetilde{W}_1(X)z}{\left(C_0^2(X)-U_0^2(X)\right)^2}\sum_{j=1}^{\infty}\left(\mathcal{C}_{jm}\alpha_j(X)\chi_j(\xi)h(X)\right),\end{aligned} \tag{5.59}$$

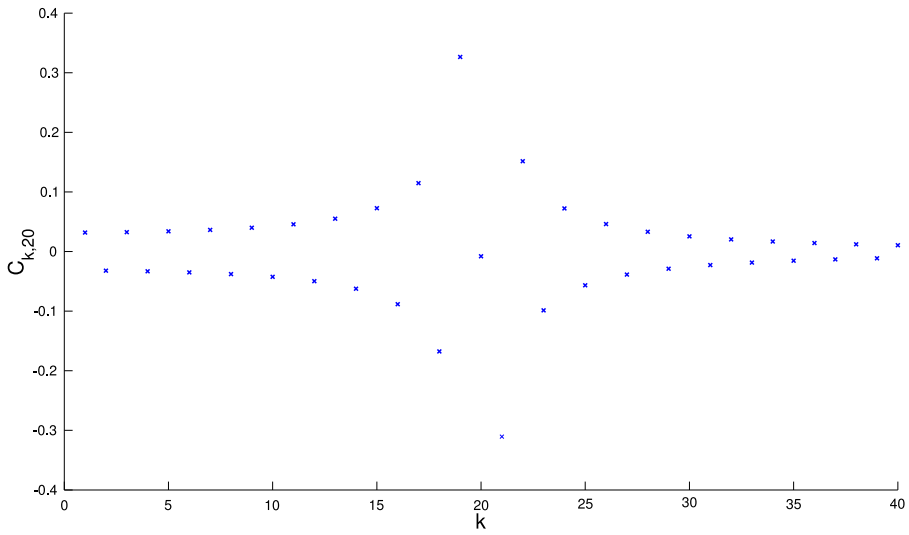

Figure 5.3: Scattering Coefficients $\mathcal{C}_{jm}$ for $1 \leq j \leq 40, m = 20$

where $\hat{\delta}_{p,t}$ is defined for convenience and is given by

$$\hat{\delta}_{p,t} = \frac{\delta_{p,t}\omega^2 C_0^2(X)}{\bar{\lambda}^2(C_0^2 - U_0^2)^2}.$$

The scattering coefficient $\mathcal{C}_{jm}$ is interesting and important because for a given j and m the magnitude of this coefficient gives an indication of the degree of modal energy that is exchanged between modes σ_j and σ_m. Figure (5.3) illustrates the values given by $\mathcal{C}_{jm}$ for $m = 20$. It is important to note that all of the modes absorb some of this energy, and that modes that are local to the incident modes absorb the largest proportion of the scattered modal energy as the incident mode undergoes cut-on cut-off transition. Modes that have $|j - m| = 1$ are deemed modes that are most local to the incident mode and thus these modes are the ones that absorb the most energy. Modes further away from the incident mode absorb less energy, increasingly so as one moves further and further away from the cut-on cut-off incident mode.

As noted in the last section, in order to achieve scattering to leading order, not only is it necessary for all of the above terms to balance within the inner region, but now the additional requirement that $\sigma_j^2 - \sigma_t^2$ must also be of the same order of magnitude as the width of the boundary layer, thus imposing the condition that

$$\sigma_j^2 - \sigma_t^2 \sim \varepsilon^{\frac{2}{3}(1+\vartheta)}.$$

Thus, in order to achieve a balance between the important terms in equation (5.57) (or equivalently equation (5.59)), a balance between all of the following

$$\varepsilon^{\frac{2}{3}(1-2\vartheta)} \sim \varepsilon^{-2\vartheta}\left(\sigma_t^2 + \delta_{p,t}\right) \sim \varepsilon^{1-\vartheta}\alpha_j$$

must be achieved, where the first term is the order of magnitude of the second derivative, the second is the size of σ_j^2, including a term representing the order of magnitude of the shift from σ_t^2, and the third term is the order of magnitude of the relevant non-parallel terms. Recall now that the incident wavenumber σ_t^2 may be expanded using a Taylor series about $X = X_t$ as

$$\begin{aligned} \sigma_t^2 &= \sigma_t^2(X_t) + \varepsilon\xi \frac{\mathrm{d}}{\mathrm{d}X}\left(\sigma_t^2\right)\Big|_{X=X_t} + \dots \\ &= \varepsilon^{\frac{2}{3}(1+\vartheta)}\xi \frac{\mathrm{d}}{\mathrm{d}X}\left(\sigma_t^2\right)\Big|_{X=X_t} + \dots \end{aligned} \tag{5.60}$$

because σ_t^2 vanishes at the turning point by definition. Thus

$$\varepsilon^{-2\vartheta}\left(\sigma_t^2\right) \sim \varepsilon^{\frac{2}{3}(1-2\vartheta)},$$

and hence yielding an automatic balance with the $\chi_m^{''}$ term as expected. For the $\delta_{p,t}$ shift term

$$\delta_{p,t} \sim \frac{\alpha_j}{\omega^2} \sim \alpha_j \varepsilon^{2\vartheta},$$

and this must balance with the non-parallel terms, both of which must balance $\varepsilon^{\frac{2}{3}(1-2\vartheta)}$, thus

$$\alpha_j \sim \varepsilon^{1-\vartheta}\alpha_j \sim \varepsilon^{\frac{2}{3}(1-2\vartheta)},$$

and so if $\vartheta = 1$ this finally yields

$$\omega \sim \varepsilon^{-1}, \quad \alpha_j \sim \varepsilon^{-\frac{2}{3}}, \quad \sigma_t^2 \sim \varepsilon^{\frac{4}{3}}, \quad X - X_t = \varepsilon^{\frac{4}{3}}\bar{\lambda}^{-1}\xi, \quad \delta_{p,t} \sim \varepsilon^{\frac{4}{3}},$$

where it is noted that the difference between σ_js neighbouring the incident σ_t is the same order of magnitude as the width as the boundary layer as required. Note that this implicitly means that the integer $M \sim \varepsilon^{-1}$; to see this, once again consider σ_t with unscaled M, α_t and ω

$$\sigma_t^2 = 1 - \left[\left(C_0^2 - U_0^2\right)\frac{\alpha_t^2 + M^2\pi^2}{\omega^2}\right]$$

and note that if σ_t^2 is truly very small in the boundary layer then the term in the square brackets on the right hand side must be very close to unity around the vicinity of the turning point. However since $\alpha_t \sim \varepsilon^{-\frac{2}{3}}$ then $\alpha_t^2/\omega^2 \sim \varepsilon^{\frac{2}{3}}$ it follows that the only way in which σ_t^2 can get close to zero is if $M^2/\omega^2 \sim 1$, which leads to $M \sim \omega \sim \varepsilon^{-1}$.

So finally then, the full balanced $O(1)$ scattering equation governing the axial amplitudes χ_m in the inner region may now be obtained, and this is given by

$$\chi_m''(\xi) + \left(\hat{\delta}_{p,t} - \xi\right)\chi_m(\xi) = \frac{2\mathrm{i}\bar{\omega}C_0^2(X_t)\widetilde{W}_1(X_t)}{\bar{\lambda}^2\left(C_0^2(X_t) - U_0^2(X_t)\right)^2}\sum_{k=1}^{\infty}\left[C_{km}\alpha_k(X_t)h(X_t)\chi_k(\xi)\right], \tag{5.61}$$

which is now referred to as the *leading order scattering equation.*

Theoretically one could now solve the above scattering equation for each χ_m and then perform an asymptotic matching to the outer solution to obtain reflection and transmission coefficients. However the problem with the above equation is that it is difficult to solve analytically, and solving the above equation numerically will only determine the mechanics of the inner region. Therefore in order to obtain some numerical results it is desirable to form a composite solution that is valid throughout the entire duct, that may then be solved numerically. The development of the composite equation is dealt with in the next section.

5.5 The Composite Equation

The outer solution breaks down as $X \to X_t$ because the second order derivatives with respect to X that were neglected in forming the approximation are the dominant terms in this region. For the inner region when $\omega \sim \varepsilon^{-\frac{1}{2}}$ the inner solution is only valid in the region where $|X - X_t| \sim \varepsilon$. Generally speaking it is desirable to form the so-called *composite solution*, which is a solution that is uniformally valid throughtout the entire duct to leading order. The composite solution encompasses both the slowly varying outer solution (both upstream and downstream) and the inner boundary later solution near the transition point X_t. There are several advantages to the composite solution in that there is no need to calculate the size of the boundary layer, and there is no need for asymptotic matching of two solutions, which is known to be quite difficult for the problem at hand. The solution will be valid for both $|X - X_t| \sim 1$ and $|X - X_t| \sim \varepsilon$. The method by which the composite solution will be derived here is similar to that shown by Ovenden [44].

Composite Equation for $\omega \sim \varepsilon^{-\frac{1}{2}}$

First start with the wave equation, but only including the terms that are known to be important in both the inner and outer regions, so

$$\left(1 - \frac{U_0^2}{C_0^2}\right)\phi_{xx} + \phi_{zz} - \frac{2\mathrm{i}\omega U_0}{C_0^2}\phi_x + \frac{\omega^2}{C_0^2}\phi + \varepsilon\left(-\frac{2\mathrm{i}\omega W}{C_0^2}\phi_z - \frac{2U_0 W}{C_0^2}\phi_{xz}\right) = 0. \tag{5.62}$$

where subscripts denote derivatives. Now let $\omega = \varepsilon^{-\frac{1}{2}}\bar{\omega}$ and let ϕ be represented by a multivariable function $F(x, z)$ multiplied by the usual convective

term

$$\phi = F(x,z)\exp\left(\frac{\mathrm{i}}{\epsilon^{\frac{3}{2}}}\int^X \frac{\bar{\omega}U_0}{C_0^2-U_0^2}\mathrm{d}X'\right). \tag{5.63}$$

The first derivative of ϕ with respect to x is

$$\frac{\partial\phi}{\partial x} = \left[F_x + \frac{\mathrm{i}\varepsilon^{-\frac{1}{2}}\bar{\omega}U_0F}{C_0^2-U_0^2}\right]\exp\left(\frac{\mathrm{i}}{\epsilon^{\frac{3}{2}}}\int^X \frac{\bar{\omega}U_0}{C_0^2-U_0^2}\mathrm{d}X'\right),$$

and the second derivative of ϕ with respect to x is

$$\begin{aligned}\frac{\partial^2\phi}{\partial x^2} &= \left[F_{xx} + \frac{2\mathrm{i}\varepsilon^{-\frac{1}{2}}\bar{\omega}U_0F_x}{C_0^2-U_0^2} - \frac{\varepsilon^{-1}\bar{\omega}^2U_0^2F}{(C_0^2-U_0^2)^2}\right] \\ &\times \exp\left(\frac{\mathrm{i}}{\epsilon^{\frac{3}{2}}}\int^X \frac{\bar{\omega}U_0}{C_0^2-U_0^2}\mathrm{d}X'\right),\end{aligned} \tag{5.64}$$

and the cross derivative is

$$\frac{\partial^2\phi}{\partial x\partial z} = \left[F_{xz} + \frac{\mathrm{i}\varepsilon^{-\frac{1}{2}}\bar{\omega}U_0F_z}{C_0^2-U_0^2}\right]\exp\left(\frac{\mathrm{i}}{\epsilon^{\frac{3}{2}}}\int^X \frac{\bar{\omega}U_0}{C_0^2-U_0^2}\mathrm{d}X'\right),$$

where the subscripts of the function F in all of the above denote differentiation with respect to that variable. Substituting the above derivatives into the governing equation (5.62) and performing some simplifications yields

$$\left(1-\frac{U_0^2}{C_0^2}\right)F_{xx} + F_{zz} + \frac{\varepsilon^{-1}\bar{\omega}^2}{(C_0^2-U_0^2)}F - \varepsilon^{\frac{1}{2}}\frac{2\mathrm{i}\bar{\omega}W}{C_0^2-U_0^2}F_z - \frac{2\varepsilon U_0W}{C_0^2}F_{xz} = O(\varepsilon^{\frac{1}{2}}). \tag{5.65}$$

Note that in order to achieve the above expression, when the derivatives were calculated and substituted into (5.62) a simplification was achieved by combining part of fifth term (which contained the cross derivative of ϕ) with the fourth term, yielding the now familiar scattering term. Thus the first four terms in the above expression now contain all of the information that is necessary to describe both the inner and outer solution, and the fifth term is no longer required meaning that the F_{xz} term in the above can now be ignored.

The function $F(X,z)$ is then split into three parts and represented as

$$F(X,z) = \sum_{k=1}^{\infty} \Phi_k(X)\chi_k(s)\cos\left(\varepsilon^{-\frac{1}{2}}\alpha_k(X)z\right), \tag{5.66}$$

where the Φ_k terms denote the slowly varying part of each mode in X, the $\chi_k(s)$ terms are functions of some new stretched variable s and denote the transitional part of the solution. The stretched variable s varies as a function of X throughout the duct via some function $g(X)$, and so

$$s = \varepsilon^{-\beta} g(X),$$

where the precise definition of $g(X)$ and hence s will be determined within this analysis, but for now it should be noted that $g(X) \sim 1$.

The various required derivatives of $F(x,z)$ with respect to z can be computed as

$$\begin{aligned} F_z &= -\varepsilon^{-\frac{1}{2}} \sum_{k=1}^{\infty} \alpha_k(X)\Phi_k(X)\chi_k(s)\sin\left(\varepsilon^{-\frac{1}{2}}\alpha_k(X)z\right), \\ F_{zz} &= -\varepsilon^{-1} \sum_{k=1}^{\infty} \alpha_k^2(X)\Phi_k(X)\chi_k(s)\cos\left(\varepsilon^{-\frac{1}{2}}\alpha_k(X)z\right), \end{aligned}$$

and in considering the derivatives in x one arrives at

$$\begin{aligned} F_x = &\sum_{k=1}^{\infty} \left(\varepsilon^{1-\beta} g' \Phi_k \chi_k' \cos\left(\varepsilon^{-\frac{1}{2}}\alpha_k z\right) - \varepsilon^{\frac{1}{2}} \alpha_k' \Phi_k \chi_k z \sin\left(\varepsilon^{-\frac{1}{2}}\alpha_k z\right)\right), \\ &+ O(\varepsilon), \\ F_{xx} = &\sum_{k=1}^{\infty} \left(\varepsilon^{2-2\beta}(g')^2 \Phi_k \chi_k'' \cos\left(\varepsilon^{-\frac{1}{2}}\alpha_k z\right) - 2\varepsilon^{\frac{3}{2}-\beta} \alpha_k' g' \Phi_k \chi_k' z \sin\left(\varepsilon^{-\frac{1}{2}}\alpha_k z\right)\right) \\ &+ O(\varepsilon^{2-\beta} + \varepsilon), \end{aligned} \tag{5.67}$$

and for the cross derivative term

$$F_{xz} = -\varepsilon^{-\frac{1}{2}} \sum_{k=1}^{\infty} \left(\varepsilon^{1-\beta} g' \alpha_k \Phi_k \chi_k' \sin\left(\varepsilon^{-\frac{1}{2}} \alpha_k z\right) + \varepsilon^{\frac{1}{2}} \alpha_k \alpha_k' \Phi_k \chi_k' z \cos\left(\varepsilon^{-\frac{1}{2}} \alpha_k z\right) \right) + O(\varepsilon). \tag{5.68}$$

It is necessary at this stage to determine the value of β, and the manner in which this task is done is to review the equation (5.65) and the various derivatives and use the knowledge obtained from the study of the inner and outer solutions in order to determine what value of β keeps in all the relevant terms and ignores the irrelevant terms. As mentioned earlier the F_{xz} term in equation (5.65) is not a significant term because this term does not feature in either the inner or outer solution to leading order. Another way of looking at this is that by noticing that the χ' and α' terms were not significant to leading order in both the inner solution and outer solution, and thus an inequality condition on β can be formed by considering values of β such that these terms are not included.

Thus for the F_{xz} to not be included in the formulation

$$\varepsilon\varepsilon^{-\frac{1}{2}}\varepsilon^{1-\beta} < \varepsilon^{\frac{1}{2}} \quad \Longrightarrow \quad \varepsilon^{\frac{3}{2}-\beta} < \varepsilon^{\frac{1}{2}},$$

which leads to

$$\frac{3}{2} - \beta \geq \frac{1}{2} \quad \Longrightarrow \quad \beta \leq 1. \tag{5.69}$$

Another condition on β can be obtained by considering the fact that it is necessary to include the χ'' term into the composite solution if the aim is to include the effects of the inner boundary layer solution. This is achieved by considering a condition on β that makes the χ'' term more significant than $\varepsilon^{\frac{1}{2}}$,

and therefore by looking at the expression (5.67) and concluding that

$$\varepsilon^{2-2\beta} > \varepsilon^{\frac{1}{2}},$$

which leads to the inequality

$$2 - 2\beta < \frac{1}{2} \qquad \Longrightarrow \qquad \beta > \frac{3}{4}. \tag{5.70}$$

Hence in combining inequalities (5.69) and (5.70) one arrives at

$$\frac{3}{4} < \beta \leq 1.$$

The method by which a differential equation for each χ_m is obtained is very similar to when the inner equation was constructed. The function F and all of the calculated derivatives are substituted into equation (5.65), and the entire system is multiplied by a cross sectional eigenfunction and integrated to give (after some manipulation)

$$\begin{aligned}\Phi_m(X)\left\{\frac{\mathrm{d}^2}{\mathrm{d}s^2}\left(\chi_m(s)\right) + \varepsilon^{2\beta-3}\frac{\bar{\omega}^2 C_0^2(X)\sigma_m^2}{[g'(X)]^2(C_0^2(X)-U_0^2(X))^2}\chi_m(s)\right\} \\ -\varepsilon^{2\beta-2}\frac{2\mathrm{i}\bar{\omega}\widetilde{W}(X)C_0^2(X)h(X)}{[g'(X)]^2(C_0^2(X)-U_0^2(X))^2}\sum_{k=1}^{\infty}\chi_k(s)\alpha_k(s)\Phi_k(s)\mathcal{C}_{km} = 0\end{aligned} \tag{5.71}$$

where $\mathcal{C}_{km}$ is defined by equation (5.58). Note that Φ_m has not yet been fixed. The above problem for χ_m is a standard WKB problem and thus in regions far from where the scattering effects are felt the solution can be expected to replicate the outer solution. Thus as with Ovenden 2005 [44] the following condition must be imposed

$$\Phi_m(X)\sqrt{\frac{C^2(X)-U^2(X)}{\omega C(X)\sigma(X)}} = \sqrt{\frac{C(X)}{\omega\sigma(X)D(X)h(X)}},$$

and therefore

$$\Phi_m(X) = \sqrt{\frac{C^2}{(C^2-U^2)D(X)h(X)}},$$

which is independent of the mode, and therefore $\Phi_m(X) = \Phi_0(X)$ for all m and thus it cancels out of the scattering equation. Now let $m = t + p$ and $k = t + q$, then equation (5.71) becomes

$$\frac{\mathrm{d}^2}{\mathrm{d}s^2}\left(\chi_{t+p}(s)\right) + \varepsilon^{2\beta-3}\frac{\bar{\omega}^2 C_0^2(X)\left(\sigma_t^2 + \delta_{t,p}\right)}{[g'(X)]^2(C_0^2(X) - U_0^2(X))^2}\chi_{t+p}(s)$$
$$-\varepsilon^{2\beta-2}\frac{2\mathrm{i}\bar{\omega}\widetilde{W}(X)C_0^2(X)h(X)}{[g'(X)]^2(C_0^2(X) - U_0^2(X))^2}\sum_{q=-t+1}^{\infty}\chi_k(s)\alpha_{t+q}(s)\mathcal{C}_{km} = 0.$$

It is possible to make a direct comparison between the above equation and the leading order scattering equation (5.61) and comparing the first two terms in the equation gives

$$\varepsilon^{2\beta-3}\frac{\bar{\omega}^2 C_0^2(X)(\sigma_t^2)}{[g'(X)]^2(C_0^2(X) - U_0^2(X))^2} = -s = -\varepsilon^{-\beta}g(X),$$

and therefore if these two terms are to balance then

$$2\beta - 3 = -\beta \quad \Longrightarrow \beta = 1.$$

Now that β is known all that remains is to determine $g(X)$, which can be found by solving the differential equation

$$\left[\frac{\mathrm{d}}{\mathrm{d}X}g(X)\right]^2 g(X) = -\frac{\bar{\omega}^2 C_0^2(X)\sigma_t^2(X)}{(C_0^2(X) - U_0^2(X))^2}$$

taking the square root of both sides and integrating yields for the axial variation variable $g(X)$

$$g(X) = \left(\pm\frac{3\mathrm{i}}{2}\int_{X_t}^{X}\frac{\bar{\omega}C_0(X')\sigma_t(X')}{C_0^2(X') - U_0^2(X')}\mathrm{d}X'\right)^{\frac{2}{3}},$$

and hence finally for the stretched variable s

$$s = \varepsilon^{-1}g(X) = \left(\frac{3\mathrm{i}}{2\varepsilon^{3/2}}\int_{X_t}^{X}\frac{\bar{\omega}C_0(X')\sigma_t(X')}{C_0^2(X') - U_0^2(X')}\mathrm{d}X'\right)^{\frac{2}{3}}.$$

and the solution branch is chosen such that s is negative for $X < X_t$ and positive for $X > X_t$.

Now, noting that

$$\frac{C_0^2(X)}{(g'(X))^2(C_0^2-U_0^2)^2} = -\frac{s}{\bar{\omega}^2\sigma_t^2} = -\frac{1}{\bar{\omega}^2\sigma_t^2}\left(\frac{3\mathrm{i}}{2}\int_{X_t}^{X}\frac{\bar{\omega}C_0(X')\sigma_t(X')}{C_0^2(X')-U_0^2(X')}\mathrm{d}X'\right)^{\frac{2}{3}}$$

the equation may now be written entirely in terms of the coordinate s as

$$\begin{aligned}&\chi''_{t+p}(s) - s\chi_{t+p}(s) - \frac{s\delta_{t,p}}{\sigma_t^2}\chi_{t+p}(s)\\ &- 2\mathrm{i}\bar{\omega}\widetilde{W}(s)h(s)\left(-\frac{s}{\bar{\omega}^2\sigma_t^2}\right)\sum_{q=-t+1}^{\infty}\chi_{t+q}(s)\alpha_{t+q}(s)C_{(t+q),(t+p)}.\end{aligned}$$

Now define $\mathscr{L}(s)$ as

$$\mathscr{L}(s) = \left(\frac{3\mathrm{i}}{2\sigma_t^3}\int_{X_t}^{X}\frac{\omega C_0\sigma_t}{C_0^2-U_0^2}\mathrm{d}X'\right)^{\frac{2}{3}} = -\frac{\bar{\omega}^2C_0^2}{(g')^2(C_0^2-U_0^2)^2} = \frac{s}{\sigma_t^2},$$

where it is noted that the definition above is <u>not</u> singular for $\sigma_t \to 0$ (see Ovenden 2005 [44]). Thus finally the equation for the composite solution is

$$\begin{aligned}&\chi''_{t+p}(s) - (s-\mathscr{L}(s)\delta_{t,p})\chi_{t+p}(s)\\ &+ \frac{2\mathrm{i}}{\bar{\omega}}\widetilde{W}(s)h(s)\mathscr{L}(s)\sum_{q=-t+1}^{\infty}\chi_{t+q}(s)\alpha_{t+q}(s)\mathcal{C}_{(t+q),(t+p)},\end{aligned} \tag{5.72}$$

and solving the equation above will yield a solution that is valid throughout the entire duct for each mode.

Summary

The purpose of the work presented in this chapter was to understand the mechanism by which modal scattering may be achieved whenever a mode undergoes cut-on cut-off transition. The phenomenon has been shown to occur using the finite element analysis in Ovenden, Eversman and Rienstra [43], but up until this point a mechanism for cut-on cut-off induced modal scattering in the presence of mean flow has not been discovered using the multiple scales

approach.

Within this chapter it was shown that the original order of magnitude estimate for ω from [43] was in fact an overestimate for flow induced scattering, although as shown by Smith, Ovenden and Bowles [58] this condition is sufficient for geometry induced scattering. The condition for flow induced modal scattering was re-examined, and on this analysis it was shown that weak modal scattering may occur at the much lower estimate of $\omega \sim \varepsilon^{-\frac{1}{2}}$. Weak scattering here actually refers to weak scattering for the excited modes, as the incident mode experiences scattering to leading order.

For the weak scattering it was noted that the scattering is weak for $\omega \sim \varepsilon^{-\frac{1}{2}}$ because the modes are not sufficiently close together to yield scattering for all modes to leading order. Thus the analysis was revisited once again with the notion that the modes should be sufficiently close together, and as a result an equation for the inner region governing scattering for all modes to leading order was obtained, and it was shown that scattering to leading order may be achieved when $\omega \sim \varepsilon^{-1}$.

Performing an asymptotic matching of the inner and outer solutions appears difficult, and is left as further work. However from a computational point of view it is desirable to form a model for the so-called composite solution, valid throughout the entire duct to leading order, and the equation governing the composite solution for each mode was given at the end of the last section.

Given that a model for the composite solution is now in place, it is possible to perform some simulations of modal scattering using a desired numerical method. However for reasons that will be briefly discussed in the next section, several difficulties lie with using the derived composite equation (5.72), most of them to do with the idea of using the derived stretch variables. Nonetheless a small simplification may be made in order to yield some very interesting and useful results without encountering too many difficulties with regard to the numerics.

Chapter 6

Numerical Results on Modal Scattering

6.1 Computational Methods

In the last chapter, a model for the composite solution, which is valid throughout the entire duct was derived. However there are several difficulties with the equation for the composite solution. The cut-on cut-off incident mode defines a new stretch variable s, and thus everything must be written as a function of this new and fairly complicated stretch variable. As an analytical solution of the equation seems unlikely at this stage, the above equation would need to be solved numerically and then converted back into physical coordinates.

As it appears that the equation is to be solved numerically in terms of the stretch variable s and then converted back into real coordinates x, it makes sense just to use real coordinates from the beginning. Therefore as an alter-

native to solving the full composite equation it is desirable to simplify the equation for the composite solution in such a way that utilising the finite difference method becomes easy to apply immediately. In this chapter matters are simplified by seeking the solution to the simpler yet related system by defining the stretch variable s as $s = \varepsilon^{-1}X = x$. With this simplification the coupled ODE system then becomes

$$\Phi(X)\left[\chi_n''(x) + \frac{\bar{\omega}^2 C_0^2 \sigma_n^2}{(C_0^2 - U_0^2)^2}\chi_n(x) - \frac{2\mathrm{i}\bar{\omega}\widetilde{W}(X)C_0^2}{(C_0^2 - U_0^2)^2}\sum_k \alpha_k(X)h(X)\chi_k \mathcal{C}_{kn}\right] = 0 \tag{6.1}$$

for $n = 1, 2, 3 \ldots N$, where it is recalled that the scattering coefficient $\mathcal{C}_{kn}$ is given by

$$\mathcal{C}_{kn} = \begin{cases} \frac{1}{2n\pi} & \text{for } k = n, \\ \frac{1}{\pi}\left(\frac{(-1)^{n+k}}{n+k} + \frac{(-1)^{k-n}}{k-n}\right) & \text{for } k \neq n, \end{cases}$$

as before, and $\Phi(X)$ is the so-called slowly-varying coefficient, given by

$$\Phi(X) = \sqrt{\frac{C_0(X)}{(C_0^2(X) - U_0^2(X))D_0(X)h(X)}},$$

with $h(X)$ being the height of the channel. Note that $\Phi(X)$ is the same for each mode as discussed at the end of the last chapter . The system defined above is the one that will be solved numerically using a finite difference scheme, the method of which is described here in some detail over the next few pages.

The Computational Domain and Non-Reflecting Boundary Conditions

The computational domain that will be used is defined as

$$x_{\min} < x < x_{\max}, \quad 0 < y < 1, \quad 0 \leq z \leq h(x) \tag{6.2}$$

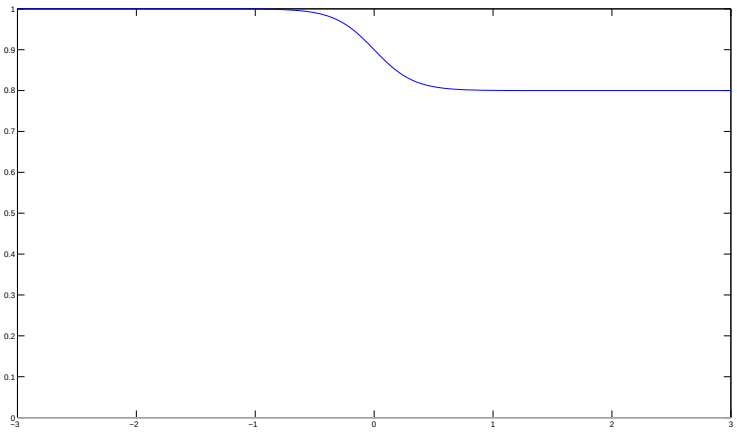

Figure 6.1: A plot of a typical computational domain

where the the height function $h(x)$ is defined as

$$h(x) = 1 - h_s - h_s \tanh(a_0 x)$$

and h_s and a_0 are constants. The flow geometry has deliberately been chosen in such a way as to make the liklihood of cut-on cut-off transition and scattering as high as possible. A sketch typical duct can be seen in figure 6.1.

Note that within the discussions outlined here it is useful to get an idea of the size of the small parameter ε, and it is usually given as a typical (or average) duct gradient. In this case an estimate for ε will be taken as

$$\varepsilon \simeq \left| \frac{1}{2x_1} \int_{-x_1}^{x_1} h'(x) \mathrm{d}x \right|,$$

for some suitably chosen x_1. It is straightforward to show then that ε may be approximated by

$$\varepsilon \simeq \frac{h_s}{x_1} \tanh(a x_1).$$

Another very important notion to consider before establishing the finite difference scheme is as follows. For many idealised problems in aeroacoustics, including this one, the domain of interest is unbounded. Suppose that this unbounded domain is denoted Ω. In order to treat the problem numerically it is necessary to consider a finite domain $D \subset \Omega$, and by doing this one introduces an artificial boundary ∂D into the numerical problem. In defining ∂D, one has to introduce boundary conditions on ∂D, and it is very important that the boundary conditions must be chosen in such a way that waves hitting ∂D from inside the computational domain are transmitted through ∂D without any spurious reflections. An incorrect choice of boundary conditions may produce large spurious reflections of waves from ∂D, leading to large errors in the computed solution. Boundary conditions that are implemented on the boundary of a finite domain with the intention of preventing spurious reflections are known as non-reflecting boundary conditions (or NRBCs for short). A well designed NRBC should be designed in such a way as to let waves generated from inside D leave the domain through ∂D without any spurious reflections. For an in-depth discussion of NRBCs the reader is directed to papers by Givoli [20] and Ching [32].

Note that the creation of non reflecting boundary conditions is not the only way in which reflections at the boundary of the computational domain may be prevented; other methods to combat spurious reflecting waves include using a sponge/buffer zone region, whereby a damping term is introduced into the governing equation at a certain distance from ∂D inside the computational domain, where the idea behind this is to diminish the strength of the outgoing

waves so that by the time they hit the boundary there is very little or no reflection. Another technique that is becoming more popular is the introduction of so-called perfectly matched layers (PMLs), which were originally formulated by Berenger in 1994 [3], and are to some extent an elegant extension of a non-reflecting boundary condition. However for the purposes discussed here a NRBC is a simple and sufficient method by which to deal with the problem of reflecting waves.

Given the geometry indicated in (6.2), it is simple to achieve an NRBC by noting that close to the domain boundaries where $x \sim x_{\min}$ and $x \sim x_{\max}$, the vertical mean flow velocity $\widetilde{W}(X) \sim 0$, and therefore near these points the system described in (6.1) may be approximated by the harmonic equation

$$\chi_n''(x) + \frac{\bar{\omega}^2 C_0^2 \sigma_n^2}{(C_0^2 - U_0^2)^2}\chi_n(x) = 0, \quad n = 1, 2, \ldots N. \tag{6.3}$$

which is a very accurate approximation for the modal propagation within this region provided that the geometry has very little variation in the applicable region. Thus for χ_n equation it is simple to form a non reflecting boundary condition (NRBC) at both the left-hand boundary and right-hand boundaries as follows. For each $x \sim x_{\min}$ the general solution for $\chi_n(x)$ is given by

$$\chi_n(x) \sim A_n e^{-\mathrm{i}k_n x} + B_n e^{\mathrm{i}k_n x}$$

where the wavenumber k_n is given by

$$k_n^2 = \frac{\bar{\omega}^2 C_0^2 \sigma_n^2}{(C_0^2 - U_0^2)^2}.$$

In this notation, A_n is the amplitude of the right-running mode and B_n is the left running mode. Note then that for this general solution

$$\chi_n'(x) - \mathrm{i}k_n\chi_n(x) = -2\mathrm{i}k_n\bar{A}_n, \quad \text{where} \quad \bar{A} = Ae^{-\mathrm{i}k_n x}$$

where $\bar{A}$ has been used to absorb a complex constant that has unit magnitude. Now in order to form a non-reflecting boundary condition at the left hand end of the channel, any right-running modes that are not incident must be eliminated. If the amplitude of the right running incident mode is given by $\bar{A}_n$, then a non reflecting boundary condition may be achieved by setting the condition that

$$\chi_n'(x) - \mathrm{i}k_n\chi_n(x) = -2\mathrm{i}k_n\bar{A}_n \quad \text{on} \quad x = x_{\min}, \tag{6.4}$$

and by setting this condition we have eliminated all spurious right running reflections at the left hand boundary. Similarly for modes entering the computational domain at the right hand boundary, for $x \sim x_{\max}$ the modes propagate according to the general formula

$$\chi_n(x) \sim C_n e^{-\mathrm{i}k_n x} + D_n e^{\mathrm{i}k_n x}.$$

At this boundary it is necessary to prevent any non-incident left-running modes from being reflected, and thus if the incident modal amplitude is given by D_n then the non reflecting boundary condition to be imposed at this boundary is

$$\chi_n'(x) + \mathrm{i}k_n\chi_n(x) = -2\mathrm{i}k_n\bar{D}_n \quad \text{on} \quad x = x_{\max},$$

where $\bar{D}_n = De^{\mathrm{i}k_n x}$. However in the results presented here all incident modes will be assumed to be right-running and so the non-reflecting boundary con-

dition at $x = x_{\max}$ reduces to

$$\chi_n'(x) + \mathrm{i}k_n\chi_n(x) = 0 \quad \text{on} \quad x = x_{\max}. \tag{6.5}$$

Description of the Finite Difference Scheme

The system that a computational solution is required for is

$$\Phi(X)\left(\chi_n''(x) + \frac{\bar{\omega}^2 C_0^2 \sigma_m^2}{(C_0^2 - U_0^2)^2}\chi_n(x)\right) = \frac{2\mathrm{i}\bar{\omega}\widetilde{W}(X)C_0^2}{(C_0^2 - U_0^2)^2}\sum_k \alpha_k(X)C_{kn}h(X)\chi_k,$$

subject to the non reflecting boundary conditions (6.4) and (6.5). In order to establish a finite difference solution to this system, first define an equally spaced mesh in the axial direction as

$$x_i = x_{\min} + i\Delta x, \quad i = 1, 2, \ldots, N.$$

The aim is to discretise the above differential system and boundary conditions such that the resulting system is tridiagonal. Once the system has been reduced to a tridiagonal system, it may be solved using an algorithm such as the Thomas algorithm.

The discretisation of the above system may be achieved using second order central differencing on the second derivative, i.e.

$$\left(\frac{\mathrm{d}^2}{\mathrm{d}x^2}\chi_n(x)\right)_{x=x_i} = \frac{\chi_n^{(i-1)} - 2\chi_n^{(i)} + \chi_n^{(i+1)}}{\Delta x^2} + O(\Delta x^2)$$

to give for the system of interest

$$\Phi^{(i)}\left(\chi_n^{(i+1)} + ((k_n^{(i)})^2\Delta x^2 - 2)\chi_n^{(i)} + \chi_n^{(i-1)}\right) = \Delta x^2\varphi^{(i)},$$

where $\chi_n^{(i)}$ denotes the i'th node in the computational domain corresponding to the sought after $\chi_n(x)$. The right hand side coefficient $\varphi^{(i)}$ is given by

$$\varphi^{(i)} = \frac{2\mathrm{i}\bar{\omega}\widetilde{W}(x_i)C_0^2(x_i)}{h}(x_i)(C_0^2(x_i) - U_0^2(x_i))^2 \sum_k \alpha_k(x_i)\mathcal{C}_{kn}\chi_j(x_i)$$

For the boundaries it is necessary to use the non-reflecting boundary conditions that were established earlier. Finite differencing the NRBC at the left hand side of the domain yields

$$\chi_n^{(1)} = \frac{1}{3 + 2\mathrm{i}k_n^{(1)}\Delta x}\left(4\mathrm{i}k_n^{(1)}A_n\Delta x + 4\chi_n^{(2)} - \chi_n^{(3)}\right),$$

and then substituting this into the finite difference scheme above one arrives at

$$\chi_n^{(2)}\left(1 - \frac{1}{3 + 2\mathrm{i}k_n^{(1)}}\right) + \chi_n^{(1)}\left((k_n^{(1)})^2\Delta x^2 - 2 + \frac{4}{3 + 2\mathrm{i}k_n^{(1)}}\right) = -\frac{4\mathrm{i}k^{(1)}A_n\Delta x}{3 + 2\mathrm{i}k_n^{(1)}},$$

which is to be applied as the left hand boundary term in the Thomas algorithm. A similar procedure for the right hand boundary yields

$$\chi_n^{(N-2)}\left(1 - \frac{1}{3 + 2\mathrm{i}k_n^{(N-1)}}\right) + \chi_n^{(N-1)}\left((k_n^{(N-1)})^2\Delta x^2 - 2 + \frac{4}{3 + 2\mathrm{i}k_n^{(N-1)}}\right)$$
$$= -\frac{4\mathrm{i}k_n^{(N-1)}A_n\Delta x}{3 + 2\mathrm{i}k_n^{(N-1)}}.$$

The scheme above is valid for all $2 \leq i \leq N-1$, and the nodes $i = 1$ and $i = N$ lie on the boundaries of the domain. The equations above are all that is required in order to solve this system numerically. The above system may be solved via several iterations using a Thomas algorithm. Several iterations are necessary here because the modal equations are coupled as the $\varphi^{(i)}$ term contains a summation involving all χ_k's for $k = 1, \ldots N$. Thus running the Thomas algorithm several times is necessary in order for the solution to converge to the correct value.

Once all of the χ_n's are known the desired solution for the acoustic field is given by the summation

$$\phi = \sum_{j=1}^{J_{\text{Max}}} \Phi(X)\chi_j(x)\cos\left(\alpha_j(X)z\right)\cos\left(M\pi y\right)\exp\left(\mathrm{i}\int_{X_t}^{X}\frac{\omega U_0}{C_0^2-U_0^2}\mathrm{d}X'\right), \quad (6.6)$$

and this may be obtained simply by multiplying each χ_j by the necessary quantities shown in the above, all of which are easily computed. For the initial incoming (right running) amplitudes, these are set by the vector A_j for $j = 1, 2, \ldots, J_{\text{Max}}$, and similarly the initial left running incoming amplitudes are set by a vector D_j. For simplicity here the amplitudes $\bar{A}_j$ and $\bar{D}_j$ are specified as the exact phase is not considered important in this investigation.

Results in this chapter were obtained using Matlab, and details of the Matlab code used in obtaining the results may be obtained from the author.

6.1.1 Results Processing

Once the code has run for a given case, it is necessary to obtain several physical quantities from the numerical results. This section gives a short description of what the quantities of interest are and how they are computed from the numerical results

Computing the Modal Amplitudes

Plotting the modal amplitudes for each mode is straightforward. All that is needed required is to plot $|\Phi(X)\chi_j(x)|$ for any mode that is required. It is usual to separate plots for the incident mode from that of the scattered modes

as typically the amplitude of the scattered modes will be much lower than that of the incident mode.

Outgoing modal Amplitudes

For both incident and scattered modes it is useful to understand to what degree individual modes are propagating out of the computational domain. If the incident mode(s) is(are) given by $j = t$, then the scattered modes are indexed by $j \neq t$. For the scattered modes there is no incoming wave ($A_{j\neq t} = 0$), and therefore to find the outgoing modal amplitude of a scattered wave this is simply given by the value of $|\Phi(X)\chi_{j\neq t}(x)|$, to be calculated at the domain boundary. In fact this formula may be used to compute the modal amplitude of a scattered mode anywhere within the computational domain.

Now for the incident modes: Assume that there is a right running incident mode $j = t$ with no incident left-running counterpart. At the left-hand end the solution is for χ_t is

$$\chi_t(x) = A_t\,\mathrm{e}^{-\mathrm{i}k_t x} + B_t\,\mathrm{e}^{+\mathrm{i}k_t x}\,.$$

In order to find the outgoing modal amplitude B_t the incident amplitude A_t may be eliminated by differentiating the above expression with respect to x and adding finding that

$$\chi_t' + \mathrm{i}k_t\chi = 2\mathrm{i}k_t\tilde{B} \quad \Longleftrightarrow \quad \tilde{B} = \frac{\chi' + \mathrm{i}k_t\chi}{2\mathrm{i}k},$$

where $\tilde{B} = B\,\mathrm{e}^{+\mathrm{i}k_t x}$. A finite difference approximation is then applied to give

$$\tilde{B} = \frac{1}{4\mathrm{i}k^{(0)}\Delta x}\left((-3 + 2\mathrm{i}k_t^{(0)}\Delta x)\chi_t^{(0)} + 4\chi_t^{(1)} - \chi_t^{(2)}\right),$$

and the quantity $\chi_t^{(0)}$ may be found by recalling that the non reflecting boundary condition at the left hand boundary is

$$\chi'_{j0} = \mathrm{i}k_j\chi_{j0} - 2\mathrm{i}k_jA_j, \tag{6.7}$$

where χ_{j0} is the value of $\chi_j(x_{\min})$ at the left-hand end of the domain. Finite differencing the above equation yields

$$\frac{-3\chi_{j0} + 4\chi_{j1} - \chi_{j2}}{2\Delta x} = \mathrm{i}k_t\chi_{j0} - 2\mathrm{i}k_jA_j,$$

where χ_{j1} and χ_{j2} are the computed values at $x = x_0 + \Delta x$ and $x = x_0 + 2\Delta x$ respectively so that

$$\chi_{j0} = \frac{4\chi_{j1} - \chi_{j2} + 4\mathrm{i}k_j\Delta xA_j}{(3 + 2\mathrm{i}k_j\Delta x)}, \tag{6.8}$$

and thus the outgoing modal amplitude B_t at the left-hand end is finally given by

$$|\Phi(x_0)B_t| = |\Phi(x_0)|\left|\frac{\chi'_t(x_0) + \mathrm{i}k_t(x_0)\chi_t(x_0)}{2k_t(x_0)}\right|.$$

Now that the outgoing modal amplitude is known it is now possible to compute the reflection coefficient $|R_t|$ as may be found by computing

$$|R_t| = \frac{\tilde{B}}{|A_t|},$$

where it is noted that although the actual modal amplitude also includes the slowly varying coefficient $\Phi(X)$, where it is noted that the slowly varying coefficient term Φ is not required as it is exactly the same for both the incident and reflected mode.

At the right-hand end, as it is assumed that there is no incoming wave from $+\infty$ the solution is

$$\chi_t = T_t\,\mathrm{e}^{-\mathrm{i}k_tx},$$

and therefore finding the modal amplitude is straightforward and a transmission coefficient can be found.

Calculation of Acoustic Pressure

As part of the results processing it is very useful to obtain contour plots of relative sound pressure level. Recall from equation (1.10) that the acoustic pressure p is given by

$$\frac{p}{D_0} = -\mathrm{i}\omega\phi - U_0\frac{\partial\phi}{\partial X}, \tag{6.9}$$

and substituting the scattered solution for ϕ into the above yields to leading order

$$|p| = D_0\Phi(X)\sum_{j=1}^{J_{\max}}\cos\left[\alpha_j(X)z\right]\left(-\frac{\mathrm{i}\omega C_0^2}{(C_0^2-U_0^2)}\chi_j - U_0\chi_j'\right).$$

This formula for $|p|$ may then be used in the pressure contour plots. It is sensible to plot these contours on the decibel scale, i.e. $20\log_{10}\left(|p(x,z)|/\max|p(x,z)|\right)$, with contour levels at every 3dB, and this is what is plotted in the pressure contours presented here.

6.2 Results

The results shown here are separated into four cases: Three of these case are for two-dimensional scattering (i.e. where $M = 0$ in equation (5.3) for example), and the final case deals with three dimensional scattering where $M \neq 0$.

Case 1: Modal Propagation consisting of a single left-running incident mode with $\omega = 35, U_0(-\infty) = \pm 0.3, M = 0$, $h_s = 0.1$, $a_0 = 3$ and $n = 10$

In this first example a two dimensional ($M = 0$) duct with a reasonably high Helmholtz number $\omega = 35$ is considered. In this case there is only one incident mode, and this mode is right-running of unit amplitude indexed by $n = 10$. All other modes (both left and right-running) have zero incident amplitude, and so $A_{10} = 1$ and $A_{n \neq 10} = 0$ for all n. Modes given by $n < 10$ are cut-on throughout the entire region, and the $n = 10$ mode cuts off at the point $X_{10t} \approx 0.64$, and the $n = 11$ mode also cuts off at some point $X_{11t} \approx -0.03$, both lying within the computational domain. A non-dimensional axial mean flow of magnitude 0.3 is imposed. Given the geometry variation the small parameter may be approximated by $\varepsilon \simeq 0.1$, and thus comparing this value to the Helmholtz number means that a strong degree of scattering is expected to occur. The model is run for two cases; one case where the mean flow is running from left to right ($U_0 = 0.3$) and another case where the mean flow is running from right to left ($U_0 = -0.3$).

According to the standard multiple scales theory where the effects of modal scattering are not taken into consideration, the mode corresponding to $n = 10$ propagates from left to right, and its reduced axial wavenumber σ_{10} decreases as the duct narrows until the point where $\sigma_{10} = 0$ at $X = X_{10t}$. Beyond X_{10t}, the reduced axial wavenumber is purely imaginary and no further acoustic energy is transmitted beyond X_{10t}, and the mode reflects at X_{10t} exchanging

its entire acoustic energy with its left-running counterpart, causing a standing wave to be formed within the duct. According to the standard multiple scales theory, energy for this mode is completely conserved. The maximum amplitude of the resulting standing wave is equal to 2, which can be seen in figures 6.2 and 6.3 for the no scattering case. No acoustic energy is transmitted beyond X_{10t} in this case, as shown by the fact that the modal amplitude reduces to zero beyond the transition point X_{10t}. Also figures 6.6 (a) and 6.7 (a) show contour plots of the acoustic pressure everywhere within the duct for this standard multiple scales case, and the region beyond the turning point at which no acoustic energy propagates may be clearly seen. Within this standard multiple scales model, it is important to note that other than the left-running counterpart of the incident mode no other modes are excited during this cut-on cut-off transition process.

Once the effects of scattering is taken into account, the results appear very different to the results obtained by the standard multiple scales model. It can now be seen that as soon as scattering effects are included, the modes neighbouring the incident mode appear to be excited within the thin narrowing region of the duct, and a cascade of reflected left-running and transmitted right-running modes are now observed. Figures 6.4 and 6.5 show amplitude plots of these modes modes for $U_0(-\infty)$ equal to 0.3 and -0.3 respectively. The modes that are directly adjacent to the incident mode (i.e. those that are indexed by $n = 9, 11$) are the modes that absorb most of the scattered acoustic energy, although in fact all modes are excited to some extent, a fact

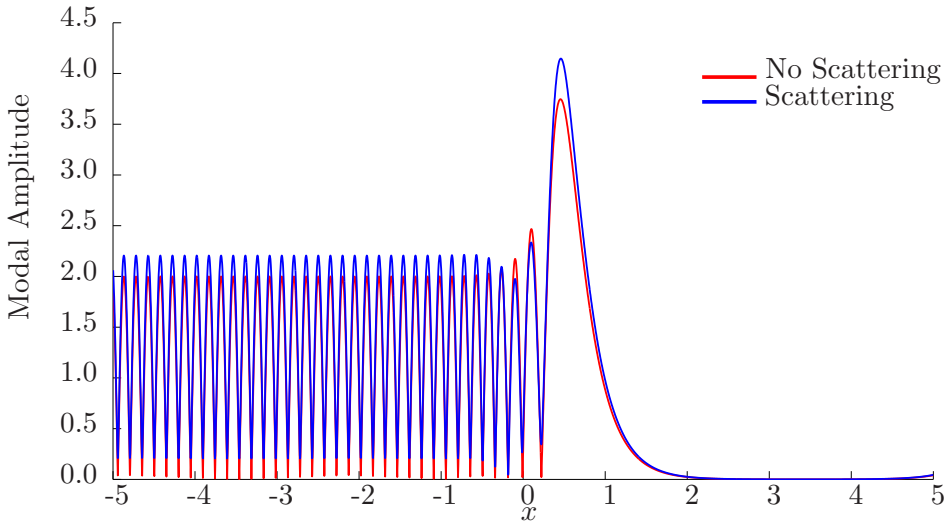

Figure 6.2: Case 1 with $U(-\infty) = +0.3$: Comparing the modal amplitude of the incident mode both with and without scattering effects included

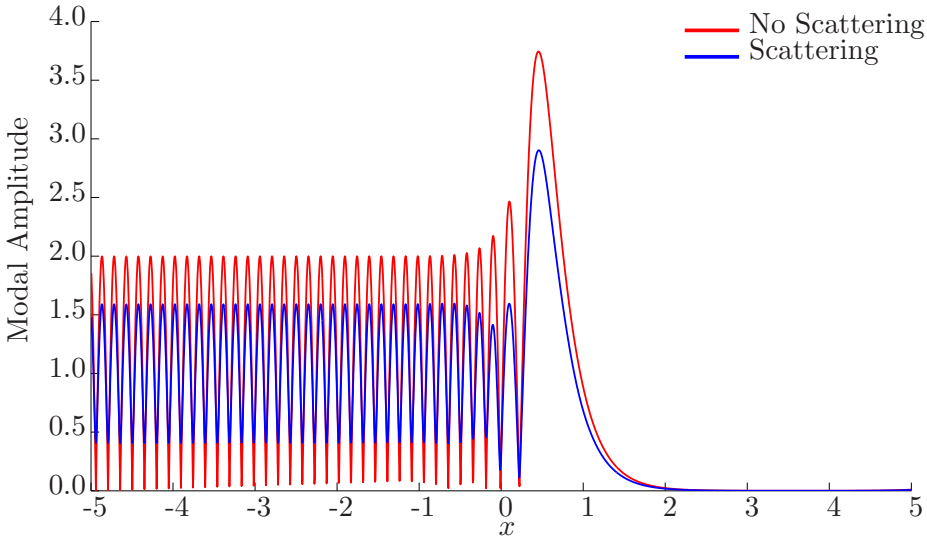

Figure 6.3: Case 1 with $U(-\infty) = -0.3$: Comparing the modal amplitude of the incident mode both with and without scattering effects included

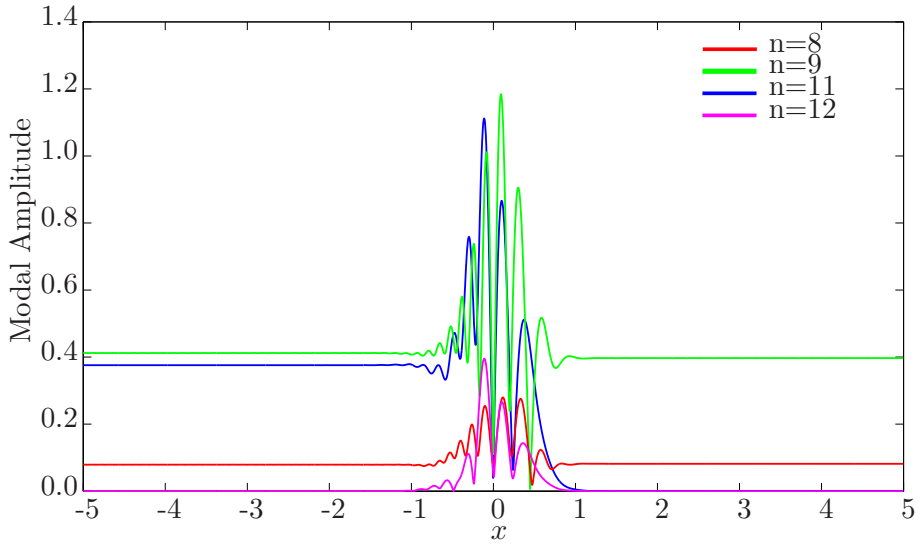

Figure 6.4: Case 1 with $U(-\infty) = +0.3$: Comparing the neighbouring modal amplitudes for $n = 8, 9, 11, 12$

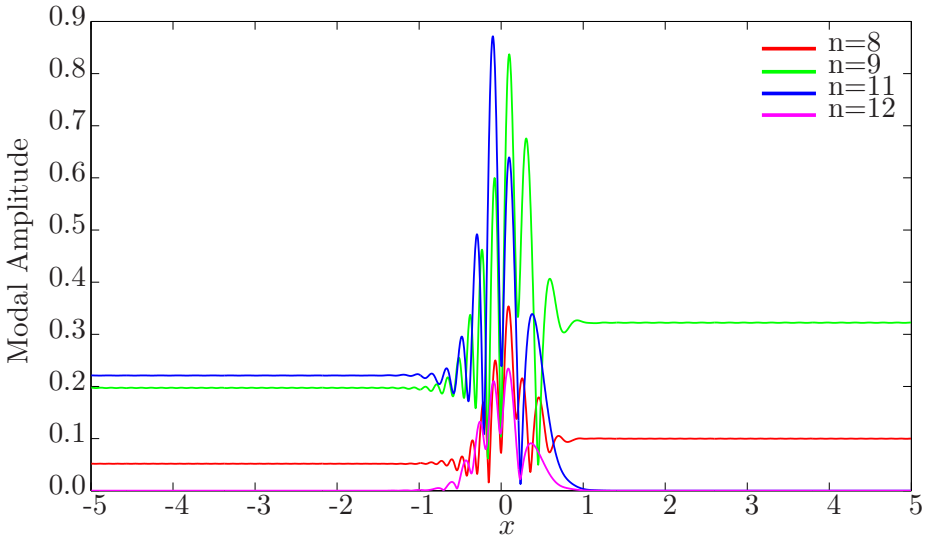

Figure 6.5: Case 1 with $U(-\infty) = -0.3$: Comparing the neighbouring modal amplitudes for $n = 8, 9, 11, 12$

which corresponds directly to the magnitude of the scattering coefficient $\mathcal{C}_{kn}$ as discussed in chapter 5. Recall that all the modes shown whose index is less than that of the incident mode (those indexed by $n < 10$) are able to propagate out of the duct in both directions. Note that modes $n < 10$ are able to fully propagate downstream provided that they themselves do not cut-off at some point further downstream, something which is possible though it is not the case here. The scattered modes indexed by $n > 10$ are unable to propagate downstream because they are already cut-off within this region. The reflection and transmission coefficients for each nearby mode are summarised in table 6.1 and are also plotted in figures 6.8 and 6.9.

A striking feature worth noting is that according to the results given by the $\omega \sim 1$ model, the mode that is indexed by $n = 11$ has a transition point at $X_{11t} \approx -0.03$ and this mode is cut on within the computational domain for $X < X_{11t}$. It may be seen in figures 6.4 and 6.5 that due to the fact that this mode must absorb a sufficient amount of acoustic energy from its cut-on cut-off neighbour, combined with the fact that it is cut-on upstream makes this enough for the mode to propagate in the negative x direction and out of the duct. This may be contrasted with the behaviour of the $n = 12$ mode, as the $\omega \sim 1$ model shows that this mode is not cut on anywhere within the duct, and so despite absorbing some energy from the $n = 10$ mode (and quite possibly the $n = 11$ mode) and being temporarily excited, it is unable to propagate upstream and out of the duct.

Recall that within the standard multiple scales model the incident mode con-

served all of its energy when undergoing cut-on cut-off transition, and this fact is reflected in non-scattered amplitudes shown in figure 6.2 and figure 6.3. These figures show that if the effects of scattering are not incorporated into the model, then a standing wave is formed that has a maximum amplitude of twice that of the incident mode. Thus, energy is completely conserved for any mode undergoing cut-on cut-off transition under the standard model. It is now interesting to compare this to the results obtained here when the effects of scattering are incorporated for $U_0(-\infty) = -0.3$. Note in this case that the incident mode actually looses some energy, and as a result of this energy loss the amplitude of the resulting standing wave is less than 2, as may be seen in figure 6.3. To be specific it is noted that for this case the reflection coefficient $|R_{10}| = 0.59$, corresponding to large reduction in acoustic energy. At first glance the cause of this considerable reduction in amplitude appears to be obvious in that the remaining energy must have been absorbed by the modes that were excited as a result of this cut-on cut-off transition process. However the idea that precisely all of the remaining energy must have been absorbed by the neighbouring modes is rapidly dispelled when looking at the results obtained for $U_0(-\infty) = +0.3$. Here it is seen that the reflected wave for $n = 10$ has a reflection coefficient with $|R_{10}| \approx 1.2$, which means that the amplitude of the reflected mode has increased by 20%, despite the fact that neighbouring modes have also been excited! This striking result appears to be an indication that an energy transfer between the mean flow and acoustic field must be taking place. Further, given the observation presented here it seems reasonable to postulate that if the mean flow is contracting as the duct narrows then energy is injected from the mean flow into the acoustic field, resulting

in an overall increase in the amount acoustic energy available to the system, something that is necessary in order for the left-running counterpart incident mode to have a transmission coefficient $|R_{10}| > 1$, which is sometimes referred to as *over reflection*. Conversely a widening duct with a diverging mean flow may in fact extract some energy from the acoustic field. This exchange in energy between the mean flow and acoustic field is a very noteworthy discovery, because up till now the conservation of acoustic energy within multiple-scales analyses for near uniform plug flow is usually taken for granted.

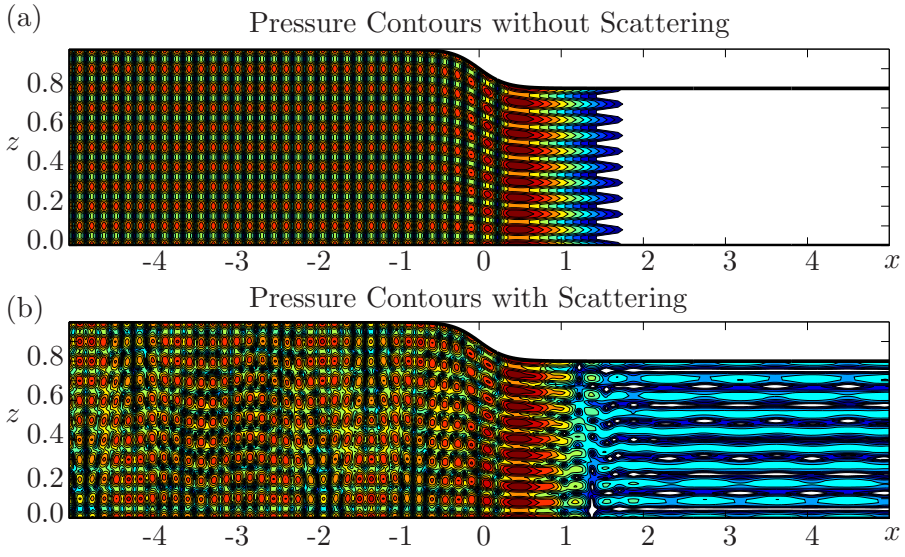

Figure 6.6: Case 1 with $U(-\infty) = +0.3$: Pressure Contours for Scattering and No Scattering

It is necessary therefore to precisely quantify the overall change in acoustic energy due to the interaction with the mean flow. This can be done by finding the difference between the acoustic power entering the domain and compar-

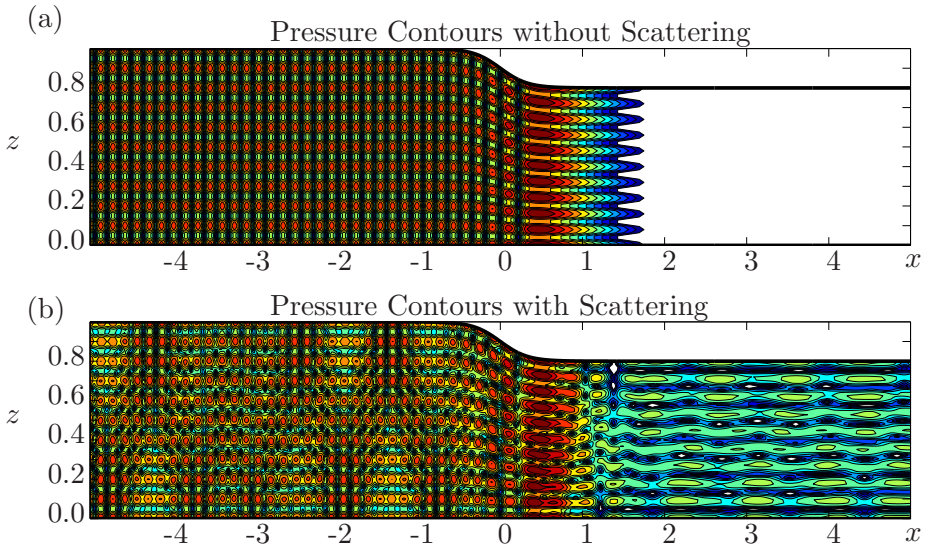

Figure 6.7: Case 1 with $U(-\infty) = -0.3$: Pressure Contours for Scattering and No Scattering

ing that with the acoustic power leaving the domain. If acoustic power is conserved then the energy leaving the domain in the form of reflected and scattered waves will be of precisely the same magnitude as the energy that was incident to the domain, and of course if energy is not conserved then these quantities will be different.

The acoustic power through the duct cross section at a given axial location x may be calculated by integrating the time-averaged acoustic intensity $\boldsymbol{I}$ over the cross section [36]: By definition then the acoustic intensity is given by

$$\boldsymbol{I} \cdot \boldsymbol{e}_x = \frac{1}{2}\mathrm{Re}\left\{ \left(\frac{p}{D} + U\frac{\partial \phi}{\partial x} \right) \left(D\frac{\partial \phi}{\partial x} + \rho U \right)^* \right\},$$

where * denotes the complex conjugate. Using $p = C^2\rho$ and the definition of

p given in equation (6.9) it may be seen that

$$\boldsymbol{I} \cdot \boldsymbol{e}_x = \frac{1}{2}\mathrm{Re}\left\{(-\mathrm{i}\omega\phi)\left(D\left(\frac{C^2-U^2}{C^2}\right)\frac{\partial\phi}{\partial x} - \frac{\mathrm{i}\omega DU}{C^2}\phi\right)^*\right\}.$$

Substituting ϕ into the above leads to

$$\boldsymbol{I} \cdot \boldsymbol{e}_x = \frac{1}{2}\frac{\omega D(C^2-U^2)}{C^2}\mathrm{Re}\left\{(-\mathrm{i}F)\left(\frac{\partial F}{\partial x}\right)^*\right\},$$

where

$$F = \sum_j \Phi(X)\chi_j(x)\cos\left[\alpha_j(x)z\right]\cos(M\pi y).$$

Now axial power $\mathcal{P}$ is the integral over an axial cross section, and as all modes are orthogonal the power may be computed separately for each mode j, and thus each $\mathcal{P}_j$ is given by

$$\mathcal{P}_j = \frac{1}{2}\frac{\omega D(C^2-U^2)}{C^2}\int_0^1\int_0^{h(X)}\cos^2\left[\alpha_j(x)z\right]\cos^2(M\pi y)\mathrm{d}z\mathrm{d}y \times \mathrm{Re}\left\{(-\mathrm{i}\Phi\chi_j)\left(\Phi'\chi_j + \Phi\chi_j'\right)^*\right\}.$$

Computing the double integral over the cosine squared terms yields

$$\int_0^1\int_0^{h(X)}\cos^2\left[\alpha_j(x)z\right]\cos^2(M\pi y)\mathrm{d}z\mathrm{d}y = \nu(m),$$

where

$$\nu(m) = \begin{cases} \frac{h}{2} & \text{for} \quad m = 0, \\ \frac{h}{4} & \text{otherwise,} \end{cases}$$

Also given that $\Phi'(X) = 0$ at the ends of the duct, the expression for $\mathcal{P}_j$ becomes

$$\mathcal{P}_j = \frac{\nu(m)\omega D(C^2-U^2)}{2C^2}\Phi^2(X)\mathrm{Re}\left\{(-\mathrm{i}\chi_j)\left(\chi_j'\right)^*\right\}.$$

In order to compute this one can use the non-reflecting boundary conditions. Recall from equation (6.4) that at the left-hand end the NRBC gave

$$\chi'_{j0} = \mathrm{i}k_j\chi_{j0} - 2\mathrm{i}k_jA_j, \tag{6.10}$$

where χ_{j0} is the value of $\chi_j(x_{\min})$ at the left-hand end of the domain. Using finite differencing then gives

$$\frac{-3\chi_{j0} + 4\chi_{j1} - \chi_{j2}}{2\Delta x} = \mathrm{i}k_t\chi_{j0} - 2\mathrm{i}k_jA_j,$$

where χ_{j1} and χ_{j2} are the computed values at $x = x_0 + \Delta x$ and $x = x_0 + 2\Delta x$ respectively so that

$$\chi_{j0} = \frac{4\chi_{j1} - \chi_{j2} + 4\mathrm{i}k_j\Delta xA_j}{(3 + 2\mathrm{i}k_j\Delta x)}, \tag{6.11}$$

and now equations (6.10) and (6.11) may be used in the power calculation to calculate the modal axial power at the left hand end.

Similarly at the right-hand end $x = x_{\max}$, assuming there is no incoming mode from $x = +\infty$ the non-reflecting boundary condition is used once again:

$$\chi'_{jN} = -\mathrm{i}k_j\chi_{jN}, \tag{6.12}$$

and applying a finite differencing approximation yields that

$$\frac{3\chi_{jN} - 4\chi_{j\,N-1} + \chi_{j\,N-2}}{2\Delta x} = -\mathrm{i}k_j\chi_{jN},$$

to obtain

$$\chi_{jN} = \frac{4\chi_{j\,N-1} - \chi_{j\,N-2}}{3 + 2\mathrm{i}k_j\Delta x}. \tag{6.13}$$

Equations (6.12) and (6.13) can now be substituted into the axial power calculations to obtain the modal axial power at the right-hand end of the domain.

It is useful to scale such axial power calculations with so-called *incident power* from the incident modes alone, and this can be calculated analytically. Let the incident modes ϕ_i be given by

$$\phi_i = \sum_{j=1}^{J_{\text{Max}}} A_j \, \mathrm{e}^{-\mathrm{i}k_j x} \cos(\alpha_j z) \cos(M\pi y) \exp\left(-\mathrm{i}\int \frac{\omega U_0}{C_0^2 - U_0^2}\mathrm{d}x\right).$$

Substituting this expression into the definition of axial power it is found that

$$\mathcal{P}_{\text{incident}} = \frac{\nu\omega D(C^2 - U^2)}{2C^2} k_t \Phi^2(X) A_j^2.$$

and using the fact that $k_t = (\omega C_0 \sigma_t)/(C_0^2 - U_0^2)$ this becomes

$$\mathcal{P}_{\text{incident}} = \omega^2 \nu \frac{D}{2C} \mathrm{Re}(\sigma_t) \Phi^2(x) A_j^2.$$

It is desirable to measure the acoustic power of the reflected and scattered modes relative to the incident mode. First note that contributions to the total energy flux at the left hand boundary $\mathcal{P}(x_{\text{max}})$ may be decomposed into an incident and reflected part, i.e.

$$\mathcal{P}(x_{\text{min}}) = \mathcal{P}_{\text{incident}} + \mathcal{P}_{\text{reflected}}.$$

where $\mathcal{P}_{\text{reflected}}$ is the total acoustic energy flux of all modes propagating towards $x = -\infty$ at the left hand boundary. The amount of acoustic energy that is lost or gained due to the presence of the mean flow may be calculated as the percentage difference of the incident and outputted acoustic energies. To do this define the flow induced power coefficient $\mathcal{EP}$ as

$$\mathcal{EP} = \frac{[\mathcal{P}(x_{\text{max}}) - \mathcal{P}_{\text{reflected}}] - \mathcal{P}_{\text{incident}}}{\mathcal{P}_{\text{inc}}} = \frac{\mathcal{P}(x_{\text{max}}) - \mathcal{P}(x_{min})}{\mathcal{P}_{\text{incident}}}.$$

The flow induced power coefficient calculates the percentage difference (as a decimal) between the energy of the flow leaving the system at the domain boundaries compared to the energy of the incident modes.

Returning to the case in hand then, it follows that for $U(\infty) = -0.3$, then $\mathcal{EP} = -0.50$, which indicates that the presence of the left propagating diverging mean flow has lead to a reduction of around 50% in the available acoustic energy, which is quite a considerable reduction in the level of noise. However when the mean flow is reversed then it follows that $\mathcal{EP} = 0.8225$, indicating a very considerable 82% increase in acoustic energy due to the interaction with the mean flow.

		$U_0(-\infty) < 0$		$U_0(-\infty) > 0$	
n	A_n	$\lvert R_n\rvert$	$\lvert T_n\rvert$	$\lvert R_n\rvert$	$\lvert T_n\rvert$
1	0	3.10e-05	1.91e-04	2.10e-05	1.86e-06
2	0	8.12e-05	4.70e-04	5.34e-05	4.77e-06
3	0	1.93e-04	1.00e-03	1.20e-04	1.18e-05
4	0	4.76e-04	2.22e-03	2.91e-04	3.88e-05
5	0	1.28e-03	5.33e-03	8.12e-04	1.46e-04
6	0	4.00e-03	0.01	2.79e-03	8.75e-04
7	0	0.01	0.04	0.01	0.01
8	0	0.05	0.12	0.08	0.10
9	0	0.20	0.38	0.41	0.47
10	1	0.55	cut-off	1.17	cut-off
11	0	0.22	cut-off	0.38	cut-off
12	0	cut-off	cut-off	cut-off	cut-off

Table 6.1: Table comparing reflection and transmission coefficients in case 1 for $U_0(-\infty) < 0$ and $U_0(-\infty) > 0$

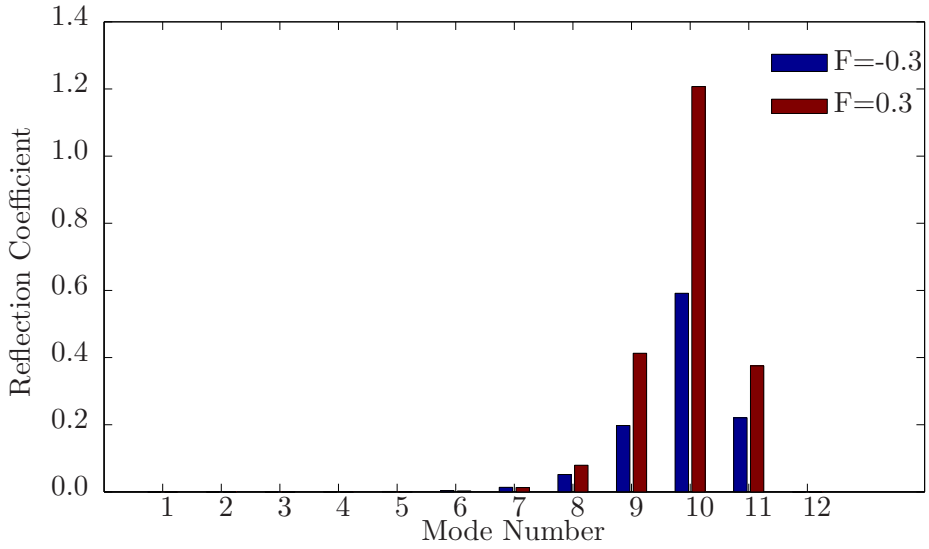

Figure 6.8: Histogram comparing reflection coefficients for $U_0(-\infty) = \pm 0.3$ in Case 1

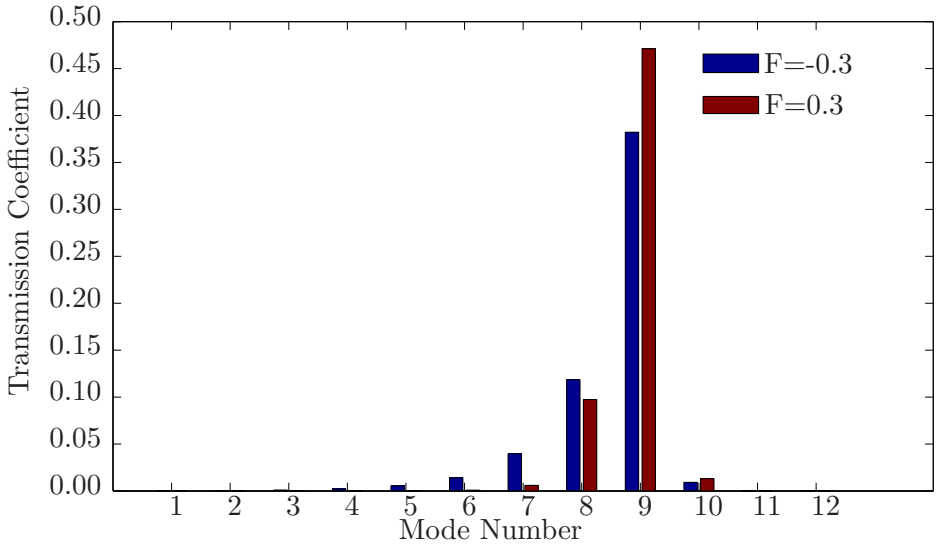

Figure 6.9: Histogram comparing transmission coefficients for $U_0(-\infty) = \pm 0.3$ in Case 1

Case 2: Modal propagation with a two incident left-running modes, $n = 9, 10$ together with $\omega = 35, U_0(-\infty) = \pm 0.3, h_s = 0.1, a_0 = 3$ and $m = 0$,

This case is very similar to the first case in the sense that the duct geometry, Helmholtz number and mean flow are completely unchanged. However instead of one incident mode as in the last case, there are now two incident modes, indexed by $n = 9$ and $n = 10$. These two incident modes are right running and have unit incident modal amplitudes, so $\bar{A}_n = 1$ for $n = 9, 10$ and zero incident amplitude for all other modes. The case with two incident modes is interesting and useful to understand because in a physical situation there are likely to be several modes that are incident. Therefore understanding the effect that a cut-on cut-off mode has on other neighbouring incident modes is very important from both a theoretical and practical point of view.

First consider the case with $U_0(-\infty) < 0$, where the mean flow is propagating from right to left. It is known from the previous example that the $n = 9$ mode is cut-on throughout the entire duct, and the $n = 10$ mode cuts off at some point X_{10t} within the duct. Thus the standard multiple scales theory anticipates that the $n = 10$ mode will cut off and form a standing wave, whilst the $n = 9$ mode propagates through without any interference from its neighbour. A pressure contour plot of this standard multiple scales scenario can be seen in the upper contour plot shown in figure 6.14(a).

Once modal scattering is taken into consideration, it is now expected that

the $n = 10$ mode that undergoes cut-on cut-off transition will scatter energy into neighbouring modes. Figure 6.10 shows a plot of the modal amplitude of the $n = 10$ modal amplitude, and compares it with two other cases: case 1, where there was only an incident $n = 10$ mode and no $n = 9$ incident mode, and situation as modelled using the standard multiple scales analysis which includes no scattering effects. As expected, a standing wave is formed for the $n = 10$ mode comprising of the incident and reflected mode, but it may also be seen that due to the presence of the incident $n = 9$ mode the amplitude of the $n = 10$ is even smaller than the case where there was no $n = 9$ incident mode and thus this mode has lost energy due to the presence of the incident $n = 9$ mode. In fact the reflection coefficient for this mode is now $R_{10} = 0.46$, considerably less than that in the previous case where there was no incident $n = 9$ mode.

For $X < X_{10t}$ the cut-on cut-off mode excites a left propagating $n = 9$ scattered mode, and this scattered mode combined with the already cut-on $n = 9$ incident mode causes an $n = 9$ partial standing wave to be formed within the duct. Figure 6.12 can be referred to in order to illustrate this fact. As a result of the scattering the amplitude of the $n = 9$ mode has increased by a considerable amount for $X < X_{10t}$, as shown in table 6.2. It should be noted however that in comparative terms this $n = 9$ mode appears to absorb less of the scattered energy than in case 1. However a mode that seems to benefit a lot from the presence of this $n = 9$ mode is its adjacent right running $n = 8$ mode, which has a transmission coefficient of $|T_8| = 0.57$, considerably larger than in the previous case, despite the fact that there is very

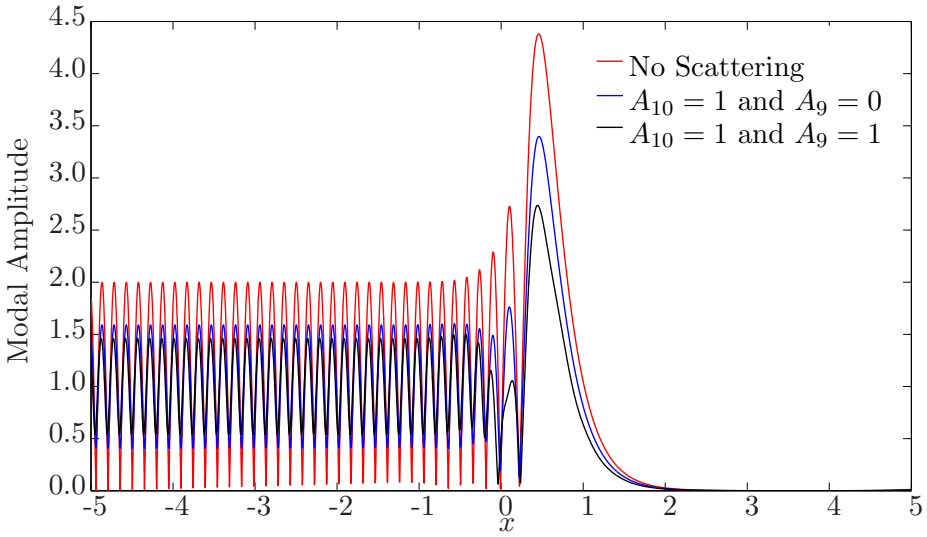

Figure 6.10: Comparing the modal amplitude for the $n = 10$ mode for $U(-\infty) < 0$ in the case of two incident modes $n = 9$ and $n = 10$ with scattering, one incident mode $n = 10$ with scattering, and two incident modes with no scattering

little movement in the reflection coefficient of its left running counterpart. A very similar situation is observed for modes indexed by $n < 8$, whereby the transmission coefficient has increased quite considerably, with the reflection coefficient relatively untouched.

Now that the effects of negative mean flow have been observed it is now necessary to switch the order of the mean flow and observe the differences. When observing the results for the reflection coefficients, it is apparent from table 6.2 that for each mode the magnitudes of this coefficient have increased from those shown in case one as a result of the extra incident $n = 9$ mode. Again however, it is interesting to note that while the reflection coefficients have increased by a small amount as expected, it is again the transmission coefficients that appear to have increased most considerably. For example,

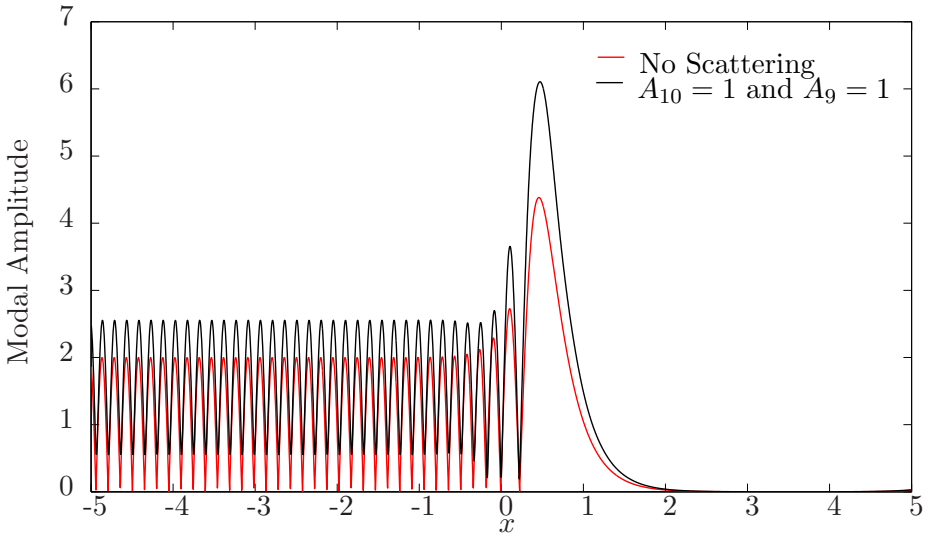

Figure 6.11: Comparing the modal amplitude for the $n = 10$ mode for $U(-\infty) > 0$ in the case of two incident modes $n = 9$ and $n = 10$, and the case with two incident modes with no scattering

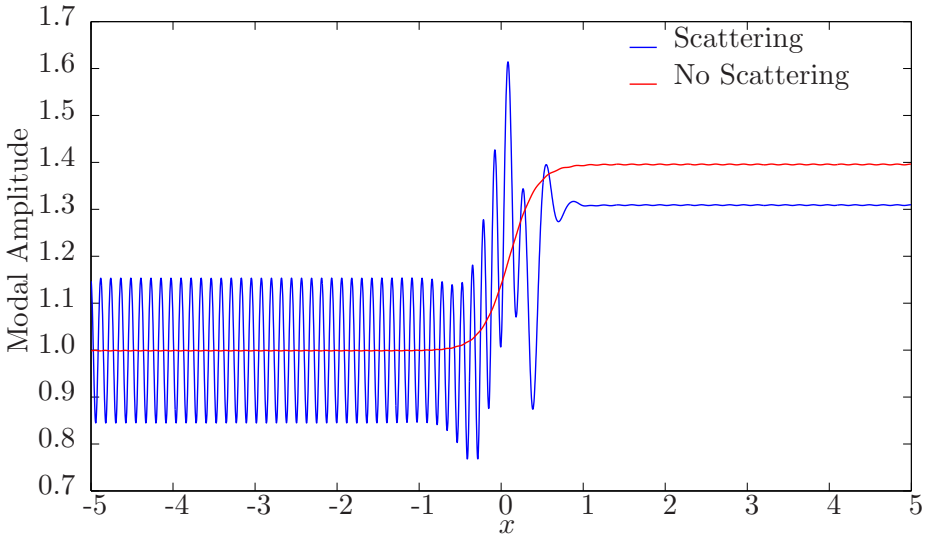

Figure 6.12: Comparing the modal amplitude for the $n = 9$ mode for $U(-\infty) < 0$ in the case of two incident modes $n = 9$ and $n = 10$, and the case with two incident modes with no scattering

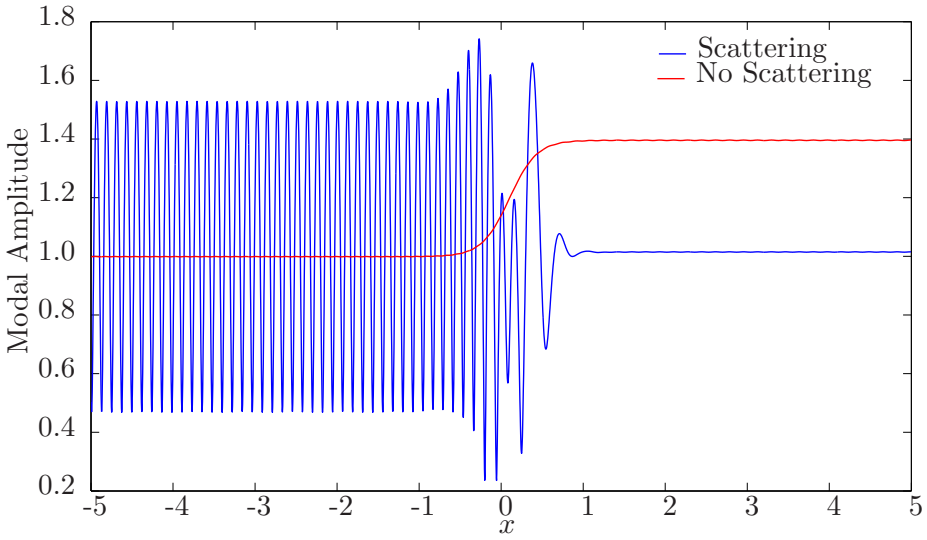

Figure 6.13: Comparing the modal amplitude for the $n = 9$ mode for $U(-\infty) > 0$ in the case of two incident modes $n = 9$ and $n = 10$, and the case with two incident modes with no scattering

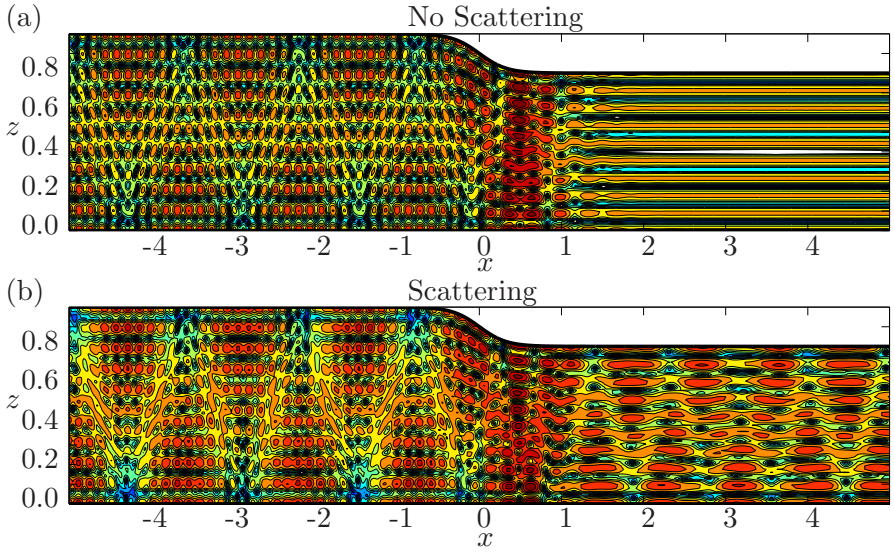

Figure 6.14: Case 1 with $U(-\infty) = -0.3$: Pressure Contours for Case 2 in the case of Scattering and for No Scattering

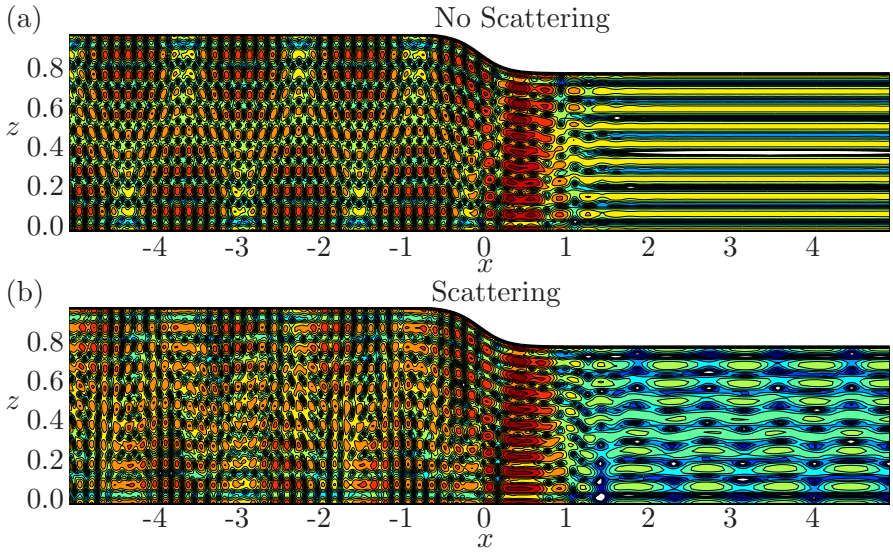

Figure 6.15: Case 1 with $U(-\infty) = 0.3$: Pressure Contours for Case 2 in the case of Scattering and for No Scattering

the $n = 8$ mode has jumped from $|T_8| = 0.1$ in case one to $|T_8| = 0.55$ here, quite a considerable increase. When looking at the behaviour of the $n = 9$ mode, this is very similar to the $U(\infty) < 0$ case, with the only noticeable difference being that the amplitude of the standing wave is larger (due to the extra energy within the system from the mean flow), and a slight peculiarity in that the right running transmitted $n = 9$ mode appears to have only absorbed about only small amount of energy as the amplitude has increased by about 1% only, less of an increase than in the case where $U_0(-\infty) < 0$. However the explanation for this may be that this appears to have been offset by an increase in around 20% for the reflected mode when compared to the first case.

For the axial power coefficients it is found that $\mathcal{EP} = -0.2622$ for the $U(-\infty) < 0$ case and for $U(-\infty) > 0$ we have $\mathcal{EP} = 0.6789$. We also have $\mathcal{P}(x_{max}) =$

143.9 and $\mathcal{P}_{\text{reflected}} = -444.41$ when $U > 0$. Also when $U < 0$ the power coefficients are $\mathcal{P}(x_{max}) = 222.66$ and $\mathcal{P}_{\text{reflected}} = -35.90$

		$U_0(-\infty) < 0$		$U_0(-\infty) > 0$	
n	A_n	$\lvert R_n\rvert$	$\lvert T_n\rvert$	$\lvert R_n\rvert$	$\lvert T_n\rvert$
6	0	0.00	0.08	0.00	0.01
7	0	0.01	0.21	0.01	0.10
8	0	0.04	0.57	0.10	0.55
9	1	0.15	0.93	0.51	0.72
10	1	0.41	cut-off	1.53	cut-off
11	0	0.21	cut-off	0.44	cut-off
12	0	cut-off	cut-off	cut-off	cut-off

Table 6.2: Table comparing reflection and transmission coefficients in case 2 for $U_0(-\infty) < 0$ and $U_0(-\infty) > 0$

Case 3: Demonstration of Weak Scattering for Low Helmholtz Number $\omega = 10, U(\infty) = \pm 0.3$ Together With One Cut-On Incident Mode $n = 3$ and Two Dimensional Flow.

The previous two cases dealt with a scenario where the flow was two dimensional and the frequency was very high, leading to a relatively large amount of energy being transferred from the cut-on cut-off incident mode into the scattered modes. The case dealt with here is an example where the various problem parameters are set up in such a way as to induce weak scattering, in accordance with the theory established in section 5.3.

Consider the case with flow geometry defined such that $h_s = 0.1$ and $a_0 = 3$, giving rise to $\varepsilon \simeq 0.1$. Recall from chapter 5 section 5.3 that a condition to induce for weak scattering is to have

$$\omega \sim \varepsilon^{-\frac{1}{2}}, \quad \alpha \sim \varepsilon^{-\frac{1}{2}},$$

thus $\omega = 10$ and $n = 3$ are chosen as they fit well with the above approximations. From the asymptotic analysis of the weak scattering it is predicted that in a case such as this, the incident mode will endure scattering to leading order, whereas the scattered modes will propagate with an amplitude that is $O(\varepsilon^{\frac{1}{2}})$.

The first set of results are for $U > 0$.

The situation for the incident mode appears quite similar to the previous two

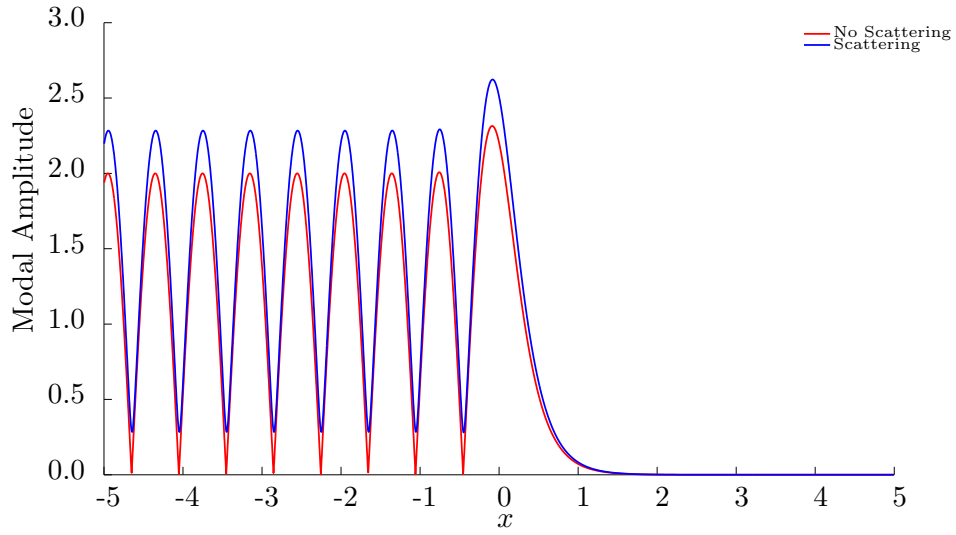

Figure 6.16: Incident Modal Amplitude for Case 3 with $U(\infty) = +0.3$

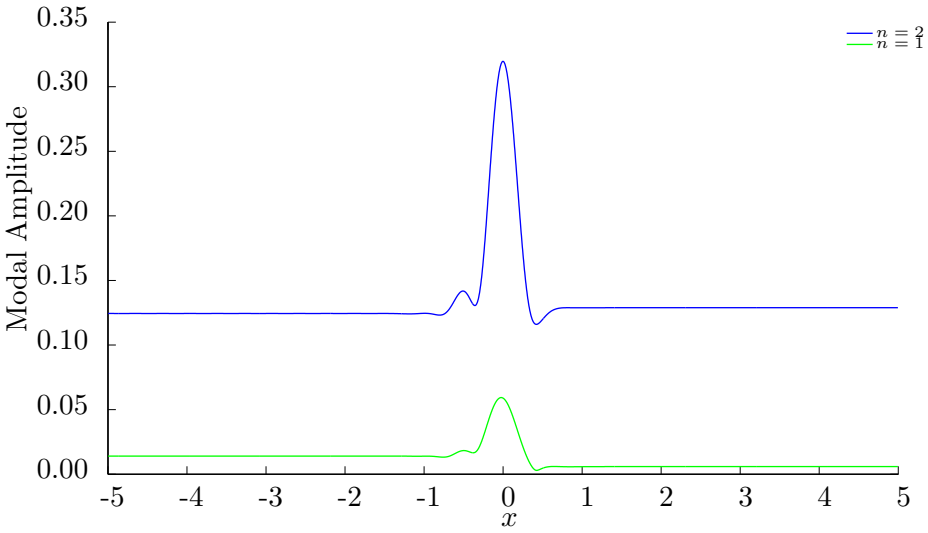

Figure 6.17: Modal Amplitudes for Case 3 with $U(\infty) = +0.3$

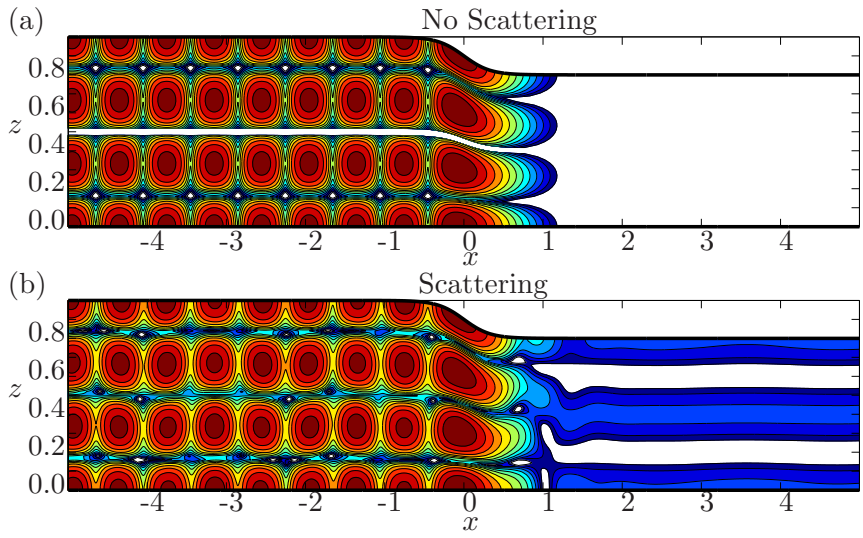

Figure 6.18: Pressure Contours for Case 3 with $U(\infty) = +0.3$

cases studied in that the cut-on cut-off mode extracts a significant proportion of energy from the mean flow, causing a large partial standing wave to be formed to the left of the turning point, as shown in figure 6.16. The axial power coefficient is given by $\mathcal{EP} = 0.7172$, indicating that there has been an increase in acoustic energy of around 70% due to the mean flow interacting with the acoustic field. However despite this large influx of extra energy into the acoustic field, only a very small amount of this appears to have been absorbed by the scattered modes. Figure 6.17 shows the amplitudes of the modes most neighbouring to the incident mode. Looking at the amplitudes of the scattered modes, it appears that most of the extra energy from the mean flow must have been absorbed by the reflected component of the incident mode as the amplitudes of the scattered modes are very small. Note that the $n = 4$ mode was cut-off throughout the entire duct. Also note that the magnitude of the scattered modal amplitudes do appear to be $O(\varepsilon^{\frac{1}{2}})$ and thus in very good

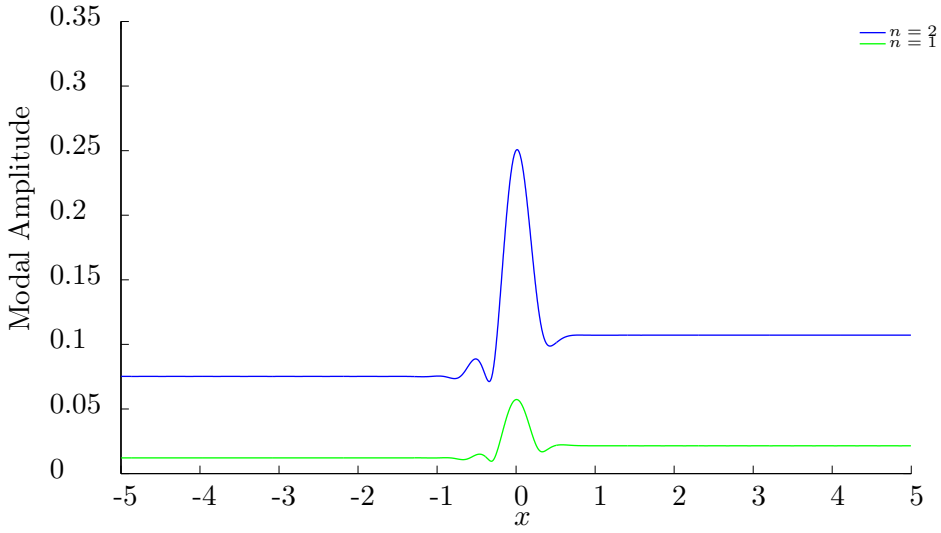

Figure 6.19: Modal Amplitudes for Case 3 with $U(\infty) = -0.3$

agreement with the asymptotic analysis on weak scattering shown in the previous chapter. Figure 6.21 shows contour plots of relative sound pressure level for case. It may be seen that there is a clear indication of acoustic disturbances beyond the turning point that may be attributed to the neighbouring modes. However, despite the fact that a large amount of energy has been extracted by the acoustic field from the mean flow these disturbances are small.

Now for the situation with $U(-\infty) < 0$. In this case the axial power coefficient is given by $\mathcal{EP} = -0.3955$, and thus of course this
means that as with the previous cases, the diverging mean causes energy to be extracted from the acoustic field, in this case to the degree of around 40%. However a weak form of modal scattering still takes place, and it is interesting to observe that despite the reduction in available acoustic energy the amplitude of the neighbouring right running $n = 2$ mode is of very similar size

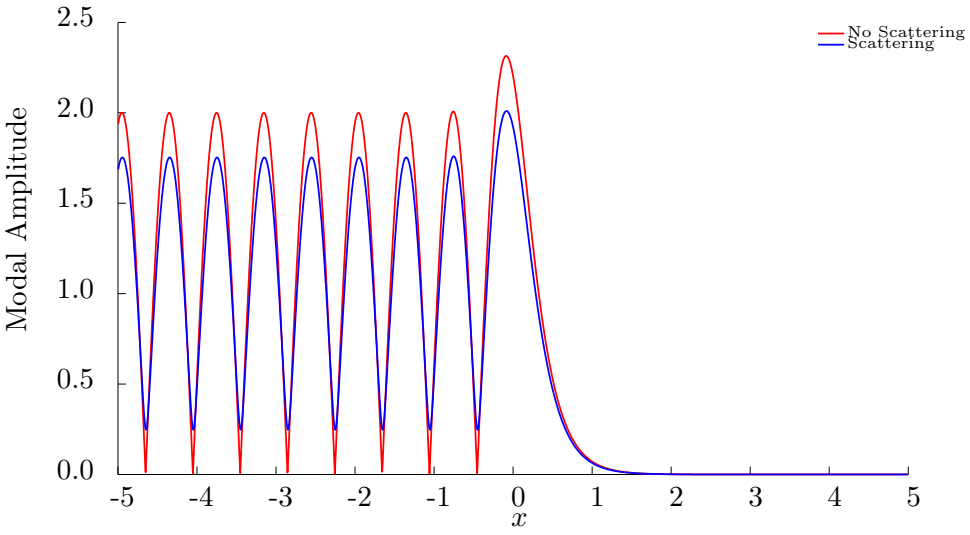

Figure 6.20: Incident Modal Amplitude for Case 3 with $U(\infty) = -0.3$

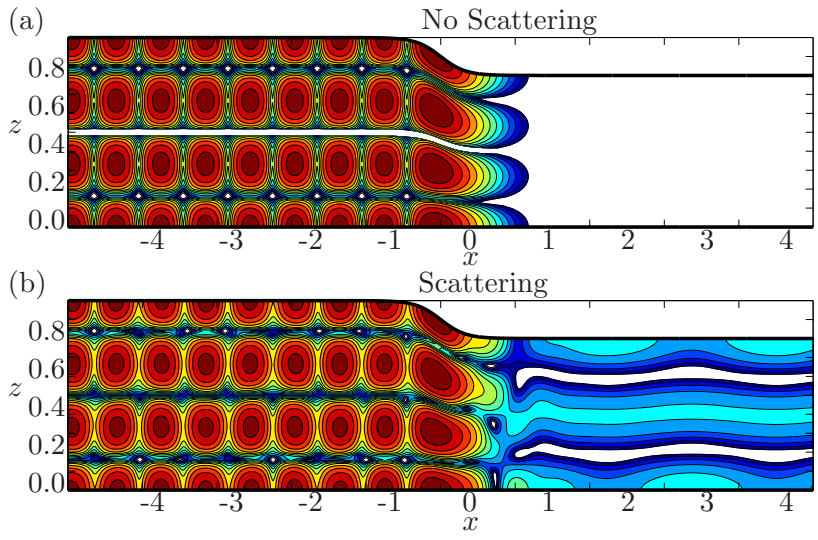

Figure 6.21: Pressure Contours for Case 3 with $U(\infty) = -0.3$

compared to the case when $U(\infty) > 0$. Also, comparing the reflection and transmission coefficients (shown in table 6.2) for the $n = 1$ mode, it may be observed that the transmission coefficient for the $U(-\infty) < 0$ is larger than for the case when $U(-\infty) > 0$. It appears therefore, that the relationship between the reflection and transmission coefficients of the scattered modes is such that for a given scattered mode, the tendency is for proportionally more energy is to be scattered into the part that propagates in the opposite direction of the mean flow. A similar conclusion may be drawn when comparing the axial power coefficients for a particular mode at both ends of the computational domain. Moreover, it may be seen that a similar trend may be seen for all results presented so far in this chapter. Therefore, a useful study to continue from the work presented here would be to compare these findings with theoretical values for the reflection and transmission coefficients. These reflection and transmission coefficients could theoretically be obtained via an analysis involving matched asymptotic expansions of the inner and outer solutions, using similar methods to those demonstrated in chapter 3. However due to the apparent complex nature of the inner solution this matching is not straightforward and is left as further work (see chapter 7).

		$U_0(-\infty) < 0$		$U_0(-\infty) > 0$	
n	A_n	$\lvert R_n\rvert$	$\lvert T_n\rvert$	$\lvert R_n\rvert$	$\lvert T_n\rvert$
1	0	0.121	0.0215	0.0140	0.0059
2	0	0.0752	0.1072	0.1244	0.1289
3	1	0.7616	cut-off	1.2924	cut-off
4	0	cut-off	cut-off	cut-off	cut-off

Table 6.3: Table comparing reflection and transmission coefficients in case 3 for $U_0(-\infty) < 0$ and $U_0(-\infty) > 0$

Case 4: Three Dimensional Scattering $\omega = 25, U(\infty) = \pm 0.3$ Together With One Cut-On Incident Mode $n = 4$

This problem considers a three dimensional flow with a slightly different geometry, defined as

$$h(x) = 1.2 - h_s \tanh(a_0 x)$$

where $h_s = 0.2$ and $a_0 = 3$. Under these geometrical conditions the small parameter ε may be approximated by $\varepsilon \approx 0.1$. Similarly to the last case, it is desirable to attempt to induce leading order scattering for all modes by setting the various problem parameters according to those described in chapter 5 section 5.4. Recall from the asymptotics performed earlier that leading order scattering may be induced via

$$\omega \sim \varepsilon^{-1}, \quad \alpha \sim \varepsilon^{-\frac{2}{3}}, \quad \sigma_t^2 \sim \varepsilon^{\frac{4}{3}}, \quad \delta_{m,t} \sim \varepsilon^{\frac{4}{3}}, \quad M \sim \varepsilon^{-1}$$

where M is the eigenvalue in the y direction. Thus for this case parameters $\omega = 25$, $n = 4$ and $M = 8$ are chosen as they are in good agreement with the approximations above. The asymptotics predict that even despite the low vertical mode and moderately high frequency, a large amount of scattering should be observed. Note that with regard to the difference between the various reduced axial wavenumbers, in running this case it was observed that this was typically some multiple of 0.05, which fits very well with the approximation that $\delta_{m,t} \sim \varepsilon^{\frac{4}{3}}$.

First start with the situation of positive mean flow. The axial power coefficient is $\mathcal{EP} = 1.4857$, indicating a large amount of energy injected into the acoustic field by the mean flow. Although the reflected component of the incident

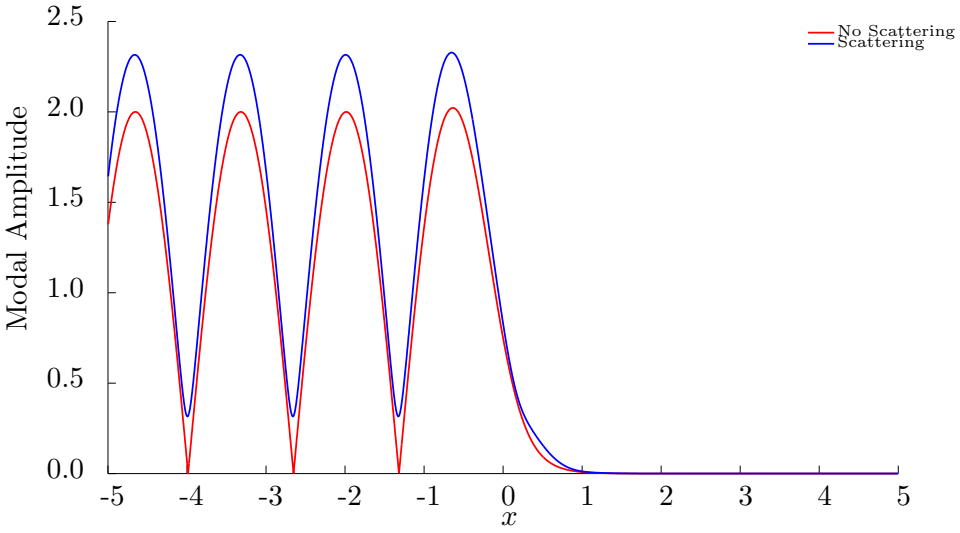

Figure 6.22: Incident Amplitudes for Case 4 with $U(\infty) = +0.3$

mode clearly absorbs some of this energy (as can be seen from figure 6.22), a rather significant amount of this energy is scattered into neighbouring modes. A clear indicator of the degree of modal scattering is given by the pressure contour plot shown in figure 6.23, where there appears to be significant levels of acoustic energy propagation beyond X_t. However it has been noted that the apparent tendency of an excited mode is that the majority of the acoustic energy should be scattered into the mode running in the opposite direction to that of the mean flow. Hence in the case with positive mean flow the majority of the scattered modal energy is reflected. This can also be seen from the modal amplitudes given in figure 6.24 and reflection and transmission coefficients shown in table 6.4.

When the direction of the mean flow is reversed the usual trends in terms of the behaviour of the incident mode may be observed, given by the fact

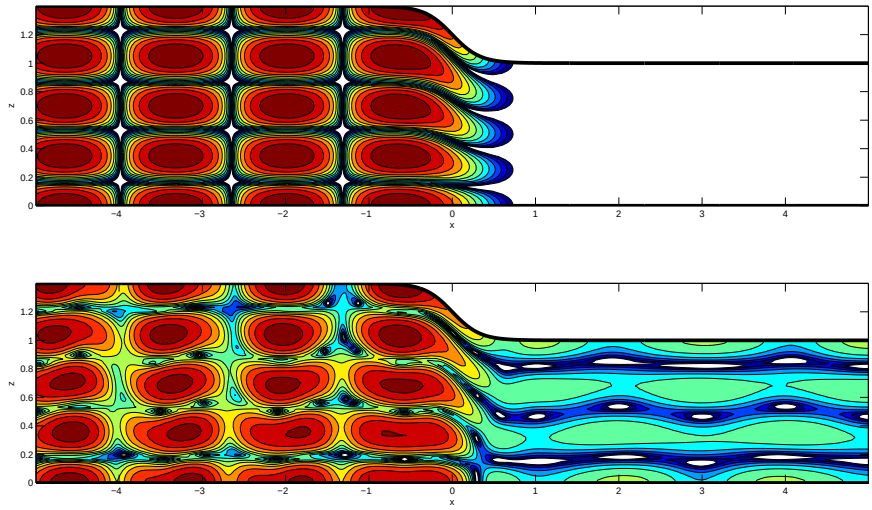

Figure 6.23: Pressure Contours for Case 4 with $U(\infty) = +0.3$

that $\mathcal{EP} = -0.5289$ in this case, and the effect of which is depicted in figure 6.27. Notice that for the individual scattered amplitudes, given in figure 6.26, these are smaller than in the case where $U(-\infty) < 0$, a consequence of the reduced level of acoustic energy due to extraction by the mean flow. However it may still be seen that the combined effect of all of these scattered modes is still leading order, and this idea reinforced by observing the acoustic pressure contours given by figure 6.25, where it may be seen that a significant amount of modal energy is able to propagate beyond the turning point of the incident mode, leading to some areas of rather high acoustic pressure. Figure 6.26 also gives a clear picture of the tendency of an excited mode to propagate in the opposite direction to that of the mean flow.

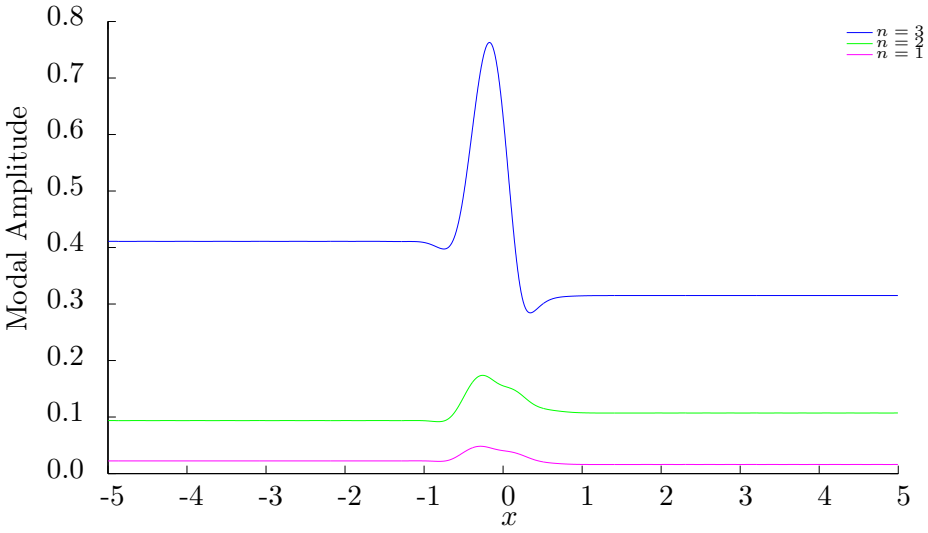

Figure 6.24: Scattered Amplitudes for Case 4 with $U(\infty) = +0.3$

Summary

Modal scattering is a phenomenon that occurs whenever an incident mode undergoes cut-on cut-off transition under suitable flow conditions and the frequency is sufficiently large. The composite solution discussed here is useful for computational and industrial purposes at it is especially suited to cases where the frequency is large, and due to the intricacy of the method the runtime of the numerical code is very fast, making it ideal for implementation within industry.

For two dimensional flow, modal scattering to leading order can only occur when the frequency is very high. Weak scattering is more likely for two dimensional flows and the results presented here show that weak scattering may be achieved under conditions that appear to be in very good agreement with the conditions outlined in section 5.3. Leading order scattering for three dimen-

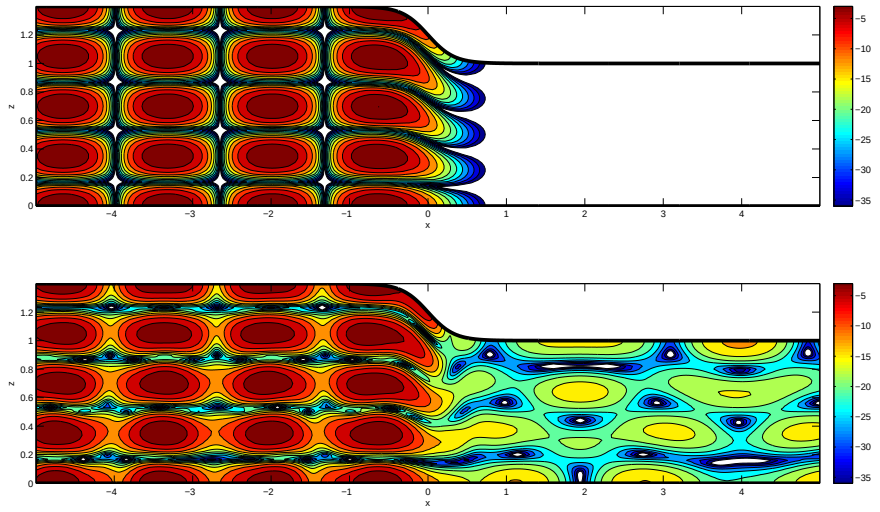

Figure 6.25: Pressure Contours for Case 4 with $U(\infty) = -0.3$

		$U_0(-\infty) < 0$		$U_0(-\infty) > 0$	
n	A_n	$\lvert R_n\rvert$	$\lvert T_n\rvert$	$\lvert R_n\rvert$	$\lvert T_n\rvert$
1	0	0.0129	0.0575	0.0224	0.0161
2	0	0.0373	0.1304	0.0937	0.1072
3	0	0.0997	0.2133	0.4109	0.3151
4	1	0.5346	cut-off	1.3228	cut-off

Table 6.4: Table comparing reflection and transmission coefficients in case 4 for $U_0(-\infty) < 0$ and $U_0(-\infty) > 0$

sional flow is possible under certain conditions, and these conditions appear to be in good agreement with those specified in section 5.4.

One interesting feature outlined in all of the cases discussed here is that there appears to be an exchange of energy between the mean flow and acoustic field during the scattering process, the like of which has not been observed within the asymptotic model before. When the mean flow is contracting, acoustic energy appears to be injected into the acoustic field, and when the mean flow is diverging, energy is extracted from the acoustic field. When the mean flow is contracting at the turning point the amplitude of the reflected component of the cut-on cut-off incident mode is larger than the incident component, and vice versa when the flow the result of which causes a partial standing wave to be formed within the duct for the incident cut-on cut-off mode. Similar conclusions were presented by Smith, Ovenden and Bowles [57]. Another paper by Smith, Ovenden and Bowles [58] also looked at the effects of both mean flow *and* geometry induced modal scattering. In this second paper it was shown that acoustic energy is fully conserved during geometry induced scattering without zero mean flow, but that an energy transfer takes place between the mean flow and the acoustic field whenever the mean flow is present.

Another interesting case shown in case 2 is the situation where there are two incident modes that propagate in the same direction and one of the modes undergoes cut-on cut-off transition. The mode that undergoes cut-on cut-off transition first causes the opposite running counterpart of the second mode to be excited, causing a partial standing wave to be formed between the second

incident mode and it's opposite running counterpart.

For a given mode that is excited via cut-on cut-off transition, there appears to be a tendency for the majority of the modal energy to be scattered into the mode that propagates in the direction that is opposite to that of the mean flow. The full extent of this relationship can be revealed by a thorough asymptotic matching of the inner and outer solutions, which is a desirable extension to the work presented in this thesis.

At this point it is noted that for a fully irrotational mean flow, acoustic energy should be completely conserved within the acoustic field, and therefore no exchange of energy with the mean flow can take place. This result is due to Cantrell and Hart [10] and Morfey [12]. Therefore the fact that there is an exchange of energy between mean flow and acoustic field in the results shown here may be attributed to the fact that irrotational mean flow has only been imposed to $O(\varepsilon)$, and in fact the mean flow velocity profile described here actually has a small ($O(\varepsilon^2)$) vorticity component. Work aimed at understanding how one might impose a fully irrotational mean flow leading to full energy conservation within the acoustic field for flow induced scattering is currently underway.

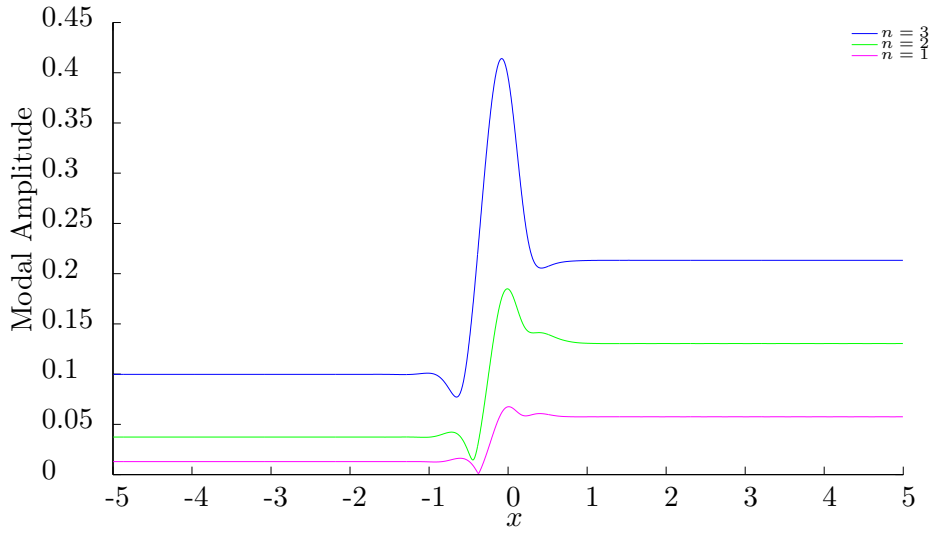

Figure 6.26: Scattered Amplitudes for Case 4 with $U(\infty) = -0.3$

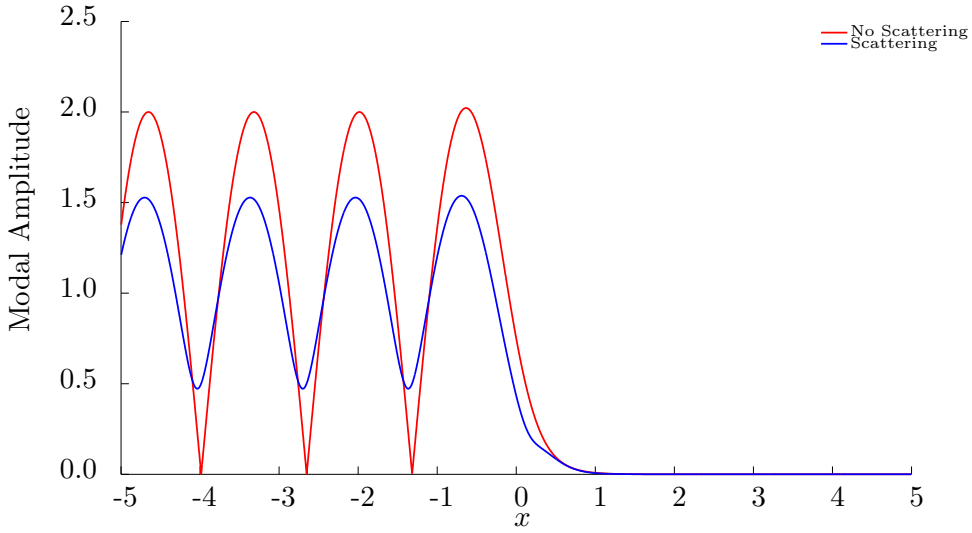

Figure 6.27: Incident Amplitudes for Case 4 with $U(\infty) = -0.3$

Chapter 7

Conclusions and Further Research

The aim of this thesis has been to obtain a deeper understanding of some of the phenomena associated with the propagation of acoustic waves within slowly varying ducts, with the main application being to improve our knowledge of some mechanisms that are related to noise associated with aircraft turbofan engines. Due to the significant number of people whose lives it effects, the understanding of this type of aeroacoustic noise is an important engineering problem, and detailed knowledge and enhancement of the topics discussed within this thesis will undoubtedly lead to improvements with regard to the design and manufacture of quieter turbofan engines.

The first part of this thesis explored the general properties of propagation and transmission of acoustic modes as modelled using the multiple scales approach. Chapter 2 discussed the general features of the propagation of acoustic modes

through a lined duct, as modelled using the standard multiple scales approach. In this analysis, an equation for the modal amplitude of a propagating mode was deduced by supressing the secular non-parallel terms on the right hand side, leading to the so-called solvability condition which in turn allowed the modal amplitude to be found. Under certain flow conditions however this solution may develop a singularity, because the slowly varying assumption that was made in the initial derivation is no longer valid, and therefore a different model must be used for the modal amplitude wherever this slowly varying assumption is invalid. For the hard-walled limit, a turning point analysis may be performed in order to form the appropriate model for the inner region, and this solution may be matched to the outer solution to reveal theoretical values for the reflection and transmission coefficient.

Chapter 3 discussed the turning point analysis in some depth, and one of the new results contained within this thesis is the matched asymptotic solution of the so-called double turning point, where the reduced axial wavenumber behaves quadratically as it approaches the turning point. There are several features of the double turning point that make it distinct from the single turning point analysis of Rienstra [49] presented in section 3.1. Firstly, the double turning point allows for the possibility of partial transmission of an acoustic mode through the turning point region. Secondly, the reflected component of the mode will lead to a partial standing wave being formed within the duct, and it was found that it is not necessary for the mode to be cut-off anywhere inside the duct in order for a partial reflection of the mode to occur. Also, in contrast to the single turning point case, the modal amplitude was shown

to exhibit the properties of Weber type functions within the turning point region (rather than Airy functions), and the resulting magnitude and phase of the reflection and transmission coefficients depend upon the behaviour and nature of the reduced axial wavenumber within the turning point region. The analysis of the double turning point is a useful result for acoustics and is likely to occur within other areas of physics. It was also shown that the reflection and transmission coefficients obtained using this asymptotic analysis appear to agree well with numerical simulations that utilise a finite difference scheme.

The focus of Chapter 4 was to develop a model for modal propagation in a slowly varying hard-walled duct of rectangular cross section at large Helmholtz number. The need for such a solution was influenced by the conclusions of Ovenden et al [43], who postulated that in order to induce modal scattering within a slowly varying hard-walled duct the frequency must be sufficiently high in order for the modes to be sufficiently close to one another to exchange energy. It was shown in this chapter a modal type solution does in fact exist for $\omega \sim \varepsilon^{-2}$, and this was achieved by truncating the Poincaré expansions of the modal amplitude and wavenumbers up to third order, eventually supplying a solvability condition that yielded the modal amplitude. The solution presented in this chapter may then be analysed further, and it may be possible to achieve a matched asymptotic solution with the solution governing the inner region. However due to the complex nature of both the inner solution and outer solutions this procedure is left as further work.

Chapter 5 then went on to look at the phenomenon of modal scattering of

acoustic modes within a slowly varying hard walled rectangular duct with mean flow. The first task used Ovenden et al's estimate for the magnitude of the frequency [43], as well as the outer solution developed in chapter 4, to attempt to describe a model for the scattering of an acoustic mode as an incident mode undergoes cut-on cut-off transition at some point within the duct. Although it was shown here that Ovenden et al's estimate was actually an overestimate, this analysis was valuable because for the first time the terms that are responsible for the scattering were revealed. It was also shown that these scattering terms appeared to be dependent upon a transverse mean flow being present within the duct, which immediately appeared to explain why the finite element model shown in [43] appeared to give scattering only in cases with high Helmholtz number *and* mean flow.

Following on from the previous analysis, the high frequency argument was then re-examined. It was shown that a balance between all of the necessary terms in the governing wave equation may be achieved using the scaling $\omega \sim \varepsilon^{-\frac{1}{2}}$, which is much lower than the previous estimate. It was then shown that simply balancing the necessary terms in the governing wave equation is not the only scaling consideration that must be undertaken in order to achieve leading order scattering for each mode. In fact $\omega \sim \varepsilon^{-\frac{1}{2}}$ actually yields weak scattering for two dimensional flows, and the reason that the scattering is weak is because at Helmholtz numbers of this magnitude the modes remain quite far apart and are unable to exchange sufficient energy to induce scattering to leading order. Weak scattering in this context actually refers to leading order scattering for the incident modes alone, and $O(\varepsilon^{\frac{1}{2}})$ scattering for all

non-incident modes. An understanding of weak scattering is still very valuable, and the equations governing this weak scattering were presented at the end of 5.3. If one's aim is to perform an asymptotic matching of the inner and outer solutions the weak scattering equations may be a good starting point.

The next development of chapter 5 was to construct a model that gave scattering to leading order for every mode. Once again the conditions required for a balance between all important terms was considered, with the additional condition that the modes should be sufficiently close to one another to achieve scattering to leading order. Once these conditions had been ascertained, a model for leading order scattering within the inner region was obtained.

The equation governing leading order scattering within the inner region appears to be difficult to solve analytically, and thus a matching with the algebraically complicated outer solution appeared to be quite laborious. It is also noted that the inner equation is only valid within the small region surrounding the turning point. From a practical point of view, it is desirable to develop the so-called composite solution, a solution that comprises of both the inner and outer solutions and is valid throughout the entire duct to leading order. Given the knowledge obtained from the previous analyses, the final development of chapter 5 was to find an equation that governed the composite solution throughout the whole duct, and this was achieved by defining a stretch variable $s = \varepsilon^{-\beta} g(X)$. Conditions on s were then established by considering values of β such that all of the terms known to be important within both the inner and outer region were included, and then once these conditions

were established the exact form for s was found by comparing it with the previously found inner equation.

A great advantage of using the multiple scales approach to model aeroacoustic problems compared to other methods is that it gives a great understanding of the physics involved within the mechanism under consideration for relatively simple geometries. For example it was shown in this thesis that flow induced modal scattering occurs as a result of a non-zero crosswise mean flow component which comes about due to the effects of the slowly varying geometry. This interaction with the mean flow is the source of the scattering, and it is thanks to the analysis shown in chapter 5 that this is known to be the case. The physical understanding of the situation revealed by this multiple scales approach means that the physics of problems that involve more complicated geometries and flow conditions may be understood.

Chapter 6 then went on to use the composite solution to obtain some numerical results. First of all, the composite model involving the stretched variable s was reformed to give a simpler yet related system involving the axial variable x, and this system was analysed using a finite difference scheme and non-reflecting boundary conditions. Results were computed and compared to the results obtained using standard multiple scales theory. In stark contrast to the standard multiple scales results, results using the scattering theory showed that when a mode undergoes cut-on cut-off transition energy is scattered into neighbouring modes, causing them to be excited and to propagate. Further to this it was also shown that there is evidence that an exchange of energy

between the mean flow and the acoustic field is taking place, as the mean flow appears to inject energy into the acoustic field whenever the mean flow is contracting (accelerating) at the turning point, and extracts energy from the acoustic field when it is diverging (slowing) around the vicinity of the turning point. This striking effect is absent from current multiple scales models of modal propagation, and it shows that energy is not conserved throughout the acoustic realm whenever scattering takes place and a mean flow exists inside the duct. Further analysis of modal scattering, including modal interaction at even higher frequencies without the effects of mean flow can be found in a paper by Smith et al [58], where it is shown that when a mean flow is not present within the duct scattering may still be induced via an even high frequency, and as there is no mean flow present energy is conserved throughout the acoustic field as one would expect.

Other cases shown within chapter 6 included scattering with two incident modes, a case which is of a great deal of practical importance as, in most practical situations, the acoustic realm will consist of several propagating incident modes, and it is important to know what happens in the situation where one of these modes cuts off. Further cases included a case of weak scattering and three dimensional scattering, and both of these cases gave results that appear to agree well with the asymptotic analysis presented in section 5.4. Some further results for this type of scattering phenomena may be found in papers by Smith, Ovenden and Bowles [57, 58].

One of the great features of a multiple scales solution is the efficiency of this

asymptotic approach, meaning that computer simulations of acoustic phenomena can be rapidly resolved, aiding the design of acoustic ducts. Typically the results presented in this thesis took around 30 seconds to compute using a single machine with an Intel Core 2 Duo CPU T7100 @ 1.80GHz processor and 2GB RAM. Such speed in processing results is a very desirable feature of any simulation that is to be used within industry. The reasons listed here should hopefully lead to a more widespread adoption of the asymptotic approach to acoustic noise problems within industry.

7.1 Further Work

There are many ways to further develop the work presented in this thesis. Examples of some of these possible studies are detailed below:

Extending the Turning Point Analysis

In chapter 3 the topic of turning points was discussed, looking at how the behaviour of a cut-on cut-off acoustic mode depends upon the nature of the reduced axial wavenumber as it approaches the turning point. This thesis has discussed the cases where σ^2 behaves linearly, and a solution where σ^2 behaves quadratically was developed here. An interesting extension of the work presented here would be to understand what happens to the solution when σ^2 behaves as a general higher order polynomial within the vicinity of the turning point, or as a general function.

Full Comparison with the Finite Element Model

The results presented here showed that acoustic scattering may indeed be modelled using the multiple scales as well as the finite difference approach. However although some comparisons between the results have been made, up to this point there are as yet no direct comparisons between results using the multiple scales and results obtained using the finite element approach as in [54, 55, 43]. Thus it would be useful to make a direct comparison between the results obtained in chapter 6 with those obtained using the finite element approach.

Extending the Analysis to More Complex Geometries

The results for modal scattering presented within this thesis assumed the case of a slowly varying rectangular ducts. For industrial applications it would be more realistic to extend the model presented here to accommodate circular, annular and elliptic ducts or even ducts of arbitrary cross section. Another interesting and useful extension from a geometrical perspective would be to extend Brambley and Peake's [8] work on strongly curved ducts.

Further Development of the Asymptotic Analysis

Chapter 4 described the features of the outer solution in the case where the frequency was very large, and chapter 5 derived a set of equations governing both weak and leading order modal scattering. Due to the complicated nature of the inner solution these solutions were not asymptotically matched and instead the more practical composite solution was developed to yield some numerical results. The composite solution was run for several cases, and from the numerics it was possible to calculate reflection and transmission coefficients. A comparison between these numerically obtained coefficients and theoretical values may be obtained via an asymptotic matching of the inner and outer solutions, and if an asymptotic matching can be done then it would be very useful to compare these numerical results to those obtained by the theory.

Another very interesting and important follow up from this would be to construct a full energy analysis of the asymptotic solution (similar to that de-

scribed in chapter 6), and compare this with the numerical results. This type of energy analysis would also be useful in developing a fuller understanding of how energy between the mean flow and acoustic field is exchanged. It was noted at the end of chapter 6 that for a fully irrotational mean flow, acoustic energy should be completely conserved within the acoustic field. This is resulting from studies by Cantrell and Hart [10] and Morfey [12]. The fact that the results presented in this thesis show an interaction between the mean flow and the acoustic field may be attributed to the fact that irrotationality has only been imposed up to $O(\varepsilon)$. One feature that does not appear to be present within the current analysis is a mechanism by which energy may be fully conserved within the acoustic field. Irrotational mean flow to $O(\varepsilon^3)$ may be imposed by allowing the second order component of the axial mean flow to take the form $U_2(X,z) = \frac{1}{2}\widetilde{W_1'}(X)z^2$, but this term has not yet shown to play a significant role within the analysis because this term occurs at $O(\varepsilon^2\omega^2)$ whereas the scattering term is $O(\varepsilon\omega^2)$. A possible way to include this term can be made via the following ansatz for the inner region:

$$\phi = \chi(\xi)\psi(y,z;X)\exp\left(-\frac{\mathrm{i}}{\varepsilon}\int_{X_t}^{X}\frac{\omega U}{C^2-U^2}\mathrm{d}X'\right),$$

where $U = U_0(X) + \varepsilon^2 U_2(X,z)$ and $C = C_0(X) + \varepsilon^2 C_2(X,z)$. However although this might seem a feasible attempt at including the required U_2 term, an ansatz of this form fails to satisfy the boundary condition at the duct walls, and actually leads to a scattering term that is active even when the walls of the duct are parallel far from the turning point, which is clearly unphysical. Therefore, a much more general form for the variation in X within the inner region must be included, and this should be matched with the outer solution

presented in chapter 4. Attempts to understand conservation of acoustic energy for flow induced modal scattering in a fully irrotational mean flow are part of an ongoing study.

It would also be useful to determine in what regimes modal scattering occurs under conditions other than when a mode undergoes cut-on cut-off transition.

Extending the Study to Include Lined Ducts

The results presented here for the double turning point and modal scattering assumed a completely hard walled duct. An interesting extension of the work presented here would be to analyse whether any similar effects occur within a ducted that is lined with an impedance wall. In 2002 Ovenden showed that if one considers the action of a single mode for $\omega \sim 1$ as $|\sigma| << 1$ then a partial reflection of modal energy occurs within the duct [42], similar to the type of reflection that occurs for a single turning point in the case of hard walls. The aim then would be to take the work of Ovenden and extend this to include scattering effects, and such a model would then be very useful in industrial applications where ducts ducts are typically lined with a wall of finite impedance. It should also be noted that as soon as the model incorporates a finite acoustic impedance then one must use a non-trivial acoustic boundary condition at the duct wall, which would normally be modelled using Myers' condition. However it is now known that the Myers' condition leads to an ill-posed problem in the time domain giving rise to surface waves that are not observed in reality and one must now use one of the corrected forms of the Myers condition presented by Rienstra and Brambley [53, 7].

Incorporating the Effects of Swirling Mean Flow

Throughout this thesis the model has assumed that both the vortical and swirling component of the mean flow is so small that it may be neglected within the model. Although the assumption of irrotational mean flow is valid within the inlet duct, it is not valid within the by-pass duct as the effects of swirl must be taken into consideration within this region. Strongly swirling flow also occurs within the gap between the fan and the stator vanes (see the turbofan engine sketch given in figure 1.2). Thus a further extension of the work presented here that is of practical importance is to study scattering of acoustic modes in the case when a swirling component is taken into consideration. Cooper and Peake [15, 13] have already successfully used the multiple scales approach to model the propagation and cut-on cut-off transition of acoustic modes within an acoustic duct and swirling mean flow, and the aim then would be to extend their work to include modal scattering.

Bibliography

[1] Milton Abramowitz and Irene A. Stegun. *Handbook of Mathematical Functions with Formulas, Graphs, and Mathematical Tables*. Dover, New York, ninth dover printing, tenth gpo printing edition, 1964.

[2] C. Bailly and D. Juvé. Numerical Solution of Acoustic Propagation Problems Using Linearized Euler Equations. *AIAA Journal*, 38:22–29, January 2000.

[3] Jean-Pierre Berenger. A perfectly matched layer for the absorption of electromagnetic waves. *Journal of Computational Physics*, 114(2):185 – 200, 1994.

[4] David T. Blackstock. *Fundementals of Physical Acoustics*. Wiley-Interscience, 1st edition, 2000.

[5] Jian bo XIE, Qi dou ZHOU, and Bin FANG. Broadband rotor noise prediction based on a new frequency-domain foumulation. *Journal of Hydrodynamics, Ser. B*, 22(3):387 – 392, 2010.

[6] E. Brambley. Low-frequency acoustic reflection at a hardsoft lining transition in a cylindrical duct with uniform flow. *Journal of Engineering Mathematics*, 65:345–354, 2009. 10.1007/s10665-009-9291-1.

[7] E. J. Brambley. A well-posed boundary condition for acoustic liners in straight ducts with flow. *AIAA Journal 0001-1452*, 49:1272–1282, 2011.

[8] E. J. Brambley and N. Peake. Sound transmission in strongly curved slowly varying cylindrical ducts with flow. *Journal of Fluid Mechanics*, 596:387–412, 2008.

[9] E. J. Brambley and N. Peake. Stability and acoustic scattering in a cylindrical thin shell containing compressible mean flow. *Journal of Fluid Mechanics*, 602:403–426, 2008.

[10] R. H. Cantrell and R. W. Hart. Interaction between sound and flow in acoustic cavities: Mass, momentum, and energy considerations. *The Journal of the Acoustical Society of America*, 36(4):697–706, 1964.

[11] X. X. Chen, X. Zhang, C. L. Morfey, and P. A. Nelson. A numerical method for computation of sound radiation from an unflanged duct. *Journal of Sound and Vibration*, 270(3):573 – 586, 2004.

[12] C.L. and Morfey. Acoustic energy in non-uniform flows. *Journal of Sound and Vibration*, 14(2):159 – 170, 1971.

[13] A. J. Cooper and N. Peake. Trapped acoustic modes in aeroengine intakes with swirling flow. *Journal of Fluid Mechanics*, 419:151–175, 2000.

[14] A. J. Cooper and N. Peake. Acoustic propagation in ducts with elliptic cross section. *Journal of Sound and Vibration*, 243:381–401, 2001.

[15] A. J. Cooper and N. Peake. Propagation of unsteady disturbances in a slowly varying duct with mean swirling flow. *Journal of Fluid Mechanics*, 445:207–234, 2001.

[16] W. Eversman. Numerical experiments on acoustic reciprocity in compressible potential flows in ducts. *Journal of Sound and Vibration*, 246(1):97 – 113, 2001.

[17] W. Eversman. A reverse flow theorem and acoustic reciprocity in compressible potential flows in ducts. *Journal of Sound and Vibration*, 246(1):71 – 95, 2001.

[18] W. Eversman and R. J. Beckemeyer. Transmission of sound in ducts with thin shear layers - convergence to the uniform flow case. *J. Acoust. Soc. Am.*, 52:216–220, 1972.

[19] Jonathan B. Freund. Noise sources in a low-reynolds-number turbulent jet at mach 0.9. *Journal of Fluid Mechanics*, 438:277–305, 2001.

[20] Dan Givoli. Non-reflecting boundary conditions. *J. Comput. Phys.*, 94:1–29, May 1991.

[21] D. O. Gough. An elementary introduction to the wkbj approximation. *Wiley-VCH Verlag GmbH Co. KGaA, Weinheim*, 180:1–13, 2007.

[22] J. C. Hardin and S. L. Lamkin. Aeroacoustic computation of cylinder wake flow. *AIAA Journal*, 22:51–57, 1984.

[23] J. C. Hardin and S. L. Lamkin. Computational aeroacoustics - Present status and future promise. In G. Comte-Bellot & J. E. Ffowcs Williams, editor, *Aero- and Hydro-Acoustics*, pages 253–259, 1986.

[24] K. U. Ingard. Influence of fluid motion past a plane boundary on sound reflection, absorption and transmission. *J. Acoust. Soc. Am.*, 31:1035–1036, 1959.

[25] Acheson D. J. *Elementary Fluid Dynamics: Oxford Applied Mathematics and Computing Science Series*. Clarendon Press, 1990.

[26] Tyler J.M. and Sofrin T.G. Axial flow compressor noise studies. *SAE Transactions*, 70:309–332, 1962.

[27] P. Britchford Joseph, K.E., and Pierre Loheac. A model of fan broadband noise due to rotor-stator interaction. pages 45–54. 5th European Conference on Turbomachinery Fluid Dynamics and Thermodynamics, Prague, Czech Republic, 2003.

[28] Batchelor G. K. *An Introduction to Fluid Dynamics*. Cambridge University Press, 2000.

[29] J D Kester and G F Pickett. Application of theoretical acoustics to the reduction of jet engine noise. *J. Phys. D: Appl. Phys.*, 5, 1972.

[30] Karl D. Kryter. *The handbook of hearing and the effects of noise: physiology, psychology, and public health*. Emerald Group Publishing Limited; 1 edition, 1994.

[31] M. J. Lighthill. On sound generated aerodynamically: I general theory. *Proc. R. Soc. Lond. A*, 211:564–587, 1952.

[32] Ching. Y. Loh. On a non-reflecting boundary condition for hyperbolic conservation laws. American Institue of Aeronautics and Aeroacoustics, 2003. Paper AIAA-2003-3975 of the 9th AIAA/CEAS Aeroacoustics Conference, 12-14 May 2003.

[33] P. M. Morse. The transmission of sound inside pipes. *J. Acoust. Soc. Am.*, 11:205–210, 1939.

[34] P. M. Morse and K. U. Ingard. *Theoretical Acoustics*. McGraw-Hill, 1968.

[35] M. K. Myers. On the acoustic boundary condition in the presence of flow. *Journal of Sound and Vibration*, 71:429–434, 1980.

[36] M.K. Myers. An exact energy corollary for homentropic flow. *Journal of Sound and Vibration*, 109(2):277 – 284, 1986.

[37] A. H. Nayfeh, D. P. Telionis, and J. E. Kaiser. Acoustics of aircraft engine-duct systems. *AIAA Journal*, 13:130–153, 1975.

[38] A. H. Nayfeh, D. P. Telionis, and S. G. Lekoudis. Acoustic propagation in ducts with varying cross sections and sheared mean flow. *Progress in aeronautics and astronautics: Aeroacoustics: Jet and combustion noise; duct acoustics*, 37:331–351, 1975.

[39] Ali Hasan Nayfeh. *Introduction to Perturbation Techniques*. John Wiley and Sons, 1981.

[40] Ali Hasan Nayfeh and Demetri P. Telionis. Acoustic propagation in ducts with varying cross sections. *J. Acoust. Soc. Am.*, 53:1654–1661, 1973.

[41] The UK Department of Transport. The future of air transport - white paper and the civil aviation bill. 2003.

[42] N. C. Ovenden. Near cut-on/cut-off transition in lined ducts with flow. 2002. Paper AIAA 2002-2445 of the Eighth AIAA/CEAS Aeroacoustics Conference in Breckenridge, CO, 17-19 June, 2002.

[43] N C Ovenden, W Eversman, and S W Rienstra. Cut-on cut-off transition in flow ducts: comparing multiple-scales and finite-element solutions.

2004. Paper AIAA-2004-2945 of the 10th AIAA/CEAS Aeroacoustics Conference, 10-12 May 2004.

[44] N.C. Ovenden. A uniformly valid multiple scales solution for cut-on cut-off transition of sound in flow ducts. *Journal of Sound and Vibration*, 286(1-2):403 – 416, 2005.

[45] W. H. Press, S. A. Teukolosky, W. T. Vetterling, and B. P. Flannery. *Numerical Recipies in C++, The Art of Scientific Computing*. Cambridge University Press, 2001.

[46] C. J. F. Riddlers. A new algorithm for computing a single root of a real continuous function. *IEEE Transactions on Circuits and Systems*, 26:979–980, 1979.

[47] S. W. Rienstra. Sound transmission in slowly varying circular and annular lined ducts with flow. *Journal of Fluid Mechanics*, 380:279–296, 1999.

[48] S. W. Rienstra. Cut-on, cut-off transition of sound in slowly varying flow ducts. contribution to the david crighton memorial issue of aerotechnica missili e spazio. *Journal of the Associazione Italiana di Aeronautica e Astronautica AIDAA*, 79:93–96, 2000.

[49] S. W. Rienstra. Sound propagation in slowly varing lined flow ducts of arbitrary cross section. *Journal of Fluid Mechanics*, 495:157–173, 2003.

[50] S. W. Rienstra. Impedance models in time domain including the extended helmholtz resonator model. American Institue of Aeronautics and Aeroacoustics, 2006. Paper AIAA-2006-2686 of the 12th AIAA/CEAS Aeroacoustics Conference, 9-10 May 2006, Cambridge, MA, USA.

[51] Sjoerd Rienstra. Acoustic scattering at a hardsoft lining transition in a flow duct. *Journal of Engineering Mathematics*, 59:451–475, 2007. 10.1007/s10665-007-9193-z.

[52] Sjoerd W. Rienstra. A classification of duct modes based on surface waves. *Wave Motion*, 37(2):119 – 135, 2003.

[53] SJOERD W. RIENSTRA and MIRELA DARAU. Boundary-layer thickness effects of the hydrodynamic instability along an impedance wall. *Journal of Fluid Mechanics*, 671:559–573, 2011.

[54] I. Danda Roy and W. Eversman. Improved finite element modeling of the turbofan engine inlet radiation problem. *Journal of Vibration and Acoustics*, 117(1):109–115, 1995.

[55] Indranil Danda Roy and Walter Eversman. Far-field calculations for turbofan noise. *AIAA Journal*, 39:2255–2261, 2001.

[56] P. Sijtsma and J.B.H.M Schulten. Wake modelling accuracy requirements for prediction of rotor wake-stator interaction noise. 2003. Paper AIAA-2003-3138 of the 9th AIAA/CEAS Aeroacoustics Conference and Exhibit 12 - 14 May 2003.

[57] A. F. Smith, N. C. Ovenden, and R. I. Bowles. Flow induced scattering of acoustic modes in slowly varying ducts. Paper AIAA-2010-3893 of the 16th AIAA/CEAS Aeroacoustics Conference, 7-9 June 2010, Stockholm, Sweden.

[58] A. F. Smith, N. C. Ovenden, and R. I. Bowles. Flow and geometry

induced scattering of high frequency acoustic modes in ducts (accepted for publication). *Wave Motion*, 2011.

[59] M. J. T. Smith. *Aircraft Noise*. Cambridge University Press, 1989.

[60] B. J. Tester. Some aspects of sound attenuation in lined ducts containing invicid mean flows with boundary layers. *Journal of Sound and Vibration*, 28:217–245, 1973.

[61] G. N. Watson. *The Theory of Bessel Functions*. Cambridge University Press, 1966.